

# Biocatalytic Tools for Enzymatic Cascades

Inaugural dissertation  
of the Faculty of Science,  
University of Bern

presented by

Valentina Marchini

from Eraclea (VE), Italy

Supervisor of the doctoral thesis:  
Prof. Dr. Francesca Paradisi

Department of Chemistry, Biochemistry and Pharmaceutical Sciences  
University of Bern

# Biocatalytic Tools for Enzymatic Cascades

Inaugural dissertation  
of the Faculty of Science,  
University of Bern

presented by

Valentina Marchini

from Eraclea (VE), Italy

Supervisor of the doctoral thesis:

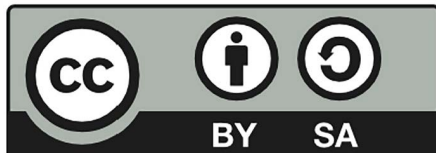
Prof. Dr. Francesca Paradisi

Department of Chemistry, Biochemistry and Pharmaceutical Sciences  
University of Bern

Accepted by the Faculty of Science.

Bern, 04 July 2022

The Dean  
Prof. Dr. Zoltan Balogh



This work is licensed under a Creative Commons Attribution-ShareAlike 4.0 International License  
<https://creativecommons.org/licenses/by-sa/4.0/>

# Table of Contents

---

<b>ABSTRACT</b> .....	<b>1</b>
<b>ABBREVIATIONS</b> .....	<b>3</b>
<b>1. INTRODUCTION</b> .....	<b>9</b>
1.1 BIOCATALYSIS.....	9
1.2 ENZYMES AS BIOCATALYSTS.....	11
1.3 AMMONIA LYASES .....	12
1.3.1 <i>Phenylalanine and tyrosine ammonia lyases (PAL - TAL)</i> .....	16
1.3.2 <i>Phenylalanine ammonia lyase from Anabaena variabilis (AvPAL)</i> .....	19
1.3.3 <i>Phenylalanine ammonia lyase from Rhodotorula glutinis (RgPAL)</i> .....	20
1.4 OXIDOREDUCTASES.....	20
1.4.1 <i>Formate dehydrogenase from Candida boidinii (CbFDH)</i> .....	21
1.5 AMINO ACID DEHYDROGENASES .....	22
1.5.1 <i>Alanine dehydrogenase from Halomonas elongata (HeAlaDH)</i> .....	24
1.5.2 <i>Glutamate dehydrogenase from Clostridium symbiosum (CsGluDH)</i> .....	25
1.5.3 <i>Phenylalanine dehydrogenase from Bacillus sphaericus (BsPheDH)</i> .....	26
1.6 HYDROXYPHENYLPYRUVATE REDUCTASES (HPPR) .....	27
1.7 BIOCATALYTIC CASCADES.....	28
1.8 ENZYME IMMOBILIZATION .....	30
1.9 FLOW BIOCATALYSIS.....	34
1.10 BIBLIOGRAPHY.....	35
<b>2. AIMS AND OBJECTIVES</b> .....	<b>45</b>
<b>3. MATERIALS AND METHODS</b> .....	<b>47</b>
3.1 MATERIALS .....	47
3.2 GENERAL METHODS .....	48
3.2.1 <i>Culture mediums</i> .....	48
3.2.2 <i>Chemically competent cells preparation</i> .....	49



3.2.3 Electro competent cells preparation.....	49
3.2.4 Agarose gel preparation.....	49
3.2.5 Transformation of competent <i>E. coli</i> cells.....	50
3.2.6 Protein overexpression.....	50
3.2.7 Protein purification.....	52
3.2.8 Purification of pTac-85 CsGluDH (without His-tag).....	54
3.2.9 SDS-PAGE preparation and execution.....	54
3.2.10 Cloning of CsGluDH - pRSETb.....	54
3.2.11 Genetic construction design of fusion proteins.....	55
3.2.12 DNA amplification: PCR of the insert.....	56
3.2.13 DNA amplification: PCR of the vector.....	57
3.2.14 Digestion with DpnI.....	58
3.2.15 Gibson assembly.....	58
3.2.16 Optimization of fusion proteins overexpression.....	60
3.2.17 HeWT preparation.....	61
3.2.18 Protein quantification.....	61
3.2.19 Size Exclusion Chromatography (SEC).....	61
3.2.20 Enzyme characterization.....	62
3.2.20.1 Activity assay of PALS.....	62
3.2.20.2 Activity of WT CsGluDH and WT CbFDH.....	63
3.2.20.3 Activity and stability of GluDH - FDH fusion protein.....	63
3.2.20.4 Activity and stability of AlaDH - FDH fusion protein.....	64
3.2.20.5 Activity assay of BsPheDH.....	65
3.2.20.6 Activity assay of MphPPR.....	65
3.2.21 Assembly prediction of GluDH-FDH fusion protein by MD.....	66
3.2.22 Biotransformations in batch.....	66
3.2.22.1 Batch Biotransformation of aliphatic substrates with AvPAL.....	66
3.2.22.2 Batch biotransformation using pTac-85 CsGluDH.....	66
3.2.22.3 Biotransformation using soluble and co-immobilized WT GluDH and WT FDH.....	67
3.2.22.4 Biotransformations of GluDH-FDH fusion protein.....	67
3.2.22.5 Batch biotransformations of AlaDH-FDH fusion protein with HeWT.....	67

3.2.22.6 Batch biotransformations of RgPAL.....	68
3.2.22.7 Batch biotransformations of BsPheDH and/or MpHPPR.....	68
3.2.23 <i>Samples preparation and analyses</i> .....	68
3.2.24 <i>Enzyme immobilization</i> .....	69
3.2.24.1 Activation of epoxy resin to obtain aldehyde groups .....	70
3.2.24.2 Quantification of aldehyde groups.....	70
3.2.24.3 Covalent immobilization on glyoxyl groups.....	70
3.2.24.4 Covalent immobilization on epoxy groups by first interaction with a metal.....	70
3.2.24.5 Covalent immobilization on epoxy groups by first interaction with ethylenediamine.....	71
3.2.24.6 Coating of epoxy or glyoxyl resin with polyethyleneimine .....	71
3.2.24.7 Qualitative assay to compare the rate of amino groups functionalization .....	71
3.2.24.8 Cross-linking with glutaraldehyde.....	72
3.2.25 <i>Immobilization and operational stability of WT CsGluDH and WT CbFDH</i> .....	72
3.2.26 <i>Immobilization and operational stability of GluDH-FDH fusion protein</i> .....	73
3.2.27 <i>Continuous flow biotransformation</i> .....	73
3.2.27.1 Continuous flow biotransformation of aliphatic substrates with AvPAL.....	74
3.2.28 <i>Extraction of L-Dopa with phenyl boronic acid (PBA)</i> .....	74
3.2.28.1 Liquid-liquid extraction (LLE) .....	74
3.2.28.2 Solid-phase extraction (SPE).....	74
3.3 BIBLIOGRAPHY .....	75
<b>4. SUSTAINABLE PRODUCTION OF ALIPHATIC ACRYLIC ACID DERIVATIVES USING PHENYLALANINE AMMONIA LYASES</b> .....	<b>77</b>
4.1 INTRODUCTION .....	78
4.2 RESULTS AND DISCUSSION.....	79
4.2.1 <i>Protein expression, purification and activity</i> .....	79
4.2.2 <i>Protein immobilization</i> .....	79
4.2.3 <i>Biotransformation of PALs towards aliphatic substrates</i> .....	83
4.2.4 <i>Biotransformation of AvPAL with coupled reaction</i> .....	85
4.2.5 <i>Biotransformation of AvPAL with coupled reaction in continuous flow</i> .....	86
4.3 CONCLUSION .....	90

4.4 BIBLIOGRAPHY .....	90
<b>5. EFFICIENT CO-IMMOBILIZATION OF GLUTAMATE AND FORMATE DEHYDROGENASE FOR A REUSABLE BIENZYMATIC TOOL TOWARDS AMMONIA REMEDIATION.....</b>	<b>92</b>
5.1 INTRODUCTION .....	93
5.2 RESULTS AND DISCUSSION .....	96
5.2.1 Protein expression, purification and activity.....	96
5.2.2 Biotransformation using pTac-85 CsGluDH.....	96
5.2.3 Cloning of GluDH.....	98
5.2.4 Expression and purification of GluDH and FDH.....	98
5.2.5 Activity of GluDH and FDH.....	100
5.2.6 Immobilization and co-immobilization of GluDH and FDH .....	101
5.2.7 Biotransformation using soluble and co-immobilized biocatalysts.....	111
5.3 CONCLUSION.....	112
5.4 BIBLIOGRAPHY .....	113
<b>6. DEVELOPMENT OF GLUTAMATE AND FORMATE DEHYDROGENASE FUSION PROTEIN AS BIFUNCTIONAL BIOCATALYTIC TOOL NFOR THE EFFICIENT CONTINUOUS REMOVAL OF AMMONIA .....</b>	<b>117</b>
6.1 INTRODUCTION .....	118
6.2 RESULTS AND DISCUSSION.....	119
6.2.1 Genetic construction of the GluDH-FDH fusion protein.....	119
6.2.2 Expression optimization.....	122
6.2.3 Larger scale overexpression and purification.....	124
6.2.4 Activity and stability.....	125
6.2.5 Assembly evaluation.....	130
6.2.6 Protein immobilization .....	132
6.2.7 Operational stability .....	134
6.2.8 Biotransformations of $\alpha$ -ketoglutarate with free and immobilized fusion protein .....	136
6.2.9 Continuous removal of ammonia via biotransformations (proof of concept).....	138
6.3 CONCLUSION .....	141

6.4 BIBLIOGRAPHY .....	141
<b>7. CREATION OF A BI-ENZYMATIC TOOL WITH ALANINE AND FORMATE DEHYDROGENASE FUSION PROTEIN FOR THE COUPLING OF TRANSAMINASE CATALYSED REACTIONS.....</b>	<b>144</b>
7.1 INTRODUCTION .....	145
7.2 RESULTS AND DISCUSSION .....	148
7.2.1 Genetic construction of the two fusion proteins .....	148
7.2.2 Expression optimization .....	150
7.2.3 Larger scale overexpression and purification .....	153
7.2.4 Activity and assembly of the two fusion proteins .....	154
7.2.5 Characterization of the AlaDH-FDH-His protein.....	160
7.2.6 Batch biotransformation.....	162
7.2.7 Dialysis assisted biotransformation.....	165
7.3 CONCLUSION.....	166
7.4 BIBLIOGRAPHY .....	167
<b>8. BIOCATALYTIC CASCADE FOR THE CONTINUOUS PRODUCTION OF DANSHENSU .....</b>	<b>170</b>
8.1 INTRODUCTION .....	171
8.2 RESULTS AND DISCUSSION.....	175
8.2.1 Purification, activity and immobilization of RgPAL.....	175
8.2.2 Batch biotransformations of RgPAL .....	178
8.2.3 L-Dopa purification and RgPAL amination in flow.....	179
8.2.4 Purification, activity and immobilization of BsPheDH.....	181
8.2.5 Batch biotransformations of BsPheDH.....	182
8.2.6 Expression, purification and characterization of MpHPPR .....	183
8.2.7 Immobilization and batch biotransformations of MpHPPR .....	187
8.2.8 Coupling of BsPheDH with MpHPPR.....	189
8.2.9 Flow reaction with BsPheDH and MpHPPR .....	194
8.2.10 Continuous production of Danshensu in the flow bioreactor .....	195
8.3 CONCLUSION .....	199

8.4 BIBLIOGRAPHY .....	200
9. CONCLUSIONS .....	204
DECLARATION OF CONSENT .....	206
CURRICULUM VITAE .....	207

## ABSTRACT

---

The field of biocatalysis is receiving increased attention over the years, owing to the incontrovertible necessity for sustainable processes. As essential part of biocatalysis, enzymes fulfil the demand for greener reactions thanks to their valuable properties, while providing simpler synthetic routes with higher selectivity than the traditional hazardous methods. Potentially, enzymes are remarkable catalysts but most of the times, they require special optimization before being effectively applied at industrial scale, which translates into significant investment of work and time. In this regard, the combination of enzymes as tool to assist a reaction or to carry out particular functions can facilitate the process.

A series of biocatalytic tools have been created in this work to tackle specific problems. Afterwards, they were tested to evaluate their efficacy during the utilization.

To enable faster conversion of alanine derivatives into acrylates, the addition of a cascade reaction was attempted for continuous depletion of the by-product ammonia, resulting in a shift of reaction equilibrium towards the product formation (chapter 4). In fact, the non-oxidative deamination of aliphatic substrates is an unnatural reaction for phenylalanine ammonia lyases, which require a tool to enhance the conversion. Consequently, the combination of a glutamate dehydrogenase with a formate dehydrogenase appeared as valid implementation, since the first enzyme consumes ammonia for the reductive amination of  $\alpha$ -ketoglutarate into glutamate with NADH, while the second protein regenerates continuously the cofactor. To optimize the two biocatalysts system, an immobilization screening was successfully performed with following co-immobilization onto the shared support, so that the faster substrate exchange could increase the reaction velocity (chapter 5). This biocatalytic tool possessed higher stability than the free proteins and could be reused several times by simply recovering the active immobilized enzymes from the bulk. These features satisfy the essential requirements for industrial application.

As further optimization of the enzymatic tool, a fusion protein has been effectively produced locating even tighter the glutamate and the formate dehydrogenase (chapter 6). The genetic linkage of the two domains did not impact on their activity, offering an efficient bifunctional protein that required less manipulation with consequent industrially appealing savings in terms of time and costs. The immobilized fusion protein could be reuse for

several cycles of biotransformations, and it proved to efficiently remove small and high amounts of ammonia (300 mM) with greater conversion rates and improved stability than the wild type enzymes.

The immobilized fusion protein was applied in continuous flow reaction as tool to assist the phenylalanine ammonia lyase. Despite this last enzyme did not apport any considerable result, the fusion protein could effectively deplete the produced ammonia for an efficient cascade reaction.

To investigate the versatility of the tool, more information on the fusion protein design was required. This has been achieved by changing the glutamate dehydrogenase with a different enzyme, the alanine dehydrogenase (chapter 7). Although more efforts were needed for their expression, two fusion proteins were successfully developed. Unfortunately, they did not retain full activity after the fusion, given the particular subunits assembly. However, the most active fusion protein showed better results than the wild type enzymes when employed in association to a transaminase biocatalyst, as optimized tool to regenerate the amino donor (alanine) and remove the inhibitory side product (pyruvate).

Finally, a cascade reaction has been developed to produce continuously danshensu (chapter 8), which is a high potential pharmacological compound that is not yet appropriately harnessed for the extremely high cost of manufacture. A novel enzyme was successfully found and characterized for the purpose, namely the hydroxy phenyl pyruvate reductase from *Mentha x piperita*, which was combined with a phenylalanine dehydrogenase to offer a sustainable tool for danshensu formation. After optimization of enzymes immobilization, the cascade reaction was successfully applied to continuous flow biotransformation, achieving a productivity of 5 mM/h.

**ABBREVIATIONS**

---

AaDH	Amino acid dehydrogenase
ACN	Acetonitrile
ADH	Alcohol dehydrogenase
AI	Autoinduction
AlaDH	Alanine dehydrogenase
API	Active Pharmaceutical Ingredient
ATA	Amino transaminase
AvPAL	Phenylalanine ammonia lyase from <i>Anabaena variabilis</i>
AzoRo	Azoreductase
BsPheDH	Phenylalanine dehydrogenase from <i>Bacillus sphaericus</i>
CbFDH	Formate dehydrogenase from <i>Candida boidinii</i>
CbHPPR	Hydroxyphenylpyruvic acid reductase from <i>Coleus blumei</i>
CHMO	Cyclohexanone monooxygenase
CLEAs	Cross-linked enzyme aggregates
CLEAs	Cross-linked enzyme crystals
CsGluDH	Glutamate dehydrogenase from <i>Clostridium symbiosum</i>
DAL	Aspartate ammonia lyases
DHPPA	3,4-dihydroxyphenylpyruvate
DNA	Deoxyribonucleic acid
DTT	Dithiothreitol
<i>E. coli</i>	<i>Escherichia coli</i>
E1cB	Elimination Unimolecular conjugate Base
EAAL	Ethanolamine ammonia lyase
EC	Enzyme Commission



## ABBREVIATIONS

EDA	Ethylenediamine
EDTA	Ethylenediaminetetraacetic acid
EWG	Electron Withdrawing Group
FDH	Formate dehydrogenase
Fmoc	Fluorenylmethyloxycarbonyl
GA	Glutaraldehyde
GC-FID	Gas chromatography with flame ionization detection
GDH	Glucose dehydrogenase
GluDH	Glutamate dehydrogenase
HAL	Histidine ammonia lyase
HeAlaDH	Alanine dehydrogenase from <i>Halomonas elongata</i>
HeWT	$\omega$ -Transaminase from <i>Halomonas elongata</i>
HPLC	High-performance liquid chromatography
HPPA	4-hydroxyphenylpyruvate
HPPR	Hydroxyphenylpyruvic acid reductase
IDA	Iminodiacetic acid
IPA	Isopropylamine
IPTG	1-thio- $\beta$ -D-galactopyranoside
KGA	$\alpha$ -Ketoglutaric acid
KCD	L-lysine cyclodeaminase
LB	Luria-Bertani broth
LDH	Lactate dehydrogenase
LeuDH	Leucine dehydrogenase
LLE	Liquid-liquid extraction
MAL	Methylaspartate ammonia lyase
MCF	Methyl chloro formate

## ABBREVIATIONS

MIO	3,5-dihydro-5-methylidene-4H-imidazol-4-one
MpHPPR	Hydroxyphenylpyruvic acid reductase from <i>Mentha piperita</i>
NAD <sup>+</sup>	Nicotinamide adenine dinucleotide
NADH	Nicotinamide adenine dinucleotide (reduced form)
NADP <sup>+</sup>	Nicotinamide adenine dinucleotide phosphate
NADPH	Nicotinamide adenine dinucleotide phosphate (reduced form)
OCD	L-ornithine cyclodeaminase
PAL	Phenylalanine ammonia lyase
PBR	Packed bed reactor
PCR	Polymerase Chain Reaction
PDB	Protein Data Bank
PEI	Polyethyleneimine
PheDH	Phenylalanine dehydrogenase
PL	Protein ladder
PLP	Pyridoxal 5'-phosphate
PMP	Pyridoxamine 5'-phosphate
PMSF	Phenylmethanesulfonyl fluoride
PTAL	Phenylalanine tyrosine ammonia lyase
RgPAL	Phenylalanine ammonia lyase from <i>Rhodotorula glutinis</i>
RsTAL	Tyrosine ammonia lyase from <i>Rhodobacter sphaeroides</i>
SDS-PAGE	Sodium dodecyl sulphate polyacrylamide gel electrophoresis
SEC	Size exclusion chromatography
βME	β-mercaptoethanol
SPE	Solid-phase extraction
TAE	Tris-acetate-EDTA
TAL	Tyrosine ammonia lyase

## ABBREVIATIONS

TB	Terrific broth
TEMED	Tetramethyl ethylenediamine
TEV	Tobacco Etch Virus
TFA	Trifluoroacetic acid
TLC	Thin layer chromatography
UV	Ultraviolet
WAL	Tryptophan ammonia lyase
WT	Wild type

### **Amino acids**

---

A - Ala	Alanine
C - Cys	Cysteine
D - Asp	Aspartic acid
E - Glu	Glutamic acid
F - Phe	Phenylalanine
G - Gly	Glycine
H - His	Histidine
I - Ile	Isoleucine
K - Lys	Lysine
L - Leu	Leucine
M - Met	Methionine
N - Asn	Asparagine
P - Pro	Proline
Q - Gln	Glutamine
R - Arg	Arginine
S - Ser	Serine

## ABBREVIATIONS

T - Thr	Threonine
V - Val	Valine
W - Trp	Tryptophan
Y - Tyr	Tyrosine

### DNA nucleotides

---

A	Adenine
C	Cytosine
T	Thymine
G	Guanine

### Units of measure / symbols

---

%	Percentage
bp	Base pair
C	Celsius
CV	Column Volume
Da	Dalton
ee	enantiomeric excess
$\epsilon$	Extinction coefficient
g	Gram
h	Hour
$K_{cat}$	Turnover number
$K_M$	Michaelis constant
L	Litre
M	Molarity

## ABBREVIATIONS

m	meter
min	Minute
mol	Mole
rpm	Rotation per minute
$R_t$	Resident Time
s	Second
U	Units
V	Volume
$V_{\max}$	Maximum Velocity
W	Weight
y	yield
$\lambda$	wavelength

## 1. INTRODUCTION

---

### 1.1 BIOCATALYSIS

Biocatalysis is a fast-developing field of synthetic chemistry, which has had an increasing impact on chemical and pharmaceutical industry during the past decades, leading to the advancement of greener, environmentally friendly, and more efficient synthetic processes.<sup>1,2</sup> In this sense, the field of biocatalysis can be inserted in the concept of Green Chemistry.

In fact, Green Chemistry is the design of chemical products and processes that minimize or eliminate the use or generation of hazardous substances with the aim of reducing pollution at its source. It applies across the life cycle of a chemical product, including its design, manufacture, use, and ultimate disposal.<sup>3</sup> Concept and guidelines of Green Chemistry have been developed by the chemists Paul Anastas and John Warner, together with a framework of a cohesive set of 12 Principles (Figure 1) which every reaction should comply with.<sup>4</sup>

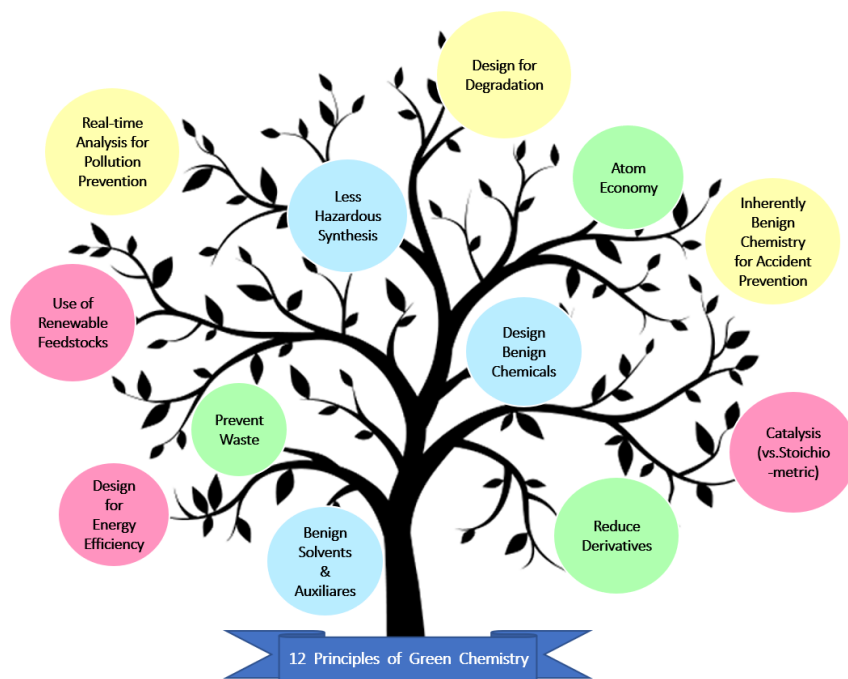


Figure 1. The 12 Principles establishing the concept of Green Chemistry.<sup>4</sup>

## 1. INTRODUCTION

Biocatalysis has emerged as one of the best solutions to achieve Green Chemistry, with many benefits over chemical synthesis. In fact, enzyme catalysed reactions fulfill almost all the demands of Green Chemistry: they normally exhibit excellent atom economy, preventing the formation of waste and undesired products. In addition, biocatalysts normally operate in mild conditions and aqueous systems, facilitating the handling of the reaction and avoiding the use of hazardous solvents or toxic reagents. Biocatalysts can also shorten the synthetic route and achieve high yields with excellent chemo-, regio-, and stereo-selectivities.<sup>5</sup>

The considerable growth of this field is being partially driven by the recent advances in several technologies, like metagenomics, bioinformatics, protein engineering, high-throughput screening and analysis. These techniques provide access to new and more productive biocatalysts which can be tuned for a wide variety of unnatural substrates and allow for reactions that are currently unknown or rare in nature.<sup>6</sup> The expanding area of biocatalysis and the adjacent technologies offer a universe of opportunities to implement advantageous and sustainable processes in industrial production of chemicals and pharmaceuticals.

Over the past 20 years, the application of enzymes as catalysts for the manufacture of complex molecules has become increasingly widespread. Nowadays, multiple molecules are synthesized via biocatalytic processes, especially to make chiral compounds for pharmaceuticals as well for the flavors and fragrance industry.<sup>7,8</sup> For example, duloxetine is an active pharmaceutical ingredient (API) that is used in the indication area of depression and incontinence.<sup>9</sup> A key intermediate in the synthesis, the duloxetine alcohol, is produced in the BASF company by the robust alcohol dehydrogenase (ADH) from *Lactobacillus brevis* and the keto reductase EbN1 from *Aromatoleum aromaticum*. Both the enzymes are highly selective for the reduction of the ketone precursor to the (S)-enantiomer. Moreover, a mutant of the second enzyme acted fast and robust in mixed solvent systems, accepting *rac*-2-butanol or isopropanol for the recycling of the expensive cofactor NADH and achieving around 90% conversion (Figure 2a).<sup>8,10</sup>

A further example is the application of the engineered transaminase ATA-117 for the synthesis of the diabetes drug Sitagliptin by Merck and Codexis from the prochiral precursor pro-Sitagliptin.<sup>11</sup> The biocatalyst was able to convert the ketone to the final API with excellent enantioselectivity at 92% yield using isopropylamine as amino

## 1. INTRODUCTION

donor (Figure 2b). The enzymatic route resulted in higher overall yield than the previously used chemical process, with 53% higher productivity, reduced total waste and elimination of the transition metal catalyst.<sup>8</sup>

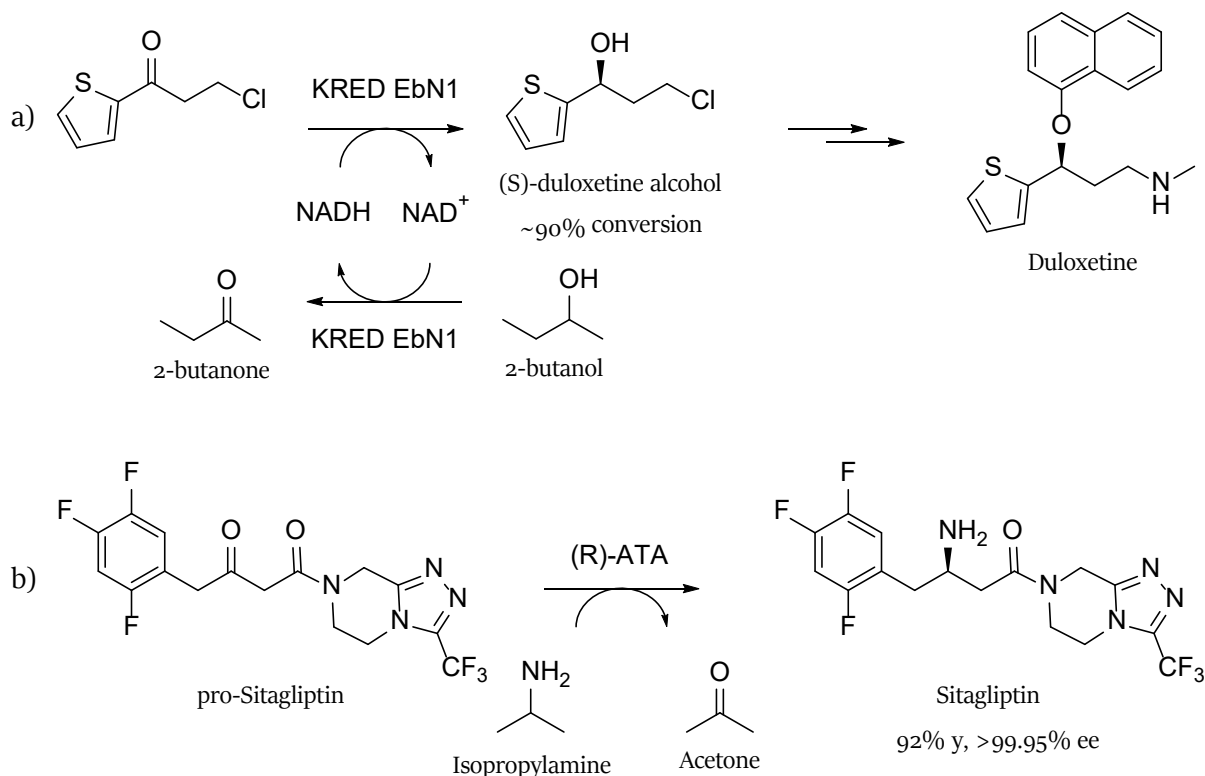


Figure 2. Enzymatic synthesis of duloxetine alcohol (a) and Sitagliptin (b).

Looking to the future, there are numerous key trends and scientific breakthroughs that are promising to have a significant influence on accelerating the discovery, development and application of biocatalysts.<sup>7</sup> Consequently, biocatalysis will become more widely used in the manufacture of chemicals, pharmaceuticals, or intermediates, realizing increasing impact in the future.<sup>5,6</sup>

### 1.2 ENZYMES AS BIOCATALYSTS

Biocatalysis involves the use of enzymes for the preparation of chemicals with added values, that are traditionally made using chemical synthesis.<sup>12</sup> Enzymes are highly effective catalysts, whose function is to lower the activation energy for a reaction and thereby enhance the rate of specific chemical reactions without being consumed in the



## 1. INTRODUCTION

process.<sup>13</sup> As macromolecular catalysts, they promote reactions through pathways that would be difficult, if not impossible, to access with small-molecule catalysts because of competition with other lower-energy reaction pathways.<sup>14</sup>

The biocatalysts are able to accept a wide range of simple or complex molecules as substrates, as well as to catalyze reactions with enantio- and regioselectivity without the need of protection and deprotection steps, that are common in selective organic synthesis. Moreover, modern enzymatic processes lead to high product concentrations with moderate undesirable by-products, provided that the enzymes do not require expensive cofactors.<sup>12</sup>

Enzymes can be considered as a toolbox which offers uncountable possibilities to successfully tackle the many challenges on the way to synthesize target molecules.<sup>15</sup> The available choice is immense. In this regard, a first selection relies on one of the classes of enzymes (Figure 3), clustered according to the nature of the required reaction.<sup>16</sup>

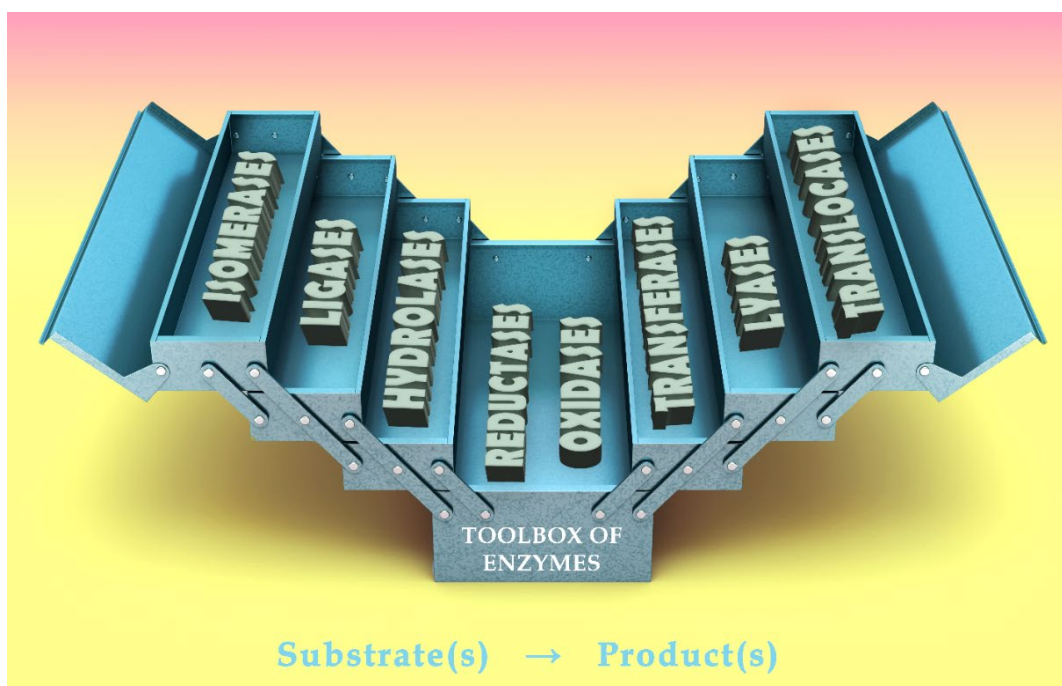


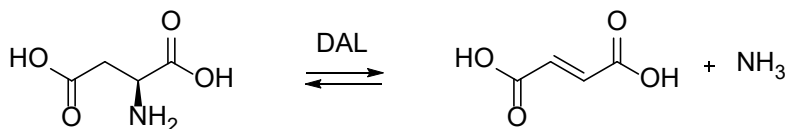
Figure 3. List of the main enzyme classification based on the reaction that the enzyme catalyzes.

Inside these classes, there are several other subclasses depending on specific features of each group of enzymes. Some examples are shown in the following paragraphs.

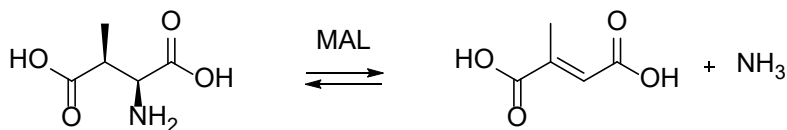
### 1.3 AMMONIA LYASES

The enzymes belonging to the family of ammonia lyases (EC 4.3.1) catalyze the reversible non-oxidative cleavage of C-N bonds, typically of  $\alpha$ -amino acids, to yield unsaturated or cyclic alkenes and ammonia. Afterwards, the structurally, functionally, and mechanistically diverse family is sorted into 31 different EC subclasses where, among others, seven main groups can be identified, based on the specific analogy in the catalyzed reaction and accepted substrates (Figure 4).<sup>1</sup>

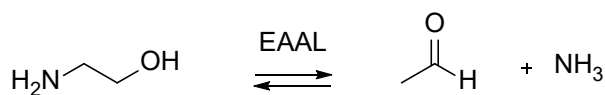
#### ASPARTATE AMMONIA LYASES



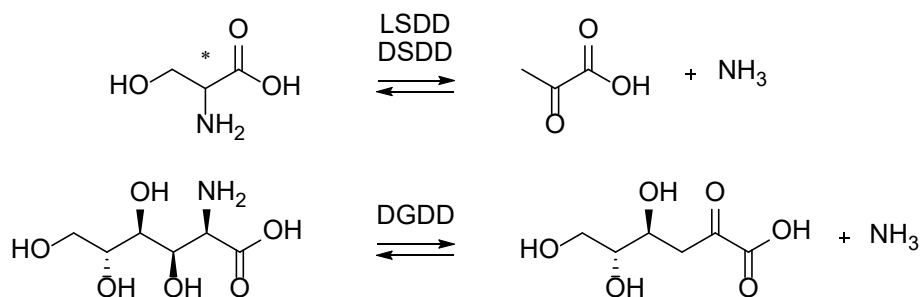
#### METHYLASPARTATE AMMONIA LYASES



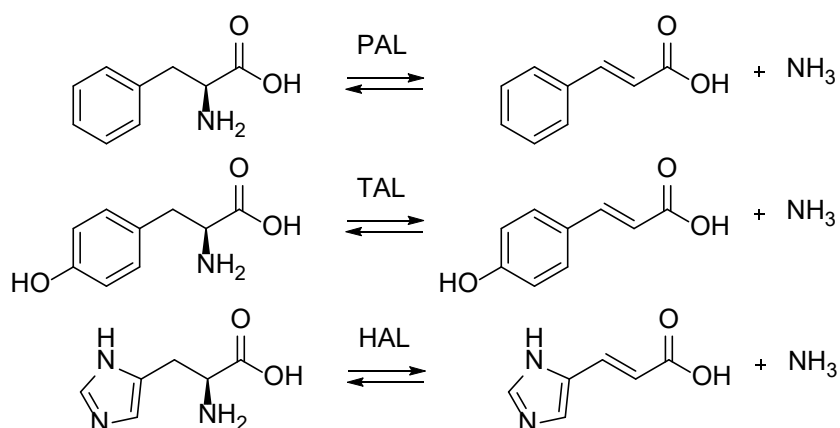
#### ETHANOLAMINE AMMONIA LYASES



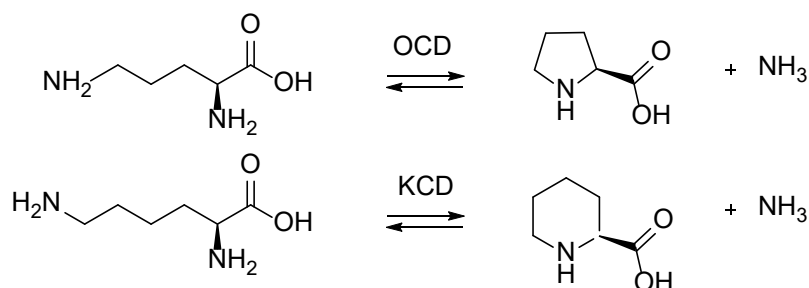
#### HYDROXY AMINO ACID DEHYDRATASE/DEAMINASES



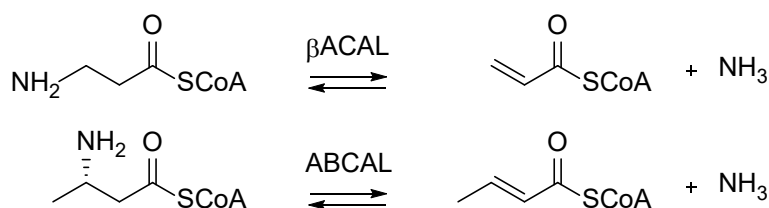
## AROMATIC AMINO ACID AMMONIA LYASES



## AMINO ACID CYCLODEAMINASES



## AMINOACYL-CoA AMMONIA LYASES

Figure 4. Representative reactions catalyzed by the most important classes of ammonia-lyases.<sup>1</sup>

Aspartate Ammonia Lyases (DALs): belong to the aspartase/fumarase superfamily and catalyze the reversible deamination of L-aspartic acid to fumaric acid. Also known as aspartases, they work in a very specific manner, and any attempt of engineering has so far failed. Thus, only a limited range of aspartic acid analogues has been synthesized with aspartases.<sup>1</sup>

Methylaspartate Ammonia Lyases (MALs): are related to the superfamily of enolases and catalyze the deamination of (2S,3S)-threo-3-methylaspartate to 2-methylfumaric acid with the presence of  $\text{Mg}^{2+}$  and  $\text{K}^+$  as cations. This

## 1. INTRODUCTION

type of enzymes accepts various substituted aspartate derivatives. Engineered MAL variants have also been developed successfully.<sup>1</sup>

Ethanolamine Ammonia Lyases (EAAL): transform ethanolamine into acetaldehyde and ammonia through the interaction of cofactor adenosylcobalamin (coenzyme B<sub>12</sub>). The synthetic applications of this subclass of enzymes is rather limited.<sup>1</sup>

Hydroxy Amino Acid Dehydratase/Deaminases (LSDD/DSDD/DGDD): are part of the PLP (pyridoxal 5'-phosphate)-dependent enzyme family, where PLP is used as an imine to convert the C-N bond of a  $\beta$ -hydroxy- $\alpha$ -amino acid to a C=O bond. As for these enzymes, no preparative application is known.<sup>1</sup>

Aminoacyl-CoA Ammonia Lyases: eliminate ammonia on previously CoA activated  $\beta$ -alanine to give acryloyl-CoA ( $\beta$ ACALs) and on 3-aminobutyryl-CoA to produce crotonyl-CoA (ABCALs). However, these biocatalysts are unlikely to be employed in large scale applications, due to the difficulty of accessing CoA derivatives as substrates.<sup>1</sup>

Amino Acid Cyclodeaminases: distinguish between L-ornithine cyclodeaminases (OCD), which result in the production of L-proline and ammonia, and L-lysine cyclodeaminases (KCD), that deaminate L-lysine to L-pipecolic acid. These reactions are carried out by nicotinamide adenine dinucleotide (NAD<sup>+</sup>) cofactor molecule. Practical applications lead to the improvement of industrial processes for cyclic amino acids generation.<sup>1</sup>

Aromatic Amino Acid Ammonia Lyases: form  $\alpha,\beta$ -unsaturated acids through nonoxidative deamination of L-phenylalanine (PALs; EC 4.3.1.24), L-tyrosine (TALS; EC 4.3.1.23), L-histidine (HALs; EC 4.3.1.3). In addition, it has been reported a putative tryptophan ammonia lyase (WAL) but its existence in nature has not been confirmed yet.<sup>17</sup>

Phenylalanine ammonia lyases are necessary for biosynthetic purposes. Indeed, these enzymes yield cinnamic acid for the biosynthesis of phenylpropanoids in plants, towards polyhydroxylated aromatic compounds, like flavonoids, lignin, anthocyanins, stilbenes, and for the biosynthesis of several antibiotic compounds in bacteria.<sup>18,19</sup>

Tyrosine ammonia lyases serve the same role producing coumaric acid from tyrosine. Their metabolic purposes are strongly related to PALs functions, but they are also involved in more specific pathways.<sup>20</sup>

This subclass of ammonia lyases do not require cofactors or a radical mechanism. With 100% atom efficiency, their productivity can be optimized through directed evolution and rational engineering, possess regio- and

enantioselectivity, are suitable for cascade reactions, and can be employed for biotherapeutic applications. Although they have already found applications in industry, and various pharmaceutical processes have been patented, aromatic amino acids ammonia lyases are expected to become considerably more relevant in the future as far as industrial and medical fields are concerned.<sup>21</sup>

### 1.3.1 Phenylalanine and tyrosine ammonia lyases (PAL - TAL)

Aromatic amino acid ammonia lyases are closely related and share high similarity to aromatic 2,3-aminomutases. Both contain the MIO (3,5-dihydro-5-methylidene-4H-imidazol-4-one) catalytic group, that mediates ammonia elimination, and further ammonia addition for the 2,3-amino shift reaction of aminomutases, acting as an electrophile.<sup>2</sup> As showed in Figure 5, the lyase activity is the step in common of these two families of enzymes.

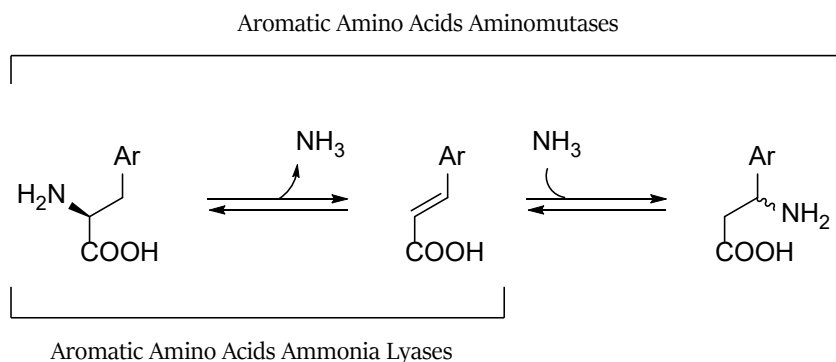


Figure 5. Reaction's plot catalyzed by aromatic amino acid ammonia lyases and aminomutases.

The MIO five-membered heterocycle is a dehydroalanine derivative formed by internal cyclization and elimination of two water molecules of an active site tripeptide, typically Ala-Ser-Gly (Figure 6). The mechanism of formation is post-translational and autocatalytic, where the neighboring protein residues of MIO moiety prevent the formation of stabilizing hydrogen bonds and to enforce the proper alignment of donor and acceptor orbitals for bond creation.<sup>22</sup> Moreover, the MIO group is located on an electropositive platform formed from six  $\alpha$ -helices which are associated with the active site and are oriented with their positive resultant dipoles aligned similarly, increasing the MIO electrophilicity further.<sup>23</sup>

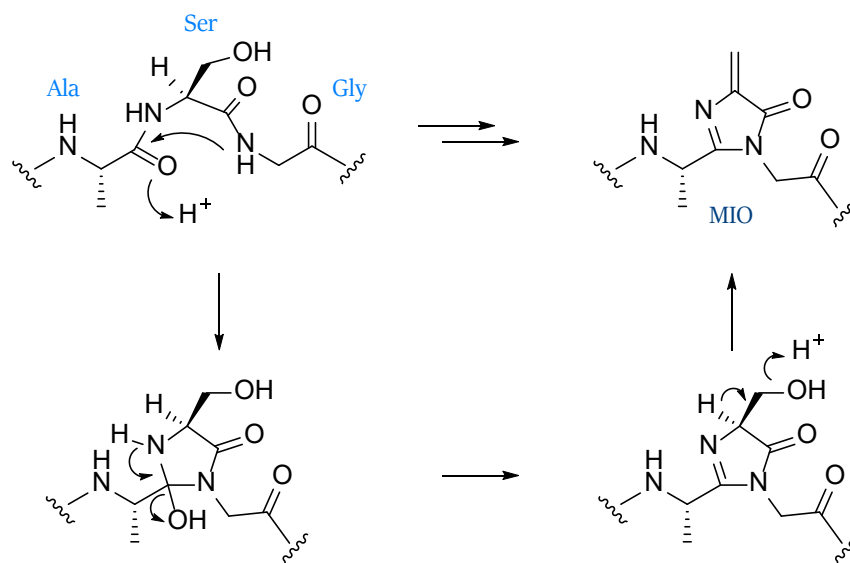


Figure 6. Mechanism of formation of the MIO electrophile by cyclization and double dehydration of the Ala-Ser-Gly motif.<sup>1</sup>

PALs and TALs are homotetramers mainly built of  $\alpha$ -helices of varying lengths. Each subunit assumes a “seahorse” shape interlocking head-to-tail with two other subunits, maximizing adjacent interactions and yielding a close-fitting construction. In addition, a complete active site comprises residues from three separate monomers, even though the MIO group and its anchoring helices are all contained within a single monomer. Thus, the four monomers in the tetrameric structure create four active sites, each consisting of a MIO catalytic moiety placed at the base of a funnel of residues leading from the active site to bulk solvent. These residues are part of the only section of  $\beta$ -sheet that is longer than three protein residues. Furthermore, most of the active-site amino acids are highly conserved or have conservative replacements.<sup>23</sup>

Eukaryotic PALs are approximately 215 residues larger than the prokaryotic PALs. These additional residues are mainly located at the N-terminal and at the C-terminal ends of the protein, with the aim to control substrate entry and product release.

Each active site is covered by two flexible loops: an inner one which is tightly packed and forms interactions with the substrate, and an outer loop which serves as an external cap, forming a barrier to bulk solvent and preventing access to the Ala-Ser-Gly triad. The inner loop contains an essential catalytic tyrosine residue, highly conserved

## 1. INTRODUCTION

among all PALs. The loop moves between a closed conformation, allowing the tyrosine catalysed abstraction of the substrate's  $\beta$ -proton, and an open conformation which permits product release and substrate access.<sup>24</sup>

A significant difference between the structures of lyases and mutases is in the loop regions. The latter enzymes generally have a more rigid catalytic loop than the former ones, to ensure the re-addition of ammonia onto the  $\alpha,\beta$ -unsaturated intermediate before product release. On the contrary, the catalytic loops are highly mobile in lyases.<sup>24</sup>

The mechanism of MIO-dependent ammonia lyases has been discussed for many decades, leading to two main possible pathways, one based on an amine-MIO group intermediate and elimination pathway, and the other on a Friedel-Crafts type reaction. The first reaction mechanism involves the direct interaction between the electrophilic catalytic triad and the deprotonated amino group of the substrate, through a covalent bond, which facilitates the formation of a better leaving group. The pro-S proton from the  $\beta$ -position is abstracted by an enzymatic base to generate a carbanion intermediate, and immediately after the secondary ammonium ion leaves through a E1cB elimination mechanism, in order to yield the product. Lastly, the amine bound to the MIO is protonated by an acidic active site residue, so that ammonia can be eliminated, along with the unsaturated acid release, and the cycle can be completed, with a regenerated active site.<sup>25</sup>

In the Friedel-Crafts type reaction the aromatic ring of the substrate attacks the MIO electrophile to form a covalent ring-MIO intermediate, which renders the  $\beta$ -hydrogens more acidic by generating a positively charged complex. This mechanism leads to the removal of the  $\beta$ -proton by an enzymatic base, followed by the ammonia's elimination and regeneration of the MIO group.<sup>23,25,26</sup>

The amino-MIO mechanism is now generally accepted as the most plausible, largely because of structural data, computational simulations, and evidence of conversion of substrates that are not able to react via a Friedel-Crafts type reaction.<sup>1</sup>

A catalytic tyrosine residue situated on an inner mobile loop lid is involved in the proton abstraction, while a second tyrosine residue interacts with the amine group of the substrate, protonating the amine-MIO complex after the release of the unsaturated acid product.<sup>27</sup> Another key catalytic site is one amino acid residue, in general phenylalanine for PALs, histidine for TALs and serine for HALs, placed near the MIO motif, indicating a role in

## 1. INTRODUCTION

forming favorable interactions with the side-chain group of the substrate. Therefore, it has been demonstrated that this conserved residue acts as a key determinant of the aromatic amino acid ammonia-lyases' substrate specificity. Comparably, its exactly consecutive residue is a highly conserved leucine in PALs and TALs, and histidine in HALs, whose position is still good to interact with the ring of the substrate. The aromatic binding pocket is very hydrophobic and is made up of multiple leucine residues, while the carboxylate binding pocket is made up from a very sensitive network of hydrogen bonding. Besides, the developing enolate on the MIO group interacts with an asparagine's hydrogen.<sup>28</sup>

Several aromatic and cyclic amino acids with or without substitutions of the ring have been demonstrated to be accepted as substrates by the phenylalanine ammonia lyases, both for the deamination and the re-amination reaction. Nevertheless, there is very little knowledge about the reactivity of these enzymes with aliphatic compounds. Indeed, only L-Propargylglycine is known to be used as non-aromatic acyclic substrate, as well as to be deaminated to form (E)-pent-2-en-4-ynoic acid. Phenylalanine ammonia lyase from *Petroselinum Crispum* is the enzyme employed and the kinetic constants' calculation gave a  $K_M$  30-times higher than for L-Phenylalanine, indicating significantly weaker binding of the non-aromatic acyclic substrate than the natural one, and a turnover number ( $K_{cat}$ ) only six-times lower than that for L-Phenylalanine, thus indicating that electronic effects in the elimination step were not significantly different between the two substrates. Kinetic constants values of L-phenylalanine and L-propargylglycine with PcPAL are respectively 0.52 mM and 16.0 mM for the  $K_M$  and 2.28 s<sup>-1</sup> and 0.37 s<sup>-1</sup> for the  $K_{cat}$  (30°C, Tris buffer 0.1 M pH 8.8, 120 µg mL<sup>-1</sup> PcPAL).<sup>29</sup>

### 1.3.2 Phenylalanine ammonia lyase from *Anabaena variabilis* (AvPAL)

The PAL from the cyanobacterium *Anabaena variabilis* is significantly similar in sequence to eukaryotic PAL enzymes, although it is more similar in size (AvPAL has 567 residues) to the smaller prokaryotic HAL enzymes than the larger plant PAL enzymes (PcPAL has 715 residues).<sup>30</sup>

As all the other PALs, this protein exists as homotetramer, weighting 64 kDa per subunit. It possesses a substrate preference for L-phenylalanine, which is converted to *trans*-cinnamic acid at the optimal pH of 8.5. Moreover,



## 1. INTRODUCTION

the formation of *p*-coumaric acid from L-tyrosine has been identified after prolonged incubation, while no detectable activity with L-histidine was found.<sup>30</sup>

AvPAL was introduced in clinical trials of phenylketonuria enzyme replacement therapy since it lacks the protease-sensitive lid loop found in all eukaryotic PALs. Being less sensitive to proteases results in greater *in vivo* stability.<sup>30-33</sup>

Furthermore, the amination reaction was tested and the biotransformation of many cinnamic acid derivatives at high concentration of  $\text{NH}_4^+$  gave high conversion numbers, proving that this bacterial PAL is a potentially attractive biocatalyst for the industrial scale synthesis of high value, non-natural amino acids.<sup>21,34-37</sup> Nevertheless, these experiments were all performed with *E. coli* whole cells harboring the AvPAL biocatalyst, meaning that the reusability of the biocatalyst has not been appropriately considered yet.

### 1.3.3 Phenylalanine ammonia lyase from *Rhodotorula glutinis* (RgPAL)

The PAL from the red yeast *Rhodotorula glutinis* exhibits MIO dependent  $\beta$ -lyase activity.<sup>38</sup> It has a molecular weight of 75 kDa with a sequence of 706 amino acids and exhibits the highest catalytic ability among the reported PALs to convert L-phenylalanine to *t*-cinnamic acid (4.3 U/mg at 50°C, pH 8.0).<sup>39</sup> In addition, RgPAL catalyzes the conversion of L-tyrosine to *p*-coumaric acid. The  $K_m$  value for L-tyrosine was calculated as 0.56 mM, which is half that of L-phenylalanine (1.3 mM), indicating that the RgPAL exhibited higher affinity towards L-tyrosine compared to L-phenylalanine.<sup>39</sup>

RgPAL has been already immobilized on a modified mesoporous silica support (MCM-41) through covalent binding, achieving high recovered activity (95% with a protein loading of 50 mg/g) and stability (80% activity was retained after 30 reuses). The immobilized enzyme was employed for the production of D-phenylalanine (ee>99%) by asymmetric resolution of racemic DL-phenylalanine in a recirculating packed-bed reactor reaching a productivity of 7.2 g L<sup>-1</sup> h<sup>-1</sup> in the scaled-up process.<sup>40</sup>

The company DSM choose this biocatalyst for the ton scale synthesis of (S)-2-indolinecarboxylic acid, which is a key intermediate in the production of angiotensin 1-converting enzyme inhibitors such as Indolapril and

Perindopril. The amino acid intermediate was obtained at 91% yield with 99% *ee* using whole *E. coli* cells containing the recombinant RgPAL protein.<sup>8</sup>

### 1.4 OXIDOREDUCTASES

One class of enzymes that is especially beneficial for industrial applications is the family of oxidoreductases. They are widely used in wastewater treatment, food and textile industry, synthesis of biologically active substances, and other technological processes, successfully replacing the conventional catalytic systems.<sup>41</sup>

Oxidoreductases are a diverse class of enzymes widely distributed among microbial, plant, animal organisms, engaged in modulating the redox homeostasis and cellular signalling cascade.<sup>42,43</sup>

They catalyze oxidative and reductive reactions, which are normally reversible.<sup>44,45</sup> Moreover, they can act on a wide range of both organic substrates including alcohols, amines and ketones and inorganic substrates including small anions such as sulfite, and metals such as mercury.<sup>46</sup> In the enzymatic reactions, the electrons' transfer takes place from one substrate to another. The substrate from where electrons are transferred is termed as an electron donor (reductant) and the substrate to which it is transferred is called an oxidant or an electron acceptor.<sup>43</sup> In particular, NAD(P)H-dependent oxidoreductases oxidize a substrate by transferring a hydride (H<sup>-</sup>) group to a nicotinamide adenine dinucleotide cofactor (either NAD<sup>+</sup> or NADP<sup>+</sup>), resulting in the reduced form NADH or NADPH.<sup>47</sup> This class has the highest average number of steps per reaction, with almost six steps in each reaction. This may indicate that, in general, redox chemistry is relatively difficult to effect.<sup>46</sup>

Oxidoreductases can be classified according to their sequence or three-dimensional structure and they can also be classified according to their signature catalysis and/or coenzyme-dependence.<sup>42</sup> The first classification relies on 22 subclasses, including dehydrogenases (for hydride transfer), oxidases (for electrons transfer to molecular oxygen), peroxidases (for electron transfer to peroxidases), and oxygenases (for oxygen transfer from molecular oxygen to the substrate).<sup>43,48,49</sup>

#### 1.4.1 Formate dehydrogenase from *Candida boidinii* (CbFDH)

Formate dehydrogenase (FDH; EC 1.17.1.9) is an oxidoreductase being involved in the NAD<sup>+</sup>-dependent oxidation of formate anion to carbon dioxide (Figure 7). It is an abundant enzyme that plays an important role in energy

## 1. INTRODUCTION

supply of methylotrophic bacteria and in response to stress in higher plants. In both eukaryotic organisms and microorganisms, the quaternary structure is composed of two chemically identical subunits and the total molecular mass ranges from 70 to 100 kDa. FDH displays relatively low specific activity, a low affinity for formate ion but is highly specific to both formate and  $\text{NAD}^+$ .<sup>50</sup>

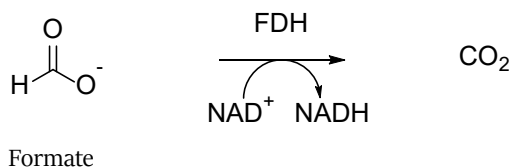


Figure 7. System of reaction of the enzymatic group of formate dehydrogenase.

FDH is widely used as NADH recycling system in enzymatic synthesis with dehydrogenases. As a notable example, the company Degussa (Germany) has developed an industrial scale process for the production of *L-tert-leucine* with FDH as coupled enzyme for cofactor regeneration, and this is one of the largest enzymatic process in medicinal chemistry.<sup>50</sup> The major advantages of the FDH are the following: the reaction is irreversible under normal conditions, shifting the equilibrium to the product formation, the sodium or ammonium formate is a cheap substrate, the  $\text{CO}_2$  is an inert product that can be easily removed from the reaction environment, the pH optimum of catalytic activity is wide, ranging from 6 to 9.<sup>49,51</sup>

The FDH from yeast *Candida boidinii* was firstly purified in 1976.<sup>52</sup> The enzyme exists as homodimer of 42 kDa per subunit.

Cristal structures of this protein are also available and many modifications were attempted over the years for various reasons, like increased stability and catalytic activity.<sup>53-55</sup>

### 1.5 AMINO ACID DEHYDROGENASES

The superfamily of amino acid dehydrogenases are oxidoreductases that catalyze the oxidation of amino acids to 2-ketoacids and the reductive amination of 2-ketoacids in the presence of ammonium salts to amino acids. They also require other molecules, such as cofactors and cosubstrates, for optimal activity.<sup>56</sup>

## 1. INTRODUCTION

Amino acid dehydrogenases are ubiquitous in nature with a central role in amino acid metabolism. They are mostly NADH-dependent and active only toward ketones bearing a carboxylic acid group in the vicinal position, and ammonia is the only reported amine accepted as substrate.<sup>57</sup>

The members of this superfamily show distinct substrate specificities; glutamate dehydrogenase recognizes and binds glutamate in preference to all other amino acids, leucine, alanine and valine dehydrogenase catalyze the oxidation of short, aliphatic amino acids only, and phenylalanine dehydrogenase has a marked preference for aromatic amino acids as substrate, although it will also accept smaller hydrophobic amino acids with reduced efficiency.<sup>58</sup>

The catalytic mechanism of amino acid dehydrogenases has been also well studied. In the case of glutamate and phenylalanine dehydrogenases, the mechanism is very similar. Initially, an Asp residue acts as a general base and abstracts a proton from the  $\alpha$ -amino group of the amino acid. Then, a hydride ion is transferred to NAD(P)<sup>+</sup> from the C $\alpha$ , forming an intermediate  $\alpha$ -imino acid. Finally, the intermediate imino acid is hydrolyzed to the corresponding  $\alpha$ -keto acid and ammonium.<sup>47</sup>

This class of enzymes has received increasing attention in the past years for their use in the preparation of enantiopure amino acids. Indeed, L- $\alpha$ -amino acids are fundamental building blocks in pharmaceutical industry.<sup>59</sup> For example, L-norvaline is a precursor for the synthesis of the antihypertensive drug perindopril, whereas L-*tert*-leucine is an intermediate for the production of the potent HIV inhibitor atazanavir.<sup>60,61</sup> Similarly, the amino acid derivative L-3-fluoroalanine is produced for its antibiotic activity and employed for the synthesis of fluoro amino drugs.<sup>62,63</sup> Then, L-phenylalanine is a starting material for the artificial sweetener aspartame.<sup>64</sup> All these four compounds are shown in Figure 8.

Biocatalysis has demonstrated a higher efficiency compared to the chemical methods to yield enantiomerically pure natural and unnatural  $\alpha$ -amino acids.<sup>59</sup> In this context, amino acids dehydrogenases assume key importance. Furthermore, this class of biocatalysts have been extensively used as cofactor recycling systems to provide NADH or NAD<sup>+</sup> to a coupled enzyme, like the alcohol dehydrogenase. Additionally, they were employed as auxiliary enzymes in combination with  $\omega$ -transaminases to *in situ* regenerate the required amine donors, while shifting the thermodynamic equilibrium towards the target transamination reaction.<sup>65</sup>

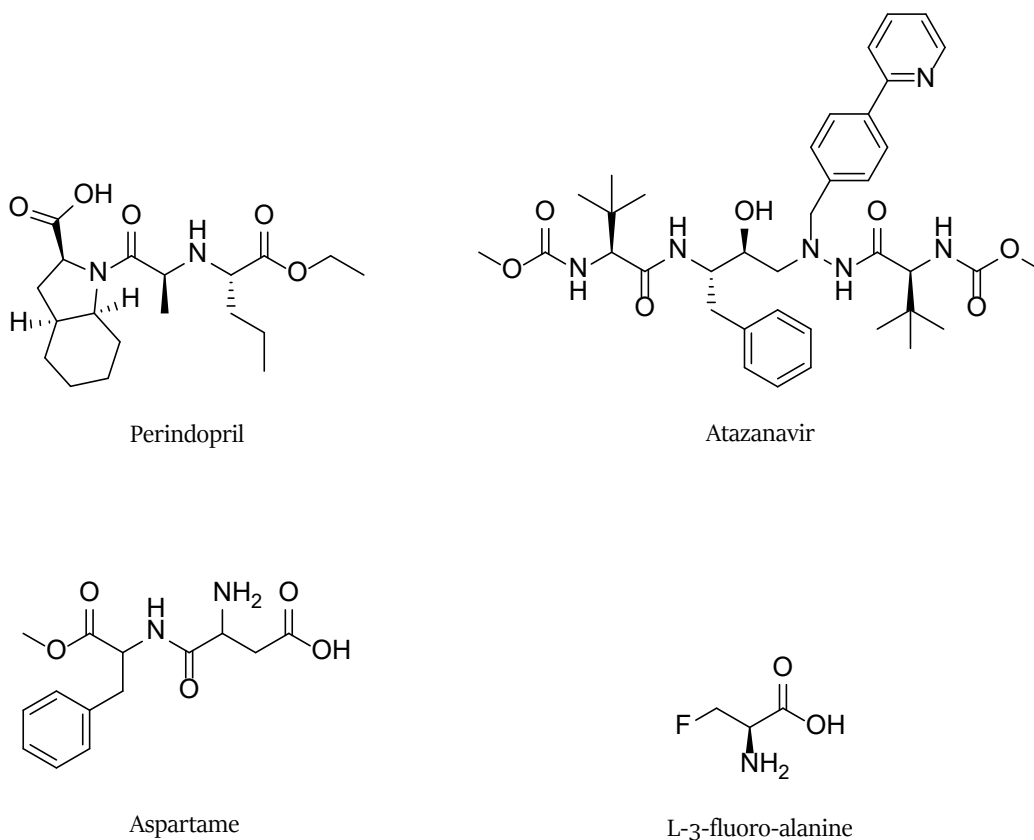


Figure 8. Chemical structure of perindopril, atazanavir, aspartame, L-3-fluoro-alanine.

### 1.5.1 Alanine dehydrogenase from *Halomonas elongata* (HeAlaDH)

Alanine dehydrogenase (AlaDH; EC 1.4.1.1) catalyzes a reversible reaction of biological and technological importance, which has been utilized for various applications of biotechnological, food and pharma industries.<sup>66</sup>

AlaDH is a physiologically important enzyme that acts at the interface of nitrogen and carbon metabolism in microorganisms.<sup>66</sup> It is a special type of amino acid dehydrogenases that has low sequence similarities with other enzymes of the same class, as glutamate and phenylalanine dehydrogenases.<sup>65</sup>

The reaction involves the reversible oxidative deamination of L-alanine to yield pyruvate and ammonia by using the cofactor  $\text{NAD}^+$  (Figure 9).

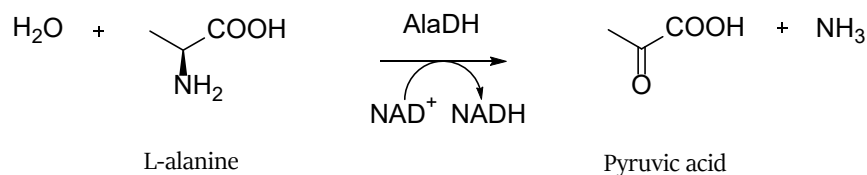


Figure 9. Reaction mechanism of the alanine dehydrogenase.

The halophilic  $\gamma$ -proteobacterium *Halomonas elongata* achieves a broad salt tolerance, in fact it can survive in salt saturated brines (>5 M, 30% NaCl).<sup>67</sup> However, *H. elongata* is a halo adapted bacterium, which allows for heterologous expression of its proteins inside *Escherichia coli*, avoiding less conventional expression systems needed for true halophilic proteins.<sup>68</sup> The alanine dehydrogenase from *H. elongata* has been recently cloned with a N-terminal His-tag as well as characterized, showing very good activity and stability at molar concentrations of sodium chloride. The enzyme is a hexamer, and each subunit has a molecular weight of 42 KDa with 399 amino acids.<sup>69</sup>

### 1.5.2 Glutamate dehydrogenase from *Clostridium symbiosum* (CsGluDH)

Glutamate dehydrogenases (GluDH; EC 1.4.1.2-4) belongs to superfamily of AaDHs and catalyze the oxidative deamination of L-glutamate to give 2-oxoglutarate and ammonia with concomitant reduction of NAD(P)<sup>+</sup> as cofactors (Figure 10).<sup>70</sup> GluDHs are found in nearly every organism and play an important role in nitrogen and carbon metabolism.<sup>71</sup>

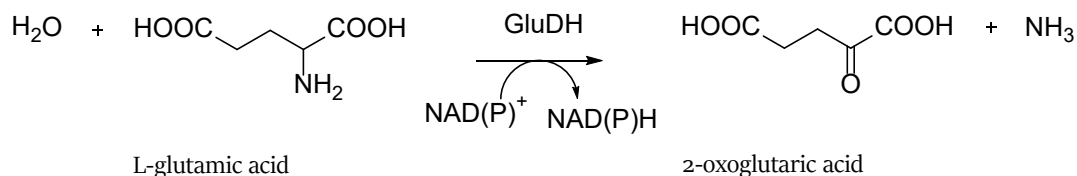


Figure 10. Mechanism of reaction of the enzymatic class of glutamate dehydrogenases.

Bacterial glutamate dehydrogenases are homohexamers that show similar structures, while the eukaryotic enzymes can be hexameric or tetrameric. The hexamer structure is possessed by mammalian enzymes, with a

## 1. INTRODUCTION

subunit molecular weight of approximately 55 kDa. They are structurally similar to their bacterial counterparts except for a nucleotide binding ‘antenna’ near the C-terminus, which is important in the regulation of catalytic activity. Instead, tetrameric enzymes have a subunit molecular weight of approximately 115 kDa.<sup>71</sup>

The GluDH from the anaerobic bacterium *Clostridium symbiosum* is a NAD<sup>+</sup>-dependent enzyme, being involved in the first step of the hydroxyglutarate pathway of glutamate fermentation. This enzyme is homohexameric like the other bacterial GluDHs and each monomer weigh 49 kDa with 450 amino acids.<sup>70</sup> Crystal structures of this protein are also available in different resolution degrees.<sup>58,70-75</sup> The six subunits of CsGluDH are arranged symmetrically as two back-to-back trimers.<sup>76</sup> Then, each subunit is organized into two domains separated by a deep cleft. The first domain, domain I, consists of the N-terminal portion of the polypeptide chain (residues 1 to 200) and residues 423 to the C-terminus. This part of the enzyme is designated for the binding of the substrate. The second smaller domain, domain II, is assembled from the contiguous stretch of residues from 201 to 366 and it is responsible for cofactor binding. In the assembled hexamer, an approximately spherical cavity is present and formed by the C-terminal end.<sup>77</sup>

This enzyme undergoes a slow reversible transition between a high-activity and slow-activity state that is pH, temperature and ionic strength dependent or triggered by the binding of various ligands.<sup>78</sup> Moreover, the enzyme shows normal Michaelis–Menten kinetics at neutral pH, whereas it is highly cooperative, with Hill coefficients of up to 6, at higher pH values.<sup>76</sup>

### 1.5.3 Phenylalanine dehydrogenase from *Bacillus sphaericus* (BsPheDH)

The NAD<sup>+</sup>-dependent L-phenylalanine dehydrogenase (PheDH; EC 1.4.1.20) is an amino acid dehydrogenase that catalyzes the reversible oxidative deamination of L-phenylalanine to phenylpyruvate (Figure 11).

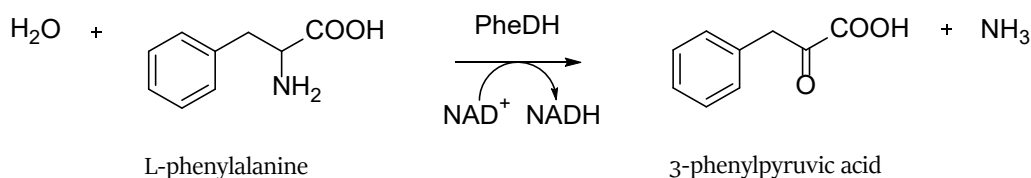


Figure 11. Reaction scheme of the phenylalanine dehydrogenase class.

PheDH is found in a limited number of Gram-positive, aerobic bacteria and shows considerable amino acid sequence homology to leucine dehydrogenases.<sup>79</sup>

The PheDH from *Bacillus sphaericus* was firstly investigated in 1987; it showed similar activity towards L-phenylalanine and L-tyrosine as well as some minor reactivity for aliphatic substrates.<sup>79-81</sup> The overall quaternary structure is octameric, while the weight of the eight singular subunits is 42 KDa with 381 amino acids.

Over the past years, this enzyme has been mutated in several positions in order to achieve different properties compared to the wild-type biocatalyst. For example, the substitution of glycine-124 and leucine-307 for alanine and valine, respectively, displayed enhanced activity for aliphatic amino acids.<sup>79</sup> In addition, the mutation of the asparagine at position 145 for alanine, leucine or valine residues resulted in improved activity towards substituted aromatic derivatives of phenyl pyruvate for creating non-natural amino acids.<sup>82</sup>

### 1.6 HYDROXYPHENYLPYRUVATE REDUCTASES (HPPR)

Rosmarinic acid is an ester of caffeic acid and 3,4-dihydroxyphenyllactic acid and a common secondary plant product in species of the Lamiaceae and Boraginaceae.<sup>83</sup> In the rosmarinic acid biosynthetic pathway, many enzymes are involved, like the already mentioned PAL, and in particular a hydroxyphenylpyruvic acid reductases (HPPR; EC 1.1.1.237) catalyze the NAD(P)H dependent reduction of 4-hydroxyphenylpyruvic acid to the corresponding lactic acid (Figure 12).<sup>84</sup>

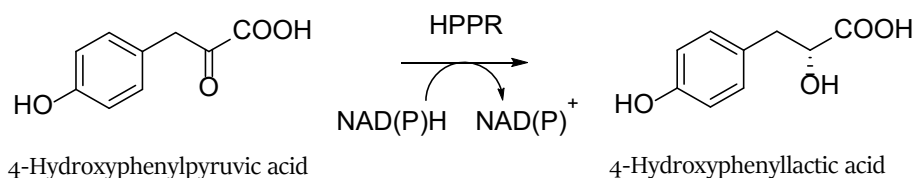


Figure 12. Scheme of reaction catalysed by the HPPR enzymes.

HPPRs are a group of enzymes belonging to the class of oxidoreductases and, more specifically, to the family of D-isomer-specific 2-hydroxyacid dehydrogenases.<sup>85</sup> Only very few HPPRs have been cloned and then isolated by purification yet, as for example the HPPR from *Coleus blumei* (Lamiaceae).<sup>86</sup> The crystal structure of the enzyme



## 1. INTRODUCTION

from *Coleus blumei* (CbHPPR) has been also determined, and confirmed that HPPR is a dimer with a molecular mass of 34113 Da per subunit. The structure was found similar to those of other members of the enzyme family and consisted of two domains separated by a deep catalytic cleft.<sup>85</sup> This enzyme showed activity with either 4-hydroxyphenylpyruvate (HPPA) or 3,4-dihydroxyphenylpyruvate (DHPPA) as substrates but needs a free 4-hydroxyl group in the substrate, consequently reduction of phenylpyruvate resulted very low (less than 2% with respect to DHPPA). Both the cofactors NADH and NADPH can serve as the electron donors.<sup>86</sup> In addition to CbHPPR, two other enzymes of this group have been characterized, which origin from *Salvia miltiorrhiza* (SmHPPR) and from *Arabidopsis thaliana* (HPPR2 and HPPR3).<sup>87,88</sup> The recombinant SmHPPR enzyme exhibited activity with phenylpyruvate (PPA), HPPA and DHPPA using NADPH as co-substrate. HPPR2 revealed both hydroxypyruvate reductase (HPR) and HPPR activities, whereas HPPR3 showed a strong preference for HPPA. In both cases, NADPH was the cofactor showing activity.<sup>88</sup>

### 1.7 BIOCATALYTIC CASCADES

In nature, biosynthetic processes exploits cascades to construct complex natural products from a relatively simple set of starting materials.<sup>89</sup>

Biocatalytic cascades are reaction sequences in which each chemical step is catalysed by an enzyme, where the product of one biocatalytic step becomes the substrate for the next transformation.<sup>7,89</sup>

Biocatalytic cascades typically feature two or more enzyme-catalysed steps (functional group interconversions or bond forming) with at least one enzymatic transformation and without intermediate isolations. Since some intermediates can be unstable to isolation and require efforts for efficient work up, the use of a cascade process can be beneficial to overcome these challenges. From an industrial perspective, biocatalytic cascades are especially attractive as they result in reduced waste, time and costs efficiency as well as more streamlined manufacturing.<sup>7</sup>

The simplest examples of industrial enzyme cascades involve combinations of a biocatalyst with a co-factor recycling enzyme and a co-substrate. Building on simple reactions, several intricate multi-step cascades have been successfully assembled, solving problems aroused by the combination of different biocatalysts. Indeed, setting up the required conditions for one enzyme may disfavour the ability of a second enzyme to work properly in the

## 1. INTRODUCTION

multi-step process. However, protein engineering has become a valuable tool to implement features to enzymes and enable their increasingly efficient optimization in the context of such cascades, where each enzyme operates in the presence of others, under continuously changing conditions as substrate, reaction intermediates, and product concentrations fluctuate over the course of the reaction.<sup>90</sup>

To cite a remarkable example, Merck and Codexis developed a total enzymatic synthesis of the HIV drug islatravir built on three key steps (Figure 13).

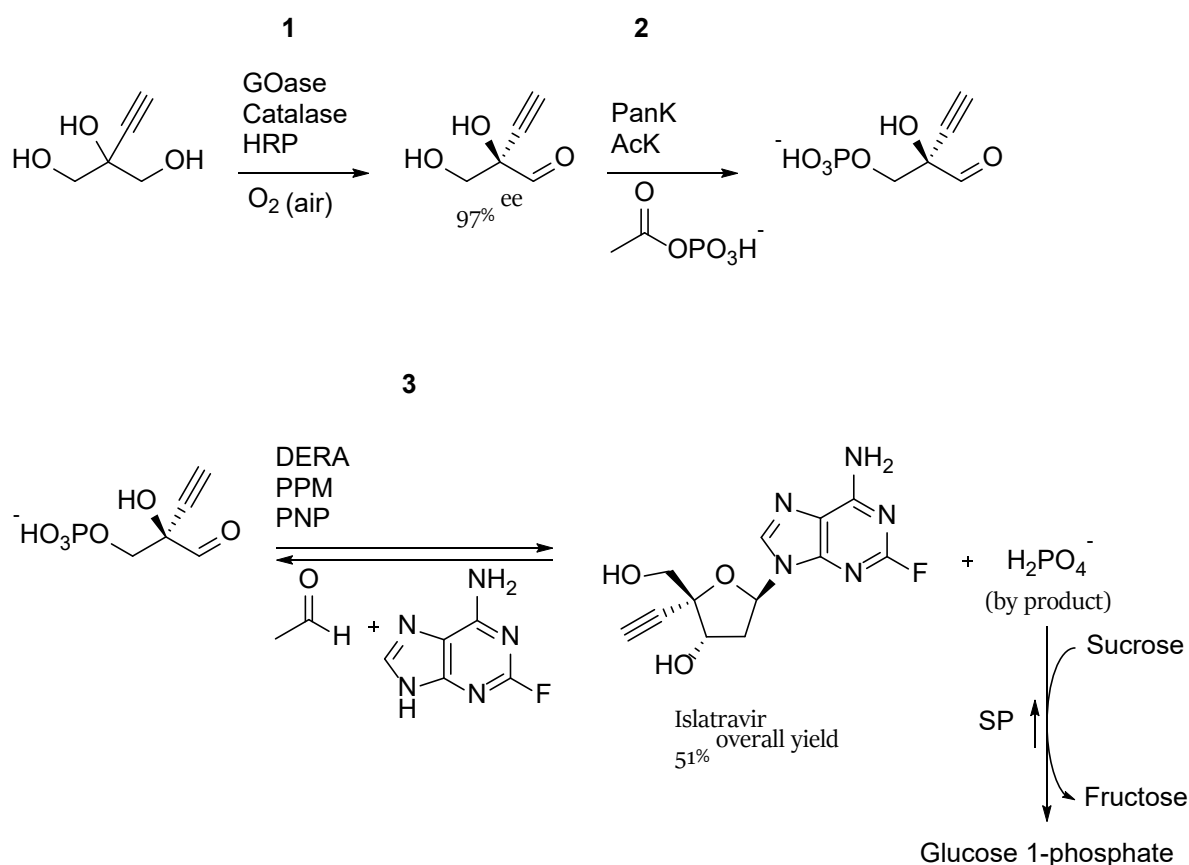


Figure 13. Multistep enzymatic synthesis of islatravir. Evolved enzymes: GOase, galactose oxidase from *Fusarium graminearum*; PanK, pantothenate kinase from *E. coli*; DERA, deoxyribose phosphate aldolase from *Shewanella halifaxensis*; PPM, phosphopentamutase from *E. coli*; PNP, purine nucleoside phosphorylase from *E. coli*. Auxiliary enzymes: HRP, horseradish peroxidase from *Amoracia rusticana*; Catalase from *Bos taurus*; AcK, acetate kinase from *Thermotoga maritima*; SP, sucrose phosphorylase from *Alloscardovia omnicolens*.<sup>91</sup>

## 1. INTRODUCTION

The overall enzymatic cascade required fewer than half the number of steps of the previously reported synthetic routes, which were ranging between 12 and 18 steps.<sup>91</sup>

The full biocatalytic cascade used five engineered biocatalysts and four auxiliary enzymes to stereoselectively assemble islatravir from simple achiral building blocks. Additionally, the nine-enzyme biocatalytic cascade reactions took place at neutral pH, in aqueous solvents, and at room temperature, which saved energy and simplified the operational footprint.<sup>90</sup>

Islatravir could be isolated in greater than 95% purity and in 51% overall yield.<sup>91</sup>

Currently, biocatalysed synthesis has become a priority in the chemical and pharmaceutical industry, owing to the economic pressure and public concern about environmental pollution. The replacement of chemical processes with cleaner, safer, and more eco-friendly biocatalytic processes has strongly demanded.<sup>92,93</sup> In this sense, the development and the application of new enzyme cascades in industry emerge to be crucial to promote a widespread adoption of biocatalysis.

### 1.8 ENZYME IMMOBILIZATION

Enzymes are active mostly at mild, near-ambient conditions of temperature and pH, and preferentially in aqueous media, requirements that became essential goals for industrial processing in order to develop a more sustainable, environmentally friendly, green chemistry.<sup>94</sup>

However, the features underlying the biological origins of enzymes constitutes in most cases a critical limitation for their exploitation as industrial catalysts given the poor stability under operation conditions. Hence, scientists have been encouraged to create new tools for increasing enzyme stability and, among all envisaged strategies, immobilization enables to build up robust and recoverable biocatalysts capable of withstanding the harsh conditions of an industrial process.<sup>95</sup>

Enzyme immobilization consists of the confinement of enzyme molecules onto/within a support/matrix preserving the enzyme catalytic activity by stabilizing the structure of the enzymes. Thus, as compared to free enzymes in solution, immobilized enzymes are more robust and more resistant to environmental changes. In addition, heterogeneous immobilized enzymes systems allow the easy recovery of both enzymes and products,

multiple reuses of enzymes, continuous operation of enzymatic processes, rapid termination of reactions, and greater variety of bioreactor designs. It is a technical process that enables the advantages listed in Figure 14 both in a practical and an economical point of view.<sup>96</sup>

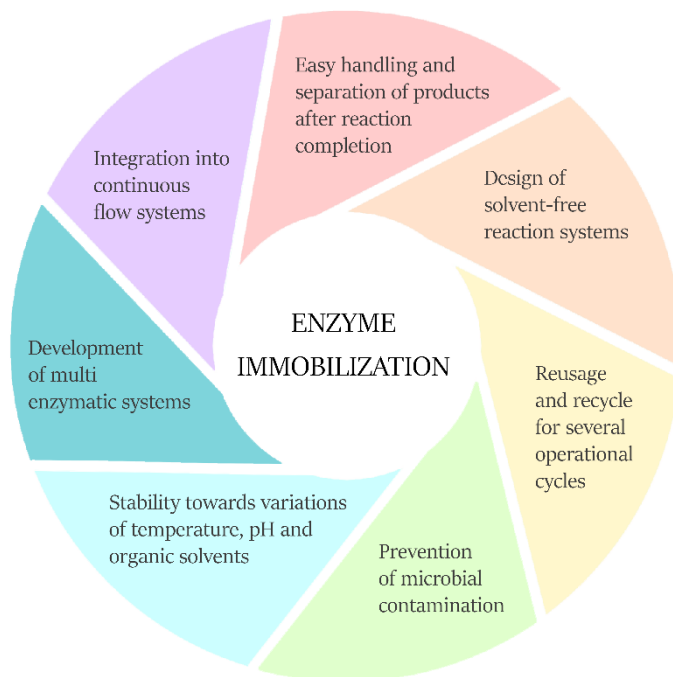


Figure 14. Advantages of enzyme immobilization.<sup>95,96</sup>

Nevertheless, there are also some drawbacks derived from enzyme immobilization, in particular mass transfer issues and loss of activity due to conformational distortions.<sup>96</sup> As a consequence, the science and technology of enzyme immobilization plays a key role in biocatalysis field as it allows and promotes the improvement of techniques and conditions required by the enzyme to be immobilized, in order to minimize side effects. Indeed, over the last few years, an array of techniques has been developed and new materials have been adapted to support biological catalysts.<sup>97</sup>

Enzymes may be immobilized by a variety of methods (Figure 15), which may be broadly classified as physical and chemical, such as reversible and irreversible, depending on the nature, stability and strength of the

interaction. As for the support, it can be a synthetic resin, an inorganic material, a hydrogel, a nanoparticle or a biopolymer.<sup>96,98</sup>

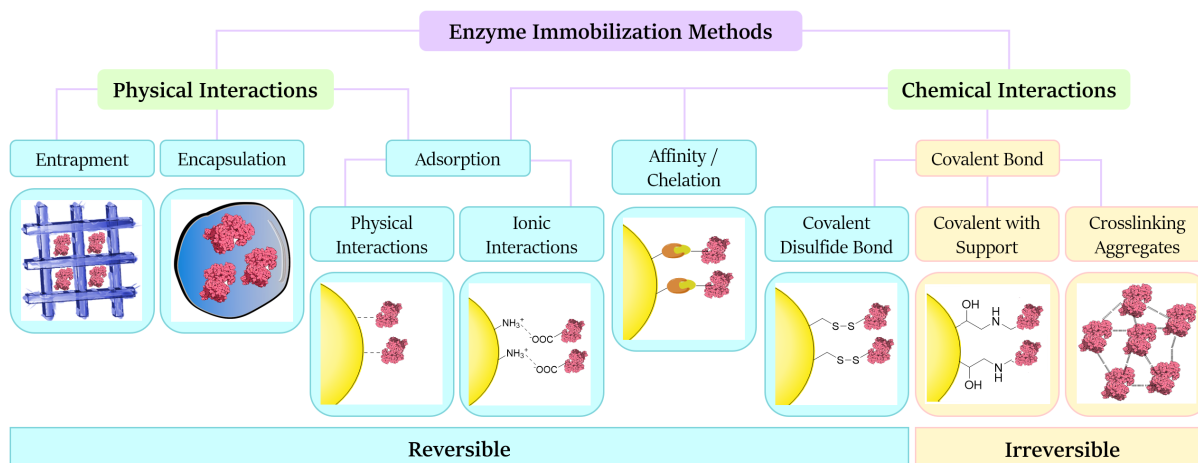


Figure 15. Methods of enzyme immobilization

The physical immobilization is used to identify methodologies in which the enzyme is constrained and physically separated from the medium via entrapment or encapsulation.<sup>99</sup>

In general, physical immobilization strategies aim at retaining the structural integrity of the enzyme without imparting any distortion to the structure, and therefore maximizing catalytic activity. Whether the enzyme is entrapped in a matrix as disordered or polydisperse aggregate, or more orderly encapsulated as oligo- or single unit in a more tailored materials, the challenge is predominately represented by the substrate diffusion from the bulk to the active site of the catalyst and of the product out.<sup>99</sup> Moreover, because it does not require the formation of covalent bonds, the physical immobilization of enzymes is (in theory) reversible.<sup>100</sup>

Chemical immobilization is intended for all processes that require direct interaction between the enzyme and the support.<sup>99</sup> This interaction can be weak (reversible) or stable (irreversible).

As for the first one, adsorption and affinity are the representative techniques involved.

The adsorption of the catalyst to the support may be driven by either physical or ionic interactions.

In physical adsorption the enzymes are linked through hydrogen bonding, van der Waals forces, or hydrophobic interactions, whereas in ionic binding the enzyme molecules are attached through salt bridges. The process

## 1. INTRODUCTION

leading to the formation of non-specific physical adsorption is mild and easy to perform and usually preserve the catalytic activity of the immobilized biocatalyst. However, the reversible nature of the interaction may cause the leaching of the enzyme from the support.<sup>101,102</sup>

On the contrary, ionic exchange interactions represent an excellent, reversible immobilization strategy that can confer a great degree of stability, often comparable with covalently immobilized systems.<sup>101</sup>

The affinity immobilization is based on the genetic modification of the enzyme with a binding element (an affinity protein, a discrete protein domain, or a peptide tag, usually fused on the N- or C- terminal end), which attaches to a matrix displaying the complementary affinity ligand or a transition metal salt. The latter one binds by coordination the enzyme element. The specificity of the affinity interaction promotes the desired orientation of the enzyme.<sup>98,99,103</sup>

The concept of irreversible immobilization means that once the biocatalyst is attached to the support, it cannot be detached without destroying either the biological activity of the enzyme or the support. Irreversibly immobilized enzymes are typically more stable under different extreme conditions, such as temperature or organic solvents, compared with their free, non-immobilized counterparts.<sup>103</sup>

One of the most common procedures of irreversible enzyme immobilization is the covalent coupling, that can greatly improve the operational performance and cost-effectiveness of biocatalytic processes thanks to the stable interaction between the support and the biocatalyst. A wide variety of reactions have been developed depending on the functional groups available on the carrier, which frequently involve the following side chains of the amino acids: lysine ( $\epsilon$ -amino group), cysteine (thiol group), aspartic and glutamic acids (carboxylic group) giving rise to enzymes linked to the support through amide, ether, thioether, or carbamate bonds.<sup>98,103</sup>

Enzymes attached covalently by disulfide bonds to solid supports are instead reversibly immobilized. Indeed, this bond can be broken by reaction with a suitable agent like dithiothreitol (DTT) under mild conditions. Additionally, since the reactivity of the thiol groups can be modulated by changing the pH, the activity yield of the methods involving disulfide bond formation is usually high, provided that an appropriate thiol-reactive adsorbent with high specificity is used.<sup>98</sup>

Immobilization of enzymes that generate insoluble, active catalysts, in the absence of a physical support by simply forming enzyme aggregates (CLEAs) or enzyme crystals (CLECs) via cross-linking of enzyme units, is also included in the irreversible chemical methods.<sup>99</sup>

Many methods, sometimes specific for a given support or enzyme have been developed. However, no single method and support is the best for all enzymes and their various applications. This is because of the widely different chemical characteristics and composition of enzymes, the different properties of substrates and products, and the various uses of the product.<sup>96</sup>

### 1.9 FLOW BIOCATALYSIS

With the growing interest in biocatalysis, a number of complementary technologies have arisen for the development of intensified, more environmentally sustainable and industrially relevant biocatalytic processes. In particular, there is growing interest in performing enzyme-catalyzed transformations in continuous flow, where the concept of “continuous flow” defines a very general range of chemical processes that occur in a continuous flowing stream.<sup>104</sup>

More in details, the continuous flow system begins with a fluid containing starting material, which is pumped through a reactor in a continuous manner to yield a stream of product. A pump (or series of pumps) injects the solution(s) into the reactor.<sup>105</sup>

The biocatalytic vessel may be a packed bed reactor (PBR), a flow coil, a microfluidic device, a membrane or a wall-coated reactor. The packed bed reactors are the most used type of flow reactor by reason of easy-handling and high stability. They consist of a tube filled with particulate biocatalyst (immobilized enzyme or cells) that remains in a fixed position while the reaction medium flows inside the column to form a continuous liquid phase between the particles. The latter ones are suspended and move constantly, consequently the clogging of the bed and the poor distribution of the flow are avoided.<sup>106</sup>

The main components of a continuous flow system for biocatalytic reactions are shown in Figure 16.

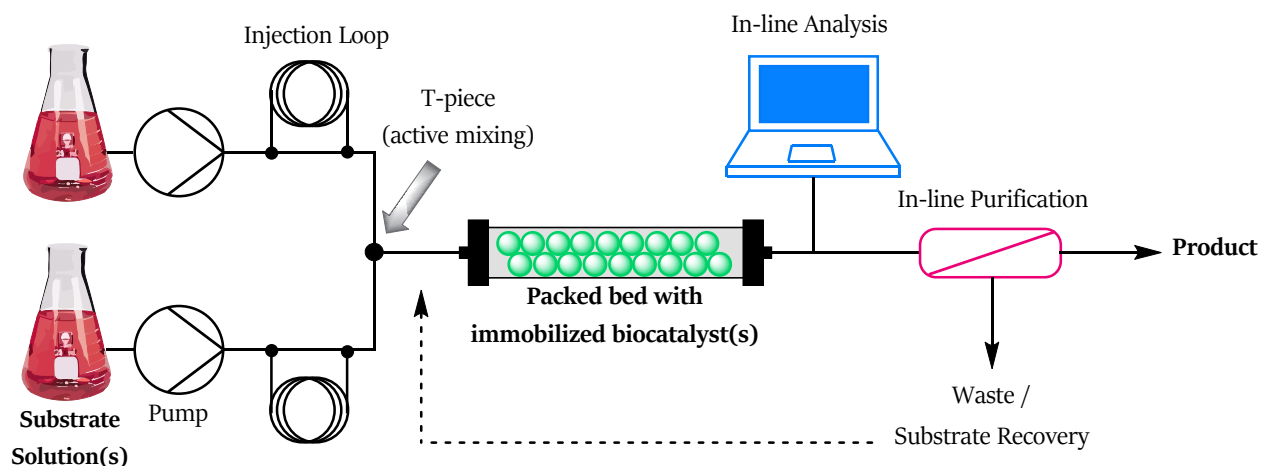


Figure 16. Continuous flow biocatalytic reactor.

Flow biocatalysis may be performed using whole-cells, immobilized enzymes or free enzymes. Immobilized enzymes are mostly chosen for flow biotransformations because the downstream processes are simpler and the reaction is performed faster than using whole cells, for the high specificity of previously purified biocatalyst. Immobilized enzymes are retained and reused unlike free enzymes, and the lifetime is longer owing to the greater stability of immobilized enzymes towards denaturing agents.<sup>105,106</sup>

Flow processing has the potential to accelerate biotransformations due to enhanced mass transfer, with a substantial decrease in reaction time, from hours to a few minutes, and an improvement in space-time yield, with increases of up to 650-fold as compared to batch processes. In addition, the continuous flow reactors permit to control and optimize parameters in real-time, like temperature and flow rate, in order to maximize the efficiency of the biocatalytic reaction and minimize the generation of waste. Biocatalysis combined with flow chemistry has also the advantage to avoid harsh mixing with subsequent increased biocatalyst stability and promote extensive application in cascade reactions. Moreover, many strategies are available with the aim to separate the product from the starting materials, so that the first one is effectively recovered and in-line purified, while the last ones can be recycled for several consecutive biotransformations, leading to a more efficient process. Besides, analytical techniques have been also interfaced with flow reactors to monitor the progress of the reaction in real time and adjust conditions for an improved productivity.<sup>104,106</sup>



Continuous flow biocatalysis is highly developed with well-established guidance on the potential advantages and challenges to implementation.<sup>104</sup> There are many examples of immobilized enzymes application in flow processes for the synthesis of pharmaceutical motifs and high-value molecules. As more enzymes become commercially available, the push towards greener and more cost-effective biotransformation's will increase, and continuous flow biocatalysis will rapidly expand and diversify over the next few years.

### 1.10 BIBLIOGRAPHY

1. Parmeggiani, F., Weise, N. J., Ahmed, S. T. & Turner, N. J. Synthetic and therapeutic applications of ammonia-lyases and aminomutases. *Chem. Rev.* **118**, 73–118 (2018).
2. Csuka, P. *et al.* Pseudomonas fluorescens Strain R124 Encodes Three Different MIO Enzymes. *ChemBioChem* **19**, 411–418 (2018).
3. EPA - Office of pollution prevention and toxics. Green Chemistry Program Fact Sheet. *Green Chem. Progr. Fact Sheet 2* (2002).
4. P. T. Anastas, J. C. W. Green chemistry: theory and practice. *OUP* (1998).
5. Sun, H., Zhang, H., Ang, E. L. & Zhao, H. Biocatalysis for the synthesis of pharmaceuticals and pharmaceutical intermediates. *Bioorganic Med. Chem.* **26**, 1275–1284 (2018).
6. Hughes, D. L. Biocatalysis in Drug Development - Highlights of the Recent Patent Literature. *Org. Process Res. Dev.* **22**, 1063–1080 (2018).
7. Bell, E. L. *et al.* Biocatalysis. **0123456789**, 1–21 (2021).
8. Wu, S., Snajdrova, R., Moore, J. C., Baldenius, K. & Bornscheuer, U. T. Biocatalysis: Enzymatic Synthesis for Industrial Applications. *Angew. Chemie - Int. Ed.* **60**, 88–119 (2021).
9. R. Stürmer, M. Kessler, B. Hauer, T. Friedrich, M. B. & Schröder, H. DE102005062662. 1–19 (2007).
10. Schneider, N. & Höffken, H. W. Biocatalysts For Manufacturing Duloxetine Alcohol. vol. US20110250 (2011).
11. Schöll, A. *et al.* Biocatalytic Asymmetric Synthesis of Chiral Amines from Ketones Applied to Sitagliptin Manufacture. *Science (80-. ).* **329**, 303–305 (2010).

12. Schmid, A. *et al.* Industrial biocatalysis today and tomorrow. *Nature* **409**, 258–268 (2001).
13. Nathan, A. J. & Scobell, A. *How China sees America. Foreign Affairs* vol. 91 (2012).
14. Arnold, F. H. Directed Evolution: Bringing New Chemistry to Life. *Angew. Chemie - Int. Ed.* **57**, 4143–4148 (2018).
15. Federsel, H. J., Moody, T. S. & Taylor, S. J. C. Recent trends in enzyme immobilization—concepts for expanding the biocatalysis toolbox. *Molecules* **26**, (2021).
16. Robinson, P. K. Enzymes: principles and biotechnological applications. *Essays Biochem.* **59**, 1–41 (2015).
17. Kumavath, R. *et al.* Isolation and Characterization of L-Tryptophan Ammonia Lyase from *Rubrivivax benzoatilyticus* Strain JA2. *Curr. Protein Pept. Sci.* **16**, 775–781 (2015).
18. Zhang, X. & Liu, C. J. Multifaceted regulations of gateway enzyme phenylalanine ammonia-lyase in the biosynthesis of phenylpropanoids. *Mol. Plant* **8**, 17–27 (2015).
19. Xiang, L. & Moore, B. S. Inactivation, complementation, and heterologous expression of *encP*, a novel bacterial phenylalanine ammonia-lyase gene. *J. Biol. Chem.* **277**, 32505–32509 (2002).
20. Kyndt, J. A., Meyer, T. E., Cusanovich, M. A. & Van Beeumen, J. J. Characterization of a bacterial tyrosine ammonia lyase, a biosynthetic enzyme for the photoactive yellow protein. *FEBS Lett.* **512**, 240–244 (2002).
21. Weise, N. J. *et al.* Intensified biocatalytic production of enantiomerically pure halophenylalanines from acrylic acids using ammonium carbamate as the ammonia source. *Catal. Sci. Technol.* **6**, 4086–4089 (2016).
22. Sánchez-Murcia, P. A., Bueren-Calabuig, J. A., Camacho-Artacho, M., Cortés-Cabrera, Á. & Gago, F. Stepwise Simulation of 3,5-Dihydro-5-methylidene-4H-imidazol-4-one (MIO) Biogenesis in Histidine Ammonia-lyase. *Biochemistry* **55**, 5854–5864 (2016).
23. Calabrese, J. C., Jordan, D. B., Boodhoo, A., Sariaslani, S. & Vannelli, T. Crystal structure of phenylalanine ammonia lyase: Multiple helix dipoles implicated in catalysis. *Biochemistry* **43**, 11403–11416 (2004).
24. Pilbák, S., Tomin, A., Rétey, J. & Poppe, L. The essential tyrosine-containing loop conformation and the role of the C-terminal multi-helix region in eukaryotic phenylalanine ammonia-lyases. *FEBSJ.* **273**, 1004–

- 1019 (2006).
25. Wang, K., Hou, Q. & Liu, Y. Insight into the mechanism of aminomutase reaction: A case study of phenylalanine aminomutase by computational approach. *J. Mol. Graph. Model.* **46**, 65–73 (2013).
  26. Krug, D. & Müller, R. Discovery of additional members of the tyrosine aminomutase enzyme family and the mutational analysis of CmdF. *ChemBioChem* **10**, 741–750 (2009).
  27. Wang, L. *et al.* Structural and Biochemical Characterization of the Therapeutic *Anabaena variabilis* Phenylalanine Ammonia Lyase. *J. Mol. Biol.* **380**, 623–635 (2008).
  28. Louie, G. V. *et al.* Structural Determinants and Modulation of Substrate Specificity in Phenylalanine-Tyrosine Ammonia-Lyases. *Chem. Biol.* **13**, 1327–1338 (2006).
  29. Weiser, D. *et al.* Phenylalanine Ammonia-Lyase-Catalyzed Deamination of an Acyclic Amino Acid: Enzyme Mechanistic Studies Aided by a Novel Microreactor Filled with Magnetic Nanoparticles. *ChemBioChem* **16**, 2283–2288 (2015).
  30. Moffitt, M. C. *et al.* Discovery of two cyanobacterial phenylalanine ammonia lyases: Kinetic and structural characterization. *Biochemistry* **46**, 1004–1012 (2007).
  31. Kang, T. S. *et al.* Converting an injectable protein therapeutic into an oral form: Phenylalanine ammonia lyase for phenylketonuria. *Mol. Genet. Metab.* **99**, 4–9 (2010).
  32. Jaliani, H. Z., Farajnia, S., Mohammadi, S. A., Barzegar, A. & Talebi, S. Engineering and kinetic stabilization of the therapeutic enzyme *Anabaena variabilis* phenylalanine ammonia lyase. *Appl. Biochem. Biotechnol.* **171**, 1805–1818 (2013).
  33. Jaliani, H. Z. *et al.* Optimized condition for enhanced soluble-expression of recombinant mutant *Anabaena variabilis* phenylalanine ammonia lyase. *Adv. Pharm. Bull.* **4**, 261–266 (2014).
  34. Lovelock, S. L. & Turner, N. J. Bacterial *Anabaena variabilis* phenylalanine ammonia lyase: A biocatalyst with broad substrate specificity. *Bioorganic Med. Chem.* **22**, 5555–5557 (2014).
  35. Lovelock, S. L., Lloyd, R. C. & Turner, N. J. Phenylalanine ammonia lyase catalyzed synthesis of amino acids by an MIO-cofactor independent pathway. *Angew. Chemie - Int. Ed.* **53**, 4652–4656 (2014).
  36. Ahmed, S. T., Parmeggiani, F., Weise, N. J., Flitsch, S. L. & Turner, N. J. Chemoenzymatic Synthesis of

- Optically Pure l- and d-Biarylalanines through Biocatalytic Asymmetric Amination and Palladium-Catalyzed Arylation. *ACS Catal.* **5**, 5410–5413 (2015).
37. Weise, N. J., Parmeggiani, F., Ahmed, S. T. & Turner, N. J. Discovery and Investigation of Mutase-like Activity in a Phenylalanine Ammonia Lyase from *Anabaena variabilis*. *Top. Catal.* **61**, 288–295 (2018).
  38. Chesters, C., Wilding, M., Goodall, M. & Micklefield, J. Thermal bifunctionality of bacterial phenylalanine aminomutase and ammonia lyase enzymes. *Angew. Chemie - Int. Ed.* **51**, 4344–4348 (2012).
  39. Zhu, L. *et al.* Cloning, expression and characterization of phenylalanine ammonia-lyase from *Rhodotorula glutinis*. *Biotechnol. Lett.* **35**, 751–756 (2013).
  40. Zhu, L. *et al.* Efficient preparation of enantiopure D-phenylalanine through asymmetric resolution using immobilized phenylalanine ammonia-lyase from *rhodotorula glutinis* JN-1 in a recirculating packed-bed reactor. *PLoS One* **9**, 1–9 (2014).
  41. Martínez, A. T. *et al.* Oxidoreductases on their way to industrial biotransformations. *Biotechnol. Adv.* **35**, 815–831 (2017).
  42. Xu, F. Applications of oxidoreductases: Recent progress. *Ind. Biotechnol.* **1**, 38–50 (2005).
  43. Sidhu, J. S., Kaur, N. & Singh, N. Trends in small organic fluorescent scaffolds for detection of oxidoreductase. *Biosens. Bioelectron.* **191**, 113441 (2021).
  44. May, S. W. Applications of oxidoreductases. *Curr. Opin. Biotechnol.* **10**, 370–375 (1999).
  45. May, S. W. & Padgette, S. R. Oxidoreductase enzymes in biotechnology: Current status and future potential. *Bio/Technology* **1**, 677–686 (1983).
  46. Holliday, G. L., Mitchell, J. B. O. & Thornton, J. M. Understanding the Functional Roles of Amino Acid Residues in Enzyme Catalysis. *J. Mol. Biol.* **390**, 560–577 (2009).
  47. Sellés Vidal, L., Kelly, C. L., Mordaka, P. M. & Heap, J. T. Review of NAD(P)H-dependent oxidoreductases: Properties, engineering and application. *Biochim. Biophys. Acta - Proteins Proteomics* **1866**, 327–347 (2018).
  48. Bissaro, B., Várnai, A., Røhr, Å. K. & Eijsink, V. G. H. Oxidoreductases and Reactive Oxygen Species in Conversion of Lignocellulosic Biomass. (2018) doi:10.1128/MMBR.00029-18.

49. Elanie Hall, M. & Bommarius, A. S. Enantioenriched Compounds via Enzyme-Catalyzed Redox Reactions. *Chem. Rev* **111**, 4088–4110 (2011).
50. Tishkov, V. I. & Popov, V. O. Catalytic mechanism and application of formate dehydrogenase. *Biochem.* **69**, 1252–1267 (2004).
51. Tishkov, V. I. & Popov, V. O. Protein engineering of formate dehydrogenase. *Biomol. Eng.* **23**, 89–110 (2006).
52. Schütte, H., Flossdorf, J., Sahm, H. & Kula, M. R. *Purification and Properties of Formaldehyde Dehydrogenase and Formate Dehydrogenase from Candida boidinii*. *European Journal of Biochemistry* vol. 62 (1976).
53. Schirwitz, K., Schmidt, A. & Lamzin, V. S. High-resolution structures of formate dehydrogenase from *Candida boidinii*. *Protein Sci.* **16**, 1146–1156 (2007).
54. Guo, Q. *et al.* Structural and Kinetic Studies of Formate Dehydrogenase from *Candida boidinii*. *Biochemistry* **55**, 2760–2771 (2016).
55. Jiang, W., Lin, P., Yang, R. & Fang, B. Identification of catalysis, substrate, and coenzyme binding sites and improvement catalytic efficiency of formate dehydrogenase from *Candida boidinii*. *Appl. Microbiol. Biotechnol.* **100**, 8425–8437 (2016).
56. J. David Rozzell, J. Method for Reductive Amination of a Ketone Using Amutated Enzyme. **2**, (2007).
57. Laurine Ducrot, Megan Bennett, Gideon Grogan, C. V.-V. NAD(P)H-Dependent Enzymes for Reductive Amination: Active Site Description and Carbonyl-Containing Compound Spectrum. *Adv. Synth. Catal.* (2014) doi:10.1002/adsc.201.
58. Baker, P. J. *et al.* Determinants of substrate specificity in the superfamily of amino acid dehydrogenases. *Biochemistry* **36**, 16109–16115 (1997).
59. Velasco-Lozano, S., da Silva, E. S., Llop, J. & López-Gallego, F. Sustainable and Continuous Synthesis of Enantiopure l-Amino Acids by Using a Versatile Immobilised Multienzyme System. *ChemBioChem* **19**, 395–403 (2018).
60. Chapman, N. *et al.* Effects of a Perindopril-Based Blood Pressure-Lowering Regimen on the Risk of

## 1. INTRODUCTION

- Recurrent Stroke According to Stroke Subtype and Medical History: The PROGRESS Trial. *Stroke* **35**, 116–121 (2004).
61. Bold, G. *et al.* New Aza-Dipeptide Analogues as Potent and Orally Absorbed HIV-1 Protease Inhibitors: Candidates for Clinical Development. *J. Med. Chem.* **41**, 3387–3401 (1998).
  62. Kollonitsch, J., Barash, L., Kahan, F. M. & Kropp, H. New antibacterial agent via photofluorination of a bacterial cell wall constituent. *Nature* **243**, 346–347 (1973).
  63. Gonçalves, L. P. B., Antunes, O. A. C., Pinto, G. F. & Oestreicher, E. G. Simultaneous enzymatic synthesis of (S)-3-fluoroalanine and (R)-3-fluorolactic acid. *Tetrahedron: Asymmetry* **11**, 1465–1468 (2000).
  64. Asano, Y. *et al.* Enantioselective Synthesis of (S)-Amino Acids by Phenylalanine Dehydrogenase from *Bacillus sphaericus*: Use of Natural and Recombinant Enzymes. *J. Org. Chem.* **55**, 5567–5571 (1990).
  65. da Silva, E. S., Gómez-Vallejo, V., Llop, J. & López-Gallego, F. Structural, kinetic and operational characterization of an immobilized L-aminoacid dehydrogenase. *Process Biochem.* **57**, 80–86 (2017).
  66. Dave, U. C. & Kadeppagari, R. K. Alanine dehydrogenase and its applications—A review. *Crit. Rev. Biotechnol.* **39**, 648–664 (2019).
  67. Kindzierski, V. *et al.* Osmoregulation in the Halophilic Bacterium *Halomonas elongata*: A Case Study for Integrative Systems Biology. *PLoS One* **12**, 1–22 (2017).
  68. Cerioli, L., Planchestainer, M., Cassidy, J., Tessaro, D. & Paradisi, F. Characterization of a novel amine transaminase from *Halomonas elongata*. *J. Mol. Catal. B Enzym.* **120**, 141–150 (2015).
  69. Padrosa, D. R., Nissar, Z. & Paradisi, F. Efficient amino donor recycling in amination reactions: Development of a new alanine dehydrogenase in continuous flow and dialysis membrane reactors. *Catalysts* **11**, (2021).
  70. Rice, D. W., Hornby, D. P. & Engel, P. C. Crystallization of an NAD<sup>+</sup>-dependent glutamate dehydrogenase from *Clostridium symbiosum*. *J. Mol. Biol.* **181**, 147–149 (1985).
  71. Oliveira, T., Sharkey, M. A., Engel, P. C. & Khan, A. R. Crystal structure of a chimaeric bacterial glutamate dehydrogenase. *Acta Crystallogr. Sect. Struct. Biol. Commun.* **72**, 462–466 (2016).
  72. Rice, D. W., Baker, P. J., Farrants, G. W. & Hornby, D. P. The crystal structure of glutamate dehydrogenase

- from *Clostridium symbiosum* at 0.6 nm resolution. *Biochem. J.* **242**, 789–795 (1987).
73. Stillman, T. J., Baker, P. J., Britton, K. L. & Rice, D. W. Conformational flexibility in glutamate dehydrogenase: Role of water in substrate recognition and catalysis. *Journal of Molecular Biology* vol. 234 1131–1139 (1993).
74. Stillman, T. J. *et al.* Insights into the mechanism of domain closure and substrate specificity of glutamate dehydrogenase from *Clostridium symbiosum*. *J. Mol. Biol.* **285**, 875–885 (1999).
75. Stillman, T. J., Baker, P. J., Britton, K. L., Rice, D. W. & Rodgers, H. F. Effect of additives on the crystallization of glutamate dehydrogenase from *Clostridium symbiosum*. Evidence for a ligand-induced conformational change. *J. Mol. Biol.* **224**, 1181–1184 (1992).
76. Sharkey, M. A. & Engel, P. C. Modular coenzyme specificity: A domain-swapped chimera of glutamate dehydrogenase. *Proteins Struct. Funct. Bioinforma.* **77**, 268–278 (2009).
77. Baker, P. J. *et al.* Subunit assembly and active site location in the structure of glutamate dehydrogenase. *Proteins Struct. Funct. Bioinforma.* **12**, 75–86 (1992).
78. Syed, S. E. H. & Engel, P. C. A pH-dependent activation-inactivation equilibrium in glutamate dehydrogenase of *Clostridium symbiosum*. *Biochem. J.* **271**, 351–355 (1990).
79. Seah, S. Y. K. *et al.* Alteration in relative activities of phenylalanine dehydrogenase towards different substrates by site-directed mutagenesis. *FEBS Lett.* **370**, 93–96 (1995).
80. Asano, Y., Nakazawa, A. & Endo, K. Novel phenylalanine dehydrogenases from *Sporosarcina ureae* and *Bacillus sphaericus*. Purification and characterization. *J. Biol. Chem.* **262**, 10346–10354 (1987).
81. Noriko, O. *et al.* Cloning and nucleotide sequencing of phenylalanine dehydrogenase gene of *Bacillus sphaericus*. *Gene* **63**, 337–341 (1988).
82. Busca, P., Paradisi, F., Moynihan, E., Maguire, A. R. & Engel, P. C. Enantioselective synthesis of non-natural amino acids using phenylalanine dehydrogenases modified by site-directed mutagenesis. *Org. Biomol. Chem.* **2**, 2684–2691 (2004).
83. Petersen, M. & Alfermann, A. W. Two New Enzymes of Rosmarinic Acid Biosynthesis from Cell Cultures of *Coleus blumei*: Hydroxyphenylpyruvate Reductase and Rosmarinic Acid Synthase. 3–6 (1988).

## 1. INTRODUCTION

84. Häusler, E., Petersen, M. & Alfermann, A. W. Hydroxyphenylpyruvate Reductase from Cell Suspension Cultures of *Coleus blumei* Benth. *Zeitschrift fur Naturforsch. - Sect. C J. Biosci.* **46**, 371–376 (1991).
85. Janiak, V., Petersen, M., Zentgraf, M., Klebe, G. & Heine, A. Structure and substrate docking of a hydroxy(phenyl)pyruvate reductase from the higher plant *Coleus blumei* Benth. *Acta Crystallogr. Sect. D Biol. Crystallogr.* **66**, 593–603 (2010).
86. Kim, K. H., Janiak, V. & Petersen, M. Purification, cloning and functional expression of hydroxyphenylpyruvate reductase involved in rosmarinic acid biosynthesis in cell cultures of *Coleus blumei*. *Plant Mol. Biol.* **54**, 311–323 (2004).
87. WANG, G. Q. *et al.* HPPR encodes the hydroxyphenylpyruvate reductase required for the biosynthesis of hydrophilic phenolic acids in *Salvia miltiorrhiza*. *Chin. J. Nat. Med.* **15**, 917–927 (2017).
88. Xu, J. J. *et al.* Characterization of *Arabidopsis thaliana* hydroxyphenylpyruvate reductases in the tyrosine conversion pathway. *Front. Plant Sci.* **9**, 1–13 (2018).
89. Kuska, J. & O'Reilly, E. Engineered biosynthetic pathways and biocatalytic cascades for sustainable synthesis. *Curr. Opin. Chem. Biol.* **58**, 146–154 (2020).
90. Nazor, J., Liu, J. & Huisman, G. Enzyme evolution for industrial biocatalytic cascades. *Curr. Opin. Biotechnol.* **69**, 182–190 (2021).
91. Huffman, M. A. *et al.* Design of an in vitro biocatalytic cascade for the manufacture of islatravir. *Science (80-. ).* **366**, 1255–1259 (2019).
92. Agostini, F. *et al.* Biocatalysis with Unnatural Amino Acids: Enzymology Meets Xenobiology. *Angew. Chemie - Int. Ed.* **56**, 9680–9703 (2017).
93. Choi, J. M., Han, S. S. & Kim, H. S. Industrial applications of enzyme biocatalysis: Current status and future aspects. *Biotechnol. Adv.* **33**, 1443–1454 (2015).
94. Bard Larry R, A. J. . F. Fundamentals and Applications Fundamentals and Applications. *John Wiley Sons, Inc.* **76**, 833 (2004).
95. Wang, H. & Shiyou, L. Immobilization of enzymes and cells. *Chem. Bull. / Huaxue Tongbao* 22–27 (1997) doi:10.1385/0-89603-386-4:319.



## 1. INTRODUCTION

96. Homaei, A. A., Sariri, R., Vianello, F. & Stevanato, R. Enzyme immobilization: An update. *J. Chem. Biol.* **6**, 185–205 (2013).
97. Romero-Fernández, M. & Paradisi, F. Protein immobilization technology for flow biocatalysis. *Curr. Opin. Chem. Biol.* **55**, 1–8 (2020).
98. Brena, B., González-Pombo, P. & Batista-Viera, F. Immobilization of enzymes: A literature survey. *Methods Mol. Biol.* **1051**, 15–31 (2013).
99. Romero-Fernández, M. & Paradisi, F. General overview on immobilization techniques of enzymes for biocatalysis. *Catal. Immobil. Methods Appl.* 409–435 (2019) doi:10.1002/9783527817290.ch12.
100. Zyuzin, M. V., Ramos-Cabrer, P. & Carregal-Romero, S. Encapsulation of Enzymes in Porous Capsules via Particle Templating. in *Methods in Molecular Biology* vol. 2100 227–241 (2020).
101. Nathan, A. J. & Scobell, A. *How China sees America. Foreign Affairs* vol. 91 (2012).
102. Milosavić, N. B., Prodanović, R. M., Veličković, D. & Dimitrijević, A. *Macroporous poly(GMA-co-EGDMA) for enzyme stabilization. Methods in Molecular Biology* vol. 1504 (2017).
103. Petroll, K., Kopp, D., Care, A., Bergquist, P. L. & Sunna, A. Tools and strategies for constructing cell-free enzyme pathways. *Biotechnology Advances* vol. 37 91–108 (2019).
104. Thompson, M. P., Peñafiel, I., Cosgrove, S. C. & Turner, N. J. Biocatalysis Using Immobilized Enzymes in Continuous Flow for the Synthesis of Fine Chemicals. *Organic Process Research and Development* vol. 23 9–18 (2019).
105. Britton, J., Majumdar, S. & Weiss, G. A. Continuous flow biocatalysis. *Chemical Society Reviews* vol. 47 5891–5918 (2018).
106. Tamborini, L., Fernandes, P., Paradisi, F. & Molinari, F. Flow Bioreactors as Complementary Tools for Biocatalytic Process Intensification. *Trends Biotechnol.* **36**, 73–88 (2018).

## 2. AIMS AND OBJECTIVES

---

The current thesis work focuses on the development of diverse systems, which allow for the application of combined biocatalysts on specific reactions. The final purpose of each optimized cascade biotransformation is summarized as follows:

1. The production of high valuable acrylate derivatives, which are extremely important building blocks to generate polymers and various products. Since the current industrial manufacture employs fossil based starting materials, an enzymatic reaction would be promising to obtain these compounds in a sustainable and alternative way. Suitable candidates are MIO-dependent aromatic amino acids ammonia lyases.
2. The determination of high levels of ammonia in solution, which might be essential in many situations, as to analyze bioreactions forming this molecule (usually by-product), to assess the quality of water samples, to monitor the ammonia levels in body fluids. In this regard, ammonia is known to be harmful for aquatic life or humans. An enzymatic tool consisting of a glutamate and a formate dehydrogenase would be of high interest, not only for the ammonia quantification but also for its removal in order to prevent toxicity or to enhance a slow bioreaction by depleting the by-product. Besides, the co-immobilization of the two biocatalysts would provide a reusable and more stable tool.
3. The development of a fusion protein, which genetically combines the two former enzymes in one bifunctional biocatalyst. In this way, the closer location of the active sites would increase the efficiency, while the simplified preparation (expression, purification, immobilization) would impact on the sustainability of the process with reduced costs and time spent for the manipulation of one enzyme instead of two. The comparison between the co-immobilized wild type enzymes and the engineered fusion protein gives the opportunity to choose the most efficient system for the ammonia treatment.
4. The evaluation of the optimized tool offered by the fusion of two proteins, by changing the glutamate dehydrogenase domain. In this context, the effective benefit of the alanine dehydrogenase in combination with the formate dehydrogenase has been already demonstrated as coupled system in the transaminase reaction. Nonetheless, their low stability in reaction conditions translates for the need of further optimization, considering that the immobilization did not provide any improvement. Consequently, the

## 2. AIMS AND OBJECTIVES

creation of a second bifunctional enzyme would allow for testing the versatility of the fusion protein system and at the same time, improving the tool assisting the transaminase.

5. The sustainable production of the active compound danshensu, which owns excellent properties but cannot be exploited in the medical field because of the excessive price. Therefore, the implementation of a biocatalytic cascade reaction for its conversion starting from a low-cost substrate would offer an alternative method for the application in industrial manufacture. This tool involves a phenylalanine ammonia lyase, a phenylalanine dehydrogenase and a novel hydroxy phenyl pyruvate reductase, that is accurately selected and then characterized for the first time.

### 3. MATERIALS AND METHODS

---

#### 3.1 MATERIALS

Q5 High-fidelity DNA polymerase, 5x Q5 reaction buffer, dNTPs, 5x Q5 high GC enhancer, Gibson assembly cloning kit, nuclease-free water, restriction enzymes (*DpnI*, *Bam*HI, *Sac*I, *Eco*RI), CutSmart buffer, unstained protein standard (broad range 10-200 kDa) and 6x gel loading dye purple were purchased from New England Biolabs (NEB). HyperLadder 1 kb was acquired from Bioline. Primers were synthesized by Microsynth.

Nicotinamide adenine dinucleotide >98% (reduced form) disodium salt (NADH), nicotinamide adenine dinucleotide >97% free acid (NAD<sup>+</sup>), Nicotinamide adenine dinucleotide phosphate reduced tetrasodium salt (NADPH) and  $\beta$ -Nicotinamide adenine dinucleotide phosphate sodium salt (NADP<sup>+</sup>) were obtained from Apollo Scientific.

LB broth, LB broth with Agar, imidazole, ampicillin sodium salt, kanamycin sulfate, sodium chloride, sodium hydroxide, tris base, sodium borohydride, SYBR Safe DNA gel stain, agarose, GeneJET Plasmid Miniprep kit, GeneJET Gel Extraction kit, N,N,N',N'-tetramethylethylenediamine, bromophenol blue, magnesium sulphate, potassium iodide, polyethyleneimine 50% aq. (solution branched MN 60,000), acetonitrile, isopropanol, chloroform were bought from Fisher Scientific.

Yeast extract, N-Z-amine, glycerol, D-sorbitol, potassium phosphate dibasic and monobasic, ammonium sulfate,  $\alpha$ -lactose monohydrate, isopropyl  $\beta$ -D-thiogalactoside, glycine, glucose, ethylenediaminetetraacetic acid, calcium chloride, magnesium chloride hexahydrate, nickel (II) chloride hexahydrate, cobalt (II) chloride, copper (II) chloride dihydrate, iron (III) chloride hexahydrate, manganese (II) chloride tetrahydrate, sodium selenite, sodium molybdate, zinc sulfate heptahydrate, L-alanine, sodium pyruvate, L-phenylalanine,  $\alpha$ -ketoglutaric acid, glutamic acid, sodium dodecyl sulfate, 2-mercaptoethanol, acetic anhydride, acrylamide/bis-acrylamide 30% solution, ammonium persulfate, Instant blue, Bradford reagent, sodium periodate, boric acid, sodium tetraborate decahydrate, sodium bicarbonate, 9-Fluorenylmethoxycarbonyl chloride, dithiothreitol, trifluoroacetic acid, iminodiacetic acid, ethylenediamine, picrylsulfonic acid, bovine serum albumin protein standard (2 mg/vial), 4,4,4-trifluorocrotonic acid, 2-amino-4-pentenoic acid, 2,4-pentadienoic acid, t-cinnamic acid, methyl

### 3. MATERIALS AND METHODS

chloroformate, L-dopa, caffeic acid, sodium phenylpyruvate, 3-Aminophenylboronic acid, 4-Mercaptophenyl boronic acid were acquired from Sigma Aldrich.

3-(3,4-dihydroxyphenyl)-2-oxopropanoic acid, (R)-3-(3,4-dihydroxyphenyl)-2-hydroxypropanoic acid, 3-(4-hydroxyphenyl)-2-oxopropanoic acid, 2-Hydroxy-3-(4-hydroxyphenyl)propanoic acid, L-3-phenyllactic Acid, (R)-2-hydroxy-3-phenylpropanoic acid were purchased by BLD pharma.

Enzyme carrier ReliSorb EP400/SS was kindly donated by Resindion S.R.L., while Lifetech ECR8204F, ECR8304F, ECR8285 were gently provided by Purolite Ltd.

Ammonium formate, ammonium chloride and ethanol absolute were acquired from VWR, while hydrochloric acid (37%) and sulfuric acid (96%) from Fluka. Formic acid was bought by Hanseler.

All other reagents were of analytical grade unless otherwise specified.

Plasmids of PALs were supplied by Prof. N. J. Turner (University of Manchester), while plasmid of glutamate dehydrogenase (CsGlutDH-pTac85) was given by Dr. M. A. Sharkey (University of Nottingham). The plasmid of MpHPPR was ordered through GenScript.

#### 3.2 GENERAL METHODS

##### 3.2.1 Culture mediums

LB medium: 25 g/L of pre-mix LB powder dissolved in dH<sub>2</sub>O. Premix powder consists of yeast extract (5 g/L), tryptone (10 g/L) and NaCl (10 g/L).

LB agar plates: 40 g/L of pre-mix LB Agar powder dissolved in dH<sub>2</sub>O. Premix powder consists of yeast extract (5 g/L), tryptone (10 g/L), NaCl (10 g/L) and 15 g/L agar.

ZYP-5052 Autoinduction media: solution consisting of N-Z-Amine (10 g/L), yeast extract (5 g/L), (NH<sub>4</sub>)<sub>2</sub>SO<sub>4</sub> 1M (25 mL/L), KH<sub>2</sub>PO<sub>4</sub> 1M (50 mL/L), K<sub>2</sub>HPO<sub>4</sub> 1M (50 mL/L) was firstly autoclaved. Then MgSO<sub>4</sub> 1M (2 mL/L), 1000x trace elements solution (2 mL/L) and 50x 5052 solution (20 mL/L; made with 250 g/L glycerol, 25 g/L glucose and 100 g/L α-lactose monohydrate in dH<sub>2</sub>O) were added in sterile conditions. Trace elements solution contains FeCl<sub>2</sub> (50 mM), CaCl<sub>2</sub> (20 mM), MnCl<sub>2</sub> (10 mM), ZnSO<sub>4</sub> (10 mM), CoCl<sub>2</sub> (2 mM), CuCl<sub>2</sub> (2 mM), NiCl<sub>2</sub> (2 mM), HCl (60 mM), Na<sub>2</sub>MoO<sub>4</sub> (2 mM), Na<sub>2</sub>SeO<sub>4</sub> (2 mM) and H<sub>3</sub>BO<sub>3</sub> (2 mM).

### 3. MATERIALS AND METHODS

**TB medium:** N-Z amine (12 g), yeast extract (24 g), glycerol (5 g),  $K_2HPO_4$  (2.2 g) and  $KH_2PO_4$  (9.4 g) and distilled  $H_2O$  (1L).

**SOB medium:** N-Z amine (5 g), yeast extract (1.25 g), NaCl (0.25 g), KCl (0.05 g),  $MgCl_2 \cdot 6H_2O$  (0.5 g),  $MgSO_4 \cdot 6H_2O$  (0.6 g) and distilled  $H_2O$  (250 mL).

#### 3.2.2 Chemically competent cells preparation

A single colony of *E. coli* of the desired strain was inoculated into 50 mL of LB media and grown at 37°C and 150 rpm to an  $OD_{600}$  of approximately 0.4. The culture was then placed on ice for 30 minutes and subsequently harvested by centrifugation at 3000 g for 15 minutes at 4°C. The supernatant was discarded, and the cell paste was resuspended in 50 mL of an ice-cold 100 mM magnesium chloride solution. After harvesting by centrifugation at 2000 g for 15 minutes at 4°C and then discarding the supernatant, the pellet was resuspended in 25 mL of an ice-cold solution of 100 mM calcium chloride and incubated on ice for 30 minutes. After centrifuging (2000 g, 15 minutes, 4°C), the pellet was resuspended in 0.5 mL of an ice-cold solution containing 85 mM calcium chloride and 15% (v/v) glycerol. Finally, 40  $\mu$ L were aliquoted in 1.5 mL microcentrifuge tubes and stored at -80°C.

#### 3.2.3 Electro competent cells preparation

A single colony of *E. coli* of the desired strain was inoculated into 50 mL of LB media and grown at 37°C and 150 rpm to an  $OD_{600}$  of approximately 0.4. The cells were chilled on ice for 30 minutes and then harvested by centrifugation at 3000 g for 15 minutes at 4°C. The pellet was then carefully resuspended in ice-cold sterilized water followed by centrifugation (3000g, 15 minutes at 4°C). The wash step was repeated with 25 mL of water and then 15 mL of glycerol 10% (v/v) in water. The pellet was finally resuspended in 0.5 mL of the same solution as the previous step and 50  $\mu$ L were aliquoted in 1.5 mL microcentrifuge tubes and stored at -80°C.

#### 3.2.4 Agarose gel preparation

DNA assay gel electrophoresis was performed using an agarose concentration of 0.8% (w/v). The solution was made by dissolving agarose powder (0.32 g) in 40 mL of TAE buffer by heating it in a standard microwave until the solution was completely clear. When the temperature was low enough without leaving it solidify, 2  $\mu$ L of SYBR safe DNA gel staining were added. The solution was then loaded into the gel cassette with the rack inserted and

### 3. MATERIALS AND METHODS

left to solidify. Samples were prepared appropriately mixing them with the gel loading dye purple (6x), generally 25  $\mu\text{L}$  of sample with 5  $\mu\text{L}$  of dye. The rack was removed, TAE buffer poured into the gel cassette and samples loaded in the wells. The DNA ladder was also added. The electrophoresis was conducted at 75 V and 150 mA for 50 minutes. A UV lamp was then employed to visualize the DNA bands in the gel.

#### 3.2.5 Transformation of competent *E. coli* cells

Transformation of chemically competent cells was performed by adding 0.5-1  $\mu\text{L}$  (100 ng) of the plasmid to a microcentrifuge tube containing 40  $\mu\text{L}$  of the chemically competent cells. The competent cells were left on ice for 30 minutes and after that, the sample was heat-shocked at 42°C for 90 seconds. The sample was then cooled on ice for 5 minutes and 250  $\mu\text{L}$  of either SOB or LB media was added to the tube. The cells were then left to grow for 1h at 37°C (150 rpm). Then, 50-150  $\mu\text{L}$  were spread onto a LB-agar plate containing the appropriate antibiotic, where the cells were grown overnight at 37°C. For the electroporation, 1  $\mu\text{L}$  of plasmid was added to 50  $\mu\text{L}$  of electrocompetent cells and then transferred into an ice-cold electroporation cuvette. Cells were electroporated at 1.8 kV for approximately 5 ms, followed by the addition of 350  $\mu\text{L}$  of SOB media immediately after. Cells were transferred to a 1.5  $\mu\text{L}$  microcentrifuge tube and left to grow for 1 hour at 37°C (150 rpm). Around 150  $\mu\text{L}$  were spread onto a LB-agar plate containing the appropriate antibiotic, where they were grown overnight at 37°C.

#### 3.2.6 Protein overexpression

A volume of 5 mL of LB media supplemented with appropriate antibiotic (100  $\mu\text{g}/\text{mL}$  ampicillin or 50  $\mu\text{g}/\text{mL}$  kanamycin) was firstly inoculated with a single colony taken from the LB-agar plate where competent cells were previously transformed. The starting culture was then incubated overnight (37°C, 250 rpm) and an aliquot was diluted 1:100 in LB or TB media (300 mL), containing suitable antibiotic, to be incubated at 37°C, while shaking (150 rpm) until  $\text{OD}_{600}$  reached approximately 0.6. After that, cells were cold-shocked for 30 minutes, then induced with 0.1-1 mM of IPTG and left to grow overnight at a specific temperature (see Table 1 for details).

Cells were harvested by centrifugation (4500 rpm, 20 minutes, 4°C) and the supernatant was accurately removed. Dry cell pellet was stored at -20°C until needed.

### 3. MATERIALS AND METHODS

When ZYP-5052 autoinduction media was employed, 300 mL of the medium containing the appropriate antibiotic were inoculated with a single colony and grown at 37°C, 150 rpm. After 8 hours, the culture was cold-shocked for 30 minutes and then incubated overnight at a specific temperature (see Table 1 for details).

Cells were harvested by centrifugation at 4500 rpm for 20 minutes at 4°C and dry cell paste was stored at -20°C.

Table 1. Expression conditions for each protein in use.

Enzyme	Plasmid Backbone	Expression Media	Temperature after induction	Antibiotic
AvPAL	pET16b	Autoinduction ZYP	20°C	Ampicillin
RgPTAL	pET16b	Autoinduction ZYP	20°C	Ampicillin
CsGluDH	pTac85	Autoinduction ZYP	30°C	Ampicillin
CsGluDH (His-tagged)	pRSETb	Autoinduction ZYP	30°C	Ampicillin
CbFDH	pET28b	Autoinduction ZYP	25°C	Kanamycin
HeAlaDH	pRSETb	TB + 1 mM IPTG	30°C	Ampicillin
Fusion Protein His <sub>6</sub> -FDH-GluDH	pET28b	LB + 0.1 mM IPTG	20°C	Kanamycin
Fusion Protein His <sub>6</sub> -FDH-AlaDH	pET28b	LB + 0.1 mM IPTG	20°C	Kanamycin
Fusion Protein AlaDH-FDH-His <sub>6</sub>	pET28b	LB + 0.1 μM IPTG	16°C	Kanamycin
BsPheDH	pRSETb	Autoinduction ZYP	25°C	Ampicillin
MpHPPR	pET15b	Autoinduction ZYP	25°C	Ampicillin



**3.2.7 Protein purification**

For cell lysis, frozen cell pellet was thawed on ice and resuspended in loading buffer (see Table 2 for details), around 2 mL per gram of dry cells. The resulting suspension was sonicated to disrupt cells, using 5 seconds pulse on, 10 seconds off for minimum 8 minutes, with 40-60% amplitude. Cell debris was removed by centrifugation (14500 rpm for 45 minutes at 4°C) to yield a cell-free extract which was filtered through a syringe filter with a 0.45 µm pore size.

For purification, the cell lysate containing crude protein was loaded onto a His-trap FF crude Ni-affinity column on the ÄKTA start Protein Purification System running UNICORN start software with Frac30 fraction collector, all from GE Healthcare. The column was firstly equilibrated with loading buffer, then loaded with crude extract, washed with loading buffer (10 column volumes), followed by an isocratic step with 10% elution buffer/ 90% loading buffer (10 column volumes) to remove any non-specific proteins bound onto the column. Recombinant proteins are finally eluted with 100% elution buffer (see Table 2 for details) in 1 mL fractions. Fractions containing purified protein were dialyzed at 4°C with mild stirring, using a cellulose membrane (14 kDa MWCO Sigma Aldrich) inserted in 800 mL of storage buffer. A first dialysis stage was left to run for 1 hour, then the buffer was changed with a fresh one, that was left for a couple of hours, and finally the proteins were dialyzed overnight with a third fresh buffer. The day after, proteins were identified by SDS-PAGE and analyzed to determine the recovered concentration.

Table 2. Purification conditions for each protein in use.

Enzyme	Loading Buffer	Elution Buffer	Storage Buffer
	50 mM potassium	50 mM potassium	
	phosphate buffer pH 8.0,	phosphate buffer pH 8.0,	50 mM borate
AvPAL	300 mM NaCl,	300 mM NaCl,	pH 8.3
	20 mM imidazole	300 mM imidazole	

### 3. MATERIALS AND METHODS

RgPAL	50 mM potassium phosphate pH 7.5,	50 mM potassium phosphate pH 7.5,	50 mM borate
	300 mM NaCl,	300 mM NaCl,	pH 8.5
	30 mM imidazole	300 mM imidazole	
CsGluDH	50 mM potassium phosphate pH 7.5,	50 mM potassium phosphate pH 7.5,	50 mM potassium phosphate pH 7.5
	100 mM NaCl,	100 mM NaCl,	
	30 mM imidazole	300 mM imidazole	
CbFDH	25 mM potassium phosphate pH 7.0,	25 mM potassium phosphate pH 7.0,	25 mM potassium phosphate pH 7.0
	100 mM NaCl,	100 mM NaCl,	
	30 mM imidazole	300 mM imidazole	
HeAlaDH	50 mM potassium phosphate pH 8.0,	50 mM potassium phosphate pH 8.0,	50 mM potassium phosphate pH 8.0
	100 mM NaCl,	100 mM NaCl,	
	30 mM imidazole	300 mM imidazole	
Fusion Proteins	50 mM potassium phosphate pH 7.5,	50 mM potassium phosphate pH 7.5,	50 mM potassium phosphate pH 7.5
	300 mM NaCl,	300 mM NaCl,	
	30 mM imidazole	300 mM imidazole	
BsPheDH	50 mM potassium phosphate pH 7.5,	50 mM potassium phosphate pH 7.5,	10 mM potassium phosphate pH 8.0,
	100 mM NaCl,	100 mM NaCl,	5 mM 2-mercaptoethanol
	30 mM imidazole	300 mM imidazole	

### 3. MATERIALS AND METHODS

	50 mM potassium	50 mM potassium	
MpHPPR	phosphate pH 7.0,	phosphate pH 7.0,	50 mM potassium
	300 mM NaCl,	300 mM NaCl,	phosphate pH 7.0
	30 mM imidazole	300 mM imidazole	

---

#### 3.2.8 Purification of pTac-85 CsGluDH (without His-tag)

Pellet obtained by harvesting cells were resuspended with 100 mM potassium phosphate buffer pH 7.5 and sonicated to disrupt cells. Cell debris was removed by centrifugation and the proteins contained in the cell-free extract were then precipitated with 70% saturation of  $(\text{NH}_4)_2\text{SO}_4$ , by leaving the salt in the solution for 2 hours at 4°C while mildly stirring. Afterwards, the solution was centrifuged for 20 minutes at 4500 rpm, the supernatant discarded, and the precipitate was resuspended with buffer to perform three dialysis at 4°C in 100 mM potassium phosphate buffer pH 7.5.

Specific activity was found by combining 25 mM  $\text{NH}_4\text{Cl}$  as ammonia source, 25 mM  $\alpha$ -ketoglutaric acid and 0.1 mM NADH.

#### 3.2.9 SDS-PAGE preparation and execution

The 12% polyacrylamide resolving gel was prepared and loaded in between two glasses pieces. When the polymerization occurred, the stacking gel was loaded in combination with a rack to shape the wells. In the meantime, samples were diluted with 2x loading dye and heated at 90°C for 10 minutes. After the two layers of gel were polymerized, running buffer was poured into the gel holder, and each gel well was filled with 5-10  $\mu\text{L}$  of sample, included one containing the protein ladder (unstained protein standard, broad range 10-200 kDa). The assay was run at 300 mV, 30 mA in SDS running buffer for around 80 minutes and then the gel was stained with Instant Blue (Expedeon®) or Coomassie blue staining.

#### 3.2.10 Cloning of CsGluDH - pRSETb

The GluDH gene (pTac85-CsGluDH) was cloned into pRSETb vector that contains a poly-histidine tag. The primers listed in Table 3 were designed for the PCR.

### 3. MATERIALS AND METHODS

Table 3. List of primers and their specifications.

Entry	Primer Name	Sequence	Length [bp]	Tm [°C]	GC content [%]	Secondary structure
1	Fwd_HisTag-GluDH	GCATTCGGATCCGATGAGCAAGTATGTTGACAGAG	35	79.4	48.6	Weak
2	Rev_HisTag-GluDH	GACTTCGAATTCTTACCAAGCAATGCCCTGAG	32	75.7	46.9	Very weak

The restriction sites *Bam*HI and *Eco*RI were employed for the cloning. The DNA was amplified by PCR using Q5 High Fidelity DNA Polymerase and following the procedure recommended by the supplier. After the thermocycling step, the sample was loaded to a 0.8% (w/v) electrophoresis agarose gel and the DNA fragment was purified with the GeneJET Gel Extraction kit. The purified PCR product (DNA insert) was digested by *Bam*HI and *Eco*RI restriction enzymes, incubating the reaction mixture at 37°C for 60 minutes. The same was done for the vector. The insert fragments and the backbone of pRSETb were purified as described before and subjected to ligation using T4 Ligase. The reaction was left overnight at 16°C, followed by ethanol precipitation using sodium acetate as salt.

The CsGluDH-pRSETb plasmid was transformed in electrocompetent *E. coli* XL10-GOLD cells. A single colony was grown in 5 mL LB supplemented with ampicillin for an overnight to propagate the plasmid, to be then collected using the GeneJET Plasmid Miniprep kit. The obtained purified plasmid was sent for sequencing to confirm the success of the cloning.

#### 3.2.11 Genetic construction design of fusion proteins

The primers in Table 4 were designed for gene cloning of GluDH–FDH fusion protein.

Table 4. List of primers and their specifications.

Entry	Primer Name	Sequence	Length [bp]	Tm [°C]	GC [%]	Secondary structure
1	Fwd_Linker-GluDH	GGCGGTGGTGGCAGCGCTAGCATGAGCAAGTATGTTGACAG	41	88	59	Moderate
2	Rev_GluDH-pET28b	TGGTGGTGGTGTCTCGAGTTTGTAGCTCTTACCAAGCAATGCCCTGAG	46	88	54	Strong
3	Fwd_GluDH-pET28b	CTCAGGGCATTGCTTGGTAAGAGCTCAAACCTCGAGCACCACCAC	44	86	55	Strong
4	Rev_FDH-Linker	GCTAGCGCTGCCACCACCGCCGATCCTTTTTTATCGTGTTTAC	44	87	55	Moderate

### 3. MATERIALS AND METHODS

The gene of the recombinant GluDH-FDH fusion protein was developed using the pET28b plasmid as backbone. A linker was implemented between the two protein domains and four restriction sites were included in specific positions of the DNA sequence (*EcoRI*, *BamHI*, *NheI*, *SacI*).

The primers in Table 5 were designed for gene cloning and site-directed mutagenesis of AlaDH-FDH fusion proteins. The gene of the two fusion proteins was developed using the pET28b plasmid as backbone and a linker was included between the two domains. The four restriction sites were added as for the previous case.

Table 5. List of primers and their specifications.

Entry	Primer Name	Sequence (5' - 3')	Length [bp]	Tm [°C]	GC [%]	Secondary structure
1	Fwd_Linkers-AlaDH	GTGGTGGCAGCGCTAGCATGAAGATCG	27	78	59	None
2	Rev_AlalDH-pET28b	CGAGTTTGAGCTCTCAGCCGATCAAGC	27	76	56	Weak
3	Fwd_AlalDH-pET28b	CTTGATCGGCTGAGAGCTCAAACCTGAGCACCACCAC	37	84	57	Strong
4	Rev_FDHL-Linker	GCTAGCGCTGCCACCACCGCCGGATCCTTTTTTATCGTGTTTAC	44	87	55	Moderate
5	Fwd_A6242C	CGGTAAACACGATAAAAAATCAGGATCCAAACTCGAGCACC	41	80	44	Weak
6	Rev_A6242C	TACGCTTTCGTCACATATTCGCCATTCAGCAGAATG	36	80	44	Weak
7	Fwd_AlalDH	ATGAAGATCGCCGTGCCGAAGGAAATCAA	29	79	48	Weak
8	Rev_AlalDH-Linker	GCTAGCGCTGCCACCACCACCGGAGCCGATCAAGCTGGCGGCTTC	45	95	69	Very strong
9	Fwd_Linkers-FDH	GGTGGTGGTGGCAGCGCTAGCCATATGGAATTCAAAAGATC	41	84	51	Strong
10	Rev_pET28b-AlalDH	CCTTCGGCACGGCGATCTTCATGCTGCTGCCCATGGTATATC	42	88	57	Strong

For the development of the AlaDH-linker-FDH-(His<sub>6</sub>-tag-C) construct, the vector FDH-pET28b was firstly mutated in a single position (6242 bp) where the stop codon is located. For the purpose, a Q5 site-directed mutagenesis kit (New England Biolabs) was employed following the protocol given by the supplier. The designed primers are listed in Table 5, entry 5 and 6.

#### 3.2.12 DNA amplification: PCR of the insert

As for the cloning of the GluDH-FDH fusion protein, primers 1 and 2 (Table 4) were employed to amplify the insert, which is displayed in Figure 1. The DNA template was the plasmid of the pRSETb-CsGluDH.

### 3. MATERIALS AND METHODS

As for the cloning of His-FDH-AlaDH, primers 1 and 2 (Table 5) were used for insert amplification. Instead, primers 7 and 8 were used for the development of AlaDH-FDH-His. In both cases, the DNA template was the plasmid of the AlaDH in pRSETb.

The reaction components were mixed with the conditions suggested by the supplier of the Q5 Polymerase and then, the thermocycling was run following a TOUCH-UP PCR protocol.

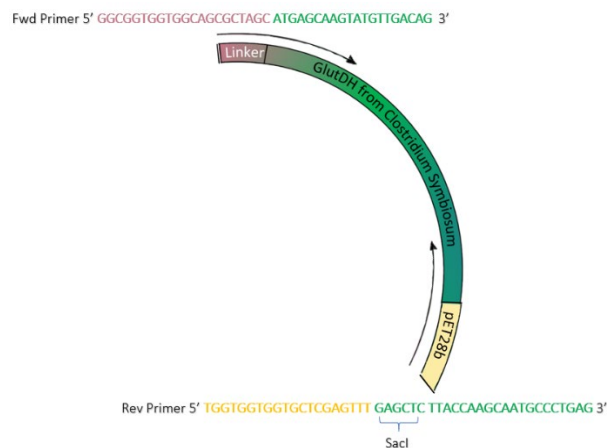


Figure 1. PCR of the insert for the GluDH-FDH fusion protein.

The annealing temperature of the first 10 cycles was programmed as a gradient increase per cycle (1°C ramp), starting from a temperature of 58°C in the first cycle to then reach 68°C in the 10<sup>th</sup> cycle. The annealing temperature of the next 20 cycles was configured as 68°C.

#### 3.2.13 DNA amplification: PCR of the vector

Primers 3 and 4 (Table 4) were added to the reaction mixture to run the PCR of the vector for the cloning of the GluDH-FDH fusion protein (Figure 2). Primers 3 and 4 (Table 5) were added to the reaction mixture to run the PCR of the vector for His-FDH-AlaDH cloning. Similarly, primers 9 and 10 were used for AlaDH-FDH-His development.

The reaction was done with the components suggested by the supplier, where the added DNA template was the plasmid pET28b-CbFDH in all the three cases.

### 3. MATERIALS AND METHODS

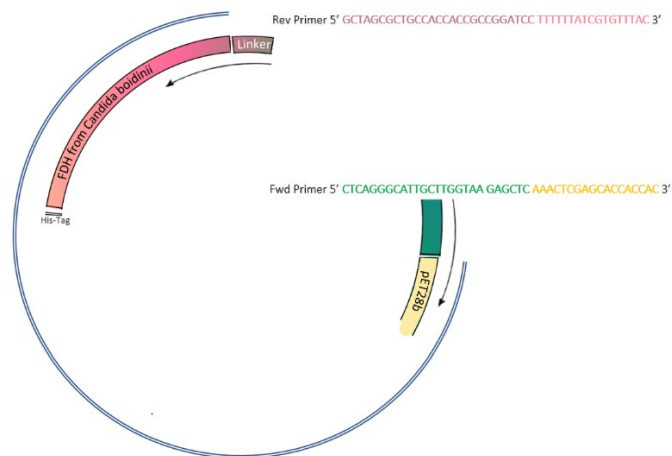


Figure 2. PCR of the vector.

The mixed solution was placed in a thermocycler and a TOUCH DOWN PCR was run. In this case the annealing temperature of the first 10 cycles was gradually decreasing (1°C ramp), while the annealing temperature of the last 20 cycles was configured at 58°C.

#### 3.2.14 Digestion with *DpnI*

The restriction enzyme *DpnI* was added in a volume of 1 µL to the PCR tube containing the 50 µL solution of amplified DNA. A further neutralization step was run by incubating the samples at 80°C for 10 minutes.

#### 3.2.15 Gibson assembly

The insert and the vector were analyzed using absorbance measurements at wavelengths of 260 nm and 280 nm. The  $A_{260}/A_{280}$  ratio provided a rapid indication of nucleic acid concentration in ng/µL. The results were overestimated, because of the presence of interfering components. Therefore, an approximation was done to then calculate the concentration in pmols (calculations were done as described in the manual provided by the supplier). Similarly, the reaction mixture was prepared according to the supplier recommendations for a total volume of 10 µL. The samples were placed in a thermocycler and incubated at 50°C for 60 minutes. The Gibson Assembly enables to incorporate the insert to the vector by combining the overlapping extremities of the DNA fragments in a single-tube isothermal reaction. This method works through three different enzymes (Figure 3):

### 3. MATERIALS AND METHODS

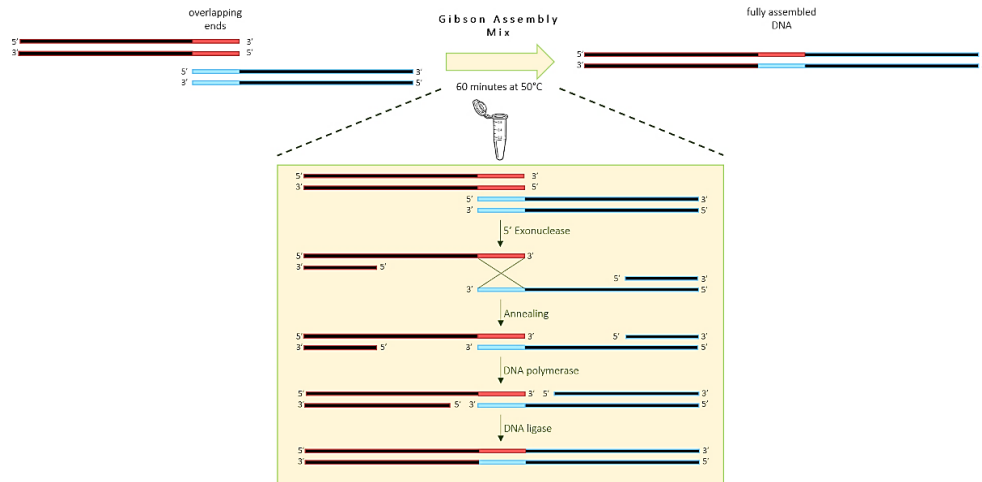


Figure 3. Overview of the Gibson Assembly method.

- The exonuclease, that creates single-stranded 3' overhangs to facilitate the annealing of fragments that share complementarity at one end.
- The polymerase, that fills in gaps within each annealed fragment.
- The DNA ligase, that seals nicks in the assembled DNA.

Both the insert and the vector contained overlapping areas that were going to anneal in the Gibson assembly, as shown in the Figure 4.

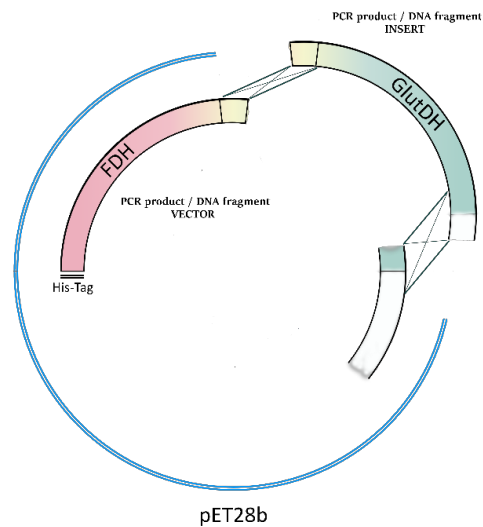


Figure 4. Overlapping areas of insert and vector DNA for GluDH-FDH fusion protein.



### 3. MATERIALS AND METHODS

A previous step of *DpnI* digestion with further heat-inactivation as well as sample refinement with the PCR purification kit were done before the assembly of the HeAlaDH with the vector containing the CbFDH sequence. After completing the Gibson Assembly of His-FDH-AlaDH gene, the assembled product was transformed and the grown colonies were subjected to PCR. The amplification was done using the T7 promoter as forward primer and T7 terminator as reverse primer. All the amplified genes were loaded to an agarose gel for a larger screening and the colony related to the sample showing a 2.5 Kb size was chosen for plasmid propagation, sequencing and further studies.

Regarding the AlaDH-FDH-His, one colony was taken after transformation of the assembled product into *E. coli* DH5 $\alpha$ , which was directly used for plasmid replication, isolation and sequencing.

#### 3.2.16 Optimization of fusion proteins overexpression

A first screening of different growth conditions was performed by pouring 1 mL of an overnight cell culture prepared with a single colony in 5 mL of LB media (kanamycin 50 mg/mL) to 50 mL of LB broth supplemented with kanamycin, using 250 mL Erlenmeyer flasks. The cultures were then incubated at 37°C with 150 rpm shaking. When the OD<sub>600</sub> reached 0.5-0.6, the flasks were cold-shocked and then induced with different concentrations of IPTG (0.1, 0.5 and 1.0 mM final concentrations). These three conditions were tested at 20 and 37°C. Moreover, 1 mL of the starting culture was added to 50 mL of autoinduction media containing kanamycin, thereafter the cells were left to grow at 37°C for 6 hours, cold-shocked and incubated at 20°C.

After the overnight, the grown cultures were harvested by centrifugation. From the cell pellet of each sample, 100 mg were taken and resuspended in 1 mL of buffer. Then, 800  $\mu$ L of the mixture were poured in a microcentrifuge tube and sonicated (6 minutes of 5 seconds on, with 5 seconds off, 30% amplitude). The disrupted cells were centrifuged (14500 rpm for 45 minutes at 4°C) and the supernatant was separated from the insoluble fraction.

The crude extracts were also submitted to two activity assays, one to assess the activity of glutamate dehydrogenase and one to determine the enzymatic activity of formate dehydrogenase. For this purpose, a 96-well plate was filled with 1.5  $\mu$ L of diluted crude extract and 236  $\mu$ L of substrates solution (see next paragraph for conditions).

### 3. MATERIALS AND METHODS

Following tests related to AlaDH-FDH-His expression were done with LB as medium, while the IPTG concentrations were reduced to 0.01 and 0.0001 mM (overexpression at 16°C). In one case, the heat shock was performed at 47°C with 30 minutes incubation of the flasks inside a water bath and in a second case, the LB media was supplemented with 94 g/L of D-sorbitol.

#### 3.2.17 HeWT preparation

The enzyme expression, purification and characterization was done following previously published protocols.<sup>1,2</sup>

#### 3.2.18 Protein quantification

The protein concentration has been determined through the Bradford assay.

The analysis was performed in a 96 well plate, where 5  $\mu\text{L}$  of the sample were mixed to 250  $\mu\text{L}$  of Bradford reagent. After incubating it for 5 minutes at room temperature, the absorbance value was measured at 595 nm. The protein concentration was calculated by creating a calibration curve with assayed samples of bovine serum albumin (BSA) having known concentrations ranging from 0.1 to 1.4 mg/mL. Samples with unknown protein quantity were prepared with different dilution factors in order to choose the results given by values included in the range. For specific proteins, the concentration was determined by measuring its absorbance at 280 nm, using molar extinction coefficients and molecular weights: 24,500  $\text{M}^{-1} \text{cm}^{-1}$  and 42 KDa for HeAlaDH, 51,465  $\text{M}^{-1} \text{cm}^{-1}$  and 43 KDa for CbFDH, 74,260  $\text{M}^{-1} \text{cm}^{-1}$  and 82 KDa for the AlaDH and FDH fusion proteins. For BsPheDH, the following molar extinction coefficient was used:  $11.7 \times 10^{-2} \text{ g}^{-1} \text{ mL cm}^{-1}$ .

#### 3.2.19 Size Exclusion Chromatography (SEC)

The purified fusion protein was applied to a gel filtration column (Superdex 200 10/300 GL, GE Healthcare), which was equilibrated with buffer (50mM Tris/HCl, 150mM NaCl, pH 7.5) and mounted onto an ÄKTA Pure instrument (GE Healthcare). The flow rate was set at 0.5 ml/min. A calibration curve was made by plotting the elution times of the following protein standards: carbonic anhydrase (29 KDa), albumin (66 KDa), alcohol dehydrogenase from yeast (150 KDa),  $\beta$ -amylase from sweet potato (200 KDa), apoferritin from horse spleen (443 KDa), thyroglobulin bovine (669 KDa). Blue dextran (2,000 KDa) was employed to determine the void volume and to check column packing. The elution of the standard proteins and the sample was followed by

absorbance readings at 280 nm. The molecular weight of the fusion protein was calculated through the elution time fitted in the equation obtained from the calibration curve.

#### **3.2.20 Enzyme characterization**

The specific activity was calculated by following the formation or depletion of a substrate or a product at a specific wavelength where only that analyzed compound absorbs. As far as the activity of oxidoreductases, it was assessed by following the production or the consumption of NADH during the catalytic reaction at a wavelength of 340 nm ( $\epsilon_{340}$  6.22 mM<sup>-1</sup> cm<sup>-1</sup>).

One unit is defined as the amount of enzyme which catalyzes the formation or depletion of 1  $\mu$ mol of product, substrate or cofactor per minute.

The specific activity assays were performed with BioTek Epoch 2 Microplate Spectrophotometer in acrylic 96 well-plates. The specific activity was measured in triplicate as change in absorbance per minute, which was then transformed in change of concentration per minute using the Lambert-Beer law and the extinction coefficient of the analyzed compound in those specific conditions. The obtained value (U/mL) was divided by the amount of protein (mg/mL) added in the reaction mixture. Consequently, the specific activity was calculated in U/mg.

The kinetic properties of the enzyme were measured in triplicate on seven or more different concentrations of substrate at same conditions of temperature and pH. The initial rate (mM/min) was calculated from the initial change in OD per minute using the molar absorption coefficient calculated from a standard calibration curve. The kinetic constants were determined by plotting concentration of the substrate versus the relative slope of concentration per minute and then fitting a non-linear regression curve using GraphPad Prism software.<sup>3</sup> The kinetic constants represent the activity per active site.

$K_M$  and  $K_{cat}$  were estimated in the following units: mM and s<sup>-1</sup>.

##### **3.2.20.1 Activity assay of PALs**

Reaction mixture was prepared with 125  $\mu$ L of purified enzyme solution (adequately diluted) and 125  $\mu$ L of 50 mM L-Phenylalanine solution in 100 mM borate buffer pH 8.3 (final concentration: 25 mM) at 30°C.

The activity was measured using the wavelength specific to *t*-cinnamic acid (300 nm, extinction coefficient 3.865 mM<sup>-1</sup> cm<sup>-1</sup>).

### 3. MATERIALS AND METHODS

#### 3.2.20.2 Activity of WT CsGluDH and WT CbFDH

Measurements of specific activity concerning GluDH were done in potassium phosphate buffer 50 mM pH 7 at 25°C using 0.3 mM NADH, 200 mM ammonium chloride, 10 mM  $\alpha$ -ketoglutaric acid disodium salt for the reductive amination, while 1 mM NAD<sup>+</sup> and 40 mM L-glutamic acid monosodium salt for the oxidative deamination. The specific activity of the formate dehydrogenase was found in 25 mM potassium phosphate buffer pH 7.5 at 25°C adding 100 mM sodium formate and 1 mM NAD<sup>+</sup>.

The kinetic parameters were determined by measuring the dependence of initial rate on substrate concentration at 25°C in potassium phosphate buffer 50 mM pH 8. For oxidative deamination reaction, glutamic acid concentration was varied from 0.1 and 20 mM in the presence of 1 mM NAD<sup>+</sup>. For the reverse reaction,  $\alpha$ -ketoglutaric acid concentration was ranging between 0.05 and 20 mM at a fixed concentration of 200 mM ammonium chloride; ammonium chloride was varied from 1 to 200 mM at 10 mM  $\alpha$ -ketoglutaric acid. In both cases, the concentration of NADH was 0.3 mM. The kinetic constants for the formate dehydrogenase were found by using a range between 1 - 100 mM formate concentration at 1 mM NAD<sup>+</sup>. Reactions were made in a 96-well plate by adding the enzyme to the substrate solution (a volume of 2.5  $\mu$ L containing around 5  $\mu$ g/mL of enzyme to 235  $\mu$ L of substrate solution in phosphate buffer) and incubating for 10 minutes to allow the enzyme to adjust to the environment. The measurement started after mixing the cofactor (12.5  $\mu$ L with 20 mM NAD<sup>+</sup> or 6 mM NADH) and following the absorbance at 340 nm with a plate reader.

#### 3.2.20.3 Activity and stability of GluDH – FDH fusion protein

Each protein domain was evaluated singularly (GluDH: 10 mM  $\alpha$ -ketoglutaric acid disodium salt and 200 mM ammonium chloride for reductive amination, 40 mM L-glutamic acid monosodium salt for oxidative deamination, in potassium phosphate buffer 50 mM pH 7.5; FDH: 100 mM sodium formate in potassium phosphate 50 mM pH 7.5). The assay was started by the addition of the cofactor in the reaction environment (0.2 mM of NADH or 1.0 mM of NAD<sup>+</sup> as final concentration).

The kinetic constants were found in triplicate by measuring the dependence of initial rate on substrate concentration at 25°C in potassium phosphate buffer 50 mM (pH 8.0 for GluDH and pH 7.5 for FDH). For oxidative deamination reaction of GluDH, glutamic acid concentration was varied from 0.1 to 100mM in the

### 3. MATERIALS AND METHODS

presence of 1 mM NAD<sup>+</sup>. For the reverse reaction,  $\alpha$ -ketoglutaric acid concentration was ranging between 0.05 and 20 mM at a fixed concentration of 200 mM ammonium chloride; ammonium chloride was varied from 1 to 200 mM at 10 mM  $\alpha$ -ketoglutaric acid. In both cases, the concentration of NADH was 0.35 mM. The kinetic constants for formic acid in the reaction of FDH were found by using a range between 1 and 100 mM formate concentration at 1 mM NAD<sup>+</sup>. The cofactor affinity was also evaluated by changing the concentration of NADH from 0.01 to 0.4 mM (10 mM  $\alpha$ -ketoglutaric acid, 200 mM ammonium chloride) and 0.1–1.0 mM for NAD<sup>+</sup> (40 mM glutamic acid for GluDH and 100 mM formic acid for FDH). Reactions were made by adding an appropriate amount of enzyme to the substrate solution and incubating the mixture for at least 10 min to allow the enzyme to adjust to the environment. The measurement started after mixing the cofactor and following the change in absorbance at 340 nm.

The stability and activity assays at different temperatures and pH were executed in triplicate by incubating the biocatalyst solution at different temperatures (pH 7.5) or at chosen pH values (temperature 25°C) and withdrawing samples at regular times for proceeding with specific activity assays of the fusion protein in parallel with the original GluDH and FDH. The activity of the enzyme was also checked using the previous protocol at several pH and temperature conditions. The reagents were prepared with the chosen pH or incubated at the chosen temperature before proceeding with the activity tests. The results were fitted in a graph showing the trend of the stability/activity of both glutamate and formate DH at chosen temperature or pH values.

#### 3.2.20.4 Activity and stability of AlaDH – FDH fusion protein

Each protein domain was evaluated singularly (AlaDH oxidative deamination: 40 mM L-alanine in 100 mM NaHCO<sub>3</sub> pH 10; 2.5 mM sodium pyruvate and 250 mM ammonium chloride in 100 mM potassium phosphate buffer 50 mM pH 8.0 for reductive amination; FDH: 100 mM sodium formate in potassium phosphate 25 mM pH 7.5). The assay was started by the addition of the cofactor in the reaction environment (0.5 mM of NADH or 1-3 mM of NAD<sup>+</sup> as final concentration).

The kinetic constants were found in triplicate by measuring the dependence of initial rate on substrate concentration at 25°C in the same buffers mentioned before. For oxidative deamination reaction of AlaDH, L-alanine concentration was varied from 0.1 to 60 mM in the presence of 1 mM NAD<sup>+</sup>, while the cofactor

### 3. MATERIALS AND METHODS

concentration ranged from 0.1 to 3.0 mM (40 mM L-alanine). For the reverse reaction, pyruvate concentration was varied from 0.1 and 4 mM at a fixed concentration of 250 mM ammonium chloride; ammonium chloride was ranged between 10 to 500 mM at 2.5 mM sodium pyruvate. In both cases, the concentration of NADH was 0.5 mM. The kinetic constants for formic acid in the reaction of FDH were found by using a range between 2 and 135 mM sodium formate concentration at 3 mM NAD<sup>+</sup>. The cofactor affinity was also evaluated by changing the concentration of NADH from 0.03 to 0.5 mM (2.5 mM pyruvate, 250 mM ammonium chloride) and 0.1–3.0 mM for NAD<sup>+</sup> (40 mM alanine for AlaDH and 100 mM formate for FDH). Reactions were made by adding an appropriate amount of enzyme, diluted in 10  $\mu$ L, and the cofactor solution (10  $\mu$ L) in the 96 well plates. The measurement started after mixing the substrates (180  $\mu$ L) and following the change in absorbance at 340 nm. The stability and activity assays at different temperatures and pH were executed in triplicate by incubating the biocatalyst solution at different temperatures (pH 7.5) or at pH values from 3 to 10 (temperature 4°C) and withdrawing samples at regular times (2, 24, 48 hours) for proceeding with specific activity assays of the fusion protein in parallel with the WT enzymes. The activity was checked using the previous protocols. The results were fitted in a graph showing the trend of the stability of both alanine and formate DH at chosen temperature or pH values.

#### 3.2.20.5 Activity assay of BsPheDH

Reaction mixture was prepared with 10  $\mu$ L of diluted enzyme solution (500-1000-fold), 10  $\mu$ L of NAD<sup>+</sup> (final concentration 2.5 mM) prepared in milliQ water and 380  $\mu$ L of L-Phenylalanine (10 mM as final concentration) in 100 mM KCl and 50 mM Gly-NaOH buffer pH 10.4 at 25°C. The activity was measured following the NADH formation at 340 nm. When L-Dopa was used as substrate, two solutions were prepared: one with L-Dopa and 5 mM  $\beta$ -mercaptoethanol in water, one with the concentrated KCl and Gly-NaOH (final concentrations 100 mM and 50 mM respectively).

#### 3.2.20.6 Activity assay of MpHPPR

Reactions were performed in a 2 mL Eppendorf by adding 10  $\mu$ L of enzyme (diluted as needed), 100  $\mu$ L of NAD(P)H (final concentration 10 mM) in milliQ water and 890  $\mu$ L of substrate (30 mM final concentration) in potassium phosphate buffer pH 7.0 (final concentration 50 mM) and 5 mM  $\beta$ -mercaptoethanol. The reaction

### 3. MATERIALS AND METHODS

mixture was incubated at 37°C, and samples were withdrawn over time to be analyzed by HPLC. The reaction product was identified and quantified through the equation obtained with a calibration curve.

#### **3.2.21 Assembly prediction of GluDH–FDH fusion protein by MD**

In silico analysis have been performed to predict the assembly of the fusion protein, when a short peptide linker of GSGGGGSAS is integrated between the two protein domains. The two 3D structures for GluDH (PDBid: 2YHF) and the formate dehydrogenase (PDBid: 5DNA) were constructed using UCSF Chimera to mimic the hexameric form, known to be the predominant with size exclusion chromatography.<sup>4</sup> After mimicking the assembly, the loop to connect both proteins was modelled using the DaReus server.<sup>5</sup> The final PDB file has been obtained after local minimization with openMM software, which is a toolkit for molecular simulation using high performance GPU code.<sup>6</sup>

#### **3.2.22 Biotransformations in batch**

The enzymatic reactions were performed in a microcentrifuge tube where a 1 mL mixture was added, containing substrate(s), cofactor (if needed) and biocatalyst in a free or immobilized form. The reaction was left in incubation at the preferred temperature for a certain amount of time. Afterward, the reaction was stopped, and samples were taken and analyzed in order to assess the rate conversion of the product(s).

##### 3.2.22.1 Batch Biotransformation of aliphatic substrates with AvPAL

Reaction mixtures were prepared in borate buffer 100 mM pH 8.3 with the following components: 10-30 mM alanine or derivative (allylglycine and 3-trifluomethyl-alanine), 30 mM  $\alpha$ -ketoglutarate, 50 mM formate, 1 mM NADH. For the biotransformation, 40 mg of immobilized AvPAL (5 mg/g) and, if added, 20 mg of immobilized fusion protein (5 mg/g) were employed. The 1 mL reaction was prepared in a 2 mL Eppendorf tube, and then incubated at 37°C, under shaking (150 rpm). The biotransformation was followed by taking samples at different times and analyzing them analytically with the GC-FID.

##### 3.2.22.2 Batch biotransformation using pTac-85 CsGluDH

The biotransformation was performed by using AvPAL (0.5 mg/mL) and CsGluDH (around 0.2 mg/mL) with 10 mM NADH, 10 mM  $\alpha$ -ketoglutaric acid, 10 mM L-phenylalanine in 100 mM borate buffer pH 8.3. Two control

### 3. MATERIALS AND METHODS

biotransformations were run in parallel by using the same substrates and only one of the two enzymes. The reaction mixtures were incubated at 30°C, while shaking, for 96 hours. Samples were taken over time, derivatized with FMOCl and analyzed by HPLC. Another biotransformation was also run in the same conditions, using 0.4 mg/mL of GluDH.

#### 3.2.22.3 Biotransformation using soluble and co-immobilized WT GluDH and WT FDH

After co-immobilizing the two biocatalysts, the biotransformations were carried out in 1 mL reaction volume containing 50 mM  $\alpha$ -ketoglutarate, 200 mM ammonium chloride, 1 mM NADH, 200 mM sodium formate in potassium phosphate buffer 50 mM pH 7.5.

The two biocatalysts were added singularly when the employed form was soluble (final concentration: GluDH 0.1 mg/mL, FDH 0.8 mg/mL) while an amount of 20 mg of resin was inserted in the reaction environment when the enzymes were co-immobilized (GluDH 5 mg/g and FDH 40 mg/g). Both the two biotransformations were started by adding the cofactor, then samples were taken over time to assess the yield of conversion by derivatizing the substrate ( $\alpha$ -ketoglutarate) and the product (glutamic acid) with methyl chloroformate, extracting with chloroform and analyzing through GC-FID.

#### 3.2.22.4 Biotransformations of GluDH-FDH fusion protein

Enough free or immobilized biocatalyst was added to a 2 mL tube containing 1 mL of reaction mixture (50/300/400 mM  $\alpha$ -ketoglutaric acid disodium salt, 200/400/300 mM ammonium chloride, 200/400 mM sodium formate and 1 mM NADH in 50 mM potassium phosphate buffer pH 7.5). A control without enzyme was run in parallel. The mixture was then incubated at 37°C under agitation (150 RPM) and aliquots were taken over time. Samples were analyzed by GC-FID after derivatization of  $\alpha$ -ketoglutarate and glutamate with methyl chloroformate.

#### 3.2.22.5 Batch biotransformations of AlaDH-FDH fusion protein with HeWT

Reactions were performed with appropriate enzymes concentration, and the desired substrates. At different times, a volume of 50  $\mu$ L was quenched with 225  $\mu$ L HCl 0.2% and 225  $\mu$ L of acetonitrile. These samples were then analyzed by HPLC.



Dialysis assisted reactions were done as previously published.<sup>7</sup>

#### 3.2.22.6 Batch biotransformations of RgPAL

The immobilized biocatalyst was weight and added in a 5 mL glass vial. The substrate solution with 5-20 mM caffeic acid, 5 mM  $\beta$ -mercaptoethanol and 0.5-2 M ammonium salt (usually ammonium sulfate) at a chosen pH was added in the glass vial. After appropriately sealing it, a stream of nitrogen was employed to remove all the oxygen present in the liquid/gas environment (with a plastic balloon previously filled with the gas and connected with the inside of the solution through a needle; a second needle was used to flow the oxygen molecules out). The vials were also wrapped with tin foil to avoid any source of light. Samples were then incubated at 37°C with 150 rpm. After 6 or 24 hours, the glass vials were open, samples were taken and quenched with HCl/ACN to be analyzed by HPLC.

#### 3.2.22.7 Batch biotransformations of BsPheDH and/or MpHPPR

Biocatalyst(s) were added in soluble or immobilized form to a 2 mL tube, where L-Dopa or another substrate (final concentration of 10 mM) was added together with 5 mM  $\beta$ -mercaptoethanol and 50 mM Tris HCl buffer pH 8.5. An appropriate amount of cofactor was inserted to start the reaction, which was then incubated at 25°C with 150 rpm.

#### **3.2.23 Samples preparation and analyses**

When the compound under monitoring was absorbing in the UV-vis, a sample of 100  $\mu$ L was withdrawn and the reaction was simply quenched by adding 450  $\mu$ L of HCl 0.2% and 450  $\mu$ L of acetonitrile. The prepared sample was then injected in the HPLC (High-Performance Liquid Chromatography) to determine the rate of conversion. When aliphatic amino acids were analyzed, the biotransformation was followed through derivatization of the amino group with Fmoc-Cl (9-Fluorenylmethoxycarbonyl chloride). Preparation of the samples was done adding 100  $\mu$ L of the reaction mixture to 200  $\mu$ L of borate buffer solution (100 mM pH 9), followed by addition of 400  $\mu$ L of Fmoc-Cl 15 mM in acetonitrile. After vortexing this solution, 200  $\mu$ L were taken and inserted in a vial; 400  $\mu$ L of acetonitrile and 400  $\mu$ L of milliQ water were incorporated to have a final volume of 1 mL inside the vial,

### 3. MATERIALS AND METHODS

that was then run in the HPLC. Standard solutions of each compound were analyzed to create calibration curves for quantification of samples after biotransformation.

The HPLC (UltiMate 3000 UHPLC Thermo Fisher Scientific) was implemented with a C18 column (Waters X-Bridge SPECIFICATIONS). The flow rate was left at 0.8 mL/min and the oven was set at 45°C. The samples were run using a gradient method from 5:95 to 95:5 (milliQ water 0.1% TFA and acetonitrile) over 4 minutes.

Samples preparation for GC-FID analyses required a previous derivatization procedure using methyl chloroformate as reagent, in combination with methanol and pyridine.<sup>8</sup> Derivatized compounds (glutamic acid and  $\alpha$ -ketoglutaric acid) were then extracted with chloroform and loaded to Agilent 8860 GC System with 7693A Automatic Liquid Sampler (temperature of inlet: 250°C, FID detector: 275°C) where the column oven temperature was initially held at 75°C for 1 minute, then increased to 200°C with a ramp of 25°C per minute and a final hold of 4 minutes, using nitrogen as gas carrier with a flow of 6.5 mL/min and CP-Chirasil-Dex CB 25m x 250  $\mu$ m x 0.25  $\mu$ m as GC column.

#### 3.2.24 Enzyme immobilization

The chosen support was left in incubation with the enzyme solubilized in the appropriate buffer. Typically, 1 g of support was added to 1 mL of a solution containing 1 mg of protein and incubated at room temperature under mild agitation. When the loading capacity was increased, 1 g of support was incubated with 1 mL of solution encompassing the desired amount of protein. The protein load is defined as the amount of protein that has been immobilized per gram of carrier (mg/g).

Small amounts of supernatant were taken over time to detect enzymatic activity, that was compared to the activity of the initial enzyme solution that was offered to the carrier (control sample). To better confirm the full immobilization, the protein concentration was then checked by Bradford assay and SDS-PAGE. When the maximum achievable yield was obtained, the support was washed.

The activity assay was performed by adding approximately 10 mg of support to a 2 mL reaction mixture containing substrates and cofactor (if needed) and monitoring it using the same procedure as for the activity assay of the free enzyme. The aim was to determine the expressed activity in U/g (units of enzyme catalyzing the formation of 1  $\mu$ mol of product per minute per gram of support), the specific activity in U/mg (expressed activity

### 3. MATERIALS AND METHODS

divided by the amount of protein loaded to the carrier) and the recovered activity, defined as a percentage calculated from the ratio between the specific activity of the immobilized enzyme and the specific activity of the free enzyme. All the procedures are done at room temperature, if not otherwise stated, under mild agitation. The washing steps are performed with deionized water. All the resins are stored at 4°C after preparation or immobilization. Samples of supernatant, of boiled support (10 mg in 20 µL of water, 10 minutes at 99°C) and samples of control were run in an SDS-PAGE to confirm the immobilization yield and the covalent binding of all the subunits of the enzyme.

#### 3.2.24.1 Activation of epoxy resin to obtain aldehyde groups

For the preparation of the support, 1 g of epoxy resin was mixed with 10 mL of 100 mM H<sub>2</sub>SO<sub>4</sub> and incubated overnight. The support was washed with deionized water, incubated with 10 mL of 30 mM NaIO<sub>4</sub> for 2 hours and washed again.

#### 3.2.24.2 Quantification of aldehyde groups

50 µL of the initial solution of 30 mM NaIO<sub>4</sub> and 50 µL of the final solution of the same after incubation with the support (flow-through) were assayed by adding 500 µL of KI 10% (w/v) in H<sub>2</sub>O and 500 µL of saturated sodium bicarbonate. The absorbance at 405 nm was measured in a 96 well plate and the number of mols of NaIO<sub>4</sub> that have reacted with the diols to form the aldehydes were calculated.

#### 3.2.24.3 Covalent immobilization on glyoxyl groups

The protein solution was prepared in 100 mM NaHCO<sub>3</sub> buffer pH 10. After washing the support with the same buffer, the protein solution was added. After incubation, the support was washed and the Schiff bases were reduced by incubating the support with 10 mg of NaBH<sub>4</sub> in 10 mL of 100 mM NaHCO<sub>3</sub> pH 10 for 30 minutes at 4°C.<sup>9</sup>

#### 3.2.24.4 Covalent immobilization on epoxy groups by first interaction with a metal

Firstly, 1 g of epoxy resin was incubated with 2 mL of modification buffer (100 mM sodium borate, 2 M iminodiacetic acid, 50 mM phosphate buffer pH 8) under gentle agitation for 2 hours. After washing, the modified support was left in incubation with 5 mL of metal buffer (1 M NaCl, 5 mg/mL CoCl<sub>2</sub> in 50 mM phosphate buffer

### 3. MATERIALS AND METHODS

pH 6) for 2 hours. The support was then washed and incubated with the protein solution in phosphate buffer 50 mM pH 8.5. When immobilization occurred, the support was washed with 3 mL of desorption buffer (50 mM EDTA, 500 mM NaCl in 50 mM phosphate buffer pH 7) to remove the metal and rinsed with deionized water. The support was left in 4 mL blocking buffer (3 M glycine in 20 mM phosphate buffer pH 8.5) for an overnight and then washed.<sup>10</sup>

#### 3.2.24.5 Covalent immobilization on epoxy groups by first interaction with ethylenediamine

Firstly, 1 g of the epoxy resin was prepared by adding 6 mL of a solution made with 2% (v/v) ethylenediamine (EDA) in 100 mM NaHCO<sub>3</sub> buffer pH 8.5. The solution was kept in contact with the support for the appropriate length of time in order to achieve the desired number of amino groups. Typically, 2 hours were enough to obtain a good ratio between the two functional groups. The support was then washed with deionized water, 1 M NaCl and again with deionized water. The protein was solubilized in 5 mM phosphate buffer pH 7 and the support was equilibrated with the same buffer before incubating it with the protein solution. When the enzyme was bound, the support was washed with buffer and successively incubated with 1 mL of 5 mM NaHCO<sub>3</sub> buffer pH 10 for at least 2 hours at 4°C. Afterwards, the support was washed, left in 4 mL blocking buffer (prepared as previously described) for an overnight and washed again.<sup>11</sup>

#### 3.2.24.6 Coating of epoxy or glyoxyl resin with polyethyleneimine

A solution of 10 mg/mL of polyethyleneimine was prepared in 100 mM NaHCO<sub>3</sub> buffer pH 10. Then, 10 mL of this solution was mixed to 1 g of support and incubated overnight. After that, the epoxy resin was washed with an excess of deionized water and stored at 4°C, while the glyoxyl resin was both washed and incubated with 1 mg of NaBH<sub>4</sub> in 10 mL of 100 mM NaHCO<sub>3</sub> buffer at pH 10 for 30 minutes under gentle shaking at 4°C. The protein solution was prepared in 5 mM phosphate buffer pH 7, the same buffer that was employed to equilibrate the support before adding the protein. When the immobilization was obtained, the resin was washed.<sup>12,13</sup>

#### 3.2.24.7 Qualitative assay to compare the rate of amino groups functionalization

After the functionalization with ethylenediamine and after the coating with polyethyleneimine, the modified support was qualitatively analyzed to estimate the presence of primary amines available on the surface by

### 3. MATERIALS AND METHODS

comparing the intensity of the color obtained after reacting them with picrylsulfonic acid. For the qualitative assay with picrylsulfonic acid, an adapted version of a previously reported protocol was used.<sup>9</sup> 200  $\mu\text{L}$  of 100 mM  $\text{NaHCO}_3$  buffer pH 10 were added to 20 mg of either the functionalized supports and the non-modified resin (blank). Then, 20  $\mu\text{L}$  of picrylsulfonic acid were inserted and left in incubation for 10 minutes at room temperature under agitation. Every support was filtered, washed 3 times with 500  $\mu\text{L}$  of saturated NaCl and 3 times with 500  $\mu\text{L}$  of 100 mM  $\text{NaHCO}_3$  buffer pH 10.

The intensity of the color increases as the amount of the primary amino groups possessed by the support.

#### 3.2.24.8 Cross-linking with glutaraldehyde

For the cross-linking of enzymes on PEI using glutaraldehyde as agent, an adapted version of a previously reported protocol was used.<sup>14</sup> A solution of 0.5% (v/v) of glutaraldehyde was prepared in 5 mM potassium phosphate buffer at pH 7.0. For 1 gram of resin, 4 mL of the solution were added and left in incubation for 2 hours, while shaking. Then, the resin was washed with an excess of the 5 mM buffer. The resin was left at room temperature for 18 hours to achieve higher degree of cross-linking.

#### **3.2.25 Immobilization and operational stability of WT CsGluDH and WT CbFDH**

Different strategies of immobilization were chosen, using the resins ReliSorb EP400/SS (Resindion S.R.L.) and Lifetech ECR8204F, ECR8304F, ECR8285 (Purolite Ltd.). The resins EP400/SS and ECR8204F were activated to obtain aldehyde groups. A part of them was employed for the covalent immobilization on glyoxyl groups, while the other part was functionalized with PEI, 60 kDa for the respective immobilization. The same epoxy resins were also modified with IDA and cobalt, with EDA or with PEI for the relative immobilizations. The biocatalysts were also immobilized directly to Lifetech ECR8304F and ECR8285 (protein eluted in 5 mM phosphate buffer pH 7).

All the carriers presenting amino groups were qualitatively analyzed using picrylsulfonic acid as reagent.

The immobilization yield and the recovered activity were calculated, by following the same conditions as for the activity assays (oxidative deamination direction for GluDH).

For the co-immobilization, ReliSorb EP400/SS was firstly treated to get glyoxyl groups and after that, it was coated with PEI 60 kDa. The two enzymes were incubated with the carrier both simultaneously and stepwise

### 3. MATERIALS AND METHODS

adding firstly GluDH and then FDH, and vice versa, to compare any difference in recovered activity. Different amounts of enzymes as well as different ratios were loaded.

The operational stability of the immobilized biocatalysts was checked by running sequential biotransformations in the same conditions (20 and 40 mg of resin in 1 mL solution containing 50 mM  $\alpha$ -ketoglutarate, 200 mM ammonium chloride, 1 mM NADH, 200 mM sodium formate in potassium phosphate buffer 50 mM pH 7.5, while the reaction was left in incubation at room temperature for 30 minutes) to then assess the loss of conversion yield over cycles. Samples were collected, derivatized with methyl chloroformate and analyzed by GC-FID. The rates of conversion obtained from the two parallel sets of biotransformations were combined to give an average value of retained activity for each cycle, which was then plotted in a graph.

#### 3.2.26 Immobilization and operational stability of GluDH-FDH fusion protein

The EP400/SS resin was firstly activated with glyoxyl groups and then coated with PEI 60 KDa. Several protein loadings were tested: 1, 5 and 10 mg per Gram of resin.

The immobilized protein was tested in terms of operational stability by performing consecutive biotransformations and checking the decrease of relative rate of conversion for each cycle of reaction. The biotransformations were prepared in 1 ml total volume containing 50 mM  $\alpha$ -ketoglutaric acid disodium salt, 200 mM ammonium chloride, 200 mM sodium formate and 1 mM NADH in potassium phosphate buffer 50 mM pH 7.5, adding 10–40 mg of immobilized biocatalyst. The reaction was left in incubation at 37°C under agitation for 30 min, then the supernatant was taken for sample preparation and subsequent GC-FID analysis.

#### 3.2.27 Continuous flow biotransformation

The flow reactors consisted of a R2S pumping module and a R-4 reactor heater, which were both commercially available from Vapourtec®. The instrument was equipped with a glass heat exchanger assembled with an Omnifit glass column (6.6 mm bore x 150 mm length), properly filled with an appropriate amount of immobilized biocatalyst (fixed bed reactor). Reagents were mixed using a T tube before entrance to the column. The flow rate was varied and optimized for each reaction, depending on length of bed reactor and required residence time ( $\text{length [cm]} \times 0.3421 = \text{total volume [mL]} / \text{residence time [min]} = \text{flow [mL/min]}$ ). The exciting flow stream was collected in different tubes, one for each cycle of reaction (collection time corresponding to residence time).

### 3. MATERIALS AND METHODS

The preparation and the analysis of the collected samples were based on the reacting substances, following the protocols described in paragraph 3.2.23.

#### 3.2.27.1 Continuous flow biotransformation of aliphatic substrates with AvPAL

Reaction mixtures were prepared in borate buffer 100 mM pH 8.3 with the following components: 15, 30 or 60 mM allylglycine or 3-trifluomethyl-alanine, 30 mM  $\alpha$ -ketoglutarate, 50 mM formate, 1 mM NADH. For the packed bed reactor, 1.6 g of immobilized AvPAL (10 mg/g) and 0.4 g of immobilized fusion protein (6 mg/g) were accurately mixed. The 1 mL reaction was prepared in a 2 mL Eppendorf tube, and then incubated at 37°C, under shaking (150 rpm). The reaction was followed by analyzing the samples of each cycle.

#### **3.2.28 Extraction of L-Dopa with phenyl boronic acid (PBA)**

The two derivatives of PBA were 3-Aminophenylboronic acid and 4-Mercaptophenylboronic acid.

##### 3.2.28.1 Liquid-liquid extraction (LLE)

A solution of 20 mM 4-Mercapto-PBA in water (with appropriate pH adjustment) and a second one of 10 mM L-Dopa in 2 M ammonium sulfate pH 8.5 were prepared. Equal volumes ( 500  $\mu$ L) of the two solutions were mixed in a 2 mL tube. Then, 1 mL of organic solvent was carefully added to the 1 mL aqueous solution. After mixing and centrifuging, the two phases were separated. The solvent phase was supplemented with 1 mL of acidic aqueous solution. After mixing and centrifuging, the water phase was collected. Samples were taken in all the LLE steps for TLC analysis (ALUGRAM® Xtra SIL G/UV – 0.2 mm silica gel 60 with fluorescent indicator) with ethyl acetate as mobile phase. TLC sheets were analyzed by UV lamp (PBA) and ninhydrin solution (L-Dopa).

##### 3.2.28.2 Solid-phase extraction (SPE)

The methacrylate resin EP400/SS was functionalized with the PBA derivatives. As for the 3-aminophenylboronic acid, the resin was previously activated to aldehydes and then 40 mM of the compound were incubated in presence of 100 mM NaHCO<sub>3</sub> buffer pH 10 (1 mL of solution for 100 mg of resin). After 3 hours incubation at 25°C while shaking, the resin was washed and incubated with NaBH<sub>4</sub> in 100 mM NaHCO<sub>3</sub> pH 10 (1 mg/mL) for 30 minutes. As for the 4-mercaptophenylboronic acid, a 40 mM solution in 100 mM NaHCO<sub>3</sub> buffer pH 10.0 was

### 3. MATERIALS AND METHODS

incubated with the epoxy resin (1 mL /100 mg resin) for 2 hours. The functionalized resins were washed with an excess of water.

For the extraction, 100 mg of the two resins were loaded separately in a 1 mL column. Firstly, they were equilibrated with an alkaline solution to obtain the reactive boronate form  $RB(OH)^3$ . Then, the 20 mM L-Dopa / 2 M ammonium sulfate solution pH 8.5 was loaded to the column. After removing the flowthrough, the resin was washed from the contaminants maintaining an alkaline pH. Finally, the resin retaining the catechol was eluted with an acidic solution and/or 50 mM Tris HCl buffer. Each sample was analyzed by HPLC to calculate the specific amounts of L-Dopa that was effectively loaded or washed away.

#### 3.3 BIBLIOGRAPHY

1. Cerioli, L., Planchestainer, M., Cassidy, J., Tessaro, D. & Paradisi, F. Characterization of a novel amine transaminase from *Halomonas elongata*. *J. Mol. Catal. B Enzym.* **120**, 141–150 (2015).
2. Padrosa, D. R., Nissar, Z. & Paradisi, F. Efficient amino donor recycling in amination reactions: Development of a new alanine dehydrogenase in continuous flow and dialysis membrane reactors. *Catalysts* **11**, 1–10 (2021).
3. GraphPad Software Inc. GraphPad Prism, version 7.02 for Windows, La Jolla California USA. (2017).
4. Pettersen, E. F. *et al.* UCSF Chimera - A visualization system for exploratory research and analysis. *J. Comput. Chem.* **25**, 1605–1612 (2004).
5. Karami, Y. *et al.* DaReUS-Loop: a web server to model multiple loops in homology models. *Nucleic Acids Res.* **47**, W423–W428 (2019).
6. Eastman, P. *et al.* OpenMM 7: Rapid development of high performance algorithms for molecular dynamics. *PLoS Comput. Biol.* **13**, (2017).
7. Padrosa, D. R., Nissar, Z. & Paradisi, F. Efficient amino donor recycling in amination reactions: Development of a new alanine dehydrogenase in continuous flow and dialysis membrane reactors. *Catalysts* **11**, (2021).
8. Walsh, R. G., He, S. & Yarnes, C. T. Compound-specific  $\delta^{13}C$  and  $\delta^{15}N$  analysis of amino acids: A rapid, chloroformate-based method for ecological studies. *Rapid Commun. Mass Spectrom.* **28**, 96–108 (2014).



### 3. MATERIALS AND METHODS

9. Guisán, J. M. Aldehyde-agarose gels as activated supports for immobilization-stabilization of enzymes. *Enzyme Microb. Technol.* **10**, 375–382 (1988).
10. Mateo, C., Palomo, J. M., Fernandez-Lorente, G., Guisan, J. M. & Fernandez-Lafuente, R. Improvement of enzyme activity, stability and selectivity via immobilization techniques. *Enzyme Microb. Technol.* **40**, 1451–1463 (2007).
11. Trobo-Maseda, L., Orrego, A. H., Romero-Fernández, M., Guisan, J. M. & Rocha-Martín, J. Immobilization of Enzymes on Hetero-Functional Supports: Physical Adsorption Plus Additional Covalent Immobilization. *Methods Mol. Biol.* **2100**, 159–174 (2020).
12. Mateo, C., Abian, O., Fernandez-Lafuente, R. & Guisan, J. M. Reversible enzyme immobilization via a very strong and nondistorting ionic adsorption on support-polyethylenimine composites. *Biotechnol. Bioeng.* **68**, 98–105 (2000).
13. Velasco-Lozano, S., Benítez-Mateos, A. I. & López-Gallego, F. Co-immobilized Phosphorylated Cofactors and Enzymes as Self-Sufficient Heterogeneous Biocatalysts for Chemical Processes. *Angew. Chemie - Int. Ed.* **56**, 771–775 (2017).
14. López-Gallego, F., Guisan, J. M. & Betancor, L. *Immobilization of Enzymes on Supports Activated with Glutaraldehyde: A Very Simple Immobilization Protocol.* *Methods in Molecular Biology* vol. 2100 (2020).

## CHAPTER 4.

# SUSTAINABLE PRODUCTION OF ALIPHATIC ACRYLIC ACID DERIVATIVES USING PHENYLALANINE AMMONIA LYASES

---



## 4.1 INTRODUCTION

Acrylic acid (IUPAC: propenoic acid) is one of the main chemicals synthetically prepared in industry. Indeed, the global annual production is around 6 million tons with a growing demand of 4-5% per year.<sup>1,2</sup>

This molecule and its derivatives are extremely important building blocks to produce polymers as well as for the manufacture of various products, such as plastics, textiles, leather, paper, coatings, elastomers, adhesives, sealants, detergents, flocculants, polishes, paints, and super absorbent products.<sup>3,4</sup>

The current industrial production of acrylic acid involves gas-phase catalytic oxidation of fossil-based 1-propene via acrolein as intermediate.<sup>1,4</sup> Nevertheless, there is a growing demand for an alternative process to obtain acrylic acid in an efficient and sustainable way, for the purpose of reducing the contribution to global warming caused by the greenhouse effect, lowering the worldwide environmental pollution, and preserving the already limited, and expensive, fossil resources. Bio-based acrylic acid, that is the material produced from renewable carbon resources, holds a great importance as precursor to obtain highly valuable intermediates and many bio-based polymers.

However, most of the alternative chemical production routes were abandoned as they were found to be economically unattractive, use non-environmental friendly catalysts or have low acrylate yields.<sup>3,4</sup> Direct biochemical routes are also taken into consideration, but the obtained concentrations of acrylic acid are low. Thus, no one has developed to date a full biotechnological process to produce acrylic acid or its esters that would give sufficiently high yields to enable a viable industrial application.<sup>1</sup>

The manufacture of acrylic acid might be realized by the action of an ammonia lyase capable of using  $\alpha$ -alanine as substrate. Nonetheless, a natural alanine ammonia lyase has not yet been found. Consequently, it would be extremely interesting to employ naturally occurring ammonia lyases to develop a biocatalyst which can effectively react with alanine, as an alternative and sustainable strategy to produce highly valuable compounds.

Suitable candidates are MIO-dependent aromatic amino acids ammonia lyases, which catalyse the non-oxidative deamination of phenylalanine, tyrosine and/or histidine to form unsaturated acids. Phenylalanine ammonia lyase from *Anabaena variabilis* has been selected for this purpose. So far, L-propargylglycine is the only aliphatic

molecule known to be accommodated as substrate by PALs. Indeed, L-propargylglycine could be reversibly transformed by PcPAL into (E)-pent-2-ene-4-ynoate.<sup>5</sup>

Consequently, more information about the behaviour of these enzymes on non-aromatic and acyclic compounds is required to then open up new opportunities on the biocatalytic production of aliphatic acrylates.

## 4.2 RESULTS AND DISCUSSION

### 4.2.1 Protein expression, purification and activity

The expression of AvPAL led to an average of 15 grams of cell pellet per liter of culture. After purification, a protein yield of around 10-15 mg/L was obtained. The final concentration was quite low, but still sufficient to work with for further analysis. The dialyzed fraction was also checked on SDS-PAGE, which confirmed the purity of the protein solution as well as the molecular weight (64 KDa). The specific activity of AvPAL was calculated as  $0.6 \pm 0.1$  U/mg at 30°C with L-Phenylalanine as substrate, in 50 mM borate buffer pH 8.3.

### 4.2.2 Protein immobilization

First tests of biotransformation of both L-phenylalanine and aliphatic substrates with AvPAL showed a visible enzyme precipitation due to loss of stability in reaction conditions. Consequently, it has been decided to perform immobilization studies with the aim of increasing the stability and the reusability of the biocatalyst.

The enzyme was firstly immobilized on EP400/SS functionalized with epoxides, IDA and cobalt (Figure 1, left).

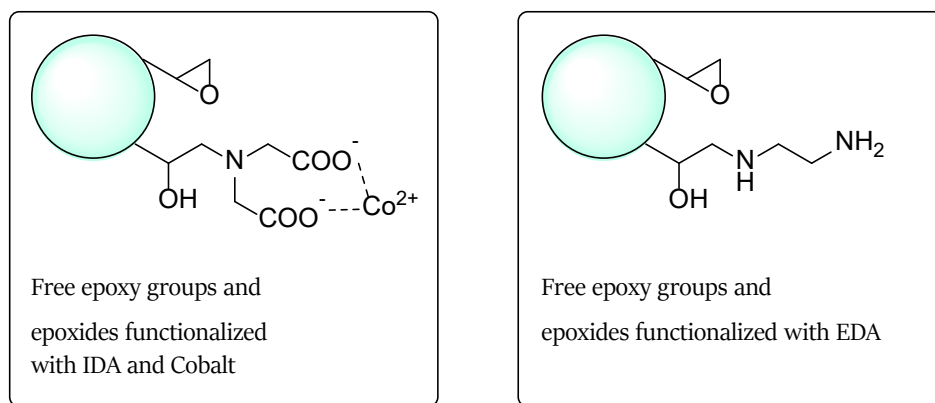


Figure 1. Heterofunctionalization of a support with the related chemistries.

However, no activity was recovered. Consequently, the enzyme stability was investigated by incubating some aliquots of AvPAL with the different reagents used during the immobilization process.

The protein was found to lose all the activity after 1 hour of incubation with 1 mM CoCl<sub>2</sub>, NiCl<sub>2</sub> and CuSO<sub>4</sub>. Due to the loss of stability with metals, the enzyme was then immobilized through a different strategy, using methacrylate resin functionalized with EDA (Figure 1, on the right).

The heterofunctionalization of the support provided two different functional groups available for the protein immobilization. The external primary amines of EDA interacted through a weak bond with one of the available side chain carboxyl groups of the enzyme (glutamate/aspartate residues) to drive its attachment on the support (mild physical absorption). Successively, the epoxy groups form covalent bonds with side chain amino groups of enzyme's lysine residues available on the surface.

In this contest, the crystal structures of AvPAL (PDBid: 3CZO and 5LTM) were analyzed in Pymol, which exhibited good amounts and well-distributed lysine and aspartate/glutamate residues.<sup>6</sup> The Figure 2 shows the tetrameric crystal structure of AvPAL, where lysine residues are colored in blue, glutamic acid residues are shown in red, while aspartic acid residues are in pink.

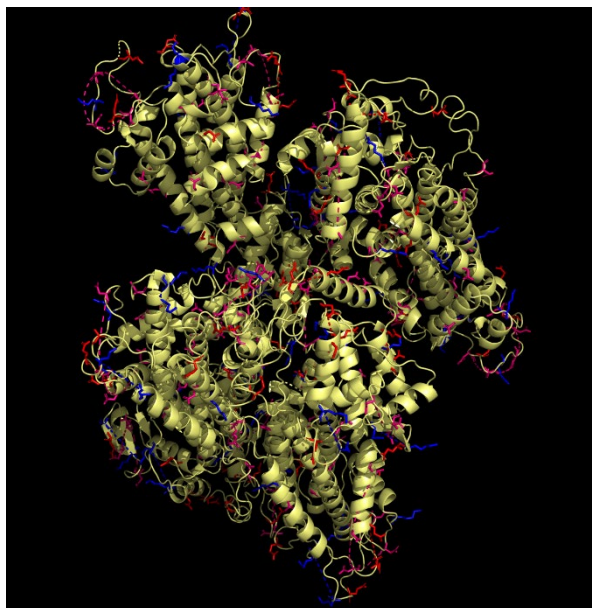


Figure 2. Crystal structure of AvPAL with Lys, Glu, Asp residues shown as licorice sticks. Visualization with Pymol.<sup>6</sup>

This image confirms the availability of the three side-chain amino acids on the surface of the quaternary structure and their regular distribution. For each carboxyl group (Asp/Glu) interacting ionically with the primary amines on the support, there would be a lysine residue forming a covalent bond with epoxides. As a result, a balanced distribution of amino ed epoxy groups on the resin is also essential.

The resin was incubated with a solution of EDA to create a covalent bond between superficial epoxides and one amine group of the molecule, while the other one being available for the enzyme interaction. Consequently, the epoxy methacrylate supports were incubated with EDA for different time frames to achieve several rates of heterofunctionalization. In this way, different ratios of epoxy and amino groups were available on the surface of the resin. After that, the resin was qualitatively assayed with picrylsulfonic acid, which reacted with the available primary amines to yield a colored product. The intensity of the color increased as the amount of the amino groups. The support not being functionalized with EDA acted as the blank color. Figure 3 shows assayed EP400/SS resin after its incubation with EDA from 2 to 24 hours. The increase of incubation time corresponded to an intensification of the color, confirming that the functionalization with amino groups was progressively developed over time.



Figure 3. EP400/SS incubated with EDA for 2, 4, 6 and 24 hours.

Results of immobilization are shown in table 1. AvPAL was immobilized onto the heterofunctionalized EP400/SS resin (loading capacity 1 mg/g) achieving 100% immobilization yield. Nevertheless, the support functionalized for 4, 6 and 24 hours with EDA reached half recovered activity compared to the value obtained for the resin incubated

for 2 hours. Therefore, the latter one was chosen for further studies. A higher number of amino groups on the carrier and thus a lower number of epoxy groups for covalent binding resulted in a less efficient immobilization. A recovered activity of  $80 \pm 5\%$  was calculated with a protein loading of 1, 5 and 10 mg per gram of resin. The expressed activity was respectively 0.48, 2.4 and 4.8 U/g.

Table 1. Results of AvPAL immobilization.

Resin	Functional groups and Immobilization strategy	Incubation time to functionalize	Protein Loading [mg/g]	Immobilization Yield [%]	Recovered Activity [%]
EP400/SS	Epoxydes + IDA + Cobalt for oriented covalent bonds		1	/	0
EP400/SS	Epoxy/Amino (EDA) for oriented covalent bonds	2 hours	1	<b>100</b>	<b>80 ± 5</b>
			5		
			10		
		4, 6, 24 hours	1	100	40 ± 5
ECR8204F	Epoxy/Amino (EDA) for oriented covalent bonds	15 min		95	50 ± 3
		30 min		95	50 ± 2
		60 min	1	94	70 ± 2
		90 min		94	60 ± 4
		120 min		94	60 ± 2

AvPAL was also immobilized on Purolite Lifetech ECR8204F. The support was incubated with EDA for different time values to achieve different ratios of heterofunctionalization. One hour with EDA gave the best results in terms of immobilization, achieving 70% recovered activity. A shorter time of contact showed lower activity (50% for 15- and 30-minutes incubation), which may be due to an insufficient number of amino groups to drive the

first interactions. A higher time of contact did not increase the recovered activity either, which resulted as 60% when EDA was incubated for 90 and 120 minutes.

Although the obtained recovered activity was high, it was 10% lower than the activity succeeded with Resindion carrier, subsequently Lifetech ECR8204F was not chosen for further studies.

The operational stability of AvPAL was tested after immobilization on EP400/SS. It showed only a 10% loss of activity after 10 cycles of biotransformations, meaning that the immobilized AvPAL was stable enough to be employed many times before reducing its biocatalytic activity.

To our knowledge, AvPAL has never been immobilized before and it has been mainly applied as whole-cell biocatalyst. Instead, RgPAL was previously immobilized using several strategies, like the loading on hollow fiber cartridges and within semipermeable microcapsules. Also, cross-linked enzyme aggregates (CLEAs) were prepared as carrier-free immobilization strategy or linked to a mesoporous silica gel as a support material. However, all these cases showed low recovered activity.<sup>7,8</sup> RgPAL was then immobilized into gelatin on polyester films for the use in phenylketonuria diagnosis, but the yield of immobilization was low, ranging around 35%.<sup>9</sup>

Similarly, PcPAL was immobilized on magnetic nanoparticles, as well as on carboxy- and amino- single-walled carbon nanotubes. Nevertheless, the enzyme presented low yield, activity and/or stability in the ammonia addition reaction.<sup>10,11</sup> No examples of PALs being immobilized on a methacrylate resin have been reported before.

#### **4.2.3 Biotransformation of PALs towards aliphatic substrates**

Because of its mechanism of conversion (E1cB), PALs do not accept alanine as substrate, which is coherent with the results of preliminary biotransformations where no product was detected. The mechanism of conversion E1cB involves the abstraction of the proton in  $\beta$ -carbon by a tyrosine residue of the enzyme (Figure 4). This is possible through the aromatic ring of the natural substrate (phenylalanine in this case) which increases the acidity of the proton. As alanine does not present any functional group near  $\beta$ -carbon that could increase the acidity of the proton, it has been decided to try some alanine derivatives that contain electron withdrawing groups (EWGs). The inductive effect of these groups increases the acidity of the proton in  $\beta$ -carbon and thus would allow its abstraction by the enzymatic base.



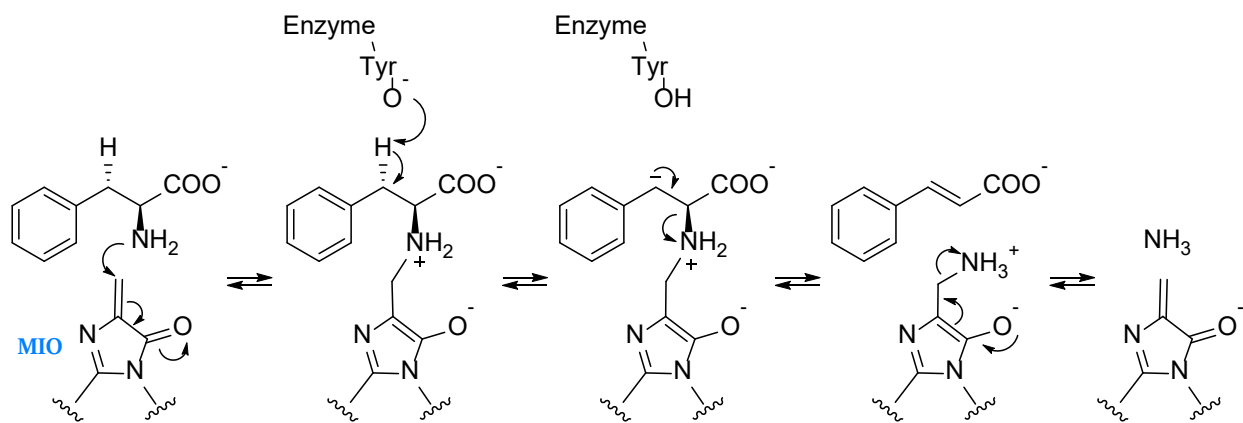


Figure 4. Scheme of PAL mechanism of reaction (Ec1B).

If the reaction takes place, AvPAL will form  $\alpha,\beta$ -unsaturated carboxylic acids which can serve as useful building blocks in organic synthesis. A sustainable and alternative way to produce  $\alpha,\beta$ -unsaturated acids is of high interest. Allylglycine and 3-trifluoromethyl-alanine were chosen as substrates for the biotransformation of the immobilized AvPAL to check whether the aliphatic substrates can be accommodated and effectively converted by the biocatalyst (Figure 5).

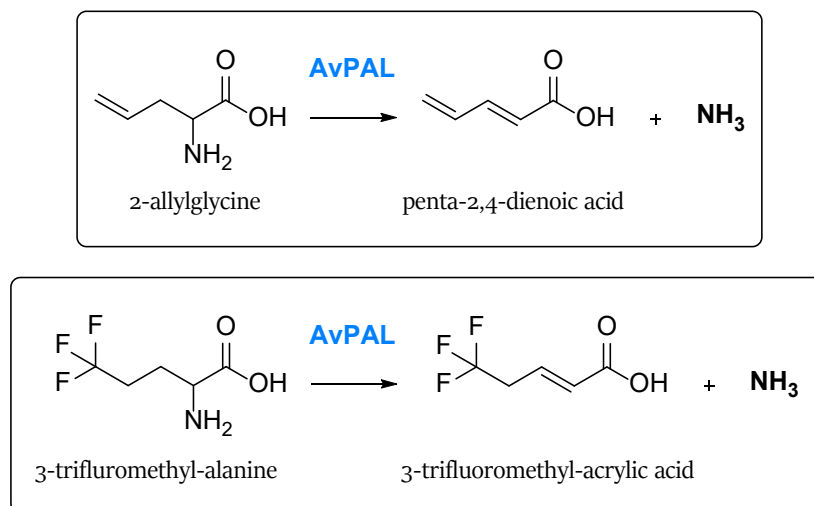


Figure 5. AvPAL deamination of allylglycine and 3-trifluoromethyl-alanine.

It is worth to mention that initially two other enzymes were tested in parallel with AvPAL, namely RgPAL and the PAL from *Planctomyces brasiliensis*. However, first attempts did show very low product formation only when

using allylglycine as substrate and AvPAL showed the highest conversion among the three enzymes. For this reason, AvPAL has been chosen as biocatalyst for the purpose of this chapter.

After 24 hours of biotransformation, 30 mM allylglycine were converted to 1 mM penta-2,4-dienoic acid, corresponding to 3.3% of conversion. After 96 hours of reaction with AvPAL, the conversion increased to a 6% with 1.9 mM of biocatalysed product. These promising results confirmed the effective conversion of an aliphatic substrate. Nevertheless, the reaction advanced very slowly achieving quite low rates of conversion. Moreover, the slow performance of the enzyme on aliphatic substrates led to an undetectable biocatalytic activity on 3-trifluoromethyl-alanine if the reaction took place. At this point, the biotransformation requires optimization to increase the level of conversion.

#### **4.2.4 Biotransformation of AvPAL with coupled reaction**

It is plausible that the deamination reaction is reversible, thus the re-amination of the product may happen in parallel as limiting step of the substrate conversion. Therefore, the coupling of the ammonia lyase reaction with a second enzyme that can scavenge the free ammonia after its production would be highly beneficial. This would prevent the reverse reaction to happen as well as boost the deamination of the unnatural substrates by removing one of the products, since the conversion proved to be very low.

Glutamate dehydrogenase catalyzes the amination of  $\alpha$ -ketoglutaric acid to glutamic acid using NADH as cofactor. It has been decided to couple this enzymatic system to the ammonia lyase reaction to avoid the re-amination of the acrylate product, depleting the availability of free ammonia. Indeed, each molecule of ammonia obtained by AvPAL activity is then employed by glutamate dehydrogenase to give glutamic acid. Moreover, the coupled reaction was associated with a formate dehydrogenase to regenerate the NADH cofactor by converting formic acid into carbon dioxide, as shown in Figure 6.

The two coupled biocatalysts were opportunely chosen, characterized and then co-immobilized to increase the stability and reusability of the system by locating them in close vicinity. Moreover, a fusion protein between the two proteins has been developed for the optimization of the coupled system.

The parts related to the glutamate dehydrogenase and the formate dehydrogenase analysis are described in Chapter 5 and 6 with the relative results and discussion. The immobilized fusion protein was used for the purpose.

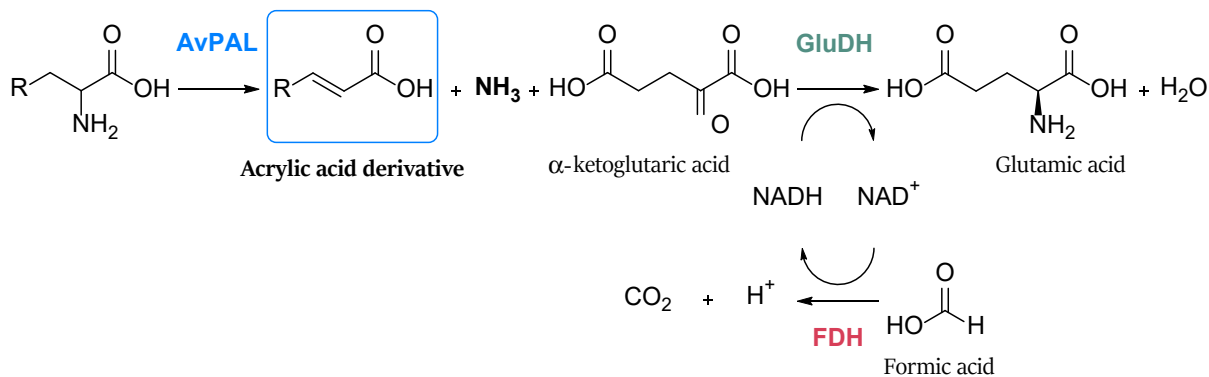


Figure 6. Reaction scheme of AvPAL deamination coupled with GluDH - FDH ammonia scavenger system.

Firstly, the activity of AvPAL was assayed in presence of each element involved in the coupled reaction, from the substrates to the products. No inhibition by any of these compounds was detected.

Afterwards, the 10 and 30 mM-scale biotransformations of allylglycine and 3-trifluoromethyl-alanine were replicated with the addition of the immobilized fusion protein. Unfortunately, the conversion did not improve, and the results stayed the same as previous batch biotransformations. This outcome revealed that the opposite reaction was not responsible of the low conversion. Also, the coupled system was not enough to shift the overall AvPAL reaction towards the product formation by depleting the ammonia from the environment. Most likely, the low rate is due to a kinetic issue where the  $K_M$  value of the aliphatic substrates is very high, resulting in very low velocity rates while working at the 10 mM or 30 mM scale. The solution of this issue may rely on higher substrate concentration and biocatalyst amount in the biotransformation system. The latter option is possible by packing grams of immobilized enzyme in a bed reactor for the use in flow biocatalysis.

It is worth to mention that different ratios of immobilized AvPAL and fusion protein were also tested for the batch biotransformation, going from 7:1 to 1:1. Nevertheless, the conversion to acrylates did not change, confirming that the fusion protein was not the limitation in the reaction.

#### 4.2.5 Biotransformation of AvPAL with coupled reaction in continuous flow

To further enhance the biocatalytic reaction, 10 mg of AvPAL were immobilized per gram of resin, corresponding to twice the loading compared to previous experiments.

Then, a sufficient amount of immobilized AvPAL was packed in the reactor to ensure high velocity of conversion (1.6 grams, meaning 16 mg of AvPAL).

The fusion protein was also immobilized on EP400/SS and 400 mg of 6 mg/g (2.4 mg of fusion protein) were mixed accurately with the previous biocatalyst. The same support for both immobilizations was employed to allow equal distribution of the two proteins, resulting in about 7:1 ratio (AvPAL - fusion protein).

Three different concentrations of substrate were prepared (15, 30 and 60 mM) to compare the conversion in the similar condition as batch biotransformation. These different amounts were also chosen to better understand how the concentration and the kinetic impact on the reaction velocity. Due to the slow rate of batch reaction, long retention times (30 or 60 minutes) were set up.

The results of allylglycine conversion are listed in table 2.

Table 2. Results of continuous flow reaction with allylglycine as substrate.

Allylglycine concentration [mM]	Residence time [minutes]	Molar conversion [%]	Product concentration [mM]
15	30	4	0.65
	60	5	0.80
30	30	3	0.90
	60	4	1.10
60	30	1	0.75
	60	2	0.95

The quantity of product was equivalent to the concentration of formed glutamic acid as stoichiometric amount (1 molecule of allylglycine produces 1 molecule of penta-2,4-dienoic acid and 1 molecule of ammonia, which then reacts with 1 molecule of  $\alpha$ -ketoglutarate to produce 1 molecule of glutamic acid, as shown in Figure 7).

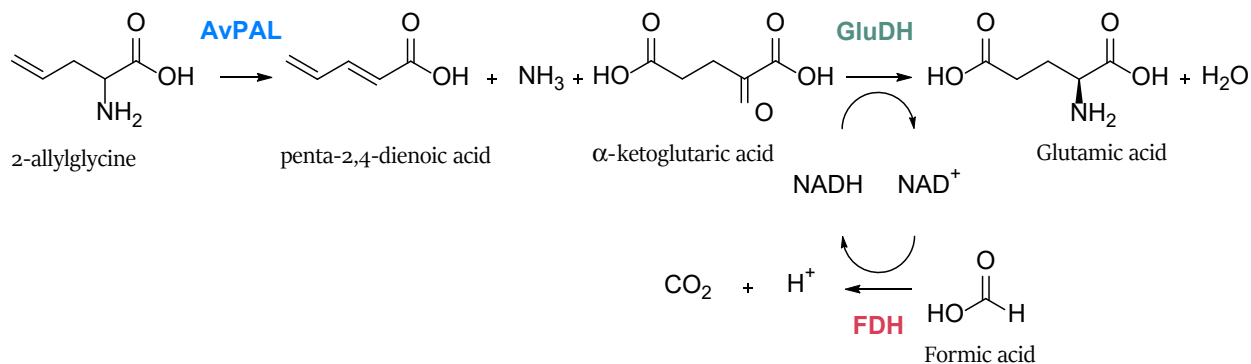


Figure 7. Reaction scheme of AvPAL deamination of allylglycine coupled with GluDH - FDH.

This confirmed that the fusion protein effectively acted as coupled system to remove the ammonia, even if the reaction was not enhanced by shifting the equilibrium towards the product generation. As a matter of fact, the penta-2,4-dienoic acid concentration was ranging around the 1 mM as achieved with the batch system. Furthermore, the comparability between the products of both AvPAL and fusion protein offered a dual confirmation of the conversion and excluded any doubts about stickiness of acrylates to the methacrylate resin used for the immobilization.

The continuous flow reaction improved positively the time scale, which was reduced from the 24 hours of batch reaction to the 30/60 minutes for analogous conversion. The highest values were obtained with the 30 mM concentration of allylglycine achieving 3-4% conversion and 0.9-1.1 mM of product with 30 and 60 minutes of residence time. The values are quite similar, meaning that doubling the residence time does not offer valuable improvement.

In addition, samples were collected for 15 cycles of each reaction condition, which were sufficient to assess any delayed increase of productivity. In this regard, the product concentration was detected in equal amount from the third to the last cycle, without showing any unspecific growth. Moreover, the mixture of the immobilized biocatalysts was tested after all the cycles of flow reaction to determine the retained activity. A batch

biotransformation with 30 mM L-Phenylalanine was run for monitoring the AvPAL activity. In parallel, the fusion protein could convert the produced ammonia into glutamic acid by using the 30 mM  $\alpha$ -ketoglutarate, 50 mM formate and 1 mM NADH available in the reaction environment. The immobilized AvPAL retained more than 90% of the initial activity, while the fusion protein was fully active as coupled system. Indeed, the concentration of *t*-cinnamic acid (product of AvPAL) and the concentration of glutamic acid were always equivalent over time (Figure 8). This confirmed that the system has been always active during the different cycles of flow biotransformation.

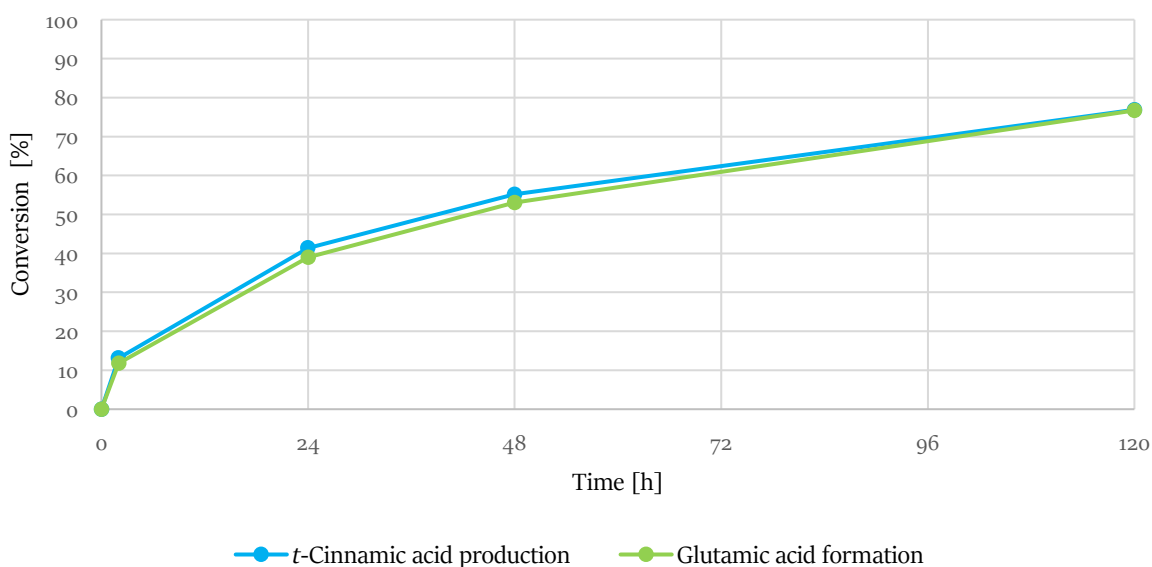


Figure 8. Results of conversion of L-Phenylalanine and  $\alpha$ -ketoglutarate using immobilized AvPAL and fusion protein after flow reaction (85 mg of resin in total, AvPAL and fusion protein with ratio 5:1)

The continuous flow reaction was also tested with 3-trifluoromethyl-alanine to see if the high quantity of packed immobilized AvPAL could yield any trace of acrylate product. Unfortunately, the 30 mM or 60 mM substrate concentration did not exhibit any decrease, while no products for both AvPAL and fusion protein were detected. Increasing the residence time up to 90 minutes did not help either.

Given that propargylglycine has been successfully converted by a PAL, allylglycine was expected to give comparable results, as they share a similar structure. The double or triple bond near the  $\beta$ -carbon is important

to offer sp<sup>2</sup>/sp hybridization. This allows for increased acidity of the β-proton with its subsequent abstraction by the enzymatic base. Instead, the β-carbon of the 3-trifluoromethyl-alanine has vicinal sp<sup>3</sup> hybridization that does not offer enough acidity to permit the β-proton abstraction, even if CF<sub>3</sub> is an EWG.

### 4.3 CONCLUSION

The natural substrates for phenylalanine ammonia lyases are aromatic. However, propargylglycine and now also allylglycine are aliphatic substrates that showed to be effectively accommodated by PALs, even if the conversion resulted very low. Other aliphatic substrates, instead, were now accepted by these enzymes, despite the presence of an EWG to increase the acidity of the β-proton. In fact, AvPAL did not convert neither alanine nor 3-trifluoromethyl-alanine to produce aliphatic acrylates. As a result, a different class of enzymes is required to perform the desired reaction and new protein candidates need to be accurately selected. Further investigations are necessary before implementing a sustainable biocatalytic process independent from the exhaustion of fossil resources for the generation of acrylates and the production of the derived bio-based polymers.

### 4.4 BIBLIOGRAPHY

1. F. Cavani, S. Albonetti, F. Basile, A. G. Chemicals and Fuels from Bio-Based Building Blocks. *Focus Catal.* **2016**, 7 (2016).
2. Wang, X., Wang, H. & Sun, Y. Synthesis of Acrylic Acid Derivatives from CO<sub>2</sub> and Ethylene. *Chem* **3**, 211–228 (2017).
3. Dishisha, T., Pyo, S. H. & Hatti-Kaul, R. Bio-based 3-hydroxypropionic- and acrylic acid production from biodiesel glycerol via integrated microbial and chemical catalysis. *Microb. Cell Fact.* **14**, 1–11 (2015).
4. Lorz, P. M. *et al.* Phthalic Acid and Derivatives. Ullmann's Encyclopedia of Industrial Chemistry. *Ullmann's Encycl. Ind. Chem.* 131–180 (2007).
5. Weiser, D. *et al.* Phenylalanine Ammonia-Lyase-Catalyzed Deamination of an Acyclic Amino Acid: Enzyme Mechanistic Studies Aided by a Novel Microreactor Filled with Magnetic Nanoparticles. *ChemBioChem* **16**, 2283–2288 (2015).
6. DeLano, W. L. Pymol: An open-source molecular graphics tool. *CCP4 Newsl. protein Crystallogr.* **40**, 82–

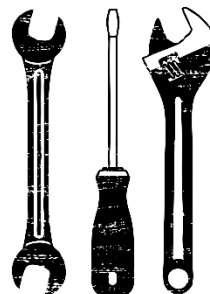
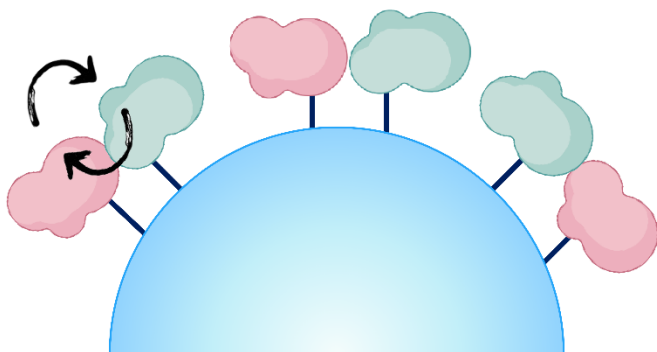
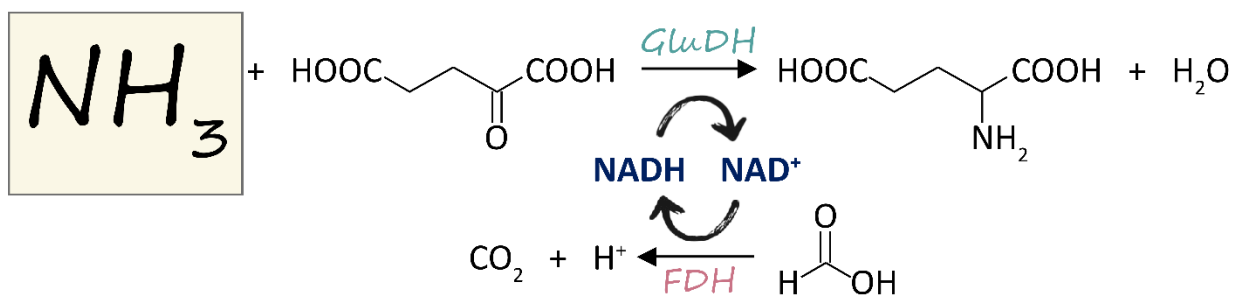
- 92 (2002).
7. Cui, J. D., Qiu, J. Q., Fan, X. W., Jia, S. R. & Tan, Z. L. Biotechnological production and applications of microbial phenylalanine ammonia lyase: A recent review. *Crit. Rev. Biotechnol.* **34**, 258–268 (2014).
  8. Cui, J. D., Li, L. L. & Bian, H. J. Immobilization of Cross-Linked Phenylalanine Ammonia Lyase Aggregates in Microporous Silica Gel. *PLoS One* **8**, 80581 (2013).
  9. Bourget, L. & Chang, T. M. S. *Phenylalanine ammonia-lyase immobilized in semipermeable microcapsules for enzyme replacement in phenylketonuria*. *FEBS Letters* vol. 180 (1985).
  10. Bartha-Vári, J. H. *et al.* Immobilization of Phenylalanine Ammonia-Lyase on Single-Walled Carbon Nanotubes for Stereoselective Biotransformations in Batch and Continuous-Flow Modes. *ChemCatChem* **7**, 1122–1128 (2015).
  11. Boros, K. *et al.* Robust, site-specifically immobilized phenylalanine ammonia-lyases for the enantioselective ammonia addition of cinnamic acids. *Catal. Sci. Technol.* **11**, 5553–5563 (2021).



## CHAPTER 5.

### EFFICIENT CO-IMMOBILIZATION OF GLUTAMATE AND FORMATE DEHYDROGENASE FOR A REUSABLE BIENZYMATIC TOOL TOWARDS AMMONIA REMEDIATION

---



## 5.1 INTRODUCTION

Ammonia ( $\text{NH}_3$ ) is a colourless, acrid smelling gas at room temperature and pressure, that readily dissolves in water and becomes liquid ammonia or ammonium, with the ratio largely depending on pH and temperature.<sup>1</sup>

It plays an important role in many circumstances. Ammonia commonly enters the environment through municipal, industrial, agricultural, and natural processes.<sup>2</sup> It is one of the most important pollutants in aquatic ecosystems, inducing ecological stress and serving as a key indicator of water quality. Higher concentrations of ammonia has been shown to be harmful to aquatic organisms.<sup>3</sup> Consequently, accurate monitoring of ammonia concentrations in natural water environments or industrial waste effluxes results essential for the control and the prevention of aquatic life toxicity.

In natural waters, concentrations of total ammonia are generally less than 0.1 mg/L, while higher levels normally indicate organic pollution.<sup>4</sup> In aquaculture systems, ammonia is at most 5 mg/L (0.28 mM), while domestic sewage typically contains 20–40 mg/L of ammonia (1.1–2.2 mM). Dairy, refinery and mineral industry effluents may reach the 100–140 mg/L (5.5–7.8 mM).<sup>5</sup> However, higher release of ammonia may happen because of accidental spills, the use and disposal of cleansing agents that contain ammonia, urban runoff, accidental releases of ammonia rich fertilizer, intensive farming, and the decomposition of livestock wasters.<sup>6</sup> For example, groundwater samples at an old municipal landfill site in Grinsted (Denmark) contained ammonia levels higher than 1 g/L (>55 mM) during the period from 1992 to 1995.<sup>7</sup> In 1991–1993, ammonia was found in the surface water collected at the Porto Alegre landfill (Brazil) at a maximum concentration of 1.63 g/L (90 mM), while the maximum amount of ammonia was 1.83 g/L (101 mM) in the leachate.<sup>8</sup>

In human body fluids, an elevated ammonia blood level (hyperammonaemia) is considered a strong indicator of an abnormality in nitrogen homeostasis, the most common related to liver dysfunction. In excess, ammonia is a potent toxin, principally of central nervous system function.<sup>9</sup> Moreover, ammonia is an important parameter to assess the quality of water exploited for human consumption or for the use as swimming water.<sup>10</sup> Therefore, the measurement of aqueous ammonia is necessary to prevent human toxicity as well as to evaluate the efficiency of medical treatments in the metabolic condition of hyperammonaemia.

Great effort has been put over the years to find an adequate system for the purpose and numerous methods are available nowadays, which include titration, colorimetric/fluorometric or chemiluminescent assays, electrode-based measurements, enzymatic reactions. Nevertheless, the majority of these methods require complicated sample pretreatment.<sup>10,11</sup> In contrast, the most common used is an enzymatic method that measures ammonia directly. Thus, sample preparation is relatively simple, because the previous liberation of ammonia from the sample is not required.<sup>9</sup> This assay is based on the reductive amination of  $\alpha$ -ketoglutaric acid to glutamic acid using NADH as cofactor, catalysed by glutamate dehydrogenase. Many reports on methods based on this enzyme have been recently reported.<sup>10</sup> However, in all the cases the ammonia content is measured by following the decrease in absorbance at 340 nm caused by the oxidation of NADH. Therefore, it allows the determination of ammonia only at lower concentrations with a maximum of 500  $\mu\text{mol/L}$  using biosensors and up to 800  $\mu\text{mol/L}$  of ammonia with commercially available assay kits.<sup>10,11</sup>

An enzymatic tool involving the glutamate dehydrogenase coupled with an enzyme able to recycle the cofactor would allow the continuous quantification of ammonia with a small loss of added cofactor. For this purpose, a formate dehydrogenase has been chosen. In addition, the determination of glutamic acid concentration over time is the method employed for the detection of aqueous ammonia from low to high concentrations, which gives a very accurate result and makes the tool application versatile.

The NAD(H)-dependent glutamate dehydrogenase from *Clostridium Symbiosum* (CsGluDH) is the chosen candidate for the system together with the formate dehydrogenase from *Candida boidinii* (CbFDH). FDH catalyses the oxidation of formate to carbon dioxide using  $\text{NAD}^+$  and possesses many advantages in the recycling of NADH: a favourable thermodynamic equilibrium, the inertness of the substrate and reaction product, its ready removal from the main product ( $\text{CO}_2$  will go to the atmosphere).<sup>12</sup>

Enzyme immobilization has been carried out with the aim to increase the stability of the biocatalysts. Furthermore, their immobilization on a carrier allows the reusability of the enzymes for further reactions and facilitates their separation from the products in the reaction environment.

The glutamate dehydrogenase from *Clostridium symbiosum* has never been immobilized before, consequently it requires a screening of different strategies of immobilization to yield an efficient and stable biocatalyst. In the

past, other glutamate dehydrogenases have been immobilized on a large variety of carriers, in particular on materials produced for probes and biosensors.<sup>13</sup> In addition, different magnetic nanoparticles and agarose beads activated with glutaraldehyde were used as supports for the hexameric bovine liver glutamate dehydrogenase, offering good outcomes even for the co-immobilization.<sup>14,15</sup> Nevertheless, the latter enzyme behaves in a different way from CsGluDH, given its mammalian origins where the protein is inserted in a more complex system. After that, a bacterial glutamate dehydrogenase has been studied for the immobilization on glyoxyl agarose with great recovered activity.<sup>16</sup> In this case, the enzyme owned a trimeric structure and, as a consequence, it could not be related to the hexameric CsGluDH. All the data previously published about glutamate dehydrogenase immobilization are only a starting point for this study. More tests are required to find an optimal strategy for this particular biocatalyst, that behaves in an unique way with changes in conformation and active/inactive forms.<sup>17,18</sup> On the other side, more information about the immobilization of formate dehydrogenase from *Candida boidinii* are available. This enzyme has been bound to many different carriers, such as membranes, silica matrixes, magnetic nanoparticles, alginate gels, polystyrene, dextran sulphate, entrapped in polyacrylamide gels and cross-linked to form enzyme aggregates (CLEAs).<sup>19-24</sup> In particular, an evaluation of different conditions and immobilization strategies was described when using agarose as support,<sup>12</sup> where the employed chemistry is very similar to the one available on polymethacrylate resin. Nevertheless, the characteristics of the agarose-based and the polymeric resins are different in terms of morphological properties (particle size, pore size, number of pores) and physical properties like hydrophilicity and mechanical strength, which means that the recovered activity may vary significantly even if the chemistry of binding the enzyme onto the support is similar. Therefore, immobilization studies of this formate dehydrogenase on polymethacrylate resin need to be implemented, given the great efficiency and stability of this carrier in comparison to the other support, especially in packed-bed reactors for continuous flow biocatalysis.<sup>25</sup>

Since the proximity of glutamate and formate dehydrogenase would increase the velocity of the biocatalytic conversion due to a closer accessibility of the recycled cofactor to the active site of the former enzyme, their co-immobilization on the same support was also tested.

The efficiency and the stability of the co-immobilized biocatalysts were assessed by running biotransformations and compared with the results obtained using the free (soluble) enzymes.

## 5.2 RESULTS AND DISCUSSION

### 5.2.1 Protein expression, purification and activity

Protein expression led to an average of 25 g of cell pellet per liter of liquid culture. After dialysis, the protein concentration was checked, and an SDS-PAGE was run to verify the purity of the protein's solution. As for the first analysis, a yield of around 100 mg of proteins was obtained per gram of pellet. Then, as shown in Figure 1, other unspecific proteins were present in the obtained solution, because of the lack of a purification system, but their concentration was low in comparison with the quantity of CsGluDH.

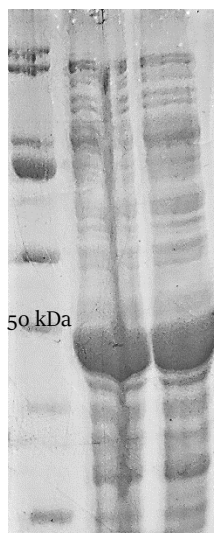


Figure 1. 12% SDS-PAGE of CsGluDH after dialysis, stained with Instant Blue.

### 5.2.2 Biotransformation using pTac-85 CsGluDH

The biotransformation was performed with AvPAL, that forms *t*-cinnamic acid and ammonia after converting L-phenylalanine, so that GluDH was coupled to use the ammonia for producing glutamic acid (Figure 2).

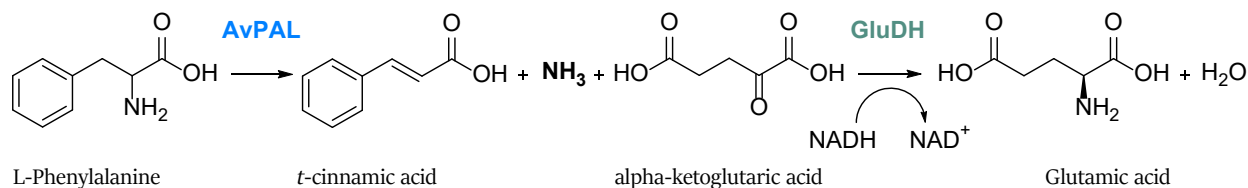


Figure 2. Biotransformation using AvPAL and CsGluDH.

One molecule of *t*-cinnamic acid formed was equivalent to one molecule of glutamic acid generated by the coupled reaction. Therefore, this test was done with the aim to assess the efficiency of the enzyme by comparing the concentration of the two products. Nevertheless, it was discovered that the control biotransformation, having only GluDH as biocatalyst, gave a slight decrease of phenylalanine and a production of small amounts of *t*-cinnamic acid (around 0.3 mM), even if AvPAL was not present. Similarly, the same sample resulted to have increasing quantities of glutamic acid formed over time, which were much higher than the *t*-cinnamic acid molecules, meaning that there was a further ammonia source. As for the first outcome, it has been found that normally *E. coli* BL21 (DE3) produces small amounts of two uncharacterized proteins possessing a 30-33% identity to other bacterial PALs. Consequently, the solution of GluDH may contain enzymes interfering with the biotransformation. Indeed, the partial purification of the overexpressed enzyme in Figure 1 showed the presence of low quantities of other proteins produced by the cells where PALs may be included.

Besides, the purification system involved the usage of high concentrations of ammonium sulphate that may not be completely removed through centrifuge and dialysis. The leftover ammonia interfered with the biotransformations, behaving as substrates. As a matter of fact, doubling the volume of GluDH added to the biotransformation turned to produce approximately the double amount of glutamic acid in the control reaction with GluDH.

Because of these factors interfering with the efficiency of the system, it has been decided to work on the development of an efficiently purified GluDH solution by the addition of a His-tag to the enzyme sequence, which allows the purification through the Ni-affinity columns and thus avoids the precipitation with ammonium sulphate. Also, the addition of FDH in the system would decrease the amount of expensive cofactor used for the reaction, enabling a continuous recycling of NADH (Figure 3).

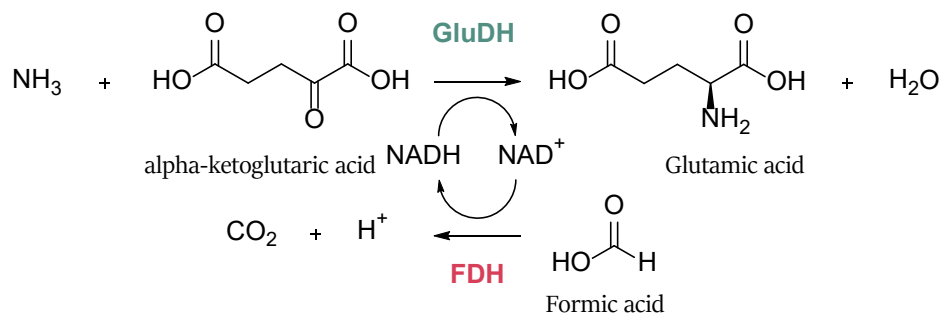


Figure 3. Scheme of GluDH and FDH coupled reaction.

### 5.2.3 Cloning of GluDH

The glutamate dehydrogenase gene (pTac85-CsGluDH) has been cloned into pRSETb as backbone, in order to obtain a protein presenting a polyhistidine tag. This sequence has been implemented to the N-terminus because the C-terminal ends are buried in the centre of the hexameric structure, as shown in Figure 4. Using the exposed N-terminal, any conformational distortion has been avoided. The gene was successfully cloned into the vector.

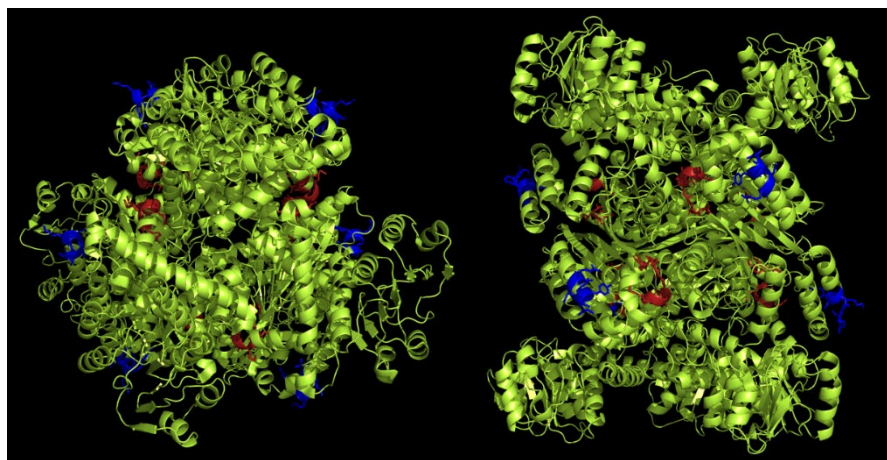


Figure 4. Crystal structure of GluDH (PDBid: 2YFH) visualized in Pymol.<sup>26</sup> N-terminal is colored in blue, C-terminal in red.

### 5.2.4 Expression and purification of GluDH and FDH

The cloned gene of CsGluDH was transformed in competent cells, and the protein was successfully expressed with an N-terminal His-tagged. After the overexpression and the purification by IMAC chromatography of both GluDH and FDH, a yield of 15 g and 22 g respectively of cell pellet per litre of culture has been achieved, as well

as an amount of 3 mg and 20 mg of protein per gram of pellet. The protein samples shown in Figure 5 confirmed the purity of the GluDH compared to the same enzyme partially purified by precipitation with ammonium sulphate (Figure 1). Consequently, the final purpose of cloning the His-tagged GluDH for its complete purification has been achieved, so that any contamination during biotransformations will be avoided.

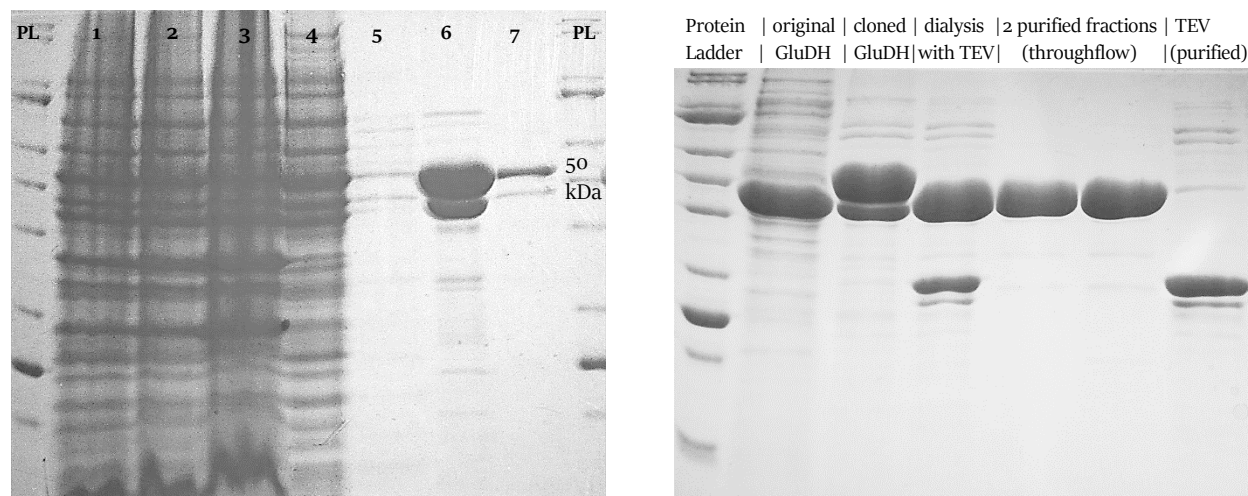


Figure 5. SDS-PAGE of the samples taken during His-GluDH purification. PL: protein ladder, 1: pellet, 2: lysate, 3: cell paste (insoluble proteins), 4: crude extract, 5: 10% buffer B, 6 - 7: after dialysis. On the right, SDS-PAGE with the samples obtained during treatment with TEV protease, compared to the half purified original GluDH (significantly diluted).

However, the purified GluDH showed 2 bands in the SDS-PAGE (Figure 5) with closed location, meaning that the monomeric molecular weights were very similar but not the same. We supposed that part of the expressed GluDH was deprived of its His-tag, showing a lower size than the remaining His-tagged GluDH. To prove this hypothesis, the purified enzyme was incubated with TEV protease, since the gene offered a TEV site between the His-tag and the GluDH sequence. The TEV protease had the aim to cleave the His-tag from all the proteins. As exhibited in the SDS-PAGE on the right (Figure 5), all the GluDH monomers presented the same size after the His-tag was removed, confirming the initial hypothesis. Also, the band of the enzyme without His-tag was located at the exact same level as the second band in the GluDH without treatment.

It is possible that only some of the subunits of the hexameric structure did not possess the His-tag, so that the assembled enzyme was still purified by interaction with the His-tagged subunits. The protease inhibitor



Phenylmethanesulfonyl fluoride (PMFS, 1 mM as final concentration) was included in the buffer used for pellet resuspension to prevent the loss of the His-tag. Still, the purified enzyme showed 2 bands, proving that the cleavage was not happening during the purification process, but in the expression phase. Since the His-tag presence or absence did not impact on the enzyme activity, it has been decided to continue working on the purified GluDH presenting both forms.

### 5.2.5 Activity of GluDH and FDH

The pure enzymes were functionally characterised by performing specific activity assays and kinetic studies with different concentrations of all substrates. Results are listed in Table 1.

Table 1. Activity and kinetic characterization of CsGluDH (both directions) and CbFDH.

	CsGluDH		CbFDH	
Specific Activity	Reaction direction		[U/mg]	[U/mg]
	Reductive Amination		220 ± 20	3.5 ± 0.3
	Oxidative Deamination		23 ± 3	
Affinity for Substrates	CsGluDH pTac85		CsGluDH pRSETb	
	K <sub>M</sub> [mM]	V <sub>max</sub> [mmol min <sup>-1</sup> mg <sup>-1</sup> ]	K <sub>M</sub> [mM]	V <sub>max</sub> [mmol min <sup>-1</sup> mg <sup>-1</sup> ]
L-Glutamate	1.93	0.047	3.0 ± 1.1	0.08 ± 0.01
α-Ketoglutarate	2.85	0.546	0.48 ± 0.31	0.13 ± 0.1
Ammonia	12.9	0.307	32.3 ± 10.0	0.36 ± 0.15
NADH	0.055	0.285	0.10 ± 0.06	0.12 ± 0.1
NAD <sup>+</sup>	0.17	0.041	0.17 ± 0.02	0.05 ± 0.02
Affinity for Substrates	CbFDH Literature		CbFDH	
	K <sub>M</sub> [mM]	V <sub>max</sub> [μmol min <sup>-1</sup> mg <sup>-1</sup> ]	K <sub>M</sub> [mM]	V <sub>max</sub> [μmol min <sup>-1</sup> mg <sup>-1</sup> ]
Formate	5.6	6	5.0 ± 1.0	3 ± 1
NAD <sup>+</sup>	0.045	6	0.168 ± 0.030	5 ± 1

The specific activity of GluDH for the oxidative deamination resulted to be  $23 \pm 3 \text{ U mg}^{-1}$  which is the same value obtained for the original biocatalyst at the same conditions (pH 7,  $25^\circ\text{C}$ ).<sup>27</sup> After cloning, results remained comparable.

Regarding GluDH kinetic characterization, all the tests were carried out at pH 8.0 as it was previously done for the pTac-85 CsGluDH.<sup>28</sup> Keeping all the same conditions gave the chance to compare this latter enzyme to the pRSETb CsGluDH after cloning and expressing it with the His-tag.

The affinity for the various substrates exhibited by His-tag GluDH is similar to that reported for the original GluDH with  $K_M$  values around 2-fold higher for the ammonia and the NADH, 1.5-fold higher for L-glutamate, and a  $K_M$  value 6 times lower for the keto acid meaning a decrease in the affinity for this substrate. The behaviour of the GluDH has not changed after the addition of 6 histidine molecules on the N-terminal of the enzyme, which confirmed they did not cause any evident steric hindrance to the quaternary structure.

Following the results of the kinetics, the standard conditions for the biotransformations were defined as 1 mM NADH, 100 mM formic acid and 50 mM  $\alpha$ -ketoglutaric acid to give enough cofactor for the first reaction to initiate while allowing the FDH to start the conversion of  $\text{NAD}^+$  into NADH.

Similarly, 2 equivalents or more of formate are necessary to avoid that the parallel recycling reaction becomes the limiting step in the system, where the excess of substrate has the aim to push the reaction to the product formation since the activity of FDH may be slower than the activity of the GluDH.

The quantity of the keto acid has been set to 50 mM considering a lower concentration of ammonia in the solution to be analysed. An excess of this substrate may be essential to overcome the lower affinity towards the ammonia, making sure that even traces are detectable.

Consequently, biotransformations were carried out with a 2-fold higher concentration of the keto acid in comparison to the cation under detection.

When higher amounts of ammonia may be present in a solution, scaling up the reaction conditions is required to ensure an excess of  $\alpha$ -ketoglutarate and formate.

### 5.2.6 Immobilization and co-immobilization of GluDH and FDH

Many strategies of immobilization were evaluated to find an effective method that offers an efficient value of recovered activity. Four different resins were tested, possessing different pore size, particle size and functional groups (see specific properties in Table 2). Moreover, the loading of the two biocatalysts was also varied in the same support to find the best immobilization conditions.

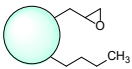
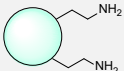
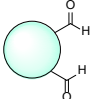
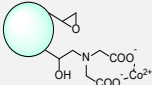
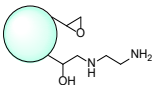
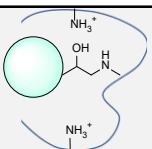
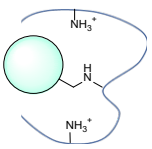
Table 2. Technical specifications of resins used for immobilization.

Resin	Brand	Matrix	Pore size [nm]	Particle Size	
				Range [μm]	Functional Group
EP400/SS	ReliSorb	polymethacrylate polymer with	40-50	50-150	Epoxide
	Resindion	highly porous structure			
ECR8204F	Lifetech	polymethacrylate polymer with	30-60	150-300	Epoxide
	Purolite	low porosity			
ECR8304F	Lifetech	polymethacrylate polymer with	30-60	150-300	Amino with short ethylene (C2) spacer
	Purolite	low porosity			
ECR8285	Lifetech	polymethacrylate polymer with	45-65	250-1000	Epoxy/Butyl
	Purolite	low porosity			

In all cases and for both the two dehydrogenases, there has been a complete immobilization yield, which was checked by measuring the activity of the supernatant containing the soluble enzyme not been immobilized and running the same sample in an SDS electrophoresis gel to assess if any protein was still present even if the activity was not detected.

As showed in Table 3, all the immobilization strategies involving a covalent bond exhibited a poor recovered activity. Indeed, the enzyme requires a certain flexibility to be active since it undergoes a conformational change from an “active” to an “inactive” form that is pH dependent, where the six subunits have the capacity for cooperative interaction.<sup>17,29</sup> Binding covalently the CsGluDH to the support may not allow the proper rearrange of conformation with a resulting decrease of activity to very low values.

Table 3. Results of immobilization of CsGluDH on different supports.

Resin	Functional groups and Immobilization strategy	Incubation time to functionalize	Loading of GluDH [mg/g]	Recovered Activity [%]
ECR8285	 Epoxy/Butyl for covalent and hydrophobic bonding	/	1	2
ECR8304F	 Amino groups for ionic bonds	/	1	2
ECR8204F EP400/SS	 Aldehydes for covalent immobilization	/	1	2
ECR8204F	 Epoxides + Iminodiacetic acid (IDA) + Cobalt for oriented covalent bonds	2 hours IDA + 2 hours Cobalt	1	0
ECR8204F EP400/SS	 Epoxy/Amino (EDA) for oriented covalent bonds	2 hours	1	1
ECR8204F EP400/SS	 Amino (PEI) for ionic interaction	overnight	1	3
ECR8204F	 Aldehydes covered with PEI for ionic interaction	overnight	1	4
EP400/SS			1	<b>85</b>
			5	<b>50</b>

Additionally, the covalent reaction happens between the epoxides of the resin and the amino acidic residues of the enzyme, which are specifically lysine side chains. The positive charges of these molecules are known to be necessary for the activity, as they stabilize the substrate before being converted.<sup>17,30</sup> When lysine amino acids are involved in the binding, the positive charges of the amino groups are not available for the stabilization of the substrate, reducing the yield of the biocatalytic conversion.

An evaluation of the amino acidic residues together with a detailed analysis of the hexameric structure has been carried out by means of the tool CapiPy, a python-based GUI-application to assist in protein immobilization.<sup>31</sup> The outcome is a PDB file exhibiting the residues of interest during the immobilization process, which are collected in clusters and coloured in blue when positive charged (lysine, histidine, and arginine amino acids), red when negative charged (aspartate and glutamate residues), in white when the side chains are hydrophobic and coloured in cyan if the cluster contains histidine chains. The final quaternary structure is shown in Figure 6, where it is evident that negative charged groups are spread all over the hexamer, offering many points of interactions with positively charged groups present on the support.

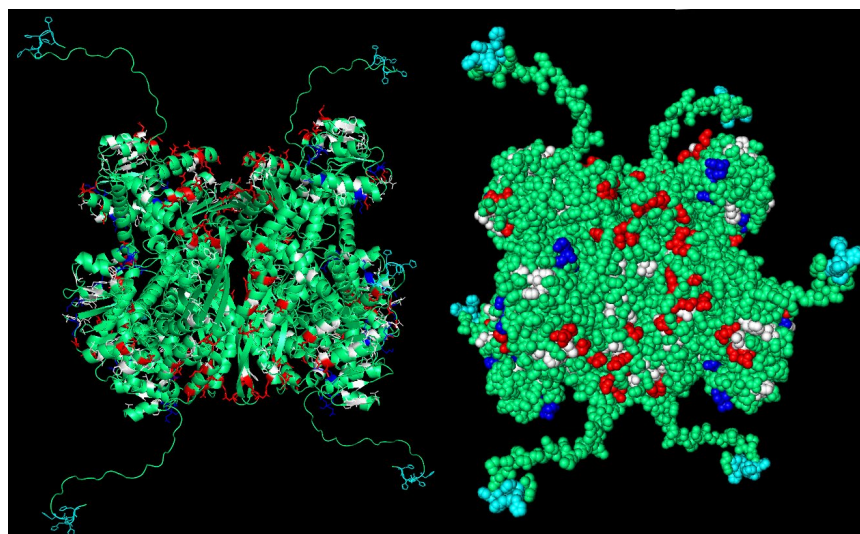


Figure 6. PDB file retrieved from CapiPy tool after the analysis of CsGluDH sequence. Visualized and edited in Pymol.<sup>26</sup>

First picture: cartoon and licorice sticks for colored amino acids, second picture: surface, spheres, and dots.

Employing EP400/SS as carrier for the immobilization as well as aiming for ionic interactions instead of rigid covalent bonds appeared to be the best choice to obtain optimum recovered activity after immobilizing the glutamate dehydrogenase. Nevertheless, the number of amino groups available on the surface of the support emerged to be important, in order to improve the stabilization of the enzyme interacting with the hydrophobic methacrylate beads, creating a more hydrophilic, and thus suitable, environment for the activity of the biocatalyst. Indeed, water molecules are essential during the conversion of the substrate into the product.<sup>32</sup> As a result,

polyethyleneimine (PEI) was used for the functionalization of the resins, both on epoxy and glyoxyl groups to compare the yield of attached polymeric chains.

The colorimetric assay with picrylsulfonic acid as reagent offers a qualitative indication of the reactive amino groups, which are available after the functionalization. As a matter of fact, picrylsulfonic acid reacts with primary amines to yield a colored product, where the intensity of the color increases as the amount of the amino groups (Figure 7).

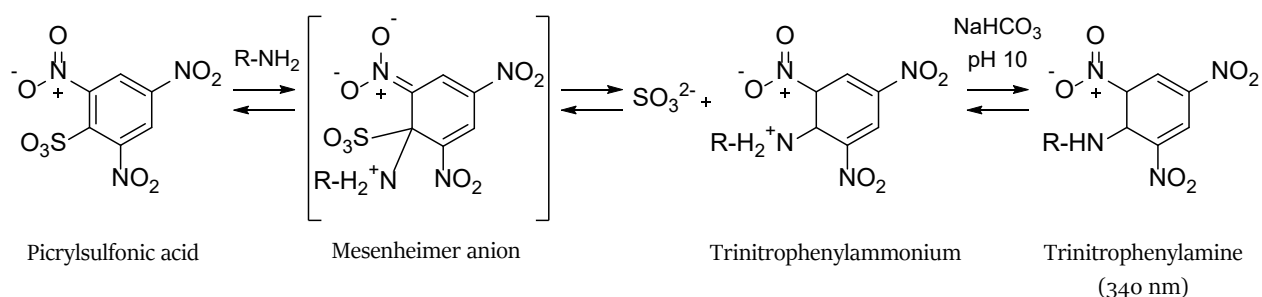


Figure 7. Reaction mechanism between picrylsulfonic acid and the enzymatic amine groups.<sup>33</sup>

In Figure 8, the Purolite resin ECR8304F having short spacer amino groups and the resin ECR8204F with different functionalization strategies are presented after being assayed.



Figure 8. Picrylsulfonic acid assay of Purolite resin, which was previously functionalised in several manners.

The color is more intense for the support that has been previously activated to aldehydes and then functionalized with PEI, confirming the higher number of amino groups located on the surface of this resin in comparison to the one being functionalized with PEI starting from the original epoxy resin. In other words, glyoxyl groups led to a higher rate of bound polyethyleneimine chains, whereas a consequent higher number of amino groups

offered an improved recovered activity of GluDH after immobilization, when the ReliSorb EP400/SS was employed. Indeed, looking at the values listed in Table 5, the best results were provided by the latter resin activated to aldehydes then covered with PEI, where specifically an overnight functionalization gave full activity while 1 hour of incubation with PEI exhibited 75% of activity.

Increasing the protein loading from 1 mg of enzyme per gram of resin to 4 caused a lower percentage of catalytic activity per gram of resin, that seemed to reflect the presence of diffusional limitations. Nevertheless, the total expressed activity is still higher when loading more enzyme, so that it becomes essential for promoting the biocatalytic conversion during the biotransformations. In any case, the chosen strategy for CsGluDH is the immobilization on EP400/SS firstly activated to aldehydes and secondly incubated with PEI for an overnight.

The same studies have been done for the formate dehydrogenase, following the same path as for the GluDH. Firstly, the amino acidic sequence was given as input to the CapiPy tool for then retrieving the outcome visible in Figure 9, demonstrating that there are many negative groups available for the ionic immobilization onto the resin functionalized with amino groups. Moreover, CbFDH includes many positively charged groups on the surface of the quaternary structure, but among them only two lysine amino acids are available for the nucleophilic attack to epoxides or aldehydes of the support for the covalent bond.

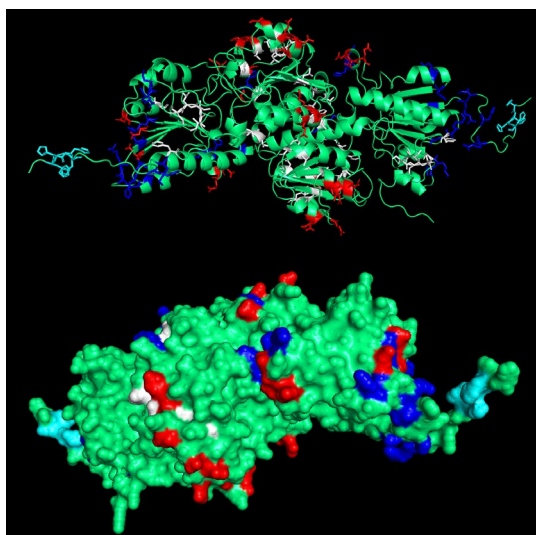
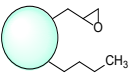
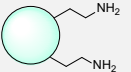
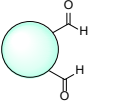
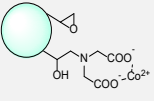
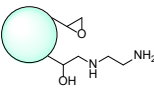
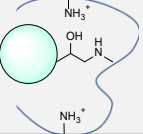
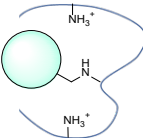


Figure 9. PDB file retrieved from CapiPy tool after the analysis of CbFDH sequence. Visualized and edited in Pymol.<sup>26</sup> First picture: cartoon and licorice sticks for coloured amino acids, second picture: surface, spheres, and dots.

Seeing the final values listed in Table 4, covalent bonds appeared to be less indicated as mechanism of immobilization for CbFDH, similarly to the previous enzyme. These permanent and rigid connections constrain the quaternary structure preventing any movement when a certain flexibility is required for the proper activity of the biocatalyst.

Table 4. Results of immobilization of CbFDH on different supports.

Resin	Functional groups and Immobilization strategy	Incubation time to functionalize	Loading of FDH [mg/g]	Recovered Activity [%]
ECR8285	 Epoxy/Butyl for covalent and hydrophobic bonding	/	1	0
ECR8304F	 Amino groups for ionic bonds	/	1	3
ECR8204F EP400/SS	 Aldehydes for covalent immobilization	/	1	10
ECR8204F	 Epoxides + Iminodiacetic acid (IDA) + Cobalt for oriented covalent bonds	2 hours IDA + 2 hours Cobalt	1	0
ECR8204F EP400/SS	 Epoxy/Amino (EDA) for oriented covalent bonds	2 hours	1	0
ECR8204F EP400/SS	 Amino (PEI) for ionic interaction	overnight	1	8
ECR8204F	 Aldehydes covered with PEI for ionic interaction	overnight	1	5
EP400/SS			1	100
			5	45



It is also important to mention that a 2 times higher recovered activity has been measured when analyzing the glyoxyl resin before the reduction step, meaning that also  $\text{NaBH}_4$  has a role in decreasing the stability of the enzyme.

On the contrary, reversible interactions between ionic groups are weak and enable higher freedom to the enzyme. Therefore, the best results of recovered activity have been achieved by using polyethyleneimine as intermediate, which surrounds the surface of the support previously activated to aldehydes, and provided a higher number of amino groups. These outcomes are comparable to the results obtained using agarose as carrier after being coated with PEI (25 KDa), which showed 100% yield and 100% recovered activity, as best strategy of immobilization for CbFDH.<sup>12</sup> In the same study, glyoxyl agarose and the further reduction step with sodium borohydride exhibited a recovered activity of 15%, slightly higher compared to the 10% achieved with the polymethacrylate resins.<sup>12</sup> In any case, a similar behavior between the two typologies of supports has been confirmed. The slightly lower percentage numbers obtained with the second resins may be due to the hydrophobicity of the material, when this enzyme prefers a more hydrophilic environment as agarose can offer.

Ultimately, the methacrylic resin EC-HFA possessing epoxy and amino groups exhibited a recovered activity of 15% when pH was 10 and 40% with neutral pH.<sup>12</sup> Bearing in mind that 40% has been the best outcome obtained in the past when using a methacrylate resin, it is interesting to see that this value can also reach a 85% recovered activity with a different chemistry of immobilization.

Concerning the loading capacity of CbFDH, when the loading was increased from 1 to 5 mg of protein per gram of resin, the recovered activity faced a decrease in the percentage rate, meaning that some diffusion limitations took place. Nonetheless, the total expressed activity yielded a greater value given the increased amount of enzyme loaded onto the support. Hence, biotransformations are carried out by adding as much protein as possible to ensure a rapid cofactor recycling activity.

Furthermore, ReliSorb EP400/SS provided better results compared to the three other resins after the immobilization of both enzymes. In addition to the type of functional groups, the main differences between the two brands of supports are the grade of porosity they possess and the particle size. Therefore, the characteristics of EP400/SS resulted to be more suitable for the two enzymes under study, creating an optimal environment for

both the dehydrogenases to perform their related biocatalytic activity. Moreover, the best choices of immobilization strategy with respect to GluDH and FDH have been alike, simplifying a lot the process of co-immobilization.

Consequently, it has been decided to use EP400/SS activated to aldehydes and functionalized with PEI (incubated overnight) to immobilize the two enzymes onto the same shared support. Moreover, in a precedent study the bacterial glutamate dehydrogenase from *Thermus thermophilus* and the formate dehydrogenase from *Candida boidinii* were also co-immobilized in the presence of PEI yielding an enzyme-PEI composite with full activity, thanks to the stabilizing effect of the polymeric chains that, generally, prevents dissociation of multimeric enzymes.<sup>16</sup>

For each protein, 1 mg per gram of resin has been loaded to the support simultaneously as well as sequentially, immobilizing firstly the CbFDH and then the CsGluDH, and vice versa, to compare and choose the best conditions. Regarding the simultaneous incubation of the two dehydrogenases with the carrier, the recovered activity was lower for the CsGluDH of around half of the original value. Similarly, the sequential immobilization of CbFDH as first enzyme and CsGluDH as second, resulted in a very low recovered activity for the former biocatalyst. On the contrary, the third method showed the best outcomes for both the enzymes with a recovered activity of 85% for the glutamate dehydrogenase and 100% for the formate dehydrogenase. The first percentage is slightly lower compared to the numbers achieved by immobilizing the single glutamate dehydrogenase, but still optimal to work with. Consequently, the first immobilization of CsGluDH and the successive co-immobilization of CbFDH onto the same support was the final procedure that has been chosen to run the biotransformations.

When increasing the enzymatic loading onto the resin, a decrease in the final percentage of recovered activity has been noted, which suggests a mass transport limitation (diffusional restrictions). Nevertheless, the value of the expressed activity is still higher compared to a lower load and the higher overall activity has the aim to increment the potentiality of the immobilized enzymes.

The co-immobilized biocatalysts were then tested to evaluate their activity and stability in operational conditions. Indeed, the possibility of re-using the same support for many sequential reactions gives a greater yield of efficiency, in particular when the tool is employed for the determination of ammonia in solution. Moreover, the

trend of any loss of activity over the sequential biocatalytic conversions becomes important to predict the effectiveness of the reaction. Firstly, the two dehydrogenases co-immobilized in a ratio 1:1 were tested, but the results showed a very low conversion of  $\alpha$ -ketoglutaric acid into glutamic acid which was limited by the low activity of the formate dehydrogenase compared to the glutamate dehydrogenase (data not shown). As a result, a faster recycling of the cofactor had to be prioritized in order to have an excess of NADH always available for the full performance of the glutamate dehydrogenase. This was achieved by increasing the loading of the FDH with a higher ratio between the latter enzyme and the GluDH.

A complete co-immobilization of 5 mg/g GluDH and 40 mg/g FDH has been obtained (ratio 1:8 between the two coupled enzymes) with a recovered activity of respectively 50% and 75% as well as an expressed activity of 50 U/g and 114 U/g.

The graph presented in Figure 10 shows the operational stability of the co-immobilized enzymes as decrease in yield of conversion over sets of biotransformations, working in the same identical conditions. In details, the biocatalysts lost an average of 6% activity for every subsequent cycle, preserving a 40% activity after a set of 10 biotransformations. A complete inactivation after 17 running cycles may be estimated. Additionally, the solution of each reaction has been collected and run in an SDS-PAGE, where no bands of the biocatalysts were found, and the chance of any protein leaching has been excluded.

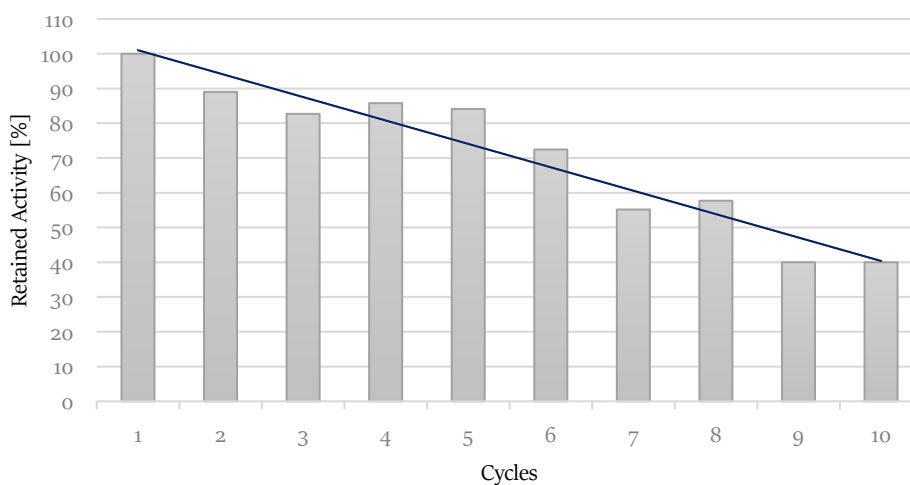


Figure 10. Operational stability of the co-immobilized enzymes. Trend shown with a dark blue line.

This outcome reveals a medium grade of stability of the system, that may be improved with further stabilization steps using compounds like glutaraldehyde to covalently bind the subunits and thus preventing their unfolding. However, the inactive enzymes could be removed as well, and the carrier reused for binding fresh and active biocatalysts, since the immobilization strategy is based on ionic interactions between the carrier and the amino acidic residues of the enzymes, which are reversible and replaceable.

### 5.2.7 Biotransformation using soluble and co-immobilized biocatalysts

Equivalent amounts of each enzyme have been used to compare the activity of the free versus the immobilized form of the two biocatalysts. Furthermore, a quantity 8 times higher of CbFDH has been loaded onto the resin with respect to the CsGluDH aiming to guarantee the continuous availability of the regenerated cofactor in the system. Samples were drawn after 10, 20 and 30 minutes of reaction and surprisingly, the 50 mM  $\alpha$ -ketoglutaric acid (1 mM NADH, 50:1) was already fully converted to glutamic acid after 20 minutes, where both the soluble and the immobilized forms were applied. In any case, the conversion yield was already 90% after 10 minutes of reaction, therefore a complete conversion may happen between the 10 and 20 minutes of biotransformation.

These results expose the great efficiency of the two dehydrogenases when employed in combination, in particular the effectiveness in terms of costs (only a very small amount of expensive cofactor is needed) as well as for the time, reaching a 100% yield only after few minutes.

Even if the operational stability reflected a loss of activity over cycles of usage, the reaction is so fast and efficient that compensates this drawback.

Furthermore, the reaction was repeated in the same conditions after 40 days of storage at 4°C and the outcomes corresponded to the previous values, proving a decent stability of the tested enzymes after the immobilization on the methacrylate support. Similarly, the activity of the soluble biocatalysts was monitored after 40 days of storage at 4°C. Nevertheless, GluDH lost 10% of its activity, while the FDH maintained only half of the initial biocatalytic activity. As a result, the soluble enzymes are less stable compared to the immobilized form.

The GluDH-FDH system was further tested to evaluate the performance in the depletion of high concentrations of ammonia, specifically 300 mM. The combination of the soluble proteins and the co-immobilized enzymes (all calculated to be in the same ratio and concentration) were employed to compare both the efficiency and the

stability in harsher conditions, where not only the 300 mM ammonium chloride but also the 400 mM  $\alpha$ -ketoglutarate and the 400 mM formate were used in an environment with high substrates concentration. Instead, the cofactor was added at only 1 mM. Surprisingly, the combination of the soluble proteins reached only 20% of conversion (Figure 11). After the 6 hours, no improvement was obtained, suggesting a stability issue of at least one of the two enzymes. On the contrary, the co-immobilized form shown increased conversion over time, reaching almost 80% conversion in the 72 hours. This probably reflects the slow regeneration of the cofactor, since the FDH amount is stoichiometric to the GluDH (same number of molecules).

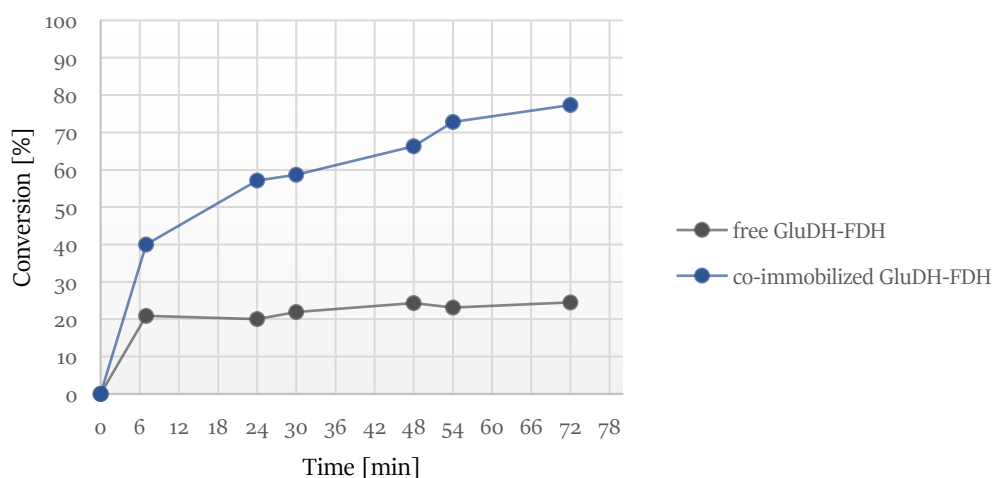


Figure 11. Conversion of GluDH and FDH in both soluble and co-immobilized forms (300 mM ammonium, 400 mM  $\alpha$ -ketoglutarate, 400 mM formate, 1 mM NADH). Protein concentration: 0.057 mg/ml for GluDH and 0.046 mg/ml for FDH.

The improved stability after immobilization is evident in such high ionic strength conditions, meaning that immobilization effectively increased the performance compared to the soluble enzymes. Also, the system can be employed for the removal of ammonia. However, it appeared to be still insufficient to fully remove the 300 mM concentration. Further optimization is required before achieving such a significant outcome.

### 5.3 CONCLUSION

Glutamate dehydrogenase from *Clostridium symbiosum* and formate dehydrogenase from *Candida boidinii* have been chosen as candidates to realize an enzymatic tool for the quantification of ammonia in solution. The efficient

coupling of the two biocatalysts was achieved through their co-immobilization on a methacrylate resin, obtaining 100% yield and high values of recovered activity. The same strategy of immobilization was applied for both dehydrogenases, meaning that less manipulation of the carrier was required, and thus shorter time of preparation and lower costs are positively involved.

The co-immobilized enzymes showed an overall good stability in storage and operational conditions, confirming the possibility to exploit them multiple times. In addition to this outcome, their efficient performance with the biocatalytic reactions has been proved with the complete conversion of  $\alpha$ -ketoglutaric acid at the 50 mM scale, which has been gained very quickly. Then, an 80% conversion of 300 mM ammonia was obtained, which was 4 times higher than for the soluble enzymes. Consequently, the co-immobilization gave increased stability in high substrates concentration.

In conclusion, the tested system has been demonstrated to be ready for its versatile application. Not only small amounts of ammonia, but also higher concentrations are detected or removed in solution. Such result cannot be achieved by usual approaches depending on NADH depletion.

The co-immobilized GluDH-FDH tool is fully available for the implementation to couple reactions in batch or flow reactions, as well as for the detection or removal of ammonia in aqueous samples.

## 5.4 BIBLIOGRAPHY

1. Molins-Legua, C., Meseguer-Lloret, S., Moliner-Martinez, Y. & Campíns-Falcó, P. A guide for selecting the most appropriate method for ammonium determination in water analysis. *TrAC - Trends Anal. Chem.* **25**, 282–290 (2006).
2. Geadah, M. L. National Inventory of Natural and Anthropogenic Sources and Emissions of Ammonia (1980). *Environ. Canada, Environ. Prot. Serv.* (1985).
3. Zhu, Y. *et al.* Development of analytical methods for ammonium determination in seawater over the last two decades. *TrAC - Trends in Analytical Chemistry* vol. 119 (2019).
4. McNeely, R. N., Neimanis, V. P. & Dwyer, L. *Water quality sourcebook: a guide to water quality parameters. Environment Canada, Inland Waters Directorate* (1979).

5. Gogoi, M. *et al.* Aquaculture effluent treatment with ammonia remover *Bacillus albus* (ASSFo1). *J. Environ. Chem. Eng.* **9**, 105697 (2021).
6. CEQG. *Canadian Water Quality Guidelines for the Protection of Aquatic Life. Canadian Environmental Quality Guidelines* (2011).
7. Kjeldsen, P., Bjerg, P. L., Rügge, K., Christensen, T. H. & Pedersen, J. K. Characterization of an old municipal landfill (Grindsted, Denmark) as a groundwater pollution source: Landfill hydrology and leachate migration. *Waste Manag. Res.* **16**, 14–22 (1998).
8. Kuajara, O., Sanchez, J. C. D., Ballestrin, R. A. & Teixeira, E. C. Environmental monitoring of the North Porto Alegre landfill, Brazil. *Water Environ. Res.* **69**, 1170–1177 (1997).
9. Barsotti, R. J. Measurement of ammonia in blood. *J. Pediatr.* **138**, (2001).
10. Azmi, N. E. *et al.* Biosensor based on glutamate dehydrogenase immobilized in chitosan for the determination of ammonium in water samples. *Anal. Biochem.* **388**, 28–32 (2009).
11. Li, D., Xu, X., Li, Z., Wang, T. & Wang, C. Detection methods of ammonia nitrogen in water: A review. *TrAC - Trends Anal. Chem.* **127**, 115890 (2020).
12. Bolivar, J. M. *et al.* Evaluation of different immobilization strategies to prepare an industrial biocatalyst of formate dehydrogenase from *Candida boidinii*. *Enzyme Microb. Technol.* **40**, 540–546 (2007).
13. Keskin, S. Y. & Keskin, C. S. Quantitative determination of glycine in aqueous solution using glutamate dehydrogenase-immobilized glyoxal agarose beads. *Appl. Biochem. Biotechnol.* **172**, 289–297 (2014).
14. Marques Netto, C. G. C. *et al.* Bovine glutamate dehydrogenase immobilization on magnetic nanoparticles: Conformational changes and catalysis. *RSC Adv.* **6**, 12977–12992 (2016).
15. Balcão, V. M., Mateo, C., Fernández-Lafuente, R., Malcata, F. X. & Guisán, J. M. Coimmobilization of L-asparaginase and glutamate dehydrogenase onto highly activated supports. *Enzyme Microb. Technol.* **28**, 696–704 (2001).
16. Bolivar, J. M. *et al.* Immobilization-stabilization of a new recombinant glutamate dehydrogenase from *Thermus thermophilus*. *Appl. Microbiol. Biotechnol.* **80**, 49–58 (2008).

17. Syed, S. E. H. & Engel, P. C. A pH-dependent activation-inactivation equilibrium in glutamate dehydrogenase of *Clostridium symbiosum*. *Biochem. J.* **271**, 351–355 (1990).
18. Hamza, M. A. & Engel, P. C. Homotropic allosteric control in clostridial glutamate dehydrogenase: Different mechanisms for glutamate and NAD<sup>+</sup>? *FEBS Lett.* **582**, 1816–1820 (2008).
19. Demir, A. S., Talpur, F. N., Betul Sopaci, S., Kohring, G. W. & Celik, A. Selective oxidation and reduction reactions with cofactor regeneration mediated by galactitol-, lactate-, and formate dehydrogenases immobilized on magnetic nanoparticles. *J. Biotechnol.* **152**, 176–183 (2011).
20. Lu, Y., Jiang, Z. yi, Xu, S. wei & Wu, H. Efficient conversion of CO<sub>2</sub> to formic acid by formate dehydrogenase immobilized in a novel alginate-silica hybrid gel. *Catal. Today* **115**, 263–268 (2006).
21. Addo, P. K., Arechederra, R. L. & Minteer, S. D. Evaluating enzyme cascades for methanol/air biofuel cells based on NAD<sup>+</sup>-dependent enzymes. *Electroanalysis* **22**, 807–812 (2010).
22. Ansorge-Schumacher, M. B., Slusarczyk, H., Schümers, J. & Hirtz, D. Directed evolution of formate dehydrogenase from *Candida boidinii* for improved stability during entrapment in polyacrylamide. *FEBS J.* **273**, 3938–3945 (2006).
23. Kim, M. H., Park, S., Kim, Y. H., Won, K. & Lee, S. H. Immobilization of formate dehydrogenase from *Candida boidinii* through cross-linked enzyme aggregates. *J. Mol. Catal. B Enzym.* **97**, 209–214 (2013).
24. Netto, C. G. C. M., Nakamura, M., Andrade, L. H. & Toma, H. E. Improving the catalytic activity of formate dehydrogenase from *Candida boidinii* by using magnetic nanoparticles. *J. Mol. Catal. B Enzym.* **84**, 136–143 (2012).
25. López-Gallego, F., Guisan, J. M. & Betancor, L. *Immobilization of Enzymes on Supports Activated with Glutaraldehyde: A Very Simple Immobilization Protocol. Methods in Molecular Biology* vol. 2100 (2020).
26. Vinet, L. & Zhedanov, A. A ‘missing’ family of classical orthogonal polynomials. *Journal of Physics A: Mathematical and Theoretical* vol. 44 (2011).
27. Hamza, M. A. & Engel, P. C. Enhancing long-term thermal stability in mesophilic glutamate dehydrogenase from *Clostridium symbiosum* by eliminating cysteine residues. *Enzyme Microb. Technol.* **41**, 706–710 (2007).

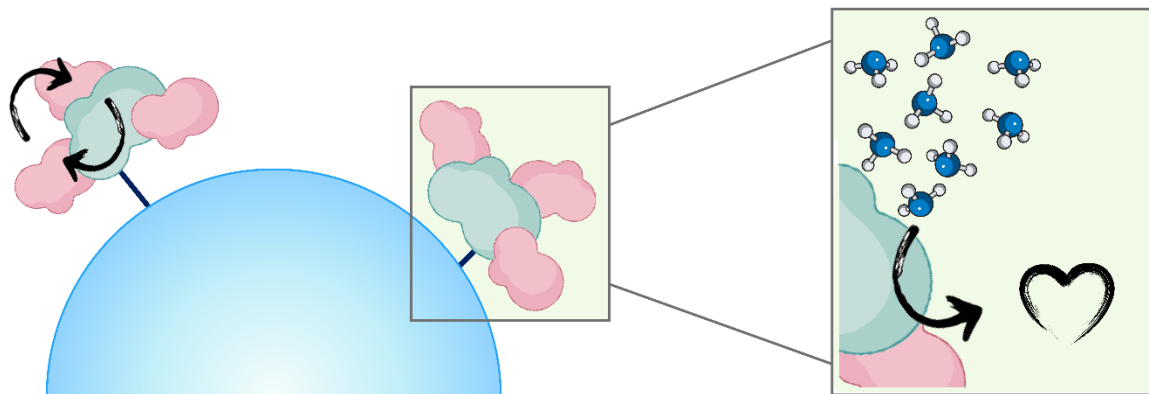
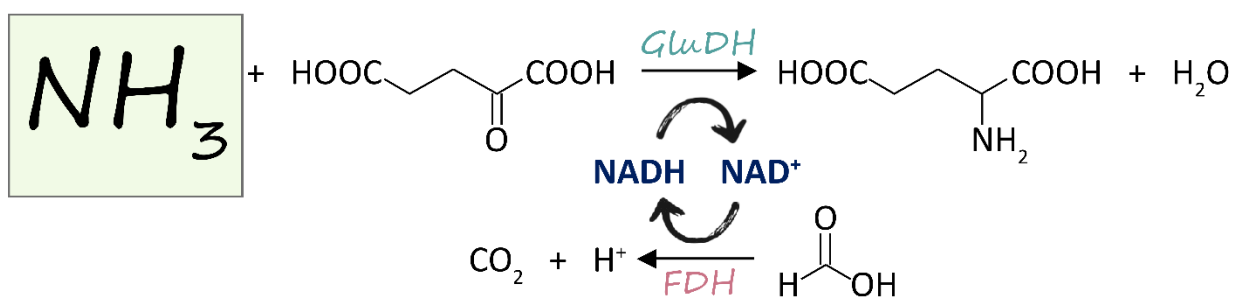


28. Sharkey, M. A. & Engel, P. C. Modular coenzyme specificity: A domain-swapped chimera of glutamate dehydrogenase. *Proteins Struct. Funct. Bioinforma.* **77**, 268–278 (2009).
29. Wang, X. G. & Engel, P. C. Positive Cooperativity with Hill Coefficients of Up to 6 in the Glutamate Concentration Dependence of Steady-State Reaction Rates Measured with Clostridial Glutamate Dehydrogenase and the Mutant A163G at High pH. *Biochemistry* **34**, 11417–11422 (1995).
30. Baker, P. J. *et al.* Subunit assembly and active site location in the structure of glutamate dehydrogenase. *Proteins Struct. Funct. Bioinforma.* **12**, 75–86 (1992).
31. Roura Padrosa, D., Marchini, V. & Paradisi, F. CapiPy: python-based GUI-application to assist in protein immobilization. *Bioinformatics* **37**, 2761–2762 (2021).
32. Stillman, T. J., Baker, P. J., Britton, K. L. & Rice, D. W. Conformational flexibility in glutamate dehydrogenase: Role of water in substrate recognition and catalysis. *Journal of Molecular Biology* vol. 234 1131–1139 (1993).
33. Cayot, P. & Tainturier, G. The quantification of protein amino groups by the trinitrobenzenesulfonic acid method: A reexamination. *Anal. Biochem.* **249**, 184–200 (1997).

## CHAPTER 6.

### DEVELOPMENT OF GLUTAMATE AND FORMATE DEHYDROGENASE FUSION PROTEIN AS BIFUNCTIONAL BIOCATALYTIC TOOL FOR THE EFFICIENT CONTINUOUS REMOVAL OF AMMONIA

---



## 6.1 INTRODUCTION

A fusion protein is a molecule consisting of two or more protein domains incorporated into one single complex. Naturally occurring fusion proteins are widespread, and their modular organization has been identified as an important evolutionary phenomenon.<sup>1,2</sup>

Artificial fusion proteins may be designed to achieve improved properties or new functionality.<sup>1</sup> For this purpose, the combination of two proteins to generate a bifunctional enzyme complex has been attempted over the years.<sup>3</sup> In particular, fusion enzyme engineering is one of the promising approaches for *in situ* efficient regeneration and reuse of the cofactors for cost-effective reactions.<sup>4</sup> As a matter of fact, the cofactor is too expensive to be applied in stoichiometric amounts, therefore a recycling system is necessary to reduce costs.<sup>5</sup> Moreover, a fusion protein can dramatically simplify the phases of expression, purification or immobilization, since one single protein presenting the activity of two (or more) distinct enzymes has to be manipulated. This results in decreased investment on time, materials and costs.

The use of GluDH to bioconvert the toxic ammonia was described in the previous chapter. Similarly, this enzyme has been coupled with the FDH to continuously regenerate the cofactor. Both the two proteins were co-immobilized on the same support and applied in biotransformations. However, the system required some optimization due to the slow conversion of high amount of ammonia, which did not achieve full conversion. As a result, these two enzymes appear perfect candidates for the development of a fusion protein to yield a more efficient biocatalyst.

The FDH is considered the enzyme of choice as recycling cofactor system, since the formate reaction is irreversible and the produced CO<sub>2</sub> can be easily separated.<sup>6</sup> Thus, including the FDH in the construction of a fusion protein is of high interest and indeed, attempts have been already accomplished with successful results: fusion proteins with the CbFDH combined to a phenylalanine dehydrogenase (PheDH), an octameric leucine dehydrogenase (LeuDH) and recently, an azoreductase (AzoRo) have been reported, even if the last protein presented a mutated form of CbFDH (C23S).<sup>7-9</sup> On the contrary, the GluDH has never been implemented to the generation of a fusion protein before the current work.

A novel fusion protein combining the hexameric CsGluDH with the dimeric CbFDH has been rationally designed, aiming for a closer proximity of the two biocatalysts. In this way, the migration of the cofactor between their active sites is accelerated through substrate channeling without first diffusing to the bulk environment.<sup>10</sup>

The reaction of interest is shown in Figure 1, where the two biocatalytic activities are combined while sharing the cofactor.

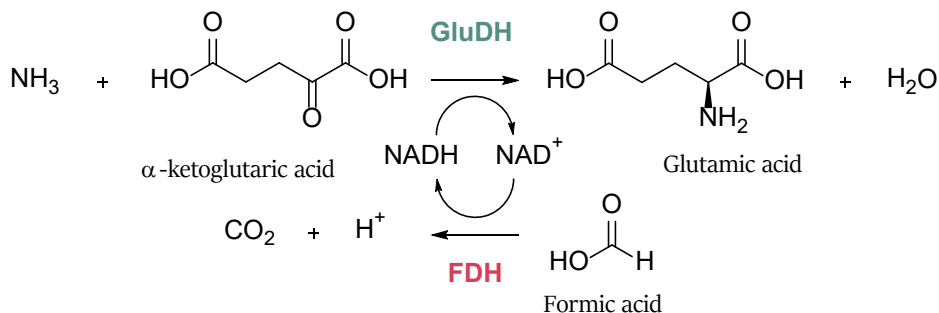


Figure 1. Reaction scheme of the bifunctional fusion protein of GluDH and FDH.

The new enzymatic complex was subjected to a series of tests to assess activity, stability, and structural conformation. Moreover, the fusion protein has been immobilized to enhance the efficiency of the bifunctional system, which was additionally proven by performing biotransformations.

The work presented in this chapter is my exclusive contribution unless otherwise stated. David Roura Padrosa worked on the MD simulation and prediction of the fusion protein assembly.

The current work has been included in the following publication:

V. Marchini, A. I. Benítez-Mateos, D. Roura Padrosa, F. Paradisi “*Fusion of glutamate dehydrogenase and formate dehydrogenase yields a bifunctional efficient biocatalyst for the continuous removal of ammonia*” *Frontiers in Catalysis* **2021**, 1, art 790461.

## 6.2 RESULTS AND DISCUSSION

### 6.2.1 Genetic construction of the GluDH-FDH fusion protein

The genetic construction of the recombinant fusion protein has been developed using the original plasmid encoding the CbFDH as a template, where the His-tag was located in the N-terminal. Then, CsGluDH gene was

inserted downstream of CbFDH DNA sequence, to enable the correct folding of the GluDH C-terminal domain which loops into the internal cavity of the hexameric complex when the quaternary structure is formed.<sup>11-13</sup> The stop codon inserted after CbFDH gene was thus removed to ensure that the overexpression was including CsGluDH in the protein formation. A 9 aa linker was inserted between the two domains acting as a spacer to avoid undesirable outcomes, including misfolding of the fusion protein, low yield in protein production or impaired bioactivity.<sup>14</sup> As a matter of fact, linkers are ubiquitously observed in naturally occurring multidomain proteins with the function of maintaining necessary distance to reduce steric hindrance and/or permit favorable domain-domain interaction between the two protein moieties.<sup>1</sup>

The final genetic construction of (N-His<sub>6</sub>-tag)-FDH-linker-GluDH is shown in Figure 2.

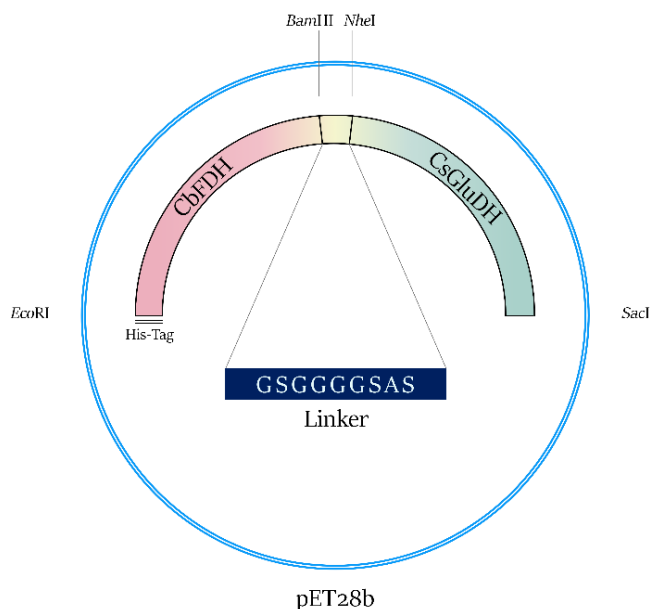


Figure 2. Genetic construction of the plasmid of recombinant fusion protein GluDH and FDH.

Firstly, the linker has been designed to present glycine and serine in the sequence, as these small polar amino acids may provide good flexibility and maintain stability in water (the linker is more likely to be exposed to the solvent). Secondly, two flanking restriction sites have been implemented to facilitate direct modification of the genetic sequence (length of the linker, flexibility, amino acids involved, etc.). *Bam*HI and *Nhe*I have been chosen for this purpose, since they are not contained in any other site of the entire construction and the translated amino acids follow the requirement described in the previous statement. Indeed, *Bam*HI restriction site encodes glycine

(GGA) and serine (TCC), while *NheI* translates alanine (GCT) and serine (AGC). Finally, the length resulted to be a compromise where the distancing between the two protein domains was effectively supplied and the primers involved in the gene cloning were not too long for being inefficient. The linker consisted of the following protein sequence: Gly-Ser-Gly-Gly-Gly-Gly-Ser-Ala-Ser.

Moreover, the genetic construction was designed to include an additional restriction site at the very beginning of CbFDH gene and one at the very end of CsGluDH DNA sequence, creating a modular and versatile system. This allows the exchange of the genes to develop other fusion proteins, as well as the incorporation of a further fusion protein involved in the catalytic reaction system. For this aim, *EcoRI* and *SacI* were chosen.

Computational studies have been performed to probe the rationale behind the gene design, before proceeding with the experimental development of the fusion protein. The PDB file resulting from the *in-silico* analyses supported the insertion of the 9 aa linker to facilitate the correct assembly of each subunit. As shown in Figure 3, the six subunits are favored to assemble, presenting the hexameric GluDH in the center (green color) of the quaternary structure. The fused FDH subunits are exposed to the bulk to form three assembled dimers (pink color) enabling proper folding without any major distortion.

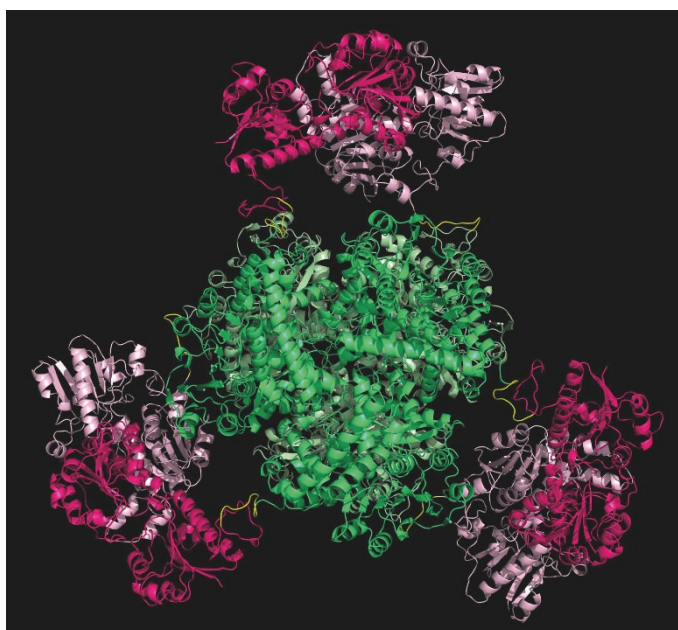


Figure 3. Modelling of the hexamer fusion protein construct created with molecular modelling and minimized with openMM.<sup>15</sup> GluDH assembly in green and FDH dimers are in pink. Graphic visualization and editing in Pymol.<sup>16</sup>

As for the amplification of the insert, the TOUCH-UP PCR was chosen for the annealing temperature increasing each cycle (from a low to a high value) that allowed to enhance the specificity of primer binding. Accordingly, the efficiency of the amplification was reduced, but the quantity of amplified insert fragments was still enough to bind the PCR product of the vector in the Gibson assembly, since the length of the first ones was only 1.4 kb while the second DNA fragments were long 6.4 kb.

On the opposite, the TOUCH-DOWN PCR of the vector involved a decreasing annealing temperature for every subsequent set of cycles (from a high to a low value) to permit more efficient amplification and so improving the yield of PCR product formation, not very high given the length of the vector (6.4 kb).

After the digestion with the restriction enzyme *DpnI*, all the methylated templates (the original plasmids of GluDH and FDH) were destroyed. Consequently, the obtained solutions were presenting only the PCR products without other DNA chains interfering.

Through the Gibson assembly method, the linker and the GluDH sequence have been joined with the sequence of the formate dehydrogenase to successfully assemble a double-stranded fully sealed DNA sequence of the recombinant fusion protein.

After transforming the assembled plasmid, the LB agar plate presented two bacterial colonies. Their purified plasmids were digested in parallel by cleaving the linker-GluDH sequence from the vector at *BamHI* and *SacI* restriction sites, and samples ran on the agarose gel.

Either the gel or the DNA sequencing confirmed that the first sample was effectively corresponding to the predicted gene, while the second sample did not match with the expected sequence.

### **6.2.2 Expression optimization**

Three different concentrations of IPTG and two temperatures were chosen to find the optimal conditions of overexpression in LB media.

All the outcomes are shown in Table 1, while the rate of production and the solubility of the overexpressed enzymes are visible in the SDS-PAGE (Figure 4).

Table 1. Outcomes for GluDH-FDH fusion protein after screening the different conditions of protein overexpression.

Expression Conditions			Weight of pellet [ g / L ]	Activity of the crude extract	
Media	IPTG Concentration [mM]	Temperature [°C]		GluDH [U/mL]	FDH [U/mL]
LB	1	20	6.8	357.6	1.02
	0.5		5.6	378.1	1.17
	0.1		6.4	407.7	1.24
LB	1	37	6.8	0.95	/
	0.5		8.4	0.85	/
	0.1		6.4	1.18	/
Autoinduction	/	20	15.4	2.2	0.13

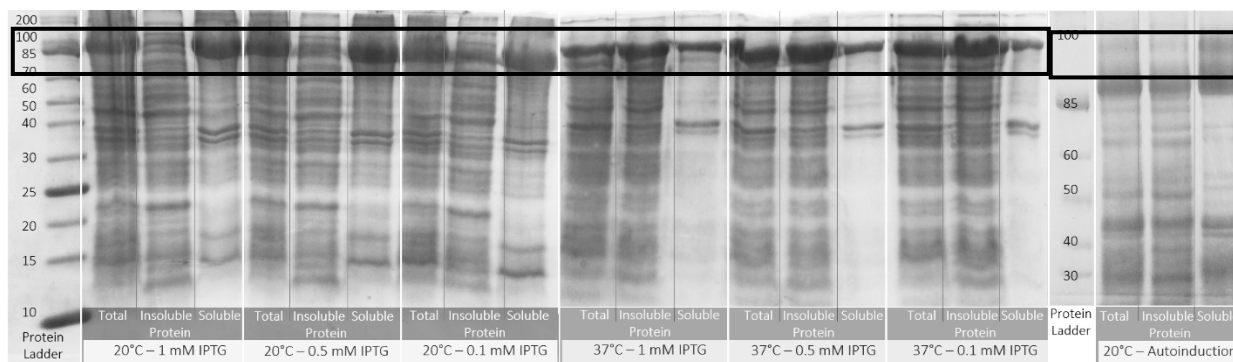


Figure 4. SDS-PAGE for screening the optimal condition of fusion protein overexpression. Scale of protein ladder: kDa.

A higher number of cells was obtained using autoinduction media, but the corresponding enzymatic activity was significantly lower than the activity given by proteins grown in LB media at 20°C, despite the probable higher protein concentration. Similarly, the activity of the crude extract obtained from the cultures grown at 37°C was very low or even undetectable.

Considering the big size of the fusion protein, a lower concentration of inducer together with a lower temperature of incubation corresponded to a slower protein synthesis rate that implied a greater amount of time for the



proteins to fold properly. The enzyme needs to be folded in the right way to be active and therefore perform the biocatalytic reaction. Furthermore, a lower temperature avoids the undesired formation of inclusion bodies. This was proved by the SDS-PAGE, because less insoluble proteins were formed by incubating the flasks at 20°C. The band of the fusion protein is placed at 93 kDa (Figure 4). A temperature of 20°C and an expression in LB media induced with 0.1 mM of IPTG were chosen as optimum conditions for larger scale overexpression.

### 6.2.3 Larger scale overexpression and purification

After overexpressing the GluDH-FDH fusion protein in 300 mL LB media, approximately 5 grams of pellet per liter of culture were produced, which were then purified and 40-60 mg of protein per liter of culture were obtained. The efficiency of the purification process was verified by SDS-PAGE, as shown in Figure 5. The fusion protein subunits were found in the flow through, meaning that there was some loss during the process. For this reason, the flow through was collected and loaded a second time to the column. Given the large dimension of the protein, it is possible that the binding between the protein and the column requires time. Although some fusion protein has been lost also in the second flow through, the collected quantity was still enough to work with. The first elution step effectively removed the unspecific proteins, so that the protein was successfully purified, as confirmed by the prevalence of overexpressed protein in the last collected sample.

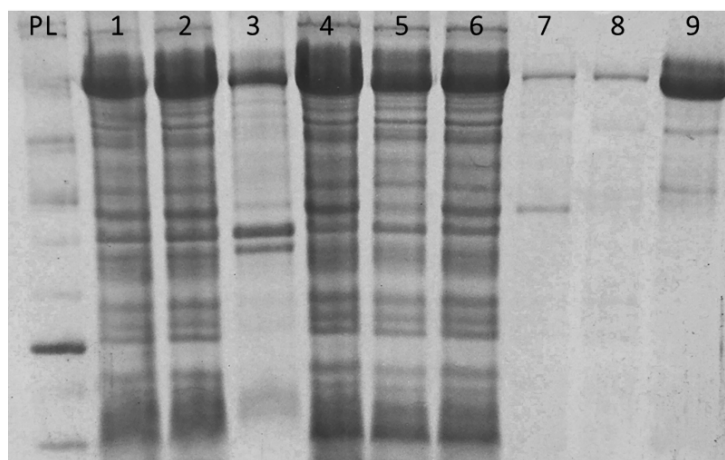


Figure 5. SDS-PAGE: purification of GluDH-FDH fusion protein. 1: pellet, 2: lysate, 3: cell paste (insoluble proteins), 4: crude extract, 5: 1st flow through, 6: 2nd flow through, 7: washing step (buffer A), 8: washing step (10% buffer B), 9: after dialysis.

### 6.2.4 Activity and stability

The specific activity of the fusion protein was determined for both catalytic domains (GluDH and FDH) and compared with the activity of the wild-type enzymes. The monomeric molecular mass of the latter ones (GluDH 53 and FDH 43 KDa) is about half than the fusion protein (93 KDa), therefore the results reported in Table 2 are normalized for concentration of each individual enzyme.

To find the weight of GluDH and FDH that contains the same moles as 1 mg of fusion protein:

$$\text{Molarity Fusion Protein} = \text{Molarity WT Protein}$$

$$\frac{\text{Weight fusion protein}}{\text{Volume} \times \text{MW fusion protein}} = \frac{\text{Weight WT protein}}{\text{Volume} \times \text{MW WT protein}}$$

$$\text{For FDH: } \frac{0,001 [g]}{0,001 [L] \times 93 [KDa]} = \frac{\text{Weight FDH [g]}}{0,001 [L] \times 43 [KDa]}$$

$$\text{Weight FDH} = \frac{0,001 [g] \times 43 [KDa]}{93 [KDa]} = \frac{43}{93} KDa = \mathbf{0.46 mg}$$

$$\text{For GluDH: } \frac{0,001 [g]}{0,001 [L] \times 93 [KDa]} = \frac{\text{Weight GluDH [g]}}{0,001 [L] \times 53 [KDa]}$$

$$\text{Weight GluDH} = \frac{0,001 [g] \times 53 [KDa]}{93 [KDa]} = \frac{53}{93} KDa = \mathbf{0.57 mg}$$

The two domains exhibited very similar activity to the wild-type proteins with an average of 86.4% of GluDH and an 80% of FDH activity. This outcome is consistent with a previous report where the FDH moiety retained less parental activity than partner enzyme.<sup>7</sup> Likewise, around an 80% of retained activity was obtained by the FDH of that fusion protein, which was presenting the flexible linker (GSSSS)<sub>2</sub>, very similar to the linker of the current study.

The great retained activity confirmed the proper folding of the subunits as predicted by the molecular modelling. They were clearly assembled without any major distortion, meaning that the GluDH possessed a hexameric quaternary structure as the wild-type, while the FDH presented a dimeric configuration.

Table 2. Specific activity of the two domains of the purified fusion protein compared to the normalized specific activity of the wild-type enzymes (shown only as reference values without the standard deviations).

	Formate dehydrogenase	Glutamate dehydrogenase	
		Amination	Deamination
Fusion protein	1.2 ± 0.2 [U/mg]	135 ± 6 [U/mg]	17.0 ± 0.5 [U/mg]
Wild-type enzymes	1.5	156	19.7

The kinetic constants for the various substrates are shown in Table 3. The assays of GluDH were performed at pH 8.0 in order to provide a better evaluation of the results of this work with respect to previously reported values.<sup>17</sup>

On the contrary, the specific activity was measured at pH 7.5 as compromise between stability/activity of both domains of the fusion protein. The different pH numbers were the reason why the values presented in Table 2 for GluDH were dissimilar from the values of the same enzyme shown in Table 3.

Table 3. Kinetic constants for the fusion protein, the glutamate- and the formate dehydrogenase.

	Fusion protein - GluDH		Wild-type CsGluDH	
	K <sub>M</sub> [mM]	V <sub>max</sub> [mmol min <sup>-1</sup> mg <sup>-1</sup> ]	K <sub>M</sub> [mM]	V <sub>max</sub> [mmol min <sup>-1</sup> mg <sup>-1</sup> ]
L-Glutamate	2.9 ± 0.8	0.04 ± 0.01	3.0 ± 1.1	0.08 ± 0.01
α-Ketoglutarate	0.41 ± 0.22	0.07 ± 0.05	0.48 ± 0.31	0.13 ± 0.1
Ammonia	32.5 ± 10.0	0.18 ± 0.06	32.3 ± 10.0	0.36 ± 0.15
NADH	0.20 ± 0.08	0.06 ± 0.05	0.10 ± 0.06	0.12 ± 0.1
NAD <sup>+</sup>	0.17 ± 0.04	0.02 ± 0.01	0.17 ± 0.02	0.05 ± 0.02
	Fusion protein - FDH		Wild-type CbFDH	
	K <sub>M</sub> [mM]	V <sub>max</sub> [μmol min <sup>-1</sup> mg <sup>-1</sup> ]	K <sub>M</sub> [mM]	V <sub>max</sub> [μmol min <sup>-1</sup> mg <sup>-1</sup> ]
Formate	6.0 ± 1.0	1.0 ± 0.3	5.0 ± 1.0	3 ± 1
NAD <sup>+</sup>	0.088 ± 0.014	1.0 ± 0.4	0.168 ± 0.030	5 ± 1

The resulting  $K_M$  values were comparable between the fusion protein and the WT enzymes. The maximum velocities ( $V_{max}$ ) of the fusion protein were the half compared to the value obtained for the WT GluDH, while 3 and 5 times lower in comparison to the WT FDH. However, this simply reflects the difference of weight between WT and fusion protein, where the last one has approximately twice the weight of the original enzymes. Therefore, the rate of conversion has been conserved after the fusion.

The FDH domain showed a lower  $K_M$  value towards  $NAD^+$  compared to the WT, while the GluDH had a decreased affinity for the NADH after the fusion. The same alteration of the cofactor kinetic parameters was found in the LeuDH-FDH fusion protein.<sup>7</sup> It has been suggested that the different affinity values towards the cofactor were caused by moiety-moiety interactions or the proximity of two cofactor binding domains in the fusion enzymes.<sup>7</sup> The affinity to the substrates has not been affected by the linkage of the two protein domains, meaning that no destabilization of the quaternary structure happened.

It has been chosen to test together the activity and the stability to avoid any change of conditions that would cause an adjustment in conformation of the enzymes with a consequent loss of the linearity of the curve to quantify the rate of conversion. Indeed, this glutamate dehydrogenase has been reported to undergo a reversible conformational change from an “active” to an “inactive” form that is pH, temperature and ionic strength dependent, where re-activation is complete after 40 minutes at 25°C but negligible even after 2 hours at 4°C<sup>18</sup>. Moreover, monitoring activity and stability at the same time has the advantage to give a better information for a practical point of view. Indeed, a biotransformation involves both the two aspects together.

The stability and activity of the fusion protein over time after its incubation at different pH values ranging from 5 to 10 are shown in Figures 6 and 7. The curves of the enzyme pairs are comparable, confirming the similar behavior of the fusion protein with the original biocatalysts.

As for the GluDH, the maximum activity was obtained at pH 7.5, while the pH values lower than 6 and higher than 9 showed to be fatal for both the biocatalysts. After 48 hours, the loss of activity was around 10-20%, indicating a good stability over time. Similarly, the activity of the FDH in both forms showed to be higher around neutral pH values as well as null at pH 5 and 10. Furthermore, the 80-90% of the activity was still retained after 48 hours at pH 7/7.5.

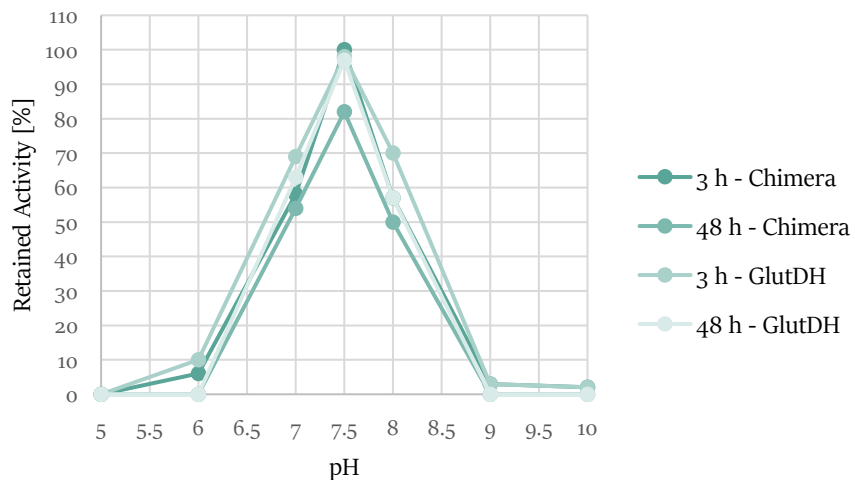


Figure 6. Stability and activity at different pH values for GluDH.

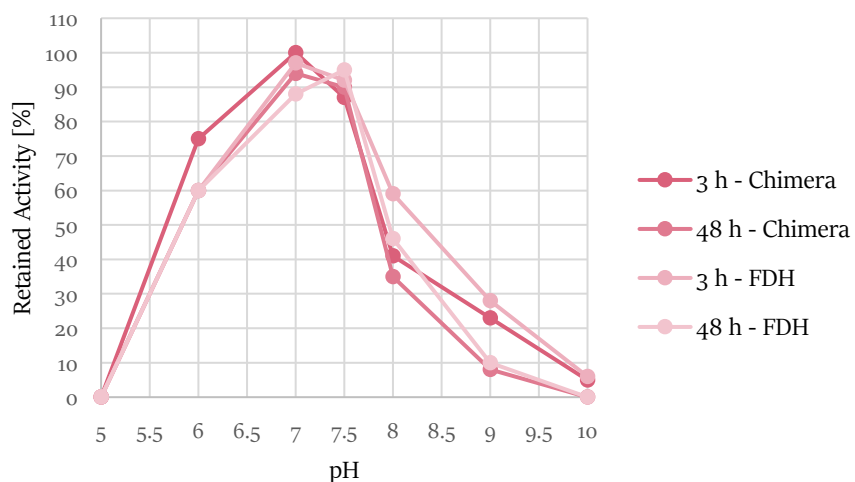


Figure 7. Stability and activity at different pH values for FDH.

The activity of the enzymes at 37°C was higher compared to the activity at 25°C with around 1.7-fold for the GluDH reaction and 1.8-fold for the FDH related to both the fusion protein and the WT biocatalyst.

After incubating them at 37°C for 24 and 48 hours, the activity was constant at its maximum with any loss in activity, as shown in Figures 8 and 9. Moreover, one hour of incubation was not enough for a complete adjustment of the quaternary structure since the activity of the GluDH in both species was a 70% in comparison to the activity of the 24 and 48 hours.

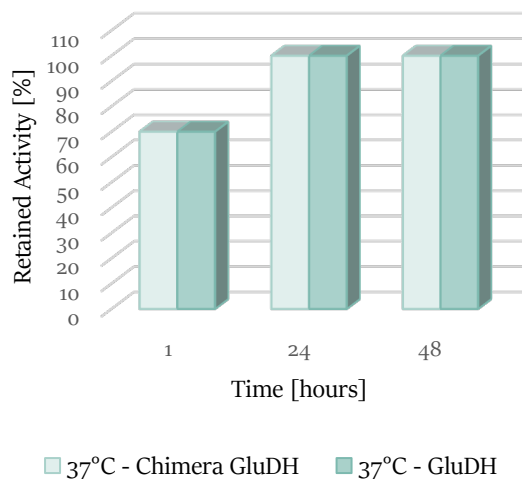


Figure 8. Stability and activity at 37°C for the glutamate dehydrogenase.

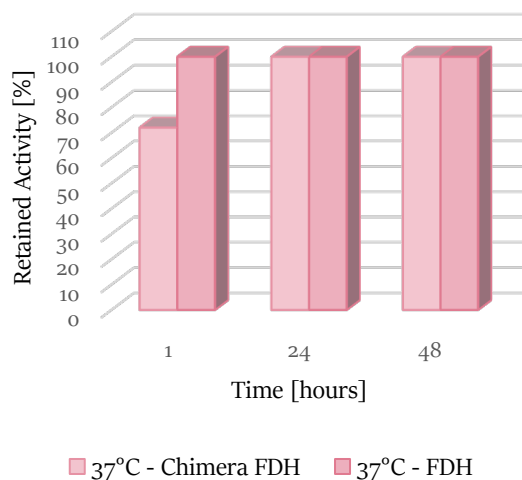


Figure 9. Stability and activity at 37°C for the formate dehydrogenase.

The WT FDH did not show this behavior of re-activation, indeed the activity after one hour of incubation was the same found for the following 24/48 hours. On the contrary, the FDH contained in the fusion protein presented a 70% activity after one hour as happens for the GluDH. Surprisingly, the conformational change of the GluDH involved a subsequent change also in the conformation of the FDH fusion protein, which developed the same reversible change from an “active” to an “inactive” form.

The fusion protein presented the same profiles as the wild-type enzymes for both pH and temperature activity/stability. Furthermore, the FDH moiety acquired a cooperative behavior that is typical of the GluDH but does not occur in the WT FDH. The fusion, therefore, led to a tight connection between the two enzymes where one domain is dependent to the other for structural modifications induced by temperature shift, for example.

### 6.2.5 Assembly evaluation

The GluDH and the FDH are typically assembled in a hexamer and a dimer, respectively, which are required to get a stable and fully active quaternary structure. Since the subunits of the fusion protein combine the two domains fused one with the other, the final assembly may be altered with drastic consequences. Thus, it is essential to investigate the oligomerization behavior of the monomers. For this purpose, two techniques were employed: the MD simulation to predict the plausible assembly of the quaternary structure, as already mentioned, and a SEC to confirm the previous data.

The calibration curve was created by running the protein standards (Figure 10).

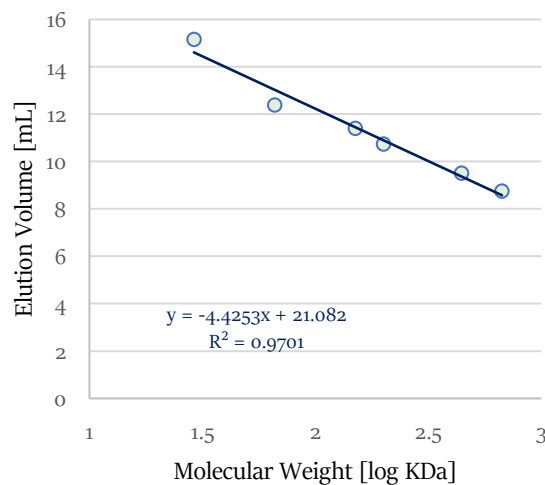


Figure 10. Graph of the protein standards applied to the gel filtration column (SEC). In ascending order by molecular weight: carbonic anhydrase (29 KDa - 15.15 min), albumin (66 KDa - 12.39 min), alcohol dehydrogenase (150 KDa - 11.4 min),  $\beta$ -amylase (200 KDa - 10.74 min), apoferritin (443 KDa - 9.51 min), thyroglobulin (669 KDa - 8.75 min). The final equation is shown in blue.

The SEC chromatogram obtained with the fusion protein is shown in Figure 11.

The different conformations were found at 7.6, 8.51, 8.98 and 11.4 minutes. By plotting these values in the calibration curve equation, the sizes 1111, 694, 544, 156 KDa were calculated. The molecular weight of the monomer is 93 KDa.

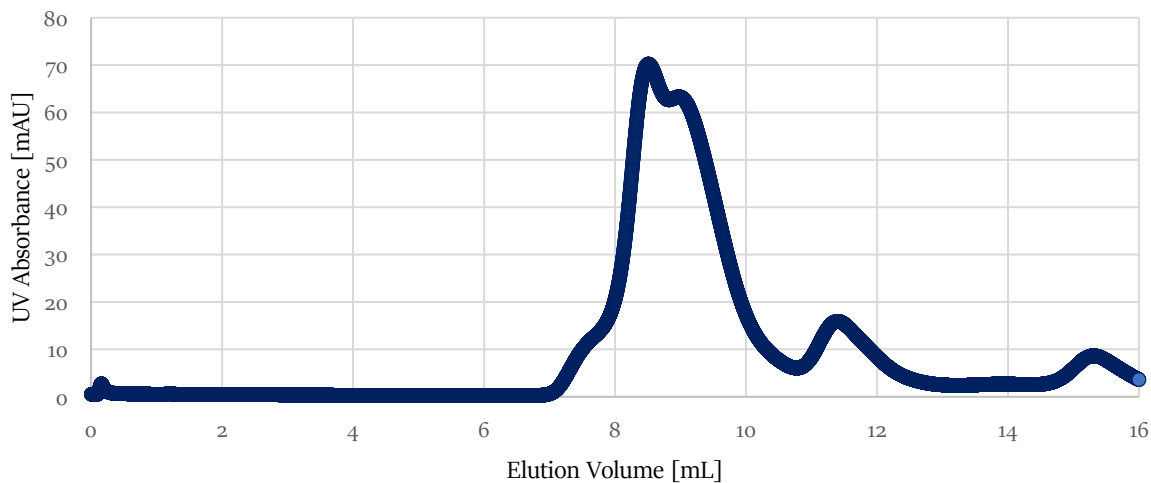


Figure 11. Chromatogram of the fusion protein conformations by SEC (blanked).

The molecular weight of the assembled fusion protein was estimated by fitting the collected data to the equation of the calibration curve, which was determined from the elution time of each protein standard.

The chromatogram showed two main large peaks, that corresponded to the molecules having six and eight subunits. In addition, other two small peaks were observed, which were related to the molecular weight of two and twelve subunits.

In accordance with the *in-silico* results, it has been confirmed that predominantly the hexameric and octameric form with traces of assembled 2 and 12 monomers are assembled.

The hypothetical configurations are shown in Figure 12.

It is worthy to remark that the final conformation is based on an equilibrium between the four different combinations of the subunits. On varying such equilibrium and the applied working conditions, the ratio may differ and accordingly, the activity of the protein domains might be subjected to small alteration.



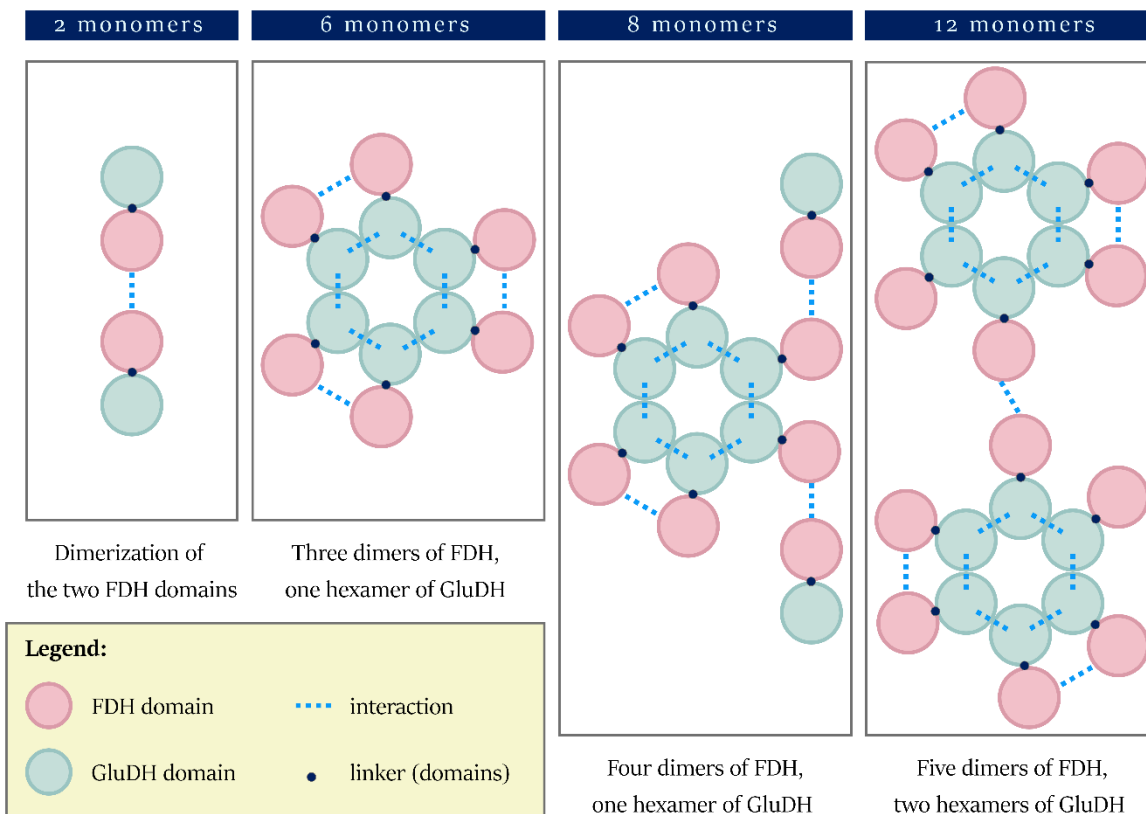


Figure 12. Schematic assembly of the fusion protein monomers.

### 6.2.6 Protein immobilization

The fusion protein has been immobilized to enhance its stability over time and over consecutive cycles of usage. Considering the results obtained in the previous chapter, it has been already demonstrated that both enzymes are efficiently immobilized on supports activated with glyoxyl groups and then coated with PEI.

Furthermore, the CapiPy tool was employed to confirm the efficiency of the immobilization strategy, since the new assembly may have changed the exposed clusters of amino acid residues available for the binding to the resin. CapiPy offered an evaluation of the protein surface through a detailed analysis of the structure, whose model was given by minimizing a manually assembled hexameric conformation followed by minimization with openMM.<sup>15</sup> The final quaternary structure is shown in Figure 13, where it is evident that negative charged groups (red) are still highly spread throughout the surface of the hexamer, offering many points of interactions with positively charged groups. Therefore, the coating of a support with PEI offers easy interaction with the aspartate

and glutamate clusters of the fusion protein. Also, the introduced high number of amino groups create a more hydrophilic, and thus favorable, environment for the enzyme.

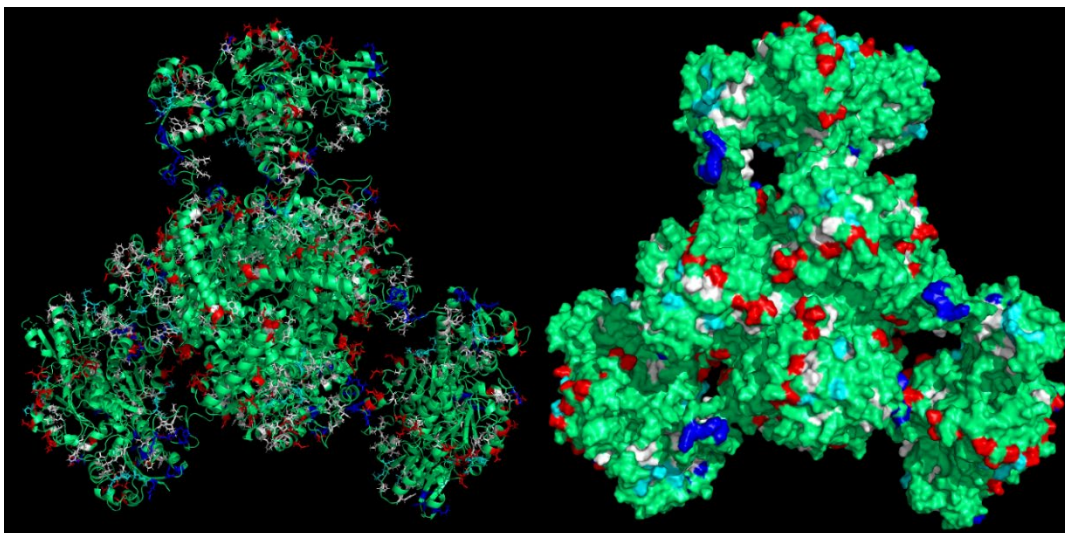


Figure 13. 3D structure of the assembled fusion protein retrieved from CapiPy tool after minimization and analysis.<sup>19</sup> Visualized and edited in Pymol.<sup>16</sup> Left: cartoon and licorice sticks for colored amino acids. Right: surface visualization.

The polymethacrylate epoxy resin ReliSorb EP400/SS has been selected as a support, since it showed good outcomes for the WT proteins. The material of the resin offered a robust support to the enzyme, while the porosity gave many points of anchoring.

The enzyme was efficiently bound through ionic interactions. This favored the retention of enzyme flexibility which is essential for its activity since it undergoes a conformational change from an “active” to an “inactive” form, where the six subunits have the capacity for cooperative interaction.<sup>18,20</sup> A complete immobilization yield was achieved, with no remaining protein in the supernatant. As indicated in Figure 14, a recovered activity of 50 and 100% for GluDH and FDH, respectively, was obtained with a loading of 1 mg of protein per Gram of support. Differently from the sequential co-immobilization of the WT enzymes, the two domains of the fusion protein have been simultaneously immobilized since their fusion did not allow for a sequential approach. Increasing the loading to 5 mg/g of support caused a slight decrease to 35% for GluDH and 85% for FDH in recovered activity. This was further reduced at 10 mg/g of loading (30% for GluDH and 60% for FDH) indicating a diffusion limitation issue. In all the cases, however, the retained activity was high and good enough to try biotransformations.

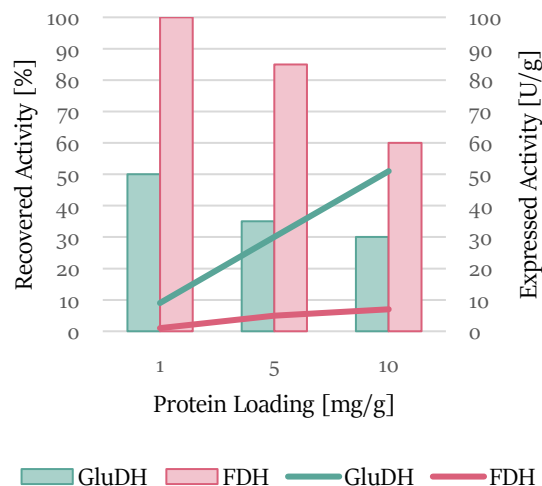


Figure 14. Recovered activity (bars) and expressed activity (lines) after the immobilization of the fusion protein onto ReliSorb EP400/SS, loading an increasing amount of protein.

The WT GluDH showed 85% recovered activity with a loading of 1 mg of protein. In comparison, the fusion protein domain achieved a lower recovered activity (50%), maybe due to a reduced flexibility when immobilized as fusion protein. On the opposite, the FDH domain recovered full activity as for the WT enzyme when loading 1 mg/g. Moreover, the WT FDH achieved only 45% recovered activity with 5 mg/g of loading, while the FDH domain of the fusion protein retained higher activity with increased loading. Consequently, the two domains behaved differently in terms of recovered activity with respect to the single enzymes, one with opposite trend compared to the other. However, favoring the activity of FDH, even if at the expense of GluDH, is required to allow an efficient cofactor recycling system, as seen in the previous chapter, where the FDH was the limiting factor when immobilized with low ratio GluDH - FDH.

### 6.2.7 Operational stability

The stability of the immobilized fusion protein was tested over different cycles of biotransformation using 50 mM  $\alpha$ -ketoglutarate as indicator of the activity for each sequential reaction. In preliminary studies, the 1 mg protein immobilized onto 1 gram of resin was employed, but the results confirmed the rate-limitation presented by the low activity of FDH (data not shown). Consequently, operational stability tests were repeated with a more active

resin prepared with 10 mg/g of biocatalyst. The linear trend of retained activity over subsequent cycles is shown in Figure 15. The immobilized biocatalyst can be reused for 10 times maintaining half of the initial activity.

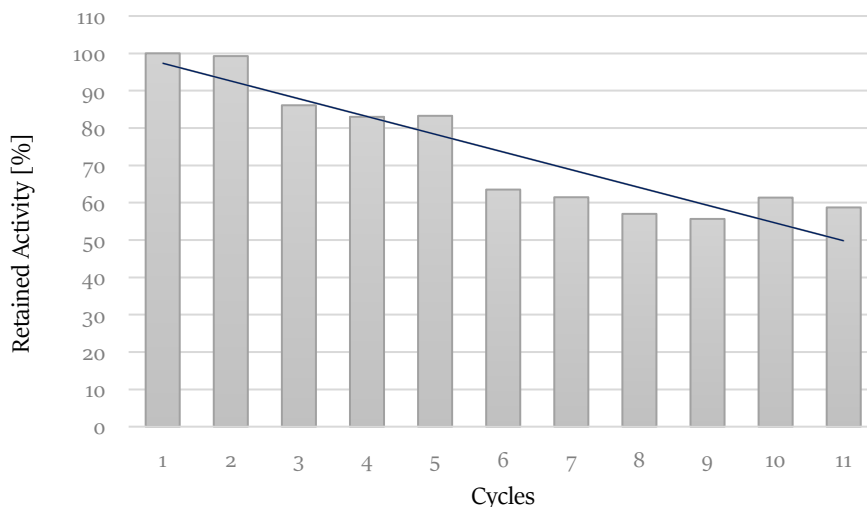


Figure 15. Operational stability of the immobilized fusion protein over 11 cycles of usage. The trendline is shown in dark blue.

Knowing that the enzyme is immobilized through reversible interactions on PEI, the good stability over cycles is a promising result for the reusability and the application in flow reactions. Indeed, this allows for a more sustainable and efficient system.

In this context, it is important to mention the use of the immobilized fusion protein in Chapter 4 in combination with AvPAL. Despite the low conversion of the PAL deamination, the fusion protein demonstrated the capacity of effectively coupling the reaction, readily converting the produced ammonia into glutamate. The immobilized fusion protein was applied in continuous flow reaction for several cycles, using different conditions. Afterwards, the activity was tested, and the enzyme showed to be fully active. Consequently, the stability of the immobilized biocatalyst has been proved even in flow system.

A stable self-sufficient biocatalyst was created and immobilized on a solid support. The construction of such bienzymatic system which enables successful immobilization is a step forward in terms of efficiency, optimization, and cost-effectiveness with respect to the well-known co-immobilization strategy of two separate enzymes.

### 6.2.8 Biotransformations of $\alpha$ -ketoglutarate with free and immobilized fusion protein

It has been decided to attempt biotransformations with the aim to assess the efficiency of the system, which involves the GluDH converting ammonia and  $\alpha$ -ketoglutarate into glutamic acid, with sub-stoichiometric amounts of NADH, and the FDH to regenerate continuously the cofactor. The reactions were performed with the immobilized fusion protein, which was compared to the results attained from the biocatalytic reaction done with the free protein.

The percentage of conversion has been defined by the depletion of the substrate  $\alpha$ -ketoglutarate compared to the control without the enzyme, and by the observed increased amount of the product glutamic acid. Initially, a 5 mg/g immobilized fusion protein with a 10 mM scale was found to achieve 72% molar conversion after 30 minutes and 100% yield in less than one hour. The same results have been seen for an equal amount of soluble enzyme in the same conditions of biotransformation.

Rising the scale to 50 mM (1 mM NADH), the free enzyme appeared to biocatalyse the reaction slightly faster than the immobilized form (Figure 16), when the reactions were performed in parallel with same conditions and presenting equal amounts of fusion protein. In any case, both forms showed a complete conversion in less than 4 hours.

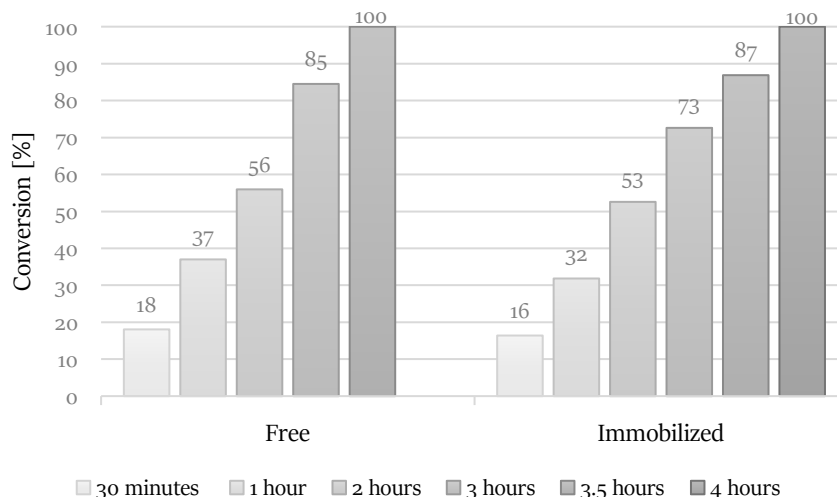


Figure 16. Percentage of conversion of 20 mg of immobilized fusion protein (5 mg/g) versus 0.1 mg/ml of the soluble form with 50 mM  $\alpha$ -ketoglutarate, 200 mM ammonium, 200 mM formate, 1 mM NADH at 37°C.

Through the activity assays and the catalytic conversion just described, the fused biocatalysts demonstrated to retain the catalytic properties of the individual enzymes. In fact, the biotransformation of the immobilized fusion protein can be compared to the biocatalytic reaction performed by the co-immobilized glutamate and formate dehydrogenases with the aim to determine whether the efficiency of the system has been improved. In the previous chapter, it has been shown that 5 mg/g GluDH co-immobilized with 40 mg/g FDH reaches 90% conversion in 10 minutes and 100% in less than 20 minutes. The 8-times higher loading of the FDH was essential to ensure a fast recycling of the cofactor without constraining the activity of the GluDH.

The comparison retrieved a limitation in the 1:1 ratio between the two fused domains, because of the slower activity of the FDH with respect to the activity of the GluDH.

To further investigate whether the FDH is the rate-limiting enzyme of the 1:1 bifunctional system, the 5 mg/g immobilized fusion protein was employed for two parallel biocatalytic reactions whose sole distinction was the amount of added NADH: 1 mM against the 15 mM. As displayed in Figure 17, the higher quantity of available NADH accelerates the activity of the GluDH, given that only 73% yield was obtained after 3 hours of biotransformation for the first reaction and 100% yield was detected as far as the second parallel reaction.

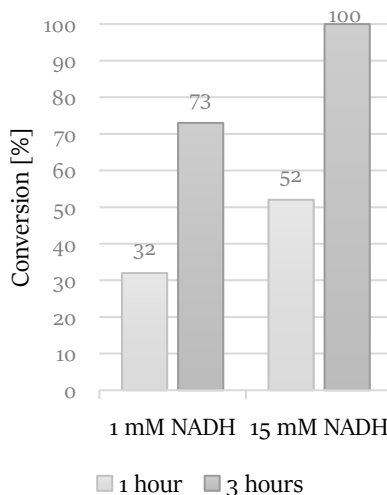


Figure 17. Comparison of activity using 1 and 15 mM NADH, with 5 mg/g immobilized fusion protein in 50 mM scale.

Even if the GluDH is limited by the slower rate of conversion of the FDH, the enzyme still works greatly with good efficiency since a full conversion is achieved in a couple of hours. The cost-effective advantage of employing a single protein instead of two overcomes this less significant drawback.

Then, a larger scale biotransformation of 300 mM  $\alpha$ -ketoglutarate (only 1 mM of NADH) was performed to push the self-sustainability of the system (Figure 18).

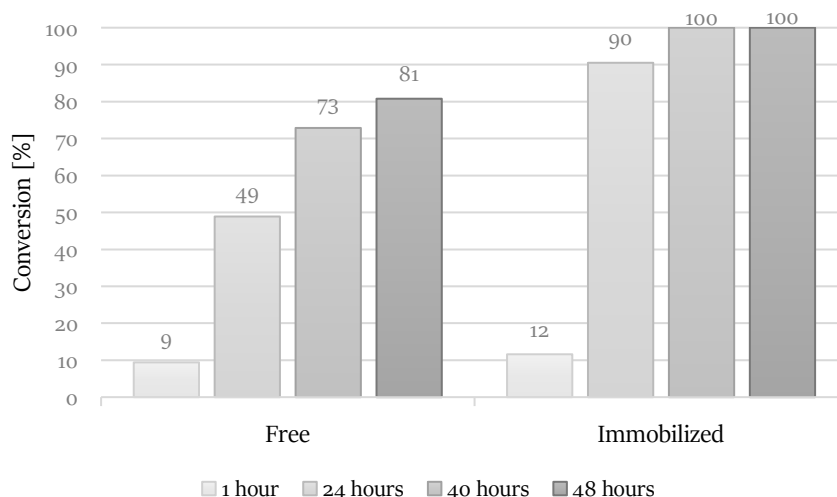


Figure 18. Percentage of conversion of 15 mg of immobilized fusion protein (10 mg/g) versus 0.15 mg/ml of the soluble form with 300 mM  $\alpha$ -ketoglutarate, 400 mM ammonium, 400 mM formate, 1 mM NADH at 37°C.

Full conversion was obtained in less than 40 hours using the immobilized enzyme, while the soluble biocatalyst achieved 70% conversion within the same timeframe.

Some protein precipitation was noted in the reaction environment with the free form, causing a decrease of activity over time. The loss of stability was probably triggered by the presence of high substrates concentration in the solution (namely, 300 mM  $\alpha$ -ketoglutarate disodium salt, 400 mM ammonium chloride, 400 mM sodium formate).

However, the immobilized enzyme worked efficiently reaching a >99% conversion, suggesting that the immobilization effectively enhanced the stability of the bifunctional system over time even at higher substrates concentration.

### 6.2.9 Continuous removal of ammonia via biotransformations (proof of concept)

The fusion protein is a bienzymatic system that can be applied as a tool to remove ammonia, for example in contaminated waters following spillages. Different experiments were performed to prove the efficiency of the

system in the depletion of small and high concentrations of ammonia, by measuring the consumption of  $\alpha$ -ketoglutarate (substrate provided in excess) combined with the rate of production of the glutamate. Indeed, the ammonia employed for the amination is stoichiometric with the consumed/formed compounds.

The first experiment wants to determine the performance of both WT and fused GluDH, with or without the assistance of FDH, in the conversion of 15 mM ammonia with an excess of  $\alpha$ -ketoglutarate (30 mM) and either stoichiometric or catalytic amounts of NADH. The activity of the FDH was permitted or not by the addition of formate as substrate in the reaction.

The reactions were monitored at 1, 2, and 24 hours. However, after 1 hour no further change in the ammonia elimination was observed. Results are shown in table 4. The fusion protein achieved full conversion only when the FDH was activated (entry 2), removing all the ammonia. In contrast, the GluDH in both forms achieved only 80% conversion, when the FDH was not activated. Therefore, it did not reach full conversion even if the cofactor was provided in stoichiometric amount (entry 1). Thus, the fusion protein with the coupled activity of the two domains was more efficient than the GluDH alone. The full depletion of 15 mM ammonia is a great result, considering that this concentration is significantly below the calculated  $K_m$  value (table 2).

Table 4. Conversion of 15 mM ammonia without (first line) and with (second line) NADH recycling.

Entry	Concentration [mM]				Conversion [%]	
	Ammonia	$\alpha$ -ketoglutarate	NADH	Formate	WT GluDH	GluDH domain
1	15	30	15	/	80%	80%
2	15	30	1	100	/	100%

After demonstrating the efficiency of the fusion protein towards low amounts of ammonia, the system was exploited against harsher conditions. In particular, 300 mM of ammonia were used together with a moderate excess of the substrates (400 mM  $\alpha$ -ketoglutarate and 400 mM formate) with still only 1 mM of cofactor. Also, the performance was compared between the soluble and the immobilized fusion protein. The chosen biocatalyst concentration was equal in both forms as well as comparable to the amounts of WT enzymes employed for the



same test in the previous chapter (paragraph 5.2.7). Indeed, the graph shown in Figure 19 also includes the results of the soluble and co-immobilized WT enzymes to provide the full comparison.

The soluble fusion protein appeared to react slowly but still achieved almost 80% conversion in 72 hours. In comparison, the free WT enzymes could not achieve more than 20% conversion, due to stability issue. Therefore, the fusion protein gained an overall higher structural stability than the single enzymes.

Furthermore, the immobilized fusion protein showed full conversion in 48 hours, meaning that also high concentrations of ammonia can be fully removed by the new biocatalyst, as proof of concept. Instead, the co-immobilized WT biocatalysts achieved only 65% conversion in the same time frame. Despite the general improved stability attained with the immobilization method, the conversion rates achieved in 48 hours with the immobilized fusion protein and the co-immobilized WT enzymes are clearly divergent with 1.5-fold higher rate for the bifunctional protein. The performance in working conditions provides a suitable method of comparison of the catalytic efficiency of the two systems (with and without the fusion) where the new enzyme is more effective timewise.

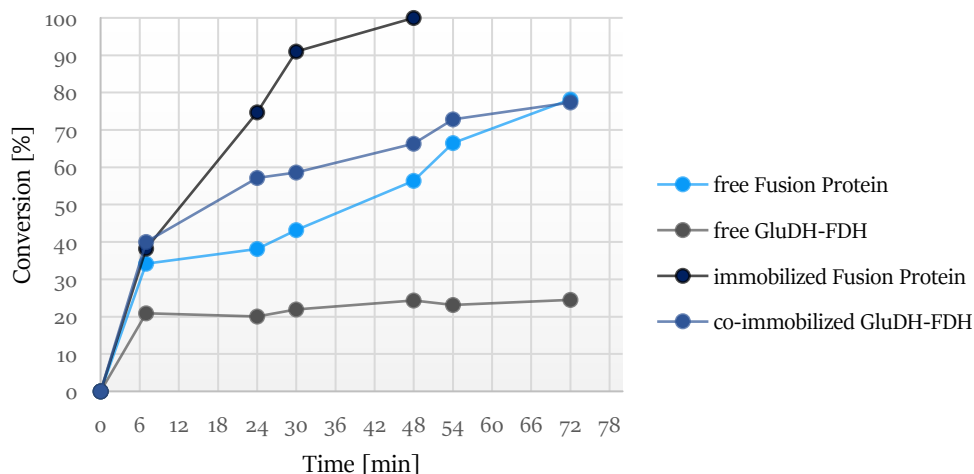


Figure 19. Conversion of the fusion protein and the WT enzymes in both soluble and immobilized form with 300 mM ammonium, 400 mM  $\alpha$ -ketoglutarate, 400 mM formate, 1 mM NADH. The final concentration of the fusion protein was 0.1 mg/ml, the final concentration of WT enzymes was 0.057 mg/ml for GluDH and 0.046 mg/ml for FDH.

Looking at the literature, also the PheDH-FDH fusion protein showed a 1.5-fold higher molecular conversion rate than the WT enzymes. In fact, the cofactor regeneration process is improved, given that the product of the first reaction can be quickly transferred to the second enzyme, leading to a lower time of diffusion.<sup>8</sup>

The immobilized fusion protein consisted of a balance arrangement of the two linked proteins so that the closed proximity of one biocatalyst to the other speeds up the cofactor regeneration system. Accordingly, the application of the new protein enhanced and highly optimized the already well-functioning co-immobilized GluDH and FDH.

### 6.3 CONCLUSION

The GluDH and the FDH have been successfully fused, overcoming all the potential drawbacks that may appear during the production of a fusion protein. One active, stable, and self-sufficient enzyme was yielded, offering a great tool for the application in small and high scale conversion of ammonia and  $\alpha$ -ketoglutarate. The fusion protein was also immobilized, providing a highly efficient and stable biocatalyst, that can be reused for several cycles of biotransformation. The close proximity of the two enzymes, given by the direct linkage, proved to enhance the activity of GluDH and FDH, showing higher conversion compared to single WT biocatalysts. Therefore, the design and development of a protein possessing the activity of two may surpass the already advantageous co-immobilization for a more industrially appealing solution, that fulfill the demand for sustainable processes. The novel fusion protein has proved to fully remove ammonia in experimental conditions, as proof of concept. Also, the immobilized fusion protein was successfully coupled to another enzyme, AvPAL, for the continuous removal of the ammonia present in solution (see chapter 4). Still, the treatment of environmental samples is a potential application, by now. The development of a system to implement effectively this tool and the required substrates for its activity is required. Nevertheless, this work provides a useful starting point for further studies and future applications to create a safer environment for us and for all the other animal species.

### 6.4 BIBLIOGRAPHY

1. Yu, K., Liu, C., Kim, B. G. & Lee, D. Y. Synthetic fusion protein design and applications. *Biotechnology Advances* vol. 33 155–164 (2015).
2. Béguin, P. Hybrid enzymes. *Curr. Opin. Biotechnol.* **10**, 336–340 (1999).

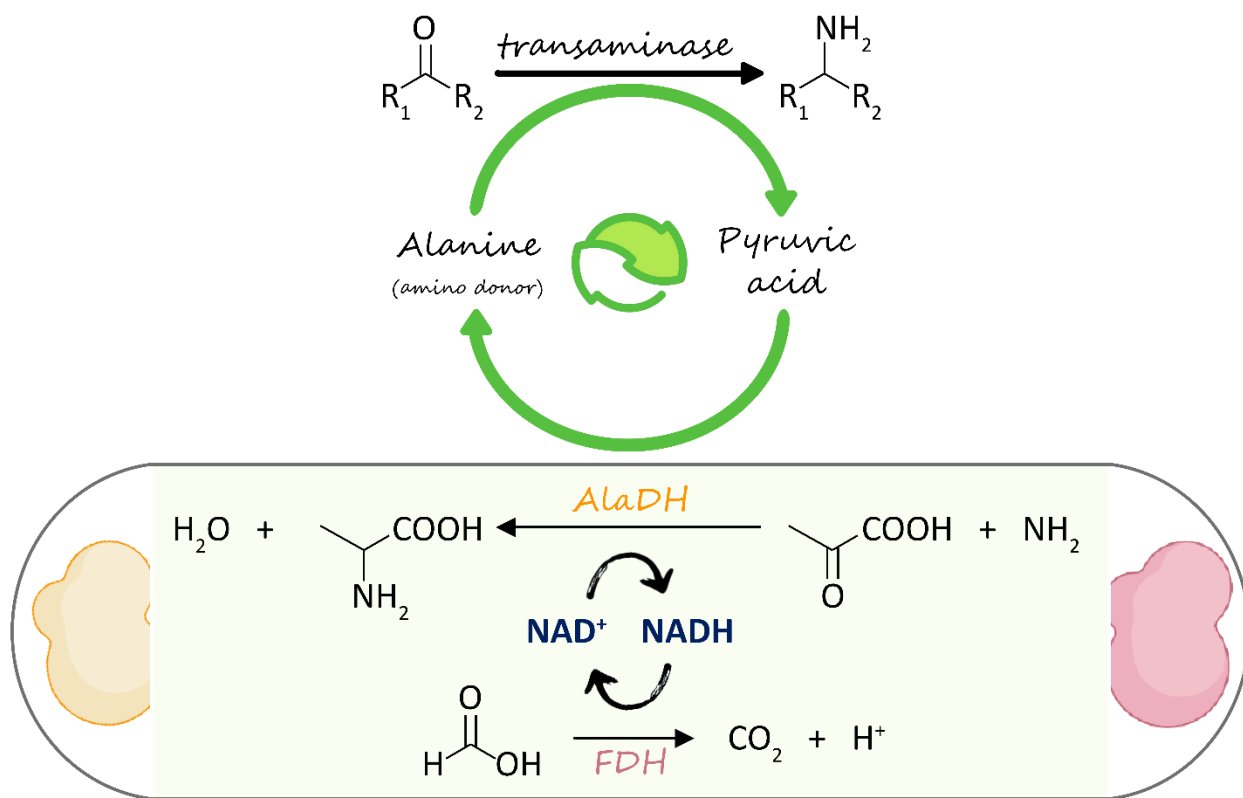
3. Lindbladh, C., Persson, M., Bülow, L. & Mosbach, K. *Characterization of a recombinant bifunctional enzyme, galactose dehydrogenase/bacterial luciferase, displaying an improved bioluminescence in a three-enzyme system. European Journal of Biochemistry* vol. 204 (1992).
4. Liu, W. & Wang, P. Cofactor regeneration for sustainable enzymatic biosynthesis. *Biotechnology Advances* vol. 25 369–384 (2007).
5. Aalbers, F. S. & Fraaije, M. W. Design of Artificial Alcohol Oxidases: Alcohol Dehydrogenase–NADPH Oxidase Fusions for Continuous Oxidations. *ChemBioChem* **20**, 51–56 (2019).
6. Bommarius, A. S., Schwarm, M. & Drauz, K. Biocatalysis to amino acid-based chiral pharmaceuticals - Examples and perspectives. in *Journal of Molecular Catalysis - B Enzymatic* vol. 5 1–11 (Elsevier, 1998).
7. Zhang, Y., Wang, Y., Wang, S. & Fang, B. Engineering bi-functional enzyme complex of formate dehydrogenase and leucine dehydrogenase by peptide linker mediated fusion for accelerating cofactor regeneration. *Eng. Life Sci.* **17**, 989–996 (2017).
8. Jiang, W. & Fang, B. S. Construction and evaluation of a novel bifunctional phenylalanine–formate dehydrogenase fusion protein for bienzyme system with cofactor regeneration. *J. Ind. Microbiol. Biotechnol.* **43**, 577–584 (2016).
9. Ngo, A. C. R., Schultes, F. P. J., Maier, A., Hadewig, S. N. H. & Tischler, D. Improving Biocatalytic Properties of an Azoreductase via the N-Terminal Fusion of Formate Dehydrogenase. *ChemBioChem* **23**, (2022).
10. Wheeldon, I. *et al.* Substrate channelling as an approach to cascade reactions. *Nat. Chem.* **8**, 299–309 (2016).
11. Rice, D. W., Hornby, D. P. & Engel, P. C. Crystallization of an NAD<sup>+</sup>-dependent glutamate dehydrogenase from *Clostridium symbiosum*. *J. Mol. Biol.* **181**, 147–149 (1985).
12. Syed, S. E. H., Engel, P. C. & Parker, D. M. Functional studies of a glutamate dehydrogenase with known three-dimensional structure: steady-state kinetics of the forward and reverse reactions catalysed by the NAD<sup>+</sup>-dependent glutamate dehydrogenase of *Clostridium symbiosum*. *BBA - Gen. Subj.* **1115**, 123–130 (1991).
13. Baker, P. J. *et al.* Subunit assembly and active site location in the structure of glutamate dehydrogenase. *Proteins Struct. Funct. Bioinforma.* **12**, 75–86 (1992).

14. Chen, X., Zaro, J. L. & Shen, W. C. Fusion protein linkers: Property, design and functionality. *Adv. Drug Deliv. Rev.* **65**, 1357–1369 (2013).
15. Eastman, P. *et al.* OpenMM 7: Rapid development of high performance algorithms for molecular dynamics. *PLoS Comput. Biol.* **13**, (2017).
16. DeLano, W. L. Pymol: An open-source molecular graphics tool. *CCP4 Newsl. protein Crystallogr.* **40**, 82–92 (2002).
17. Sharkey, M. A. & Engel, P. C. Modular coenzyme specificity: A domain-swapped chimera of glutamate dehydrogenase. *Proteins Struct. Funct. Bioinforma.* **77**, 268–278 (2009).
18. Syed, S. E. H. & Engel, P. C. A pH-dependent activation-inactivation equilibrium in glutamate dehydrogenase of *Clostridium symbiosum*. *Biochem. J.* **271**, 351–355 (1990).
19. Roura Padrosa, D., Marchini, V. & Paradisi, F. CapiPy: python-based GUI-application to assist in protein immobilization. *Bioinformatics* **37**, 2761–2762 (2021).
20. Wang, X. G. & Engel, P. C. Positive Cooperativity with Hill Coefficients of Up to 6 in the Glutamate Concentration Dependence of Steady-State Reaction Rates Measured with Clostridial Glutamate Dehydrogenase and the Mutant A163G at High pH. *Biochemistry* **34**, 11417–11422 (1995).

## CHAPTER 7.

### CREATION OF A BI-ENZYMATIC TOOL WITH ALANINE AND FORMATE DEHYDROGENASE FUSION PROTEIN FOR THE COUPLING OF TRANSAMINASE CATALYSED REACTIONS

---



## 7.1 INTRODUCTION

An  $\omega$ -transaminase ( $\omega$ -TA) catalyzes the reversible amination of a ketone or aldehyde (amine acceptor) and the concomitant deamination of a primary amine (amine donor); overall an amino moiety is transferred between two molecules. For this reaction, the transaminase requires a vitamin B<sub>6</sub>-based cofactor, pyridoxal 5'-phosphate (PLP), acting as an intermediate amine acceptor and electron sink.<sup>1</sup>

Among the group of  $\omega$ -TAs, the amino transaminases (ATAs, EC 2.6.1.-) are particularly interesting, since they do not require the presence of a carboxylic group in the substrate molecule, being able to accept a large variety of carbonyl compounds. In this contest, ATAs have attracted considerable interest in their use as biocatalysts for the enantioselective synthesis of valuable chiral amine compounds, which are widespread within the pharmaceutical, agrochemical, and fine chemical industry.<sup>2</sup> Indeed, they are considered a convenient alternative to classical chemical approaches and, thanks to their compatibility with other enzymes, they are often employed in multiple-enzymes cascade reactions.<sup>1</sup>

ATAs have been implemented in the industrial scale synthesis of important compounds and one example was mentioned in the introduction. The Sitagliptin molecule was efficiently produced with the engineered transaminase ATA-117, using isopropylamine (IPA) as amine donor.

Nonetheless, the insufficient stability of ATAs under operating conditions, still, constitutes a major hurdle for industrial applications.<sup>3</sup> As a matter of fact, high amine donor concentrations are required to shift the unfavorable reaction equilibrium towards the production of the desired amine, but this is detrimental for the enzyme.<sup>4</sup> The high amounts of amine donor react with the PLP and induce accumulation of the less stable intermediate form (E:PMP) constituted by the aminated cofactor, pyridoxamine 5'-phosphate (PMP).<sup>3</sup> Instead of recycling E:PMP to the stable E-PLP (internal aldimine) form, ATAs tends to release PMP in the absence of the produced ketone/aldehyde (very low ratio compared to the amine donor).<sup>5</sup> The resulting loss of cofactor causes monomer dissociation, unfolding and irreversible protein aggregation.<sup>3</sup>

A second source of instability is then enzyme inhibition by various amines as well as by amino acceptors, either reactive aldehydes or keto acids such as pyruvate.<sup>6</sup>

Several methods have been developed to displace the equilibrium and avoid byproduct inhibition. In this regard, the amine donor IPA used for the Sitagliptin synthesis produces acetone, which can be removed easily under low pressure or slight heating. However, IPA is not widely accepted from ATAs, and this fact compromises its wide applicability.<sup>7</sup> More than that, IPA can significantly affect the operational stability of the enzyme, since high concentrations are required.<sup>3</sup>

Using other amine donors (e.g., 1-aminotetralin) improved the levels of conversion slightly, but no general approach could be identified and most case studies reported highly substrate-dependent transamination reactions.<sup>1</sup>

Alanine is widely used as amine donor, since it is accepted by almost any ATAs, if not all of them. Furthermore, L-alanine is economically advantageous.<sup>7</sup> The scheme of transaminase reaction with L-alanine as amine donor is shown in Figure 1.

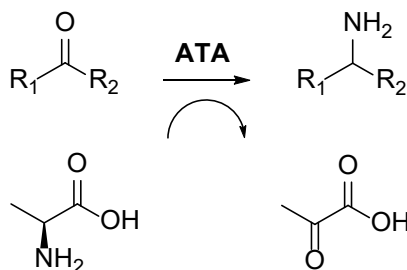


Figure 1. Scheme of the transaminase catalysed reaction where L-Alanine is the amine donor converted to pyruvic acid.

Like for the IPA, large excess is employed to shift the equilibrium towards the product formation.

An approach for equilibrium displacement and prevention of byproduct inhibition involves the addition of a second enzyme, such as a lactate dehydrogenase (LDH). This biocatalyst converts the pyruvate into lactic acid at the expense of NADH, removing the byproduct from the reaction environment.<sup>2</sup> To recycle NADH, a third enzyme such as glucose dehydrogenase (GDH) is added. The formed byproduct, however, causes a pH shift that might not be compatible with the transaminase.<sup>1</sup> Similar approaches employed a pyruvate decarboxylase to remove pyruvate by converting it to acetaldehyde, but this molecule competes with the substrate to be aminated, leading to ethylamine as side product.<sup>1,2</sup>

An amino acid dehydrogenase like AlaDH could be an alternative candidate in this scenario. In fact, it removes the pyruvate from the reaction bulk by consuming ammonium and NADH and simultaneously, and it recycles alanine so that the amine donor is continuously available for the transaminase reaction, without the need to use it in excessive amounts. Therefore, both equilibrium displacement and byproduct inhibition are most likely solved. Then, the cofactor can be efficiently recycled by adding FDH as coupled biocatalyst. The reaction of interest is shown in Figure 2, where the two biocatalytic activities are combined for cofactor regeneration.

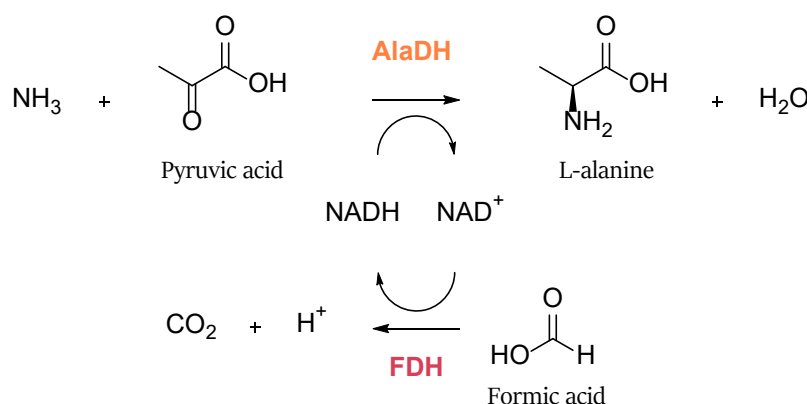


Figure 2. Reaction scheme of the combination of AlaDH with FDH.

This system has been previously reported, showing high conversion rates (mainly >90%) and high enantioselectivity with the soluble enzymes.<sup>8,9</sup>

To be sustainable and industrially appealing, though, the system requires to be reused efficiently for several cycles. Accordingly, the enzyme immobilization onto a solid support was attempted using the transaminase from the halotolerant bacteria *Halomonas elongata* (HewT), the AlaDH also from *Halomonas elongata* (HeAlaDH) combined with the FDH from *Candida boidinii* (CbFDH).<sup>9</sup> However, the immobilized biocatalysts did not reach comparable rates of conversion as the free enzymes. Indeed, only a 40% molar conversion of 10 mM vanillin was obtained for the co-immobilized enzymes (Epoxy-Agarose as carrier), with respect to the full conversion achieved in 2 hours with the free form. The limiting factor of the reaction was the regeneration of the cofactor, due to the very low activity recovered by the CbFDH.<sup>9</sup>



In a second approach, the three biocatalysts were mixed in their soluble form and trapped inside a dialysis membrane, which allowed for reusability in subsequent reactions without losing the enzyme in the reaction bulk. Almost full conversion was reached in the first cycle, but, unfortunately, the enzyme stability was rapidly lost in the following 2 cycles. Afterwards, the addition of stabilizing agents in the reaction vessel showed beneficial effects on the stability, presenting a maximum of 70% final yield after 3 cycles when using 150 mg/mL glycerol.<sup>9</sup>

The optimization of the AlaDH - FDH pair would be of high interest, in order to yield more stable biocatalysts which can be used in the transaminase reaction without the addition of stabilizing agents.

With the intention to further investigate the versatility of engineered fusion proteins, a second bifunctional enzyme has been developed by exchanging the GluDH domain with the previously described HeAlaDH. Indeed, this last enzyme has a hexameric structure like the GluDH, so that the assembly should be efficient as observed for the GluDH-FDH fusion protein. To our knowledge, the AlaDH enzyme has never been implemented in a fusion protein before the current work. Furthermore, two different constructs were developed, where the position of the two domains was swapped. This enables further analysis on the effect of the domain location and gives the opportunity to choose the most active version of fusion protein.

Indeed, past works on the fusion of proteins revealed that the orientation of the domains can drastically change the activity of the final protein. For example, the fusion of an alcohol dehydrogenase (ADH) with a cyclohexanone monooxygenase (CHMO) was studied and one orientation showed the expected catalytic efficiency, while the other one showed low to no activity.<sup>10</sup> It was suggested that structural changes happened to the inactive fusion protein. In fact, the orientation of the two domains or the fusion itself may hinder the association between the subunits to form the oligomers. It is in fact possible that one protein domain covers the oligomerization interface of its fusion partner, preventing the multimeric assembly, essential for the activity.<sup>10</sup>

Consequently, the activity of the two developed fusion proteins was evaluated and the most active form was chosen. Then, specific studies were completed to compare the wild-type enzymes with the chosen recombinant protein for the application to the transaminase reaction.

The work presented in this chapter is my exclusive contribution unless otherwise stated. Sophia Lena Hutter helped with the cloning and the characterization of the AlaDH-linker-FDH-(His<sub>6</sub>-tag-C).

## 7.2 RESULTS AND DISCUSSION

### 7.2.1 Genetic construction of the two fusion proteins

The genetic construction of (N-His<sub>6</sub>-tag)-FDH-linker-AlaDH has been performed using the same strategy employed for the cloning of the recombinant fusion protein of GluDH-FDH (chapter 6). Unfortunately, replacing the gene of GluDH from the previous fusion protein with the gene of AlaDH by double digestion and ligation (through *NheI* and *SacI* restriction sites) was not successful and the generation of the construct was attempted via Gibson assembly. The amplification of both the insert and the vector was effective, as checked by agarose gel and sequencing of the vector, yielding good amounts of DNA fragments to work with for the following step. However, despite several attempts and optimization, the sequencing of random clones was not successful. Therefore, a colony PCR was performed to speed up the process analyzing as many colonies as possible without sequencing all of them. By means of the colony PCR, only few among 30 screened colonies seemed to be efficiently assembled (Figure 3).

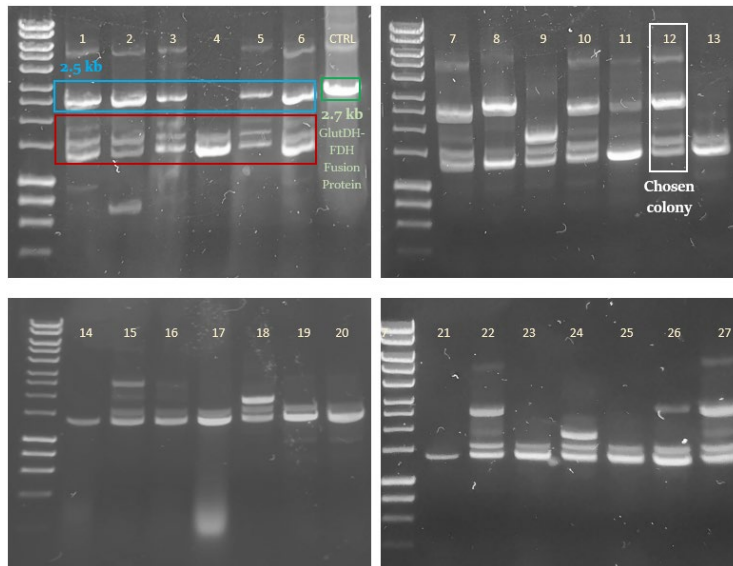


Figure 3. Colony PCR of the His-FDH-AlaDH fusion protein.

The chosen candidate exhibited a more intense band in the expected size line (2.5 kb) of the agarose gel and after sequencing, the purified plasmid was confirmed to contain the His-FDH-AlaDH fusion protein.

On the other hand, the genetic construction AlaDH-linker-FDH-(His<sub>6</sub>-tag-C) was designed considering the assembly of the hexameric structure, where the AlaDH is most likely located in the center surrounded by the FDH dimers. For this reason, it has been decided to insert the His-tag at the C-terminal of the FDH domain, exposed to the bulk, so that the six subunits of AlaDH are able to fully assemble without any distortion. Furthermore, the activity of the GluDH-FDH fusion protein confirmed that the presence of a His-tag in the dimeric FDH structure was not detrimental for the assembly.

The plasmid backbone was again pET28b in order to maintain the same properties as the previous fusion protein and allow for a fair comparison between the two new enzymes.

For the development of this second fusion protein, a first mutation was performed to remove the stop codon at the end of the FDH gene. In this way, the His-tag available in the vector template was encoded in the protein sequence at the C-terminal of the FDH domain. The one-point mutation resulted in the exchange of the base A contained in the TAA stop codon for a C base, developing a TCA triplet, which translates for a serine in the amino acidic structure. After the PCR amplification of both insert (gene fragment of AlaDH) and vector (FDH-pET28b), the Gibson assembly was performed.

One of the colonies obtained with the subsequent bacterial transformation was employed for plasmid propagation and purification. After sequencing, the plasmid was confirmed to contain the right DNA of AlaDH-FDH-His fusion protein.

### 7.2.2 Expression optimization

The His-FDH-AlaDH fusion protein was expressed in small scale to evaluate the best conditions, using LB as culture media, different concentration of the inducer IPTG and two different temperatures of incubation (20°C and 37°C). The results of the crude activity are shown in Table 1. The SDS-PAGE of the related samples is exposed in Figure 4 where the rate of production and the solubility of the overexpressed enzymes are compared.

The activity in the crude extract obtained from the cultures grown at 37°C was almost undetectable. In fact, no activity of the FDH was found, while the AlaDH had very low values with respect to the results obtained from the cultures grown at 20°C. The latter ones offered an active enzyme for both domains as well as a higher level of

overexpression. However, in all cases the majority of the fusion protein was found in the insoluble fraction and among the three different amounts of IPTG, the 0.1 mM seemed to yield the most soluble and active enzyme.

Table 1. Outcomes for His-FDH-AlaDH after screening the different conditions of protein overexpression.

Expression Conditions			Weight of pellet [ g / L ]	Activity of the crude extract		
Media	IPTG Concentration [mM]	Temperature [°C]		AlaDH deamination [U/mL]	AlaDH amination [U/mL]	FDH [U/mL]
LB	1	20	8	0.16	1.0	0.09
	0.5		5	0.19	1.1	0.09
	0.1		5	0.30	1.7	0.07
LB	1	37	4	0.02	0.6	/
	0.5		4	0.02	0.6	/
	0.1		5	0.02	0.7	/

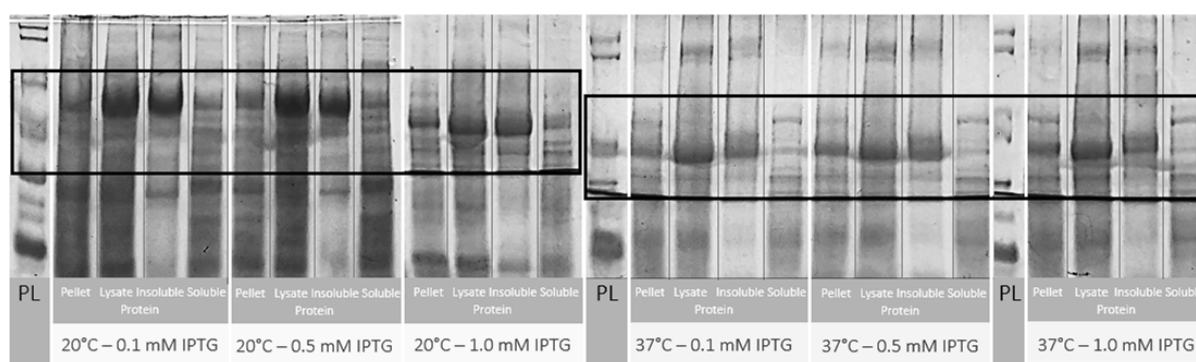


Figure 4. SDS-PAGE for screening the optimal condition of His-FDH-AlaDH fusion protein overexpression. PL: protein ladder.

Consequently, a temperature of 20°C and an induction with 0.1 mM of IPTG were chosen as optimum conditions for larger scale expression of His-FDH-AlaDH fusion protein. It is worth to mention that these conditions were also chosen for the previous fusion protein, having the same pattern (His-FDH-GluDH).

The fusion protein of AlaDH-FDH-His was firstly expressed following the same conditions as before. Unfortunately, the protein was completely insoluble, and no activity was detected.

Reducing protein synthesis rate is one of the strategies often employed to minimize the formation of inclusion bodies.<sup>11</sup> Furthermore, reducing IPTG concentrations in the culture medium decrease the rates of protein expression to manageable levels without placing a metabolic burden on *E. coli* cells, which is ultimately favorable for the proper folding of recombinant proteins.<sup>12,13</sup> Consequently, the IPTG concentration was further reduced to 10  $\mu\text{M}$ , which was unsuccessful, and then 0.1  $\mu\text{M}$  (as final concentration) was also attempted. Likewise, the culture temperature in induction phase was further decreased from 20°C to 16°C. In parallel, a 30-minutes heat shock at 47°C prior to induction (10  $\mu\text{M}$  IPTG) was trialed to induce chaperons' production. Indeed, exposure of the cells to heat stress triggers the expression of heat-shock proteins, many of which act as molecular chaperons. These molecular chaperones assist protein refolding, disassemble aggregated proteins, or prevent protein aggregation.<sup>14</sup> Osmotic stress-triggering chemicals display beneficial effects on the expression of soluble recombinant proteins. For example, the presence of sorbitol in the culture media triggers high osmotic pressure. Then, the *E. coli* cells adapts to this osmotic stress by synthesizing/up-taking small organic compounds known as osmolytes, which can act as "chemical chaperones" by increasing the stability of native proteins and assisting in the refolding of unfolded polypeptides.<sup>14,15</sup>

Therefore, the LB culture media was supplemented with D-sorbitol (0.5 M), as previously described.<sup>16</sup>

These last three conditions are shown in Figure 5 with the comparison between insoluble and soluble recombinant proteins. When performing the heat-shock before induction, some soluble proteins were successfully produced. Instead, the addition of sorbitol appeared to completely inhibit the expression of the fusion protein, which is not present neither as soluble nor as insoluble protein. Lowering the IPTG concentration to 0.1  $\mu\text{M}$  gave the best outcome (highlighted with a black rectangle in Figure 5), because no insoluble protein was present, and the desired soluble proteins seemed to be slightly more concentrated compared to the heat-shock condition.

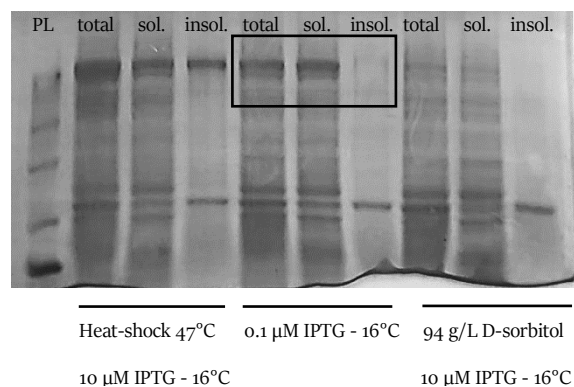


Figure 5. SDS-PAGE of AlaDH-FDH-His protein overexpression. PL: protein ladder, sol.: soluble, insol.: insoluble proteins.

The larger scale overexpression was performed with 0.1 μM of IPTG and an induction temperature of 16°C.

### 7.2.3 Larger scale overexpression and purification

The His-FDH-AlaDH fusion protein was overexpressed in 300 mL of LB media, yielding 12 grams of pellet per liter of culture. Considering the parameters used for LB overexpression, other culture medias were tried in parallel, namely the TB (with 0.1 mM IPTG) and the AI (without IPTG). Nevertheless, the protein yield was half compared to the LB in both cases, while the specific activity in the crude was half for the AI and similar for the TB. Since no improvement was obtained, the LB remained the best choice.

After the purification of the overexpressed His-FDH-AlaDH fusion protein (in LB), 8 mg of proteins per liter of media was obtained. Unfortunately, the expression level was not very high, but sufficient for the following studies. In the SDS-PAGE with the purified fraction (Figure 6), the band of the overexpressed protein is placed at 82 KDa, confirming the proper molecular weight of the monomers.

A fraction of insoluble proteins is clearly present (line 3), nevertheless the soluble fusion protein was successfully purified to be then properly characterized (line 5, inside the square).

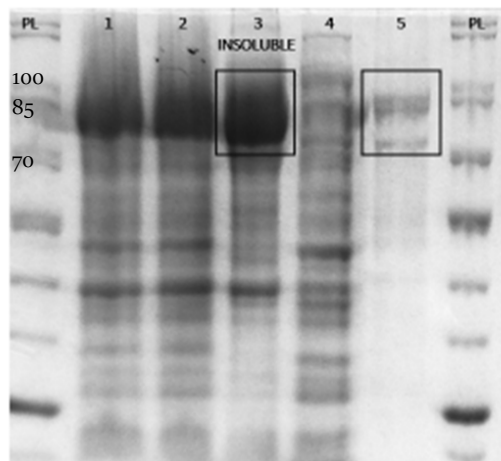


Figure 6. SDS-PAGE stained with Coomassie with samples taken during the purification of His-FDH-AlaDH fusion protein. Sample are as follows 1: pellet, 2: lysate, 3: cell paste, 4: crude extract, 5: after dialysis, PL: protein ladder.

The AlaDH-FDH-His fusion protein was also overexpressed in 300 mL of culture media. The yields of pellet and purified enzyme were in the same range as for the His-FDH-AlaDH fusion protein, even if the expression conditions were not the same.

In figure 7, the SDS-PAGE related to the purification process is shown, where the final protein fraction is highlighted with the black square.

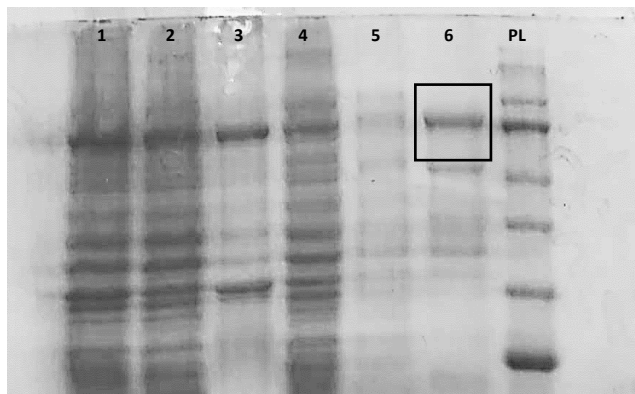


Figure 7. SDS-PAGE stained with Coomassie with samples taken during the purification of His-FDH-AlaDH fusion protein. Sample are as follows 1: pellet, 2: lysate, 3: cell paste, 4: crude extract, 5: after dialysis, PL: protein ladder.

Increasing the volume of expression from 50 to 300 mL caused some formation of insoluble proteins (line 3). However, the ratio between insoluble and soluble proteins is almost 1:1, which is a great improvement compared to the samples in Figure 6, where the ratio is clearly greater for the insoluble fraction compared to the soluble recombinant protein.

Considering that the level of expression was similar between the two conformations, the second fusion protein seemed more efficient in terms of reduced loss of proteins caused by aggregation and unfolding.

#### 7.2.4 Activity and assembly of the two fusion proteins

To better normalize the values for fair comparison, the activity of the two catalysts of the fusion protein (U/mg) was aligned to half of the activity of the wild type (WT) AlaDH and half of that for the WT FDH. The weights of WT AlaDH and WT FDH that contains the same moles as 1 mg of fusion protein were calculated as follows:

$$\text{Eq. 1:} \quad \text{Molarity Fusion Protein} = \text{Molarity WT Protein}$$

$$\text{That can be written also as:} \quad \frac{\text{Weight fusion protein}}{\text{Volume} \times \text{MW fusion protein}} = \frac{\text{Weight WT protein}}{\text{Volume} \times \text{MW WT protein}}$$

$$\text{Including FDH parameters:} \quad \frac{0,001 [g]}{0,001 [L] \times 82.415 [KDa]} = \frac{\text{Weight FDH [g]}}{0,001 [L] \times 42.95 [KDa]}$$

$$\text{Weight FDH} = \frac{0,001 [g] \times 42.95 [KDa]}{82.415 [KDa]}$$

$$\text{Normalized WT FDH weight:} \quad \frac{42.95}{82.415} \text{ KDa} = \mathbf{0.5 \text{ mg}}$$

$$\text{Including AlaDH parameters:} \quad \frac{0,001 [g]}{0,001 [L] \times 82.415 [KDa]} = \frac{\text{Weight AlaDH [g]}}{0,001 [L] \times 41.72 [KDa]}$$

$$\text{Weight AlaDH} = \frac{0,001 [g] \times 41.72 [KDa]}{82.415 [KDa]}$$

$$\text{Normalized WT AlaDH weight:} \quad \frac{41.72}{82.415} \text{ KDa} = \mathbf{0.5 \text{ mg}}$$

The specific activity of both protein domains has been measured in triplicates to calculate the retained activity of the enzymes after being cloned in the His-FDH-AlaDH fusion protein (Table 2).



Table 2. Specific activity of the purified His-FDH-AlaDH compared to the normalized specific activity of the wild-type enzymes (shown only as reference values without the standard deviations).

	FDH	Amination AlaDH	Deamination AlaDH
Wild-type enzymes	1.75	58	12
His-FDH-AlaDH	0.40 ± 0.08 U/mg	6.5 ± 1 U/mg	1.4 ± 0.1 U/mg
Retained activity	23 ± 5 %	11 ± 2 %	12 ± 1 %

The activity of the alanine dehydrogenase was detected in both amination and deamination reaction to confirm the accuracy of the results, which were found to be consistent as they gave a very similar outcome. Only 11-12% of the activity was retained with respect to the WT AlaDH, meaning that the assembled quaternary structure was likely subjected to conformational changes impacting on the usual folding and activity of the enzymes. In addition, 22% of the activity of the FDH domain was retained compared to the WT protein, which is 2-times higher than the activity of the AlaDH. This behavior may be due to a different ratio of correct folding between the protein domains. Indeed, the FDH presents only two subunits that need to interact for complete assembly, while the hexameric AlaDH requires six assembled monomers to be active. Generally, two subunits are easier to assemble than six. Accordingly, a size exclusion chromatography of the His-FDH-AlaDH fusion protein was done to analyze the oligomerization behavior of the monomers.

The calibration curve was created as shown in the chapter 6 and the chromatogram obtained with the fusion protein is shown in Figure 8.

Two different conformations were found at 8.42 and 9.36 mL of elution. The molecular weight of the monomer is 82,415 Da. By plotting these values in the calibration curve equation (shown in Figure 10 of chapter 6), the protein sizes were calculated, which corresponded to the molecular weight of the assembled eight (659 KDa) and twelve subunits (989 KDa).

The hypothetical configurations are shown in Figure 9.

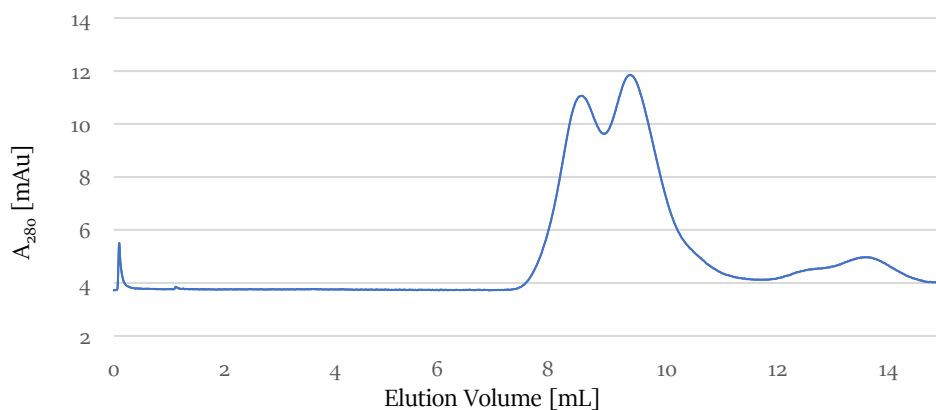


Figure 8. Chromatogram of His-FDH-AlaDH fusion protein by SEC.

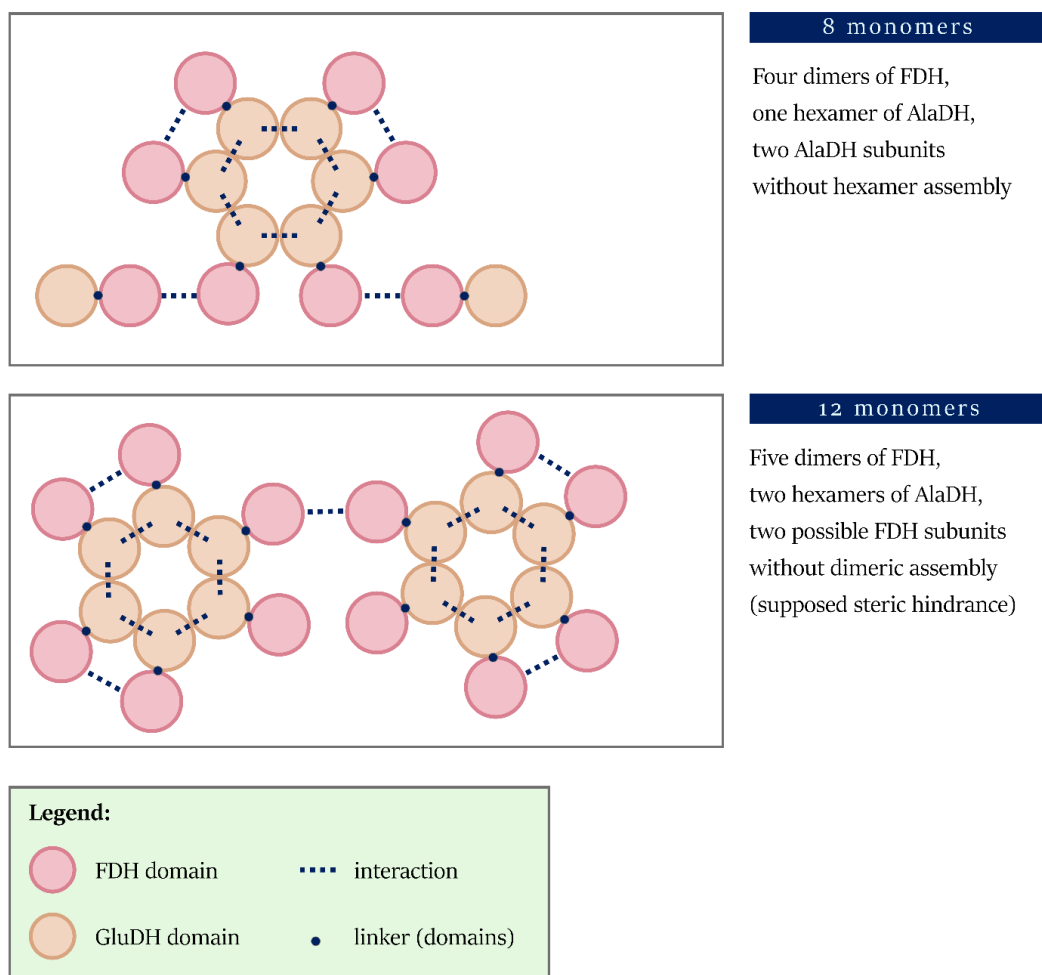


Figure 9. Schematic assembly of the His-FDH-AlaDH fusion protein monomers.

In the case of the octameric configuration, the eight FDH subunits are fully assembled in four dimers. Then, six of the linked AlaDH domains interact to form a hexameric structure, same as the WT. However, two subunits of AlaDH are not interacting with other AlaDH monomers. These two lone domains are connected to the octamer through the fused FDH that forms a dimer with the core hexameric structure.

As for the second conformation, two hexameric AlaDH domains are fully assembled, and connected through the dimerization of the fused FDH. This last domain forms most likely five assembled dimers (ten subunits). It can be speculated that the other two FDH domains do not interact together because of the steric hindrance between the vicinal subunits. Also, it is possible that the full interaction of all the FDH subunits would cause high rigidity to the final structure.

The results of the SEC confirmed that the AlaDH and the FDH domains were not fully assembled in hexamers and dimers, respectively, in all the two main conformations. This leads to a loss of activity, as confirmed by the low retained specific activity compared to the WT enzymes.

The specific activity of the second fusion protein (AlaDH-FDH-His) was calculated and compared to the WT enzymes (Table 3).

Table 3. Specific activity of the purified His-FDH-AlaDH compared to the normalized specific activity of the wild-type enzymes (shown only as reference values without the standard deviations).

	FDH	Amination AlaDH	Deamination AlaDH
Wild-type enzymes	1.75	58	12
AlaDH-FDH-His	1.0 ± 0.2 U/mg	16.0 ± 2.3 U/mg	2.4 ± 0.5 U/mg
Retained activity	57 ± 11 %	28 ± 4 %	20 ± 4 %

The specific activity of the FDH domain was twice the activity of the AlaDH domain, as seen for the previous fusion protein. In this case, around a 60% of FDH activity was retained after the fusion. Instead, the AlaDH domain retained between 20 and 30% of the original activity, considering both directions of reaction. The values obtained with the amination are still consistent with the results acquired with the deamination reaction if we consider the error.

The AlaDH-FDH-His fusion protein presented 2/2.5-fold higher activity than the His-FDH-AlaDH fusion protein. Consequently, the AlaDH-FDH-His enzyme was chosen as the most active version of the bifunctional AlaDH and FDH system. This protein was thus characterized and used for the biotransformations. Knowing that the cofactor regeneration is usually slower than the coupled reaction, the 2-fold higher activity of FDH compared to AlaDH may be beneficial to ensure fast recycling of NADH without limiting the overall conversion.

The GluDH-FDH fusion protein retained almost all the activity after the fusion, showing comparable results between the two domains. In comparison, the fusion of the AlaDH with the FDH preserved much lower activity. Developing two fusion proteins with equal WT conformation offers the possibility to assess the versatility of the system, when changing only one of the two domains. In this case, the high-efficient GluDH-FDH fusion protein showed special behaviors inherited from the CsGluDH. Thanks to the attributes of this latter enzyme, a new protein with optimal characteristics was developed. Interchanging the GluDH with a different hexameric protein did not offer the same results.

A study on the development of three bifunctional fusion proteins with both orientations of each domain was reported in the literature.<sup>10</sup> The six fusion constructs had a domain in common (CHMO from *Thermocristum municipale*) which retained full activity in 5 cases, independently of the orientation. One of them showed half activity, even if the same orientation in the other 2 cases did not have any impact. This means that the loss of half activity was related to the different fused partner that caused possible structural changes. As for the second domain, three different ADH enzymes were employed (TbADH from *Thermoanaerobacter brockii*, ADHA from *Pyrococcus furiosus*, ADHMi from *Mesotoga infera*) and all of them behaved differently. ADHA domain was not active in both orientations. Then, ADHMi domain was active in one construct, but not active in the opposite orientation, which was confirmed by the different structural conformation (the trimer was inactive, while the tetramer was active). Instead, TbADH showed a less drastic effect, but still orientation-dependent, where one retained 4-times lower activity compared to the other fully active fusion protein. Although the CHMO domain was consistently active in all the constructs, the three ADH domains produced very diverse outcomes.<sup>10</sup>

In a similar way, the FDH domain of all the three here described fusion proteins (His-FDH-GluDH, His-FDH-AlaDH, AlaDH-FDH-His) retained very different levels of activity. Moreover, the published PheDH-FDH-His

protein reported a lower catalytic activity compared to the WT enzymes.<sup>17</sup> While the six previously developed FDH-LeuDH fusion proteins showed different levels of activity depending on the linker inserted between the domains (the rigid EAAAK or the flexible GGGGS, with 1, 2 or 3 repetitions). The LeuDH domain retained more activity than the FDH domain, apart from one construct where the FDH activity was even 1.5-fold higher than the original CbFDH. The recently reported His-AzoRo-FDH and His-FDH-AzoRo fusion proteins presented similar retained activities for the FDH domain (FDH with the residue Cys23 mutated to Ser) but lower than the WT FDH. The specific activity of these two proteins was around 1 U/mg, like the value shown in Table 3 for the AlaDH-FDH-His.

Therefore, the fusion of two biocatalysts can lead to very diverse outcomes even when one of the two domains is kept unaltered. Fusing two enzymes is still a delicate process, and it is difficult to predict the efficiency of a fusion protein before analyzing it. The fusion protein systems are not as versatile as initially supposed.

### 7.2.5 Characterization of the AlaDH-FDH-His protein

The AlaDH-FDH-His fusion protein was further characterized. Firstly, the affinity of the domains towards the natural substrates was assessed. The results are shown in Table 4, where the values related to the WT enzymes are also inserted for a comparison.

The resulting  $K_M$  values were comparable between fusion protein and WT domains with most of the substrates. Only NADH for the AlaDH domain and  $NAD^+$  for FDH suffered a decrease of affinity, where the values were both around 3.5-fold higher than the WT enzymes. A similar behavior was found for the GluDH domain in the GluDH-FDH protein, where the  $K_M$  was 2-fold higher. On the contrary, the FDH domain had half the value found with the WT protein (Table 3 of chapter 6), meaning that, in comparison, the AlaDH-FDH-His fusion protein significantly worsened. The  $K_M$  values of the FDH domain in the His-FDH-AzoRo fusion protein increased by at least 10-fold for formate and almost 2-fold for  $NAD^+$ .<sup>18</sup> Similarly, the PheDH-FDH-His fusion protein had 2-fold higher  $K_M$  values for the substrates phenylpyruvate and formate than the WT enzymes.<sup>17</sup> Consequently, the AlaDH-FDH-His protein still maintained overall similarity to HeAlaDH and CbFDH despite the increased  $K_M$  for the cofactor, which was also found in other fusion proteins, like the Leu-FDH mentioned in the previous chapter.<sup>19</sup>

Table 4. Kinetic constants for the fusion protein, the alanine- and the formate dehydrogenase.

	Fusion protein - AlaDH	Wild-type HeAlaDH
	$K_M$ [mM]	$K_M$ [mM]
L-Alanine	$11.4 \pm 1.5$	$10.3 \pm 2.4$
Pyruvate	$0.44 \pm 0.06$	$0.60 \pm 0.11$
Ammonia	$93.3 \pm 16.2$	$77.8 \pm 12.6$
NADH	<b><math>0.18 \pm 0.02</math></b>	$0.05 \pm 0.01$
NAD <sup>+</sup>	$0.26 \pm 0.02$	$0.20 \pm 0.04$
	Fusion protein - FDH	Wild-type CbFDH
	$K_M$ [mM]	$K_M$ [mM]
Formate	$7.8 \pm 1.4$	$5.0 \pm 1.0$
NAD <sup>+</sup>	<b><math>0.57 \pm 0.03</math></b>	$0.17 \pm 0.03$

The AlaDH-FDH-His fusion protein was then subjected to stability assays. The two enzymes were analyzed after 2, 24 and 48 hours of incubation in different pH values, as shown in Figure 10. Concerning the AlaDH domain, the profile of pH stability is in accordance with the published results.<sup>9</sup>

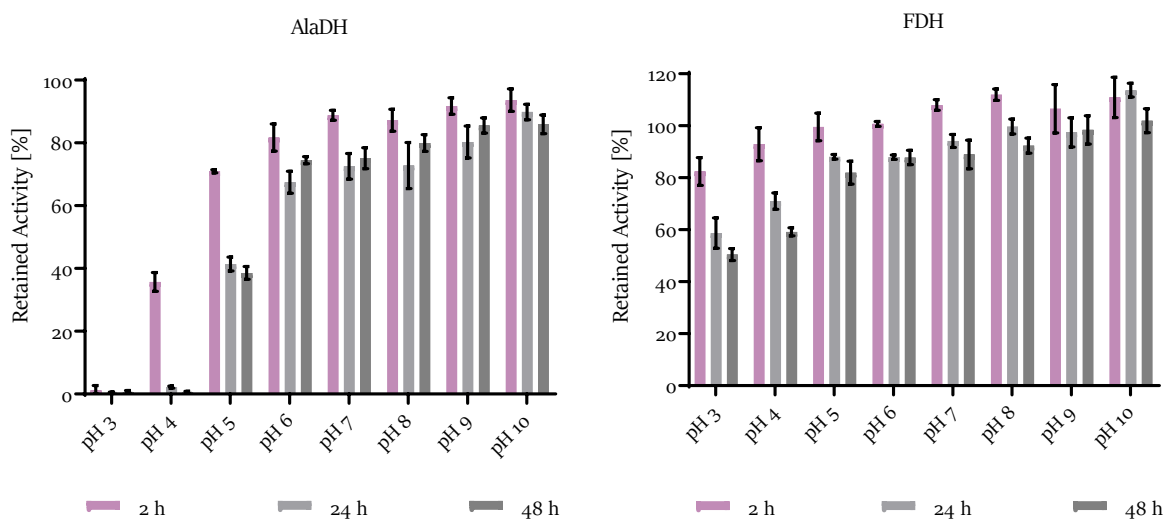


Figure 10. pH effect on the stability of AlaDH and FDH domains.

The FDH domain did not seem to lose activity after incubation at very low pH, even if the AlaDH stability was considerably affected in the same conditions. The FDH maintained overall stability at all the tested pH values.

The stability of the fusion protein at various temperatures was checked over time (2, 24, 48 hours). The graphs are shown in Figure 11 with the profiles of the WT enzymes.

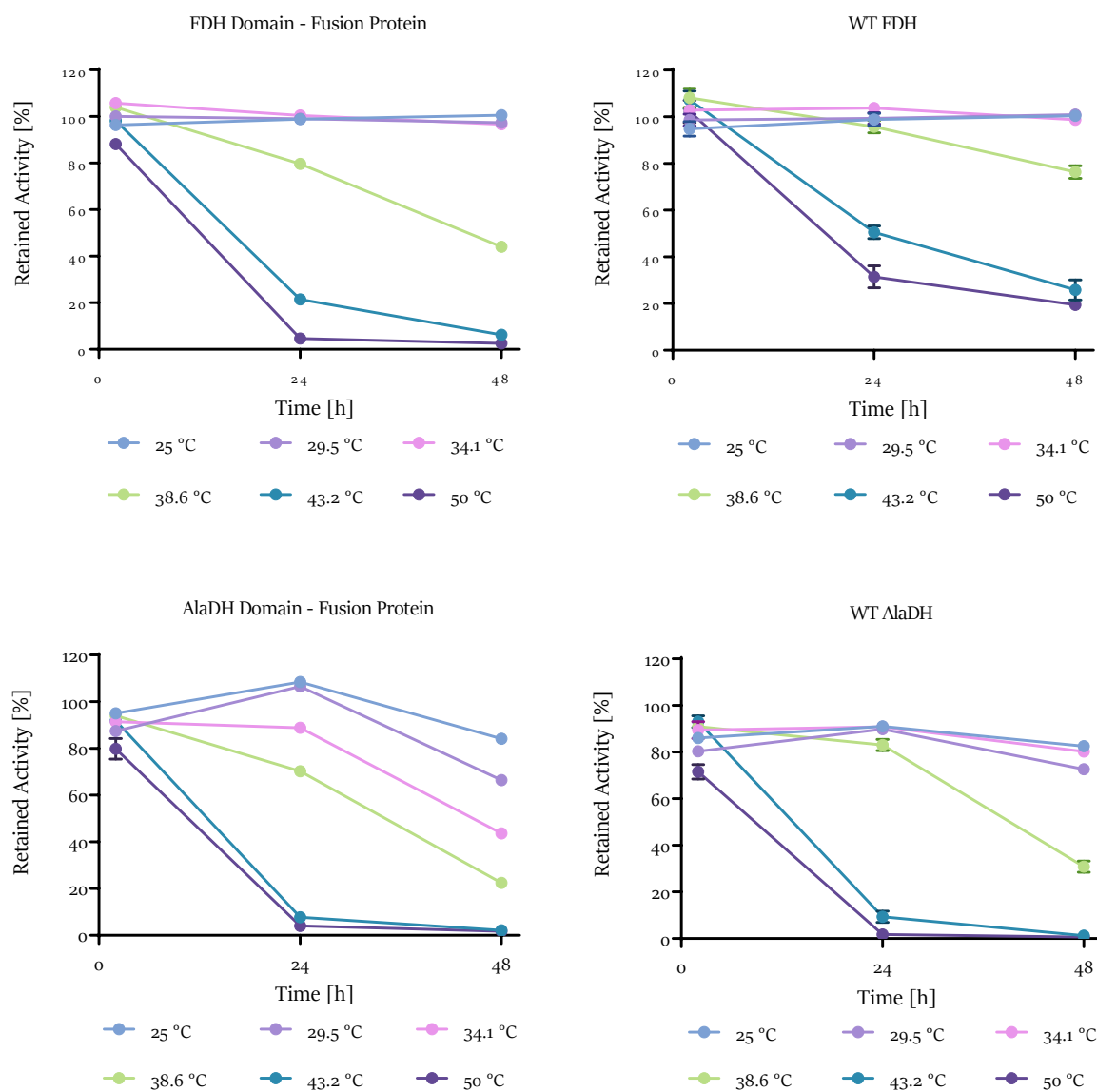


Figure 11. Temperature effect on the stability of AlaDH and FDH domains compared to the WT enzymes.

The FDH domain showed reduced stability at higher temperatures over the 24 and 48 hours compared to the WT FDH, while no difference was noticed between the 25°C and 34°C. In contrast, the AlaDH domain exhibited a comparable profile as the WT AlaDH, without any significant loss of stability.

After the fusion, both AlaDH and FDH domains effectively preserved their overall properties.

### 7.2.6 Batch biotransformation

Vanillin (10 mM) was employed as substrate for the transaminase reaction with only 1 equivalent of L-alanine and accordingly, the ability of the fusion protein to recycle the amino donor was examined (1 mM NAD<sup>+</sup>, ratio 1:10). The reaction scheme is shown in Figure 12.

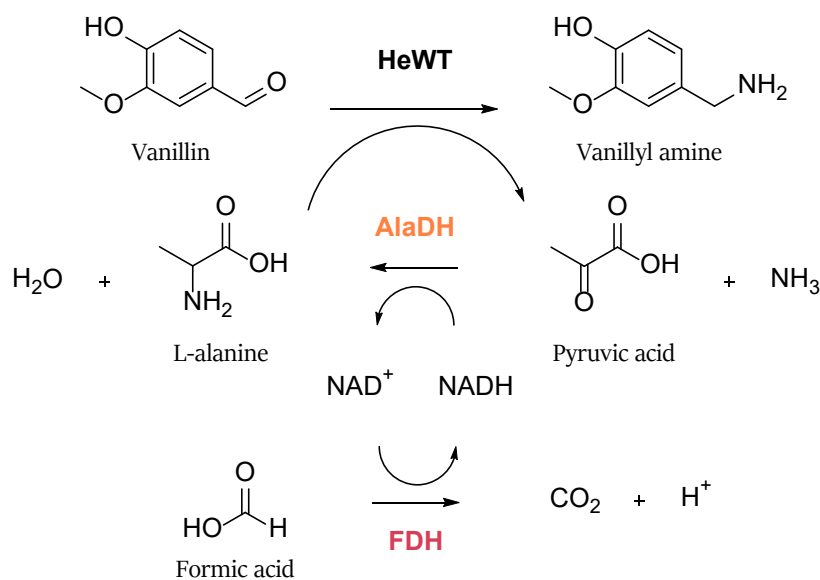


Figure 12. Reaction scheme of the transaminase reaction (HeWT) coupled with AlaDH and FDH.

The AlaDH-FDH-His fusion protein was tested in batch biotransformation with the presence of the transaminase HeWT (Figure 13). In parallel, the same reaction was performed with the WT enzymes instead of the fusion protein, adding half protein concentration with respect to the fusion protein (0.15 and 0.30 mg/mL). In this way, the fusion protein domains and the WT enzymes presented the exact same ratio (1:1).



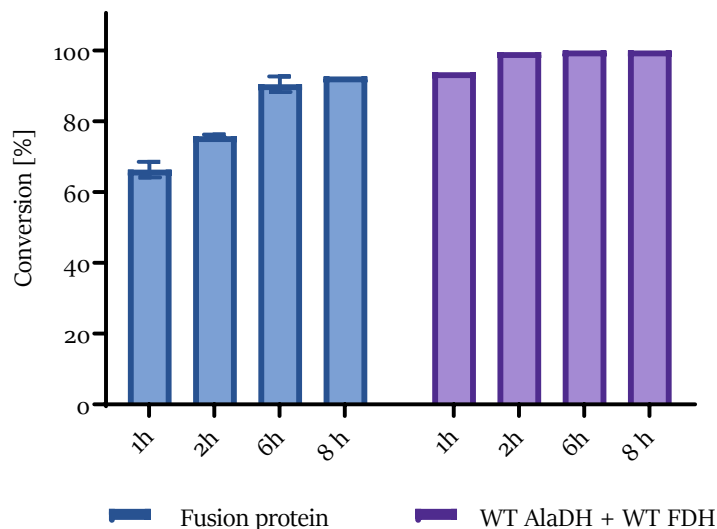


Figure 13. Conversion of vanillin to vanillyl amine over time. Reaction components: 0.3 mg/ml of fusion protein or 0.15 mg/ml of WT AlaDH and 0.15 mg/ml of WT FDH, 0.6 mg/ml HeWT, 10 mM vanillin, 10 mM L-alanine, 100 mM ammonium formate, 1 mM NAD<sup>+</sup>, 0.1 mM PLP, 100 mM phosphate buffer pH 8.0, 10% DMSO. Reaction performed in 1 mL volume, at 37°C and 150 rpm.

After 1 hour of reaction, the transaminase HeWT coupled with the WT enzymes achieved 94% of conversion. After 2 hours, the reaction was completed, with all the 10 mM vanillin converted to vanillyl amine. In comparison, the coupling with the fusion protein reached 66% conversion after 1 hour and 76% after 2 hours. These results confirmed the efficacy of the fusion protein to recycle the amino donor (L-alanine) by removing the inhibiting by-product (pyruvate) for an efficient transaminase reaction. However, the fusion protein was slower than the WT enzymes. Also, the full conversion was not achieved before the 8 hours, with very small increase between the 6 and the 8 hours of reaction (90% and 93% conversion, respectively). Considering that the activity of the fusion protein domains was significantly lower than the activity of the WT enzymes, the results seemed promising. Indeed, the AlaDH domain presented only a 20-30% retained activity, while the conversion rate reached 70% compared to the conversion obtained with the WT AlaDH after the first hour of reaction. To see whether the fusion protein could achieve comparable rates as the WT, a second batch biotransformation was performed with twice the amount of enzyme, from the 0.30 mg/mL to the 0.60 mg/mL. In this case, the 76% conversion obtained

in the 2 hours improved to 88% conversion, meaning that fine tuning the concentration, the fusion protein can proportionally achieve higher conversion.

### 7.2.7 Dialysis assisted biotransformation

A dialysis membrane enclosed system was previously reported as strategy to reuse the three coupled enzymes (HeWT, AlaDH, FDH) as mentioned before, since the FDH was inactivated after covalently binding to the resin.<sup>9</sup> The dialysis assisted biotransformation achieved completion over 24 hours and the enzymatic mix could be reused for a maximum of three cycles of usage.<sup>9</sup>

The same reaction was set-up with the fusion protein to assess its performance and stability in comparison to the wild type AlaDH and FDH. The first cycle of biotransformation was tested over time, as shown in Figure 14.

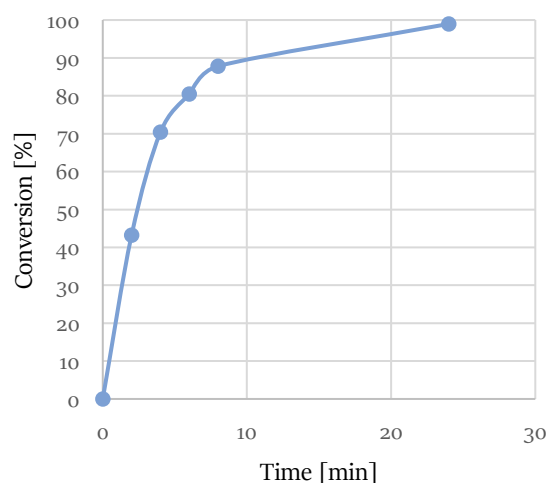


Figure 14. Conversion of 10 mM vanillin to vanillyl amine over time, mixing 0.3 mg/mL fusion protein and 0.6 mg/mL HeWT inside a dialysis bag. The reaction was performed in a glass vial incubated in a water bath at 37°C. The reaction volume of 5 mL also contained 1 mM NAD<sup>+</sup>, 100 mM ammonium formate, 10 mM L-alanine, 0.1 mM PLP, 100 mM potassium phosphate buffer pH 8.0.

Remarkably, almost 50% conversion could be achieved after only 2 hours, despite the 5 times higher volume than the previous biotransformations. After 6 hours, the conversion was 80% and full conversion was found after 24 hours. The dialysis assisted approach did not obstacle the enzyme mix to biocatalyse the reaction. Even if the

velocity decreased (76% vs 43% in 2 hours), it did not impact as much as in the wild-type system (99% vs 30% in 2 hours) containing higher quantity of enzymes.<sup>9</sup>

The same biotransformation was repeated two more times to evaluate the reusability of the system, taking the samples after the 24 hours (Figure 15). Full conversion was achieved in all the three consecutive reactions, confirming the better stability of the fusion protein compared to the WT enzymes, even without the need for additional agents.

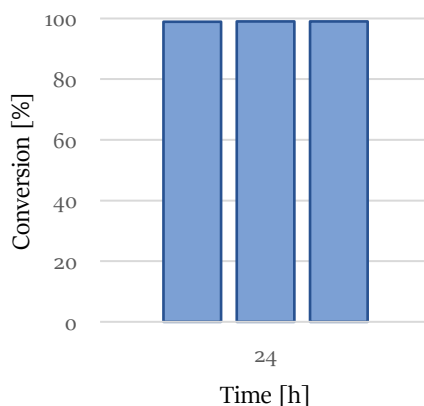


Figure 15. Three cycles of the 24-hours reaction using the same biocatalysts enclosed in a dialysis bag.

### 7.3 CONCLUSION

After accurate optimization of the expression conditions, two bifunctional fusion proteins of AlaDH and FDH were produced. The two enzymes were both active, even if at different degree. It has been confirmed that the lower activity was related to the different structural conformation of the assembled subunits compared to the original enzymes.

The AlaDH-FDH-His fusion protein demonstrated twice the activity as the His-FDH-AlaDH assembly. Consequently, this enzyme was successfully characterized, confirming similar stability and affinity as the wild type HeAlaDH and CbFDH. Moreover, the efficiency of the chosen fusion protein was proved in combination with the transaminase reaction. The biotransformations showed good conversion rates despite the low retained activity. However, the reduced velocity compared to the WT enzymes could be improved by adding increased amount of biocatalyst.

In the last experiment, the soluble fusion protein showed higher stability during consecutive reactions. An analogous outcome was seen in the GluDH and FDH fusion protein (chapter 6) when tested in high scale biotransformation of ammonia. Consequently, it can be assumed that the fusion protein is an optimized system that enhance the stabilization level of the connected biocatalysts, increasing the overall efficiency, if the activity is maintained. As future work, the AlaDH-FDH-His fusion protein could be immobilized following the same procedures as the WT enzymes to compare the final recovered activity of the covalently bound FDH domain, which typically lose all the activity. Perhaps, the fusion of the two domains could impact also on the immobilization outcomes yielding an efficient immobilized bifunctional protein.

#### 7.4 BIBLIOGRAPHY

1. Fuchs, M., Farnberger, J. E. & Kroutil, W. The Industrial Age of Biocatalytic Transamination. *European J. Org. Chem.* **2015**, 6965–6982 (2015).
2. Slabu, I., Galman, J. L., Lloyd, R. C. & Turner, N. J. Discovery, Engineering, and Synthetic Application of Transaminase Biocatalysts. (2017) doi:10.1021/acscatal.7b02686.
3. Börner, T. *et al.* Three in One: Temperature, Solvent and Catalytic Stability by Engineering the Cofactor-Binding Element of Amine Transaminase. *ChemBioChem* **18**, 1482–1486 (2017).
4. Börner, T. *et al.* Explaining Operational Instability of Amine Transaminases: Substrate-Induced Inactivation Mechanism and Influence of Quaternary Structure on Enzyme-Cofactor Intermediate Stability. *ACS Catal.* **7**, 1259–1269 (2017).
5. Chen, S., Campillo-Brocal, J. C., Berglund, P. & Humble, M. S. Characterization of the stability of *Vibrio fluvialis* JS17 amine transaminase. *J. Biotechnol.* **282**, 10–17 (2018).
6. Shin, J. S. & Kim, B. G. Substrate inhibition mode of  $\omega$ -transaminase from *Vibrio fluvialis* JS17 is dependent on the chirality of substrate. *Biotechnol. Bioeng.* **77**, 832–837 (2002).
7. Kelefiotis-Stratidakis, P., Tyrikos-Ergas, T. & Pavlidis, I. V. The challenge of using isopropylamine as an amine donor in transaminase catalysed reactions. *Org. Biomol. Chem.* **17**, 1634–1642 (2019).
8. Koszelewski, D. *et al.* Formal asymmetric biocatalytic reductive amination. *Angew. Chemie - Int. Ed.* **47**, 9337–9340 (2008).

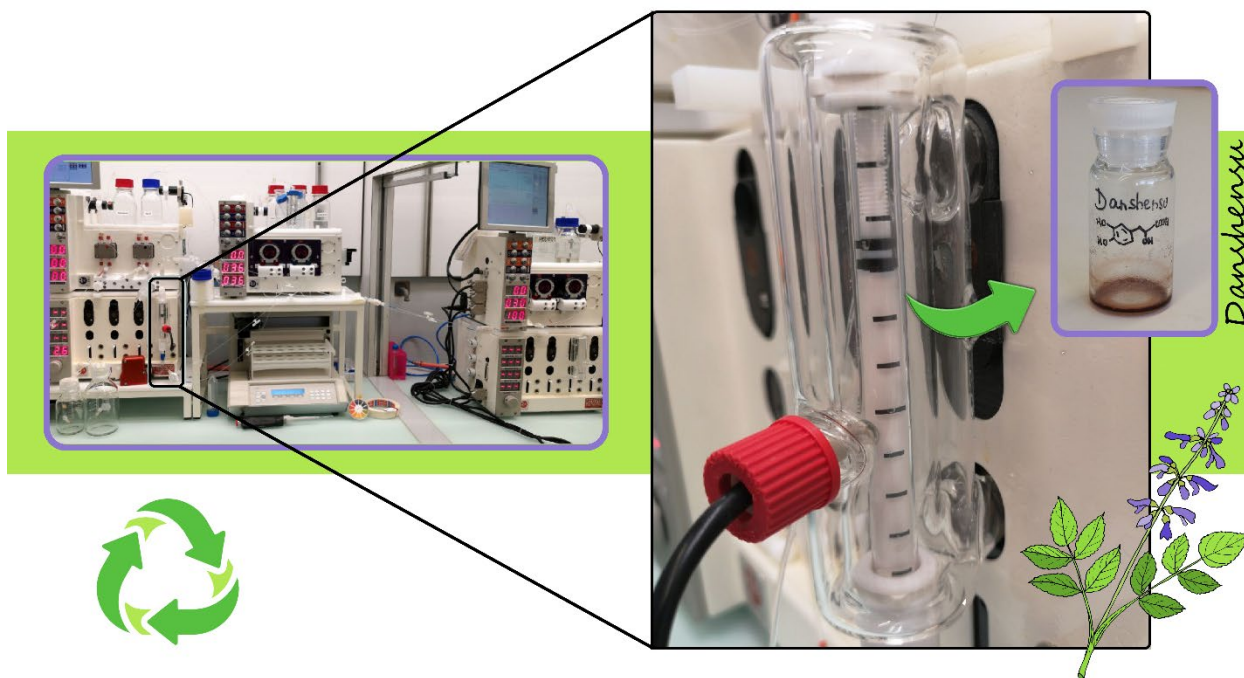
9. Padrosa, D. R., Nissar, Z. & Paradisi, F. Efficient amino donor recycling in amination reactions: Development of a new alanine dehydrogenase in continuous flow and dialysis membrane reactors. *Catalysts* **11**, (2021).
10. Aalbers, F. S. & Fraaije, M. W. Coupled reactions by coupled enzymes: alcohol to lactone cascade with alcohol dehydrogenase–cyclohexanone monooxygenase fusions. *Appl. Microbiol. Biotechnol.* **101**, 7557–7565 (2017).
11. Bhatwa, A. *et al.* Challenges Associated With the Formation of Recombinant Protein Inclusion Bodies in *Escherichia coli* and Strategies to Address Them for Industrial Applications. *Front. Bioeng. Biotechnol.* **9**, 65 (2021).
12. Donovan, R. S., Robinson, C. W. & Click, B. R. Review: Optimizing inducer and culture conditions for expression of foreign proteins under the control of the lac promoter. *J. Ind. Microbiol.* **16**, 145–154 (1996).
13. Jhamb, K. & Sahoo, D. K. Production of soluble recombinant proteins in *Escherichia coli*: Effects of process conditions and chaperone co-expression on cell growth and production of xylanase. *Bioresour. Technol.* **123**, 135–143 (2012).
14. Oganessian, N., Ankoudinova, I., Kim, S. H. & Kim, R. Effect of osmotic stress and heat shock in recombinant protein overexpression and crystallization. *Protein Expr. Purif.* **52**, 280–285 (2007).
15. Blackwell, J. R. & Horgan, R. *A novel strategy for production of a highly expressed recombinant protein in an active form.* *FEBS Letters* vol. 295 (1991).
16. Sarch, C., Suzuki, H., Master, E. R. & Wang, W. Kinetics and regioselectivity of three GH62  $\alpha$ -L-arabinofuranosidases from plant pathogenic fungi. *Biochim. Biophys. Acta - Gen. Subj.* **1863**, 1070–1078 (2019).
17. Jiang, W. & Fang, B. S. Construction and evaluation of a novel bifunctional phenylalanine–formate dehydrogenase fusion protein for bienzyme system with cofactor regeneration. *J. Ind. Microbiol. Biotechnol.* **43**, 577–584 (2016).
18. Ngo, A. C. R., Schultes, F. P. J., Maier, A., Hadewig, S. N. H. & Tischler, D. Improving Biocatalytic Properties of an Azoreductase via the N-Terminal Fusion of Formate Dehydrogenase. *ChemBioChem* **23**, (2022).

19. Zhang, Y., Wang, Y., Wang, S. & Fang, B. Engineering bi-functional enzyme complex of formate dehydrogenase and leucine dehydrogenase by peptide linker mediated fusion for accelerating cofactor regeneration. *Eng. Life Sci.* **17**, 989–996 (2017).

## CHAPTER 8.

### BIOCATALYTIC CASCADE FOR THE CONTINUOUS PRODUCTION OF DANSHENSU

---



## 8.1 INTRODUCTION

The dried root of the plant *Salvia miltiorrhiza*, also known as red sage or Danshen in Chinese, is one of the major traditional herb medicines and the most widely used for more than a thousand years in China.<sup>1</sup> Danshen is also listed in the Chinese Pharmacopeia for its well-known pharmacological effects.<sup>2</sup> In this regard, the consumption of this crude drug was estimated at about 80 million kilogram a year in China.<sup>3</sup>

The traditional medical prescription suggests the administration as decoction preparation.<sup>1</sup> During the process, many root components are extracted, of which danshensu, rosmarinic acid and salvianolic acid B are the highest water-soluble constituents.<sup>4</sup>

Danshensu [3-(3,4-dihydroxy-phenyl) lactic acid], also called Salvianic acid A, is an active component that has been extensively studied over the years, offering a list of numerous pharmacological activities.<sup>5</sup> Danshensu is structurally composed of a catechol and a lactic acid (Figure 1). The catechol is the major active group that exerts an antioxidant effect.<sup>6</sup> In this context, it exhibited higher scavenging activity against radicals than vitamin C, possessing excellent antioxidant property, which is in agreement with its protective effects against cell injury from oxidative stresses.<sup>4</sup>

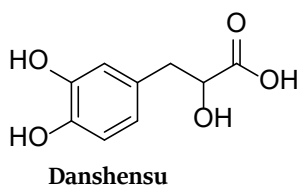


Figure 1. Chemical structure of danshensu.

Danshensu demonstrated therapeutic effects in cardiovascular diseases (e.g., myocardial ischemia and reperfusion, atherosclerosis, hypertension, Angina Pectoris, cardiac fibrosis), cerebral lesions and disorders (e.g., ischemia, cognitive decline, anxiety), and other health problems (e.g., thrombosis, tumorigenesis, pancreatitis, preeclampsia).<sup>6</sup> It can activate and improve blood microcirculation in association with vasodilation, hypotensive action and inhibition of platelet aggregation.<sup>7-9</sup> Other mechanisms behind the beneficial effects include anti-apoptosis, inflammation regulation, lipidemia control, through several molecular signaling pathways.<sup>6,10,11</sup>



Most recently, *in vitro* and *in vivo* studies identified antiviral activity against severe acute respiratory syndrome coronavirus 2 (SARS-CoV-2). Moreover, the SARS-CoV-2-triggered respiratory inflammation, which may cause severe damage to lung tissue leading to mortality, was effectively inhibited by this pharmaceutical compound. Thus, danshensu is also a potential treatment for COVID-19 patients.<sup>12</sup>

In addition to all these positive effects, single or repeated dose toxicity studies suggested that danshensu does not cause any sign of adverse effect and toxicity, making it a safe compound.<sup>13</sup>

The administration of danshensu in combination with classical cardiovascular drugs as metoprolol, nicardipine, perindopril, benazepril has already proved to improve therapeutic efficiency in comparison with the well-established drugs taken alone.<sup>6</sup> Danshensu might even be more effective than conventional drugs.<sup>6</sup>

Nevertheless, this promising pharmaceutical compound is too expensive for widespread commercialization. As an example, the current price of danshensu sodium salt (CAS 81075-52-7) in Sigma Aldrich is \$330 (USA) and €329 (Europe) for 25 mg, which results in €13,160 per gram.

Nowadays, danshensu is mostly produced by extraction from the root of Danshen, but the yield is typically low.<sup>9,14</sup> Isolation and purification from natural resources are difficult and time consuming due to the chemical instability of phenolic hydroxyl groups, low content of danshensu in Danshen and the presence of a variety of structural analogs as impurities.<sup>15</sup> Moreover, it is hard to obtain from chemical synthesis due to its chiral structure.<sup>15</sup> Indeed, only the pure (R)-danshensu is desirable, since the (S)-enantiomer has not been studied yet.<sup>16</sup> Several synthetic strategies have been explored, but they suffered from complicated procedures, low yields, low enantiopurity and very expensive costs due to the need for chiral catalysts.<sup>14,17</sup>

Metabolic engineering of *E. coli* was also developed to produce danshensu via biosynthetic strategy. In this case, the production was accomplished by the integration of two enzymes in the metabolic pathway, in particular *E. coli* endogenous hydroxylase complex HpaBC and D-lactate dehydrogenase (D-LDH) from *Lactobacillus pentosus* (Figure 2).<sup>17</sup> However, the product was achieved by adding 4-hydroxyphenyl pyruvate (HPPA) as a precursor, which is mainly prepared via a multistep process that involves harsh conditions and causes environmental pollution.<sup>18</sup>

A similar problem arises for the reaction based on whole-cell biotransformation, that employed *E. coli* BL21 co-expressing the LDH from *Lactobacillus reuteri* and a glucose dehydrogenase (GDH), as shown in Figure 3.<sup>19</sup> This

system was optimized for the conversion of DHPPA, although its chemical synthesis in large quantities is limited by the complicated process and the use of toxic heavy metals.<sup>14</sup>

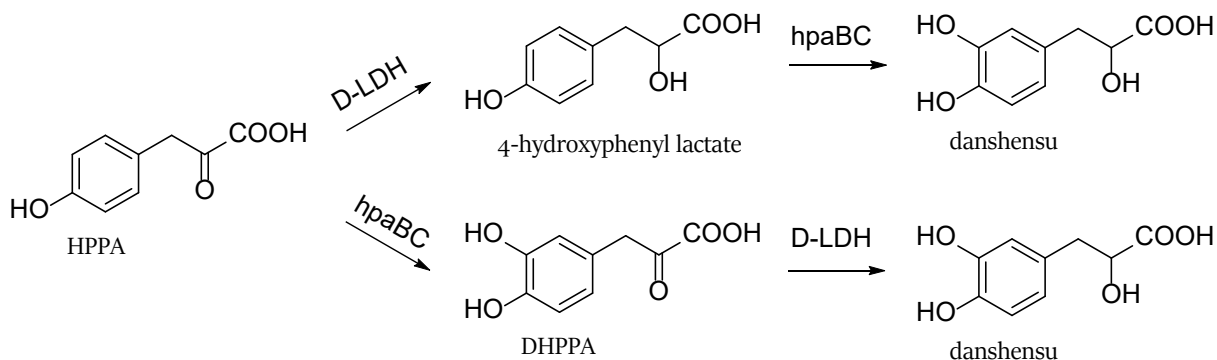


Figure 2. Reaction scheme of danshensu production via hpaBC and D-LDH in *E. coli* cells.<sup>17</sup>

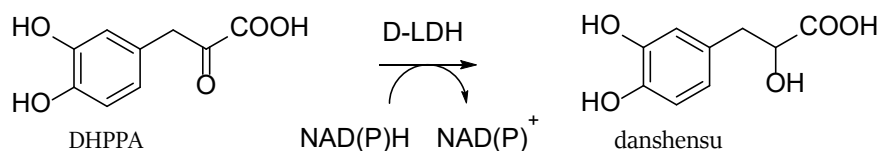


Figure 3. Reaction scheme of danshensu production with D-LDH from *Lactobacillus reuteri* starting from DHPPA.<sup>19</sup>

To our knowledge, only one publication investigated the production of danshensu starting from the renewable substrate L-dopa. In this work, the whole-cell biotransformation was achieved with the combination of three enzymes, namely tyrosine aminotransferase from *Escherichia coli* (tyrB), glutamate dehydrogenase from *Clostridium difficile* (cdgdh) and D-aromatic lactate dehydrogenase from *Clostridium sporogenes* (csldhD).<sup>14</sup> The addition of the glutamate dehydrogenase had the purpose to regenerate the amino acceptor for the transaminase reaction as well as the cofactor for the DHPPA (intermediate) reduction, achieved with csldhD (Figure 4). However, the conversion of L-dopa to danshensu could be performed with only two enzymes instead of three and reduced substrates content if the amino acceptor is not required. This would lead to cost- and material-effectiveness.

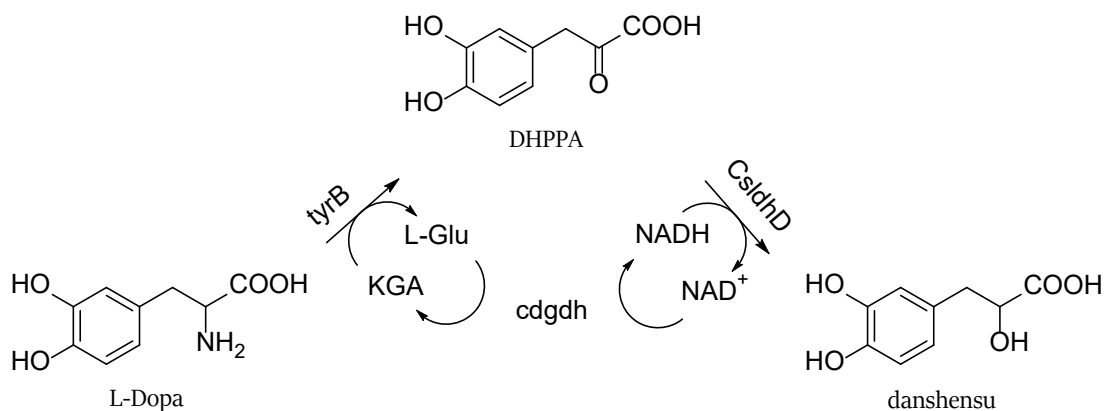


Figure 4. Reaction scheme of danshensu production starting from L-dopa. KGA: α-ketoglutaric acid.<sup>14</sup>

In this work, a sustainable system has been investigated to produce danshensu starting from the low-priced substrates caffeic acid and L-dopa without the need for a supplementary enzyme (Figure 5). In details, the first reaction is completed with the PAL from *Rhodotorula glutinis* (RgPAL) which aminates caffeic acid to L-dopa in the presence of an ammonium source. Then, the PheDH from *Bacillus subtilis* (BsPheDH) is coupled with a new, uncharacterized, hydroxy phenyl pyruvate reductase (HPPR) for the continuous conversion of L-dopa to danshensu. This system provides continuous regeneration of the cofactor, while no additional substrate is added.

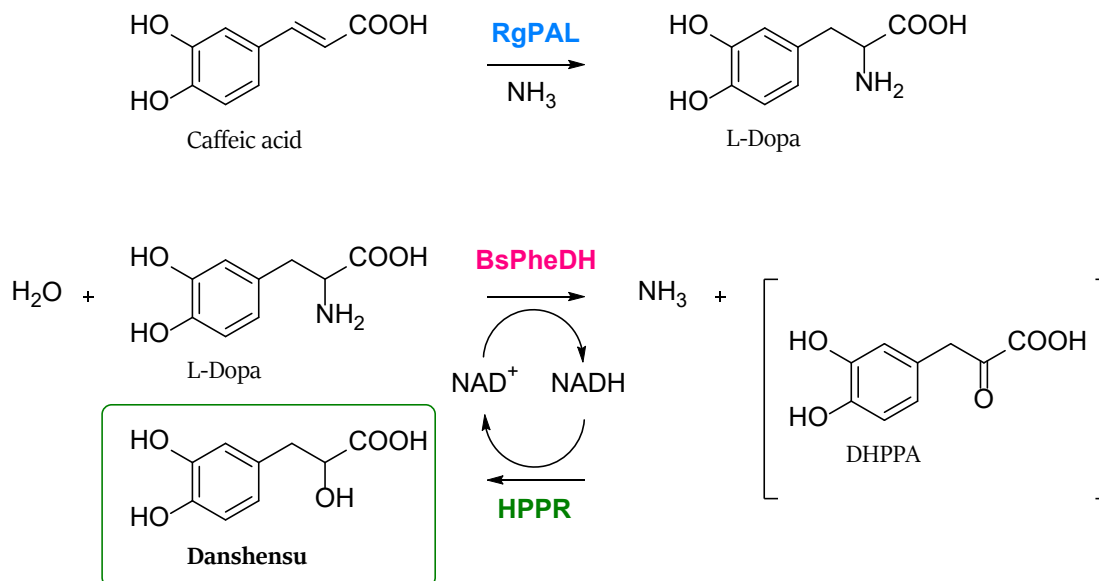


Figure 5. Reaction scheme of danshensu production using RgPAL, BsPheDH, HPPR.

## 8.2 RESULTS AND DISCUSSION

### 8.2.1 Purification, activity and immobilization of RgPAL

The expression of RgPAL yielded 17 grams of pellet per liter of culture. After purification, around 55 mg of pure protein were obtained. L-phenylalanine is the natural substrate for the non-oxidative deamination reaction performed by RgPAL. However, this enzyme is known to have activity towards L-tyrosine, inserting it in the class of PTALs (phenylalanine tyrosine ammonia lyases). Since the presence of the *para*-hydroxy group on the aromatic moiety showed activity, L-dopa was also tested as substrate containing a second OH in *meta*-position. The reaction schemes are available in Figure 6, while the results of the specific activity towards the three mentioned substrates are shown in Table 1.

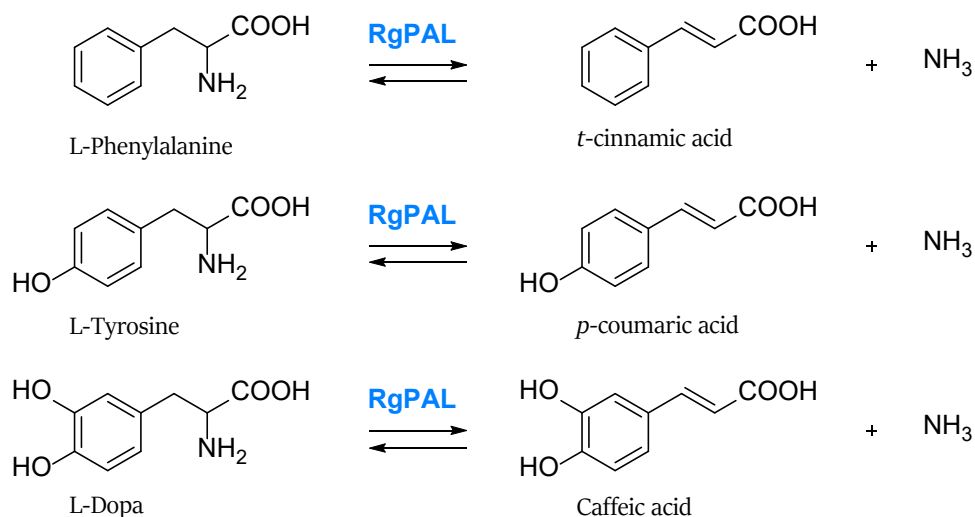


Figure 6. Scheme of the reactions catalyzed by RgPAL, using L-phenylalanine, L-tyrosine, and L-dopa as substrates.

Table 1. Specific activity of RgPAL for L-phenylalanine ( $\lambda$ : 300 nm,  $\epsilon$ : 3.865 mM<sup>-1</sup> cm<sup>-1</sup>), L-tyrosine ( $\lambda$ : 290 nm,  $\epsilon$ : 20.575 mM<sup>-1</sup> cm<sup>-1</sup>) and L-dopa ( $\lambda$ : 325 nm,  $\epsilon$ : 17.621 mM<sup>-1</sup> cm<sup>-1</sup>) in 50 mM borate buffer pH 8.5 at 30°C.

Substrate	Concentration [mM]	Specific activity [U/mg]	Comparison to L-Phe [%]
L-phenylalanine	20	2.5 ± 0.1	/
L-tyrosine	5	0.50 ± 0.05	20
L-dopa	10	0.016 ± 0.003	0.64

RgPAL presented 5-fold lower specific activity for L-tyrosine, compared to the activity for L-phenylalanine. Instead, the activity for L-dopa was only a 0.64% with respect to L-phenylalanine. Probably, this low value was caused by the higher steric hindrance of the substrate in the active site. Indeed, the presence of only one of the two hydroxy groups in the ring caused already an 80% activity loss.

Accordingly, a mutated form of RgPAL (Ile472Val) was developed with the aim to offer more space in the aromatic *para* and *meta* positions of the substrate. The exchange of the isoleucine with a smaller amino acid was suggested in a previous publication where several mutations of a PAL were analyzed, mapping the conserved amino acidic residues of the active site.<sup>20</sup> Moreover, the TAL from *Rhodobacter sphaeroides* was found to have activity towards L-dopa and that exact position (409) presented a valine.<sup>21</sup> Consequently, the isoleucine of RgPAL was mutated for a valine in position 472. Although the mutant retained almost full activity towards L-phenylalanine, the activity for L-dopa was significantly reduced with only a 4% retained activity compared to the wild-type (0.0007 U/mg). Since the specific activity was low for both WT RgPAL and RgPAL I472V, the biocatalysts were tested in a 10-hour batch biotransformations with all the three substrates as starting materials (Figure 7).

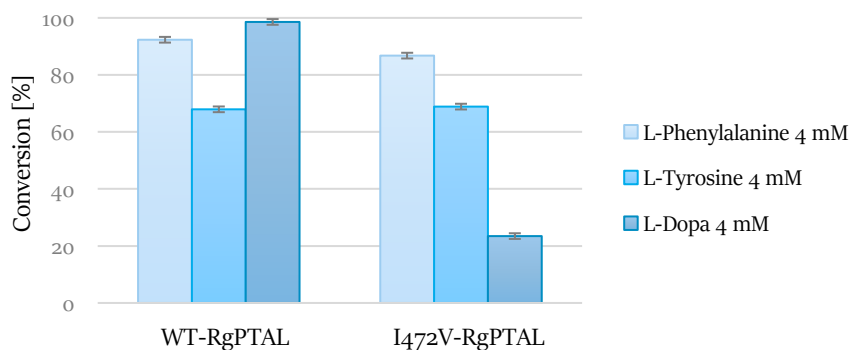
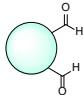
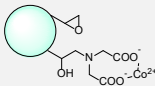
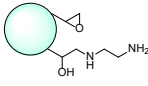
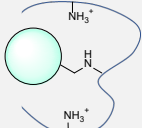


Figure 7. Conversion of 4 mM L-phenylalanine, L-tyrosine, or L-dopa at 37°C, after 10 hours of biotransformation using 1 mg/mL (final concentration) of WT-RgPAL or I472V-RgPAL

Surprisingly, the wild-type enzyme achieved almost full conversion of 4 mM L-dopa when in parallel the other two substrates, at the same concentrations, were not converted as fast. On the contrary, the mutant did not offer any improvement, reaching a 4 times lower conversion compared to the WT-RgPAL. Thus, WT-RgPAL was chosen for the next experiments.

The PALs amination reaction is performed with high ammonium salt concentrations, from 2 to even 6 M, to achieve decent conversions. A first attempt of reaction was done with the free RgPAL, however the enzyme rapidly precipitated in such high ionic strength without showing any product formation. For this reason, the biocatalyst was immobilized onto a resin to enhance its stability (Table 2).

Table 2. Screening of immobilization strategies of RgPAL onto a methacrylate resin.

Resin	Functional groups and Immobilization strategy	Loading of RgPAL [mg/g]	Immobilization Yield [%]	Recovered Activity [%]
EP400/SS	 Aldehydes for covalent immobilization	1	>99	0
EP400/SS	 Epoxides + Iminodiacetic acid (IDA) + Cobalt for oriented covalent bonds	1	99	65 ± 4
EP400/SS	 Epoxy/Amino (EDA) for oriented covalent bonds	1	99	75 ± 4
EP400/SS	 Aldehydes covered with PEI for ionic interaction	1	99	55 ± 7

The highest recovered activity was obtained with the resin functionalized with amino and epoxy groups, where the enzyme was covalently bound. This preparation was used for the biotransformations.

Due to the fast oxidation of L-dopa and the caffeate catechol group, the substrate solution was prepared with the addition of an antioxidant. Firstly, 10 or 20 mM of ascorbic acid were used to ensure antioxidant activity, but the enzyme was completely inhibited by the compound. Then, glutathione (5 or 10 mM), dithiothreitol (DTT, 5 mM) and  $\beta$ -mercaptoethanol (5 mM) were tested in 24-hours biotransformations.

The conversion of L-phenylalanine or L-dopa was not affected by the presence of the reagents and in 24 hours visible oxidation (formation of darker color over time) was not observed at all with  $\beta$ -mercaptoethanol. Therefore, it was chosen as antioxidant agent, also for its cheaper price.

### 8.2.2 Batch biotransformations of RgPAL

The biocatalyst was immobilized with higher loading (10 mg/g) yielding full immobilization and 75% recovered activity. The 24-hours biotransformations with 10 mg of immobilized RgPAL achieved full conversion of 5 mM L-dopa, 82% with 10 mM and 52% with 20 mM, confirming the efficiency of the immobilized form in the deamination reaction (1 mL reaction in 50 mM potassium phosphate buffer pH 8.0, incubation at 37°C).

Regarding the amination of caffeic acid to produce L-dopa, the biotransformations were performed in a degassed environment (after N<sub>2</sub> bubbling) to avoid oxidation caused by the presence of the salt at basic pH (Figure 8). With the deamination reaction, it was confirmed that the process did not affect the conversion and, accordingly, the immobilized enzyme (Figure 8 A).

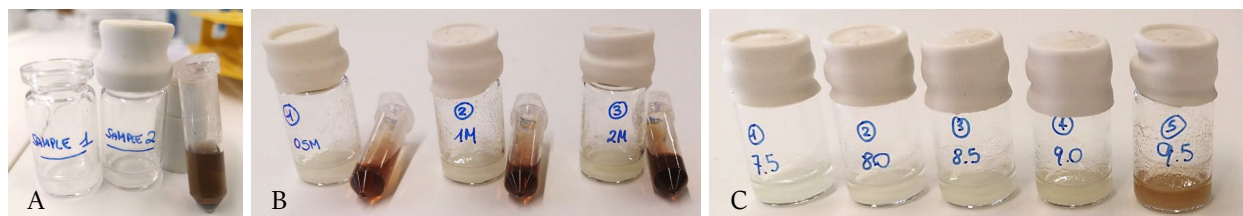


Figure 8. Biotransformation performed in degassed environment (glass vial with septum) and in presence of oxygen (tube).

Different ammonium sources were trialed at pH 8.5 and 9.5. Carbamate (2 M) and chloride (4 M) salts accelerated the oxidation process even in absence of oxygen and in presence of  $\beta$ -mercaptoethanol, showing no product formation. Probably the oxidation started before the degassed reaction, during the solution preparation, and it propagated after.

Ammonium formate (4 M) gave very low conversion. Instead, ammonium sulfate was effectively used in the amination reaction with decent conversion rate, so it was chosen as ammonium source.

Different pH values and different salt concentrations were tested.

The best results were obtained with 2 M and pH 8.5 for a balanced ratio between conversion and rate of oxidation (faster with higher pH or ionic strength, as shown in Figure 8 B and 8 C). In 24 hours, RgPAL could effectively convert  $18 \pm 2\%$  of 5, 10 or 20 mM caffeic acid.

### 8.2.3 L-Dopa purification and RgPAL amination in flow

The presence of 2 M ammonium sulfate in the reaction environment highly impacted the oxidative deamination of L-dopa to DHPPA (BsPheDH reaction), shifting the equilibrium to the re-amination. For this reason, a method to separate the L-dopa product from the ammonium salt was investigated. The compound could not be extracted with any solvent, so a liquid-liquid extraction (LLE) on a complexed form of L-dopa was attempted to separate it from the salt-aqueous phase and reintroduce it to a fresh buffer solution. This involved the use of phenylboronic acid (PBA) derivatives, since the boronate form obtained at alkaline pH reacts with the catechol to produce a reversible complex. At acidic pH, the boronic acid is not bound to the catechol, and it is released as free form (Figure 9). In this case, 3-aminophenylboronic acid and 4-mercaptophenylboronic acid were employed.

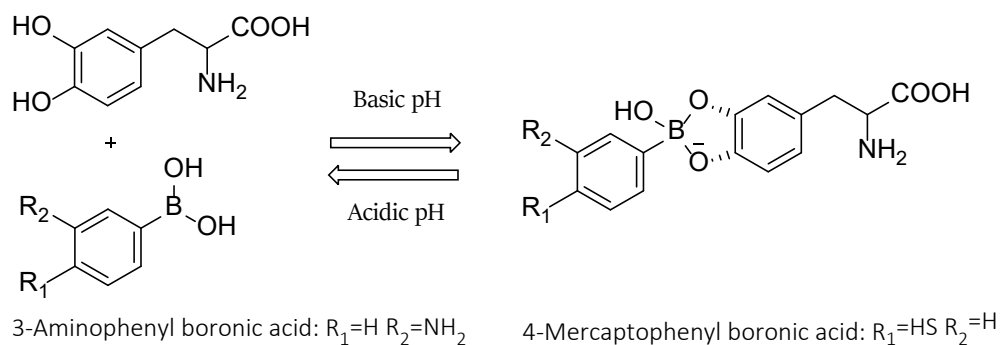


Figure 9. Complexation between PBA derivatives and L-dopa depending on pH.

Around half extracted complex was obtained with a mixture of butanol, ethanol, and ethyl acetate. However, an efficient extraction of the PBA-L-dopa complex was hard to achieve even trying different solvent mixtures at different ratios, so another method was attempted. A solid-phase extraction (SPE) based on the same complexation strategy was performed after functionalizing the methacrylate resin EP400/SS with the PBA derivatives (Figure 10). The L-dopa solution was incubated with the reactive boronate groups on the two resins, which were then washed to remove contaminants. Finally, the complexed catechol compounds were eluted by incubating the resin with Tris HCl buffer or acidic pH. Nevertheless, most of the bound L-dopa was lost in the washing step and only a 20% could be finally eluted in the fresh buffer, even trying different conditions.



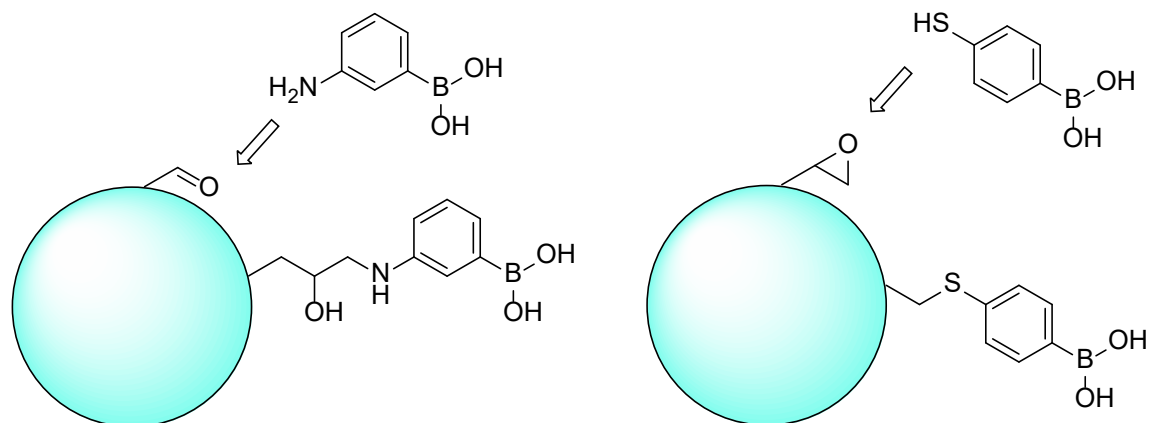


Figure 10. Functionalization of methacrylate beads presenting glyoxyl or epoxy groups with 3-amino- and 4-mercapto-PBA.

The optimization of a method for the purification of L-dopa was not investigated further also because of the results of the RgPAL amination reaction in continuous flow. In fact, the conversion reached maximum a 6% with 30 minutes of residence time (Table 3).

Table 3. Results of the continuous flow reaction with RgPAL, 20 mM caffeic acid, 5 mM  $\beta$ -mercaptoethanol ( $\beta$ SME), 2 M ammonium sulfate pH 8.5 at 37°C.

Amount of resin [g]	Loading of RgPAL [mg/g <sub>resin</sub> ]	Residence Time [min]	Conversion [%]	Product concentration [mM]
1.6	5	15	3	0.6
		30	6	1.2
		60	3	0.6
Amount of resin [g]	Loading of RgPAL [mg/g <sub>resin</sub> ]	Contact time [h]	Conversion [%]	Product concentration [mM]
1.4	10	2.5	8	1.6

The recirculation of the collected solution (10.27 mL corresponding to 5 column volumes of the packed bed reactor) reached only 8% conversion despite the higher protein concentration (10 mg/g, 100% immobilization yield, 65% recovered activity). Moreover, the biocatalyst lost activity over cycles of usage, and only 20% of activity was retained after one reaction and the following overnight incubation at 4°C, probably because of the stickiness of oxidized substrate/(by)product onto resin.

Considering the low efficiency of the RgPAL amination and thus the impact on costs and time spent for the reaction or the preparation of new active biocatalyst and the accumulation of waste over reactions (2 M ammonium sulfate, oxidized L-dopa), the production of danshensu starting from caffeic acid was abandoned. At the present time, the price of L-dopa is €3.36 per gram (CAS 59-92-7; Sigma-Aldrich Europe; product D9628-500G: €1,680), therefore in terms of cost it appears to be an excellent option also.

#### **8.2.4 Purification, activity and immobilization of BsPheDH**

The expression of BsPheDH yielded 16 g of pellet and 32 mg of purified enzyme (per L of culture).

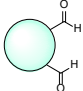
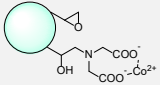
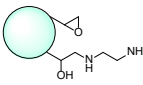
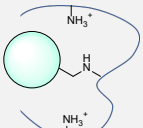
The specific activity towards L-phenylalanine was  $100 \pm 10$  U/mg in the oxidative deamination reaction, as already described in literature.<sup>22-24</sup> In comparison, BsPheDH showed lower activity for L-dopa, ranging around 17 U/mg. The biocatalyst was immobilized onto the methacrylate resin EP400/SS using four different strategies, as shown in Table 4.

The covalent immobilization did not hamper the enzyme activity, which was sufficiently good. Among the three strategies of covalent binding, the immobilization on epoxides in presence of IDA and cobalt gave the highest recovered activity, which was approximately 36% with a protein loading of 1 mg/g.

The reversible immobilization on PEI achieved around 90% of recovered activity, meaning that the enzyme retained considerable flexibility required for the full activity.

Given the high activity of BsPheDH immobilized on PEI and the reversible nature of the interactions, the operational stability was checked by running several cycles of 4-hours biotransformations with 10 mM L-phenylalanine and 20 mM NAD<sup>+</sup> (in 50 mM Tris HCl buffer pH 8.5). After 10 reactions, the immobilized enzyme retained 60% of the initial activity. Therefore, the biocatalyst was sufficiently stable, although the binding on the resin was reversible and the enzyme could have been deactivated after leaching in the bulk environment.

Table 4. Screening of immobilization strategies of BsPheDH onto a methacrylate resin.

Functional groups and Immobilization strategy	Loading of BsPheDH [mg/g]	Immobilization Yield [%]	Recovered Activity [%]
 Aldehydes for covalent immobilization	1	99	27 ± 3
 Epoxides + Iminodiacetic acid (IDA) + Cobalt for oriented covalent bonds	1	>99	36 ± 2
	5	>99	14 ± 4
 Epoxy/Amino (EDA) for oriented covalent bonds	1	>99	26 ± 3
 Aldehydes covered with PEI for ionic interaction	1	>99	92 ± 5
	3	>99	90 ± 3

### 8.2.5 Batch biotransformations of BsPheDH

The free and immobilized enzyme was tested in batch biotransformations (1 mL of reaction volume) with L-phenylalanine or L-dopa as substrates (final concentration of 10 mM). These reactions were run at pH 10.4, which was ideal for BsPheDH deamination, and pH 8.5 for the stability of both the L-dopa and the cofactor since they are less stable under basic conditions. Compared to pH 10.4, at pH 8.5 the enzyme retained 60% of the activity, while the substrates did not show any breakdown. Without the addition of a cofactor recycling system, the reaction required high initial concentrations of NAD<sup>+</sup> to show increased conversion rates. As a matter of the fact, the presence of 2 equivalents of cofactor (20 mM) resulted in 2-fold higher conversion than for 1 equivalent. The same was noticed with the amount of protein in the reaction, where the addition of more BsPheDH increased the molar conversion.

When using 20 mg of immobilized enzyme (3 mg/g on PEI) in the biotransformation of 10 mM L-dopa and 20 mM cofactor, a conversion of 19% was achieved in 6 hours (Figure 11). After 24 hours of reaction, no further conversion was found. The addition of 20% ethyl acetate in the biotransformation environment showed slightly

lower conversion (18%) meaning that the immobilized enzyme was still stable. An increase of substrate or product recovery was not seen either, confirming that the two compounds were not sticking onto the methacrylate resin. The reaction performed in 20% toluene yielded a reduced conversion rate (11%), as toluene clearly impacted the enzyme stability.

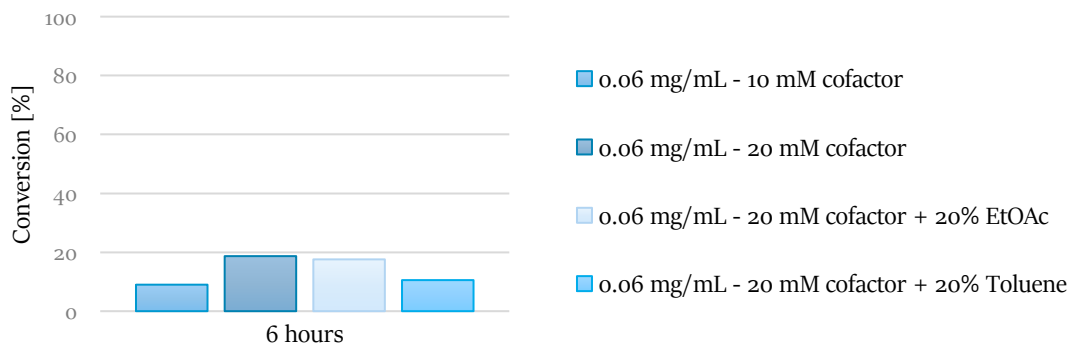


Figure 11. Batch biotransformations (1 mL volume) of 10 mM L-dopa with immobilized BsPheDH, 10 - 20 mM NAD<sup>+</sup>, 5 mM βME, 50 mM Tris HCl buffer pH 8.5 at 25°C, 150 rpm.

Improved values were expected after the coupling of BsPheDH with MpHPPR, since lower amounts of cofactor were required, thanks to the continuous *in situ* recycling. Also, the reaction equilibrium was expected to be shifted towards the product formation. Indeed, the product of BsPheDH (DHPPA) is converted to danshensu by the HPPR as soon as it is formed.

### 8.2.6 Expression, purification and characterization of MpHPPR

The sequence of HPPR from *Mentha x piperita* (MpHPPR) was found by sequence alignment to the only characterized enzyme of this class up to now. In this regard, MpHPPR possessed high identity with CbHPPR (91.4%). The gene was ordered to GenScript with pET15b as backbone.

The enzyme MpHPPR has never been expressed and characterized before, so a first screening of different expression conditions was done. The enzyme was overexpressed in 50 mL of LB or AI media at 37°C or 25°C, induced with 1 or 0.1 mM IPTG when LB media was used. An SDS-PAGE was run with the samples of the described expression conditions to compare the yield of insoluble/soluble proteins (Figure 12). The molecular weight of the MpHPPR monomers was confirmed to be around 36 kDa, as expected from the genetic sequence.

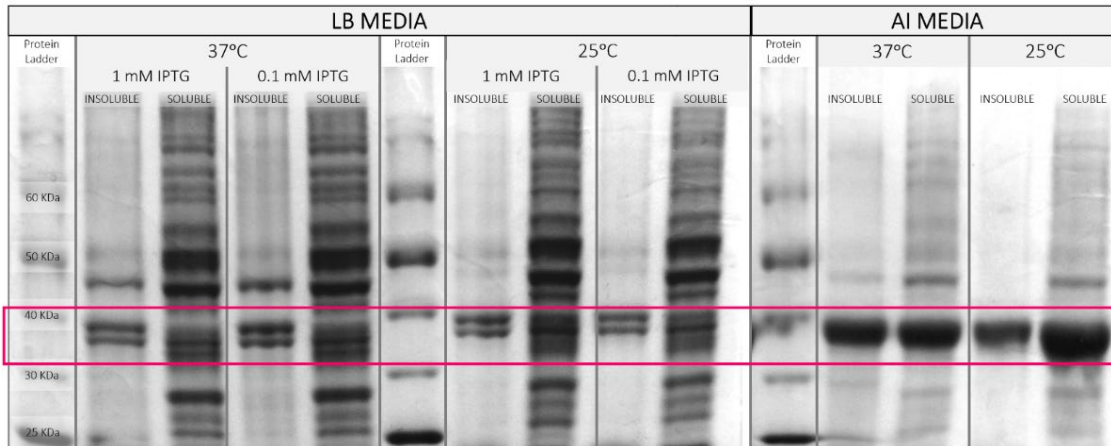


Figure 12. SDS-PAGE of expression conditions. The bands related to MpHPPR are located inside the pink rectangular.

Both insoluble and soluble fractions were found in all the tested conditions. However, the expression in autoinduction media at 25°C offered the highest amount of soluble overexpressed protein. Moreover, it gave the best ratio between soluble and insoluble proteins, where the soluble were predominant compared to the insoluble. The activity of the crude extract was checked with DHPPA and NADH as substrates, and all the conditions seemed to give active proteins.

The larger scale expression (AI - 25°C) produced 20 grams of pellet per liter of culture. Enzyme purification was performed by Nickel-affinity chromatography using a 5 mL His-trap column. A significant amount of MpHPPR was effectively purified, specifically 300 mg per liter of culture media, as shown in Figure 13.

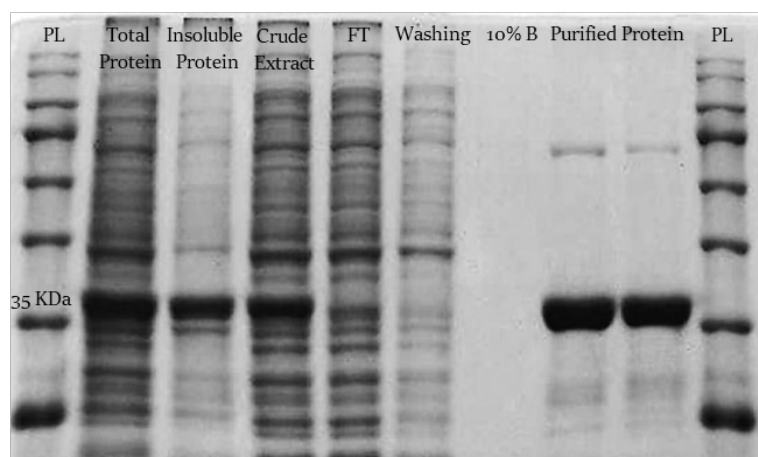


Figure 13. SDS-PAGE of MpHPPR purification process.

The specific activity of the purified enzyme was monitored by stopping 1 mL reactions at specific time points and analyzing the samples by HPLC. The activity was then calculated on the increase of product concentration per minute.

Firstly, the specific activity towards phenyl pyruvate and phenyl lactic acid (R and S enantiomers) was analyzed with the appropriate buffer to assess the activity over pH (Figure 14).

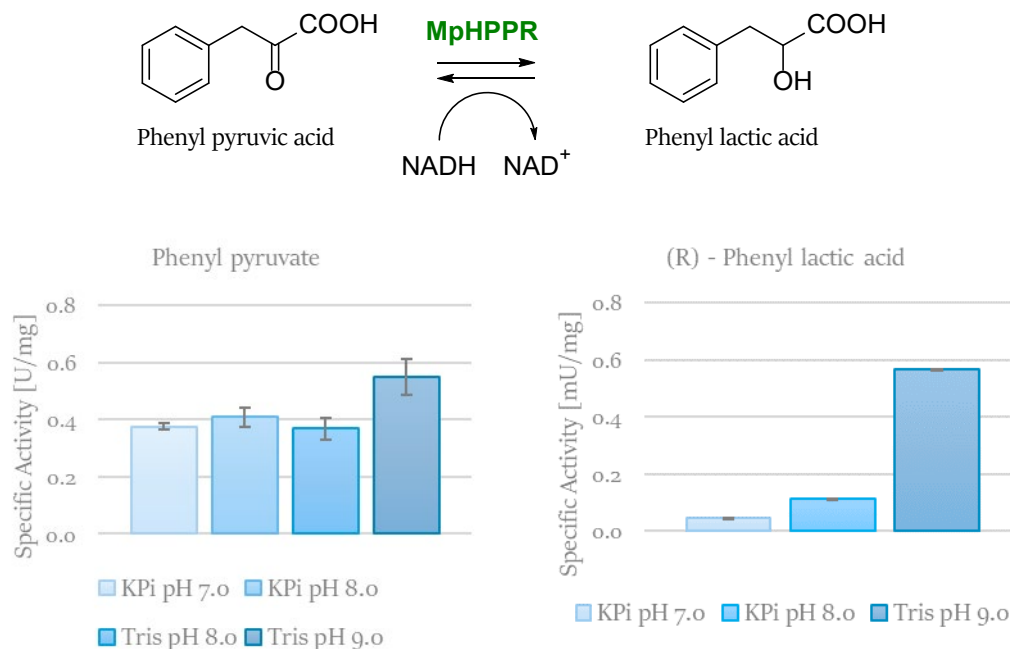


Figure 14. Scheme of reaction and specific activity of MpHPPR for phenylpyruvate and (R)-phenyl lactic acid at 37°C, employing 30 mM substrate, 10 mM NADH, 5 mM  $\beta$ -mercaptoethanol and the appropriate buffer: potassium phosphate (KPi) or Tris HCl buffer.

The biocatalyst did not exhibit any activity for the (S)-enantiomer, confirming the great specificity of MpHPPR to the (R)-enantiomer. Furthermore, the reduction of phenylpyruvate is preferred compared to the opposite reaction, that showed 1000-times lower activity with a clear difference between pH 7 and pH 9.

As for the activity towards phenyl pyruvate, the results were very similar from pH 7 to pH 8 with slightly higher activity at pH 9 but still in the range considering the error. Nonetheless, the same test gave different outcomes when 4-hydroxyphenylpyruvic acid (HPPA) was employed as substrate (Figure 15). The highest activity was achieved at pH 7.0 while increasing the pH revealed a faster oxidation rate of the substrate solution (visible brown

color formation). Consequently, the lower activity obtained at higher pH may be caused by the reduced availability of the substrate, which was below the  $K_M$ . To avoid any error, all activity assays were performed at pH 7 in phosphate buffer. The temperature of 37°C was also chosen as standard condition for the activity assays since it showed the best outcome. In a similar way, CbHPPR was assessed to develop maximal activity at 37°C and at pH of 6.5 to 7.0 with HPPA or DHPPA as substrates.<sup>25</sup>

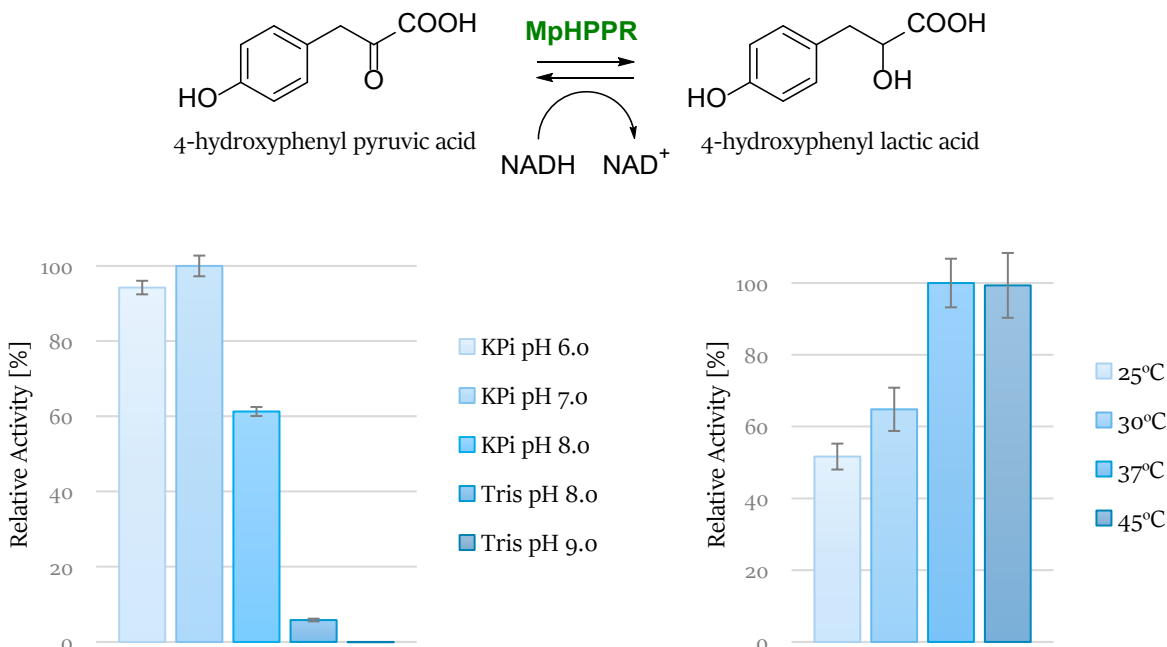


Figure 15. Scheme of reaction and specific activity of MpHPPR for HPPA, employing 30 mM substrate, 10 mM NADH, 5 mM  $\beta$ -mercaptoethanol and the appropriate buffer: potassium phosphate (KPi) or Tris HCl buffer for the graph on the left (at 37°C), and KPi pH 7 over temperature for the graph on the right. Relative activity to pH 7 (left) and 37°C (right).

The specific activity of MpHPPR for the different substrates is listed in Table 5, where also 3,4-dihydroxyphenyl pyruvic acid (DHPPA) is included. The specific assays were done with either NADH or NADPH.

The enzyme showed a preference for NADPH as cofactor with higher specific activity for HPPA (almost 4-times) and DHPPA (more than the double) compared to the activity achieved with NADH.

A similar trend was described for CbHPPR, where the activity for DHPPA was 2.6-fold higher with NADPH than NADH and 4 times higher for HPPA and NADPH compared to the same substrate in presence of NADH.<sup>26</sup>

However, CbHPPR did not accept phenyl pyruvate as substrate, since the reduction occurred only to a very low

extent, which was less than 2% of the activity towards DHPPA.<sup>26</sup> On the contrary, MpHPPR exhibited decent activity for phenyl pyruvate, that was comparable to the specific activity for HPPA. Notably, the activity assays of CbHPPR were also performed in 100 mM potassium phosphate buffer pH 7.0.

In addition, MpHPPR demonstrated a clear preference for DHPPA as seen with CbHPPR, although the affinity was approximately 4-fold lower for DHPPA with respect to phenyl pyruvate. Indeed, the  $K_M$  values raised with the increasing number of hydroxy groups on the aromatic moiety and, accordingly, with the increasing steric hindrance. The different polarity of the substrates might also be involved. In comparison, CbHPPR presented lower  $K_M$  for HPPA and DHPPA, respectively 0.01 and 0.13 mM, but similar lower affinity for DHPPA with respect to HPPA.<sup>25</sup>

Table 5. Specific activity and  $K_M$  for phenylpyruvate, HPPA and DHPPA at pH 7.0 (100 mM potassium phosphate buffer) and 37°C, using 30 mM substrate (specific activity) or different amounts from 0.5 to 30 mM ( $K_M$ ), 10 mM NAD(P)H, 5 mM  $\beta$ -mercaptoethanol.

	Cofactor	Specific activity [U/mg]	$K_M$ [mM]
Phenyl pyruvate	NADH	0.38 ± 0.01	1.7 ± 0.5
HPPA	NADH	0.44 ± 0.03	2.8 ± 0.5
	NADPH	1.6 ± 0.1	
DHPPA	NADH	3.3 ± 0.6	6.5 ± 0.5
	NADPH	7.2 ± 0.4	

MpHPPR proved to accept DHPPA and NADH as substrates, therefore it can be further studied and optimized for danshensu production inside the biocatalytic cascade.

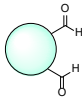
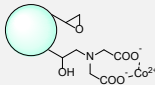
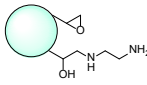
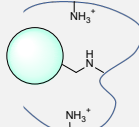
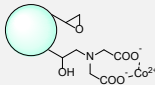
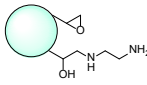
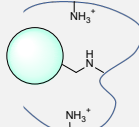
### 8.2.7 Immobilization and batch biotransformations of MpHPPR

To increase the enzyme stability and enhance the reusability, MpHPPR was immobilized onto EP400/SS using different strategies of immobilization and testing two loading capacities to ensure a sufficient level of activity (Table 6). Indeed, the low activity recovered after immobilization of 1 mg/g MpHPPR on epoxy-EDA resin was not easy to assess, while a 5 times higher loading provided a more precise outcome. In any case, the activity was



too low to consider this immobilization strategy as a choice. The same was observed for the covalent immobilization on glyoxyl groups. In fact, the enzyme was killed after the incubation step with  $\text{NaBH}_4$  and no activity was detected even with higher loading.

Table 6. Screening of immobilization strategies of MpHPPR onto a methacrylate resin. The recovered activity was measured with HPPA and NADPH as substrates.

Functional groups and Immobilization strategy	Loading of MpHPPR [mg/g]	Immobilization Yield [%]	Recovered Activity [%]																					
 Aldehydes for covalent immobilization	1	>99	0																					
	5			 Epoxides + Iminodiacetic acid (IDA) + Cobalt for oriented covalent bonds	1	>99	$39 \pm 1$	5	>99	$39 \pm 1$	40	>99	$37 \pm 1$	 Epoxy/Amino (EDA) for oriented covalent bonds	1	70	<1	5	70	$7 \pm 2$	 Aldehydes covered with PEI for ionic interaction	1	>99	$83 \pm 1$
 Epoxides + Iminodiacetic acid (IDA) + Cobalt for oriented covalent bonds	1	>99	$39 \pm 1$																					
	5	>99	$39 \pm 1$																					
	40	>99	$37 \pm 1$																					
 Epoxy/Amino (EDA) for oriented covalent bonds	1	70	<1																					
	5	70	$7 \pm 2$																					
 Aldehydes covered with PEI for ionic interaction	1	>99	$83 \pm 1$																					
	5	>99	$89 \pm 2$																					

The best recovered activity was achieved through the reversible immobilization on PEI, which was more than 80%. After this strategy, the covalent immobilization on epoxides (in presence of IDA and cobalt) offered good recovery of activity (39%), that was half than the previous one but still sufficient to provide satisfactory conversion rates. In fact, these two immobilized enzymes were evaluated in batch biotransformation to compare their performance over time, in parallel with the soluble biocatalyst. As shown in Figure 16, the enzyme immobilized on PEI was faster in the conversion of HPPA compared to MpHPPR immobilized on epoxides. However, both the immobilized forms worked well, reaching respectively 84% and 69% of conversion in 24 hours.

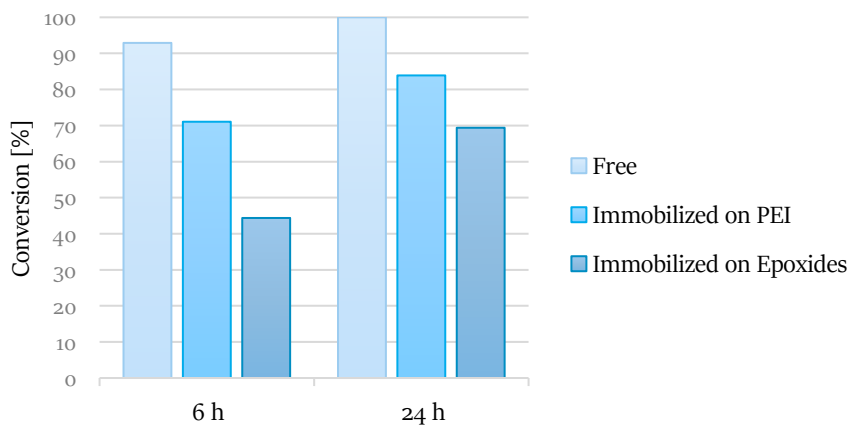


Figure 16. Batch biotransformations of 0.1 mg/mL MpHPPR in free or immobilized form (20 mg of resin with 5 mg/g biocatalyst) using 15 mM HPPA and 30 mM NADH (5 mM  $\beta$ -ME, 100 mM KPi pH 7). Further conditions: 37°C, 150 rpm, 1 mL total volume, 6 - 24 hours incubation.

### 8.2.8 Coupling of BsPheDH with MpHPPR

As first test, the two soluble biocatalysts were coupled in batch biotransformations to evaluate the efficiency of the system, that involved the concomitant conversion of L-dopa to DHPPA and then DHPPA to Danshensu together with the continuous regeneration of the cofactor (Figure 5). To assess whether the second enzyme was limiting the overall conversion rate, one biotransformation was supplemented with 2 equivalents of  $\text{NAD}^+$  (20 mM) while the other parallel reaction contained only 2 mM of cofactor (Figure 17).

The biotransformation was incubated at 25°C to prioritize the first reaction, as BsPheDH was poorly active at 37°C compared to room temperature. A control reaction was run at the same conditions with only MpHPPR as biocatalyst and as expected, no substrate depletion or product formation was detected. Similarly, another reaction was prepared with only BsPheDH as enzyme and 20 mM of cofactor. In this case, the conversion achieved 21% in 6 hours without any further increase after the 24 hours. Instead, the presence of MpHPPR enhanced the conversion of BsPheDH, that reached 59% with 20 mM cofactor and 37% with 2 mM  $\text{NAD}^+$  in the same 6 hours. The significant improvement from 21% to 59% conversion was given by the continuous removal of the intermediate DHPPA from the bulk with consequent shift of the BsPheDH reaction equilibrium towards the product generation.

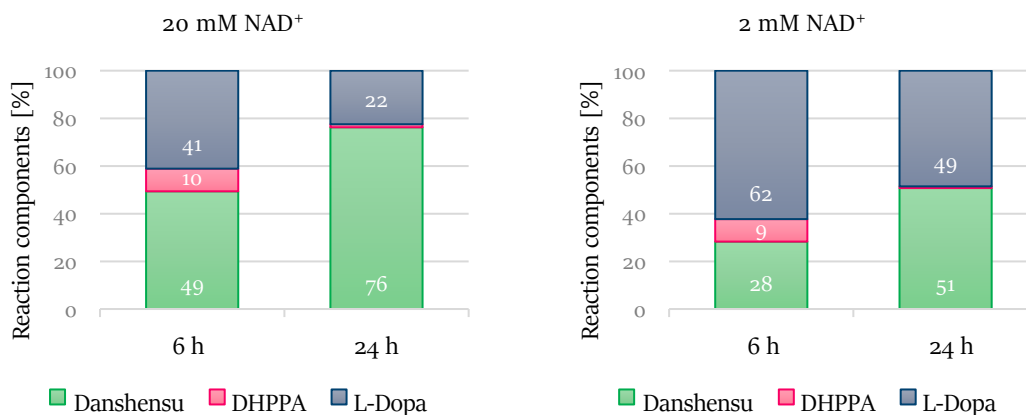


Figure 17. Batch biotransformations of 0.15 mg/mL BsPheDH and 0.25 mg/mL MpHPPR (soluble form) using 10 mM L-Dopa and 2 - 20 mM NAD<sup>+</sup> (5 mM  $\beta$ -ME, 50 mM Tris HCl pH 8.5). Further conditions: 25°C, 150 rpm, 1 mL total volume, 6 - 24 hours incubation.

Comparing the results of the two graphs in Figure 15, the cofactor recycling was not fast enough for the first reaction. Indeed, the lower availability of NAD<sup>+</sup> affected the conversion showing reduced rates with respect to the biotransformation having full availability of the cofactor. Furthermore, the intermediate was accumulated in the 6-hours reactions, meaning that the second enzyme was not fast enough to convert it. Therefore, an increased amount of MpHPPR had to be implemented to ensure higher efficiency.

The coupling of BsPheDH with MpHPPR showed promising results with high conversion rates, that reached even 76% in 24 hours. With a proper optimization, the outcomes could be further improved.

The two biocatalysts were both immobilized onto EP400/ss with high recovered activities. To enable a faster exchange of NAD(H) and DHPPA between the active sites, the two enzymes were co-immobilized yielding a closer location. Different strategies were employed, considering the results obtained with the immobilization screenings of the single enzymes (Tables 3 and 5). In particular, the co-immobilization on PEI or epoxides in simultaneous or sequential mode (first BsPheDH, then MpHPPR, and vice versa) and the immobilization of PheDH on aldehydes followed by the immobilization of MpHPPR on PEI (Figure 18) were attempted. This latter strategy has been previously described for the immobilization of other enzymes.<sup>27,28</sup> A loading of 3 mg/g of BsPheDH and 5 mg/g of MpHPPR was used as first analysis.

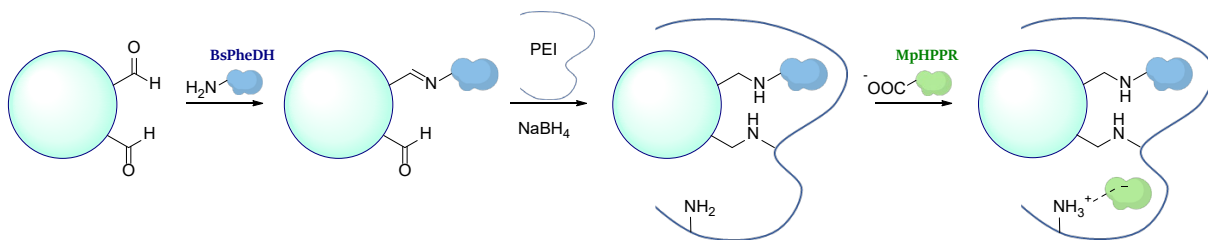


Figure 18. Co-immobilization by first interaction of BsPheDH with aldehydes, then coated with PEI followed by reduction, and last interaction of MpHPPR with PEI.

Complete immobilization was obtained with all the strategies. Afterwards, biotransformations were run to assess the performance of the co-immobilized enzymes, in terms of activity and operational stability. Unfortunately, it was hard to measure the recovered activity of each immobilized enzyme since they share the same substrates. The biotransformation using the coupled system could give a better hint on the final purpose of this work, that is the production of danshensu.

As for the activity, the highest conversion rates were achieved with the simultaneous immobilization on PEI, simultaneous immobilization on epoxides and sequential immobilization on aldehydes and PEI (Figure 19). These three best strategies were chosen for the evaluation of the operational stability.

It is interesting to mention that no intermediate was found for the three modalities of immobilizations on PEI. Most likely, the activity of MpHPPR was higher than the activity of BsPheDH after the co-immobilization, even if the recovered activities of the single enzymes were similar (around 90%).

In literature, CbHPPR was described as a dimeric assembled protein.<sup>29</sup> Consequently, it is plausible that MpHPPR had the same quaternary structure. Considering the dimeric form of this enzyme and the octameric conformation of BsPheDH, it was possible that the MpHPPR immobilization was happening faster than the BsPheDH binding, resulting in higher activity for the HPPR. The sequential immobilization on glyoxyl groups and PEI gave no intermediate as well, but in this case it can be explained by the lower recovered activity of BsPheDH on glyoxyl groups (27%, Table 4) compared to MpHPPR on PEI (89%, Table 6). The higher activity of the latter biocatalyst translated into faster conversion of the intermediate compound, with no accumulation over time. Instead, the immobilization on epoxides showed 6-7% of DHPPA (intermediate) when testing the simultaneous or sequential

(BsPheDH first, MpHPPR after) loading, meaning that these two strategies were more similar to the results obtained with the free enzymes (Figure 17).

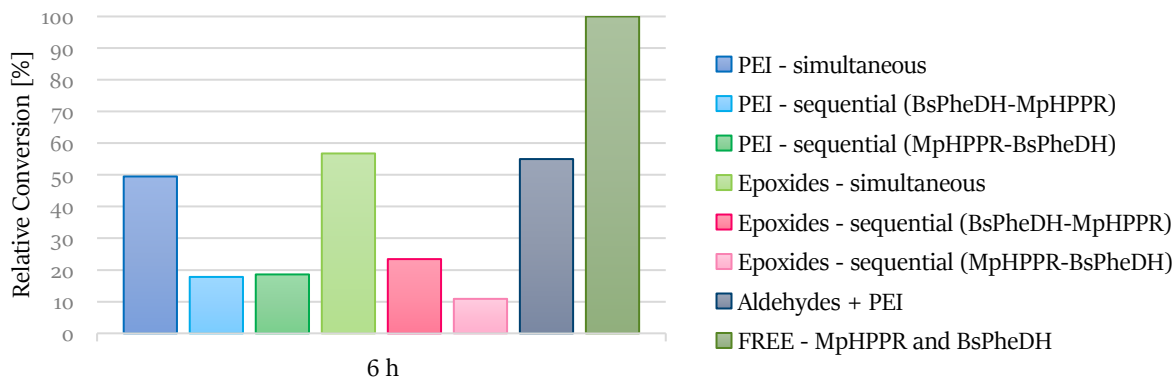


Figure 19. Conversion of 10 mM L-dopa to Danshensu as final product, with 1 mM NAD<sup>+</sup>, 5 mM βME, 50 mM Tris pH 8.5 at 25°C, 150 rpm, 1 mL total volume, 6 hours incubation. The results are relative to the conversion of the free enzymes (0.15 mg/mL BsPheDH and 0.25 mg/mL MpHPPR) at the same concentrations as the co-immobilized biocatalysts (50 mg).

With further biotransformations combining the free enzymes, enhanced rates of conversions were reached raising either the amount of MpHPPR (with equal concentration of the PheDH) or the amount of BsPheDH (with the same MpHPPR concentrations), as displayed in Figure 20.

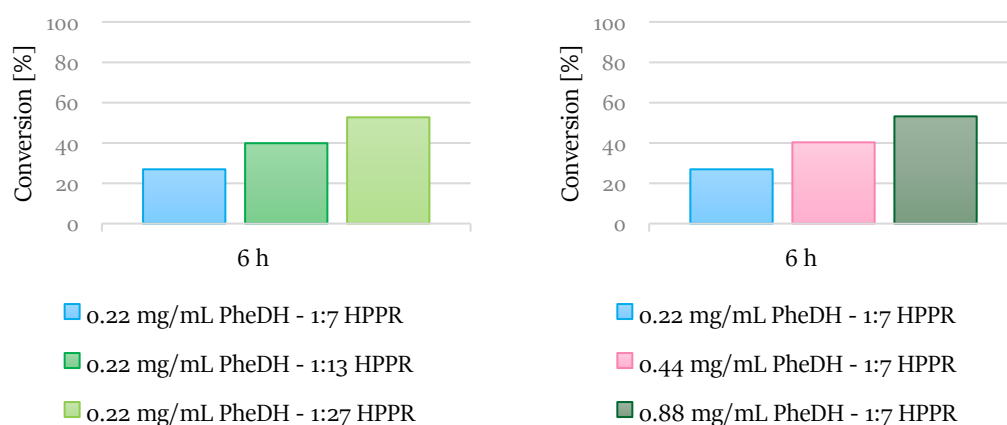


Figure 20. Conversion of 10 mM L-dopa to danshensu as final product, with 0.1 mM NAD<sup>+</sup> (ratio 1:100), 5 mM βME, 50 mM Tris pH 8.5 at 25°C, 150 rpm, 1 mL total volume. The BsPheDH : MpHPPR ratio is relative to the enzyme concentration.

As a result, more enzyme was loaded in the co-immobilization on EP400/SS (5 mg/g PheDH and 40 mg/g HPPR) to assess the operational stability.

The immobilized biocatalysts were tested over 6 cycles of 2 hours reactions. The covalent immobilization on epoxides was the most stable preparation, without any loss of activity after sixth biotransformations. The reversible immobilization on PEI maintained 60% of the initial conversion, while the sequential immobilization on glyoxyl groups and PEI retained only 25% of the starting activity after 6 cycles of usage. With this strategy, the enzyme activity was rapidly dropped within the third cycle, due to enzyme leaching. Therefore, the cross-linking of MpHPPR with glutaraldehyde (GA) was trialed to covalently stabilize the enzyme on the support and avoid any leaching in working conditions. The protein was cross-linked without the reduction step since it was known to be detrimental for the enzyme stability. However, MpHPPR retained only 8% of the initial recovered activity after the treatment with GA. Given the unsuccessful outcome, the immobilization on epoxides was chosen as best strategy, due to the high stability and good activity in the biotransformations of L-dopa.

The co-immobilization on epoxy groups was compared with a combination of resins supporting individual enzymes in order to evaluate the efficiency of the two systems. For the single immobilization, the recovered activities were calculated, which were 14% for the 5 mg/g BsPheDH (Table 4) and 37% for the 40 mg/g (Table 6). The co-immobilization did not seem to provide any improvement (Figure 21).

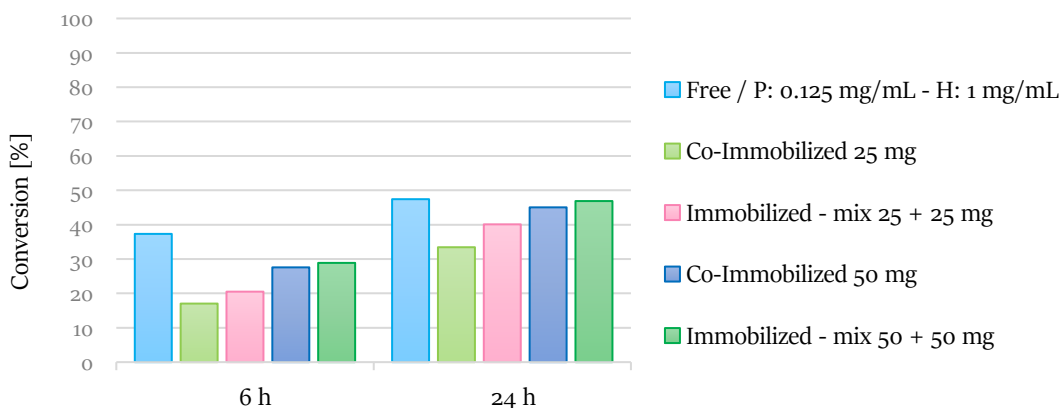


Figure 21. Conversion of 10 mM L-dopa to danshensu as final product, with 1 mM NAD<sup>+</sup> (ratio 1:10), 5 mM βME, 50 mM Tris pH 8.5 at 25°C, 150 rpm, 1 mL total volume. P: BsPheDH; H: MpHPPR. The free enzymes correspond to the 25 mg of (co-) immobilized form (5 mg/g BsPheDH and 40 mg/g MpHPPR).

Besides, the preparation of distinct biocatalysts offered the possibility to change the two enzymes ratio depending on the need. Consequently, the immobilization of separate enzymes was chosen for the flow continuous reactions.

### 8.2.9 Flow reaction with BsPheDH and MpHPPR

The packed-bed reactor was filled with 0.6 g of immobilized BsPheDH (5 mg/g) and 1 g of immobilized MpHPPR (40 mg/g) properly mixed for equal enzymes distribution in the column. The flow set-up is shown in Figure 22.

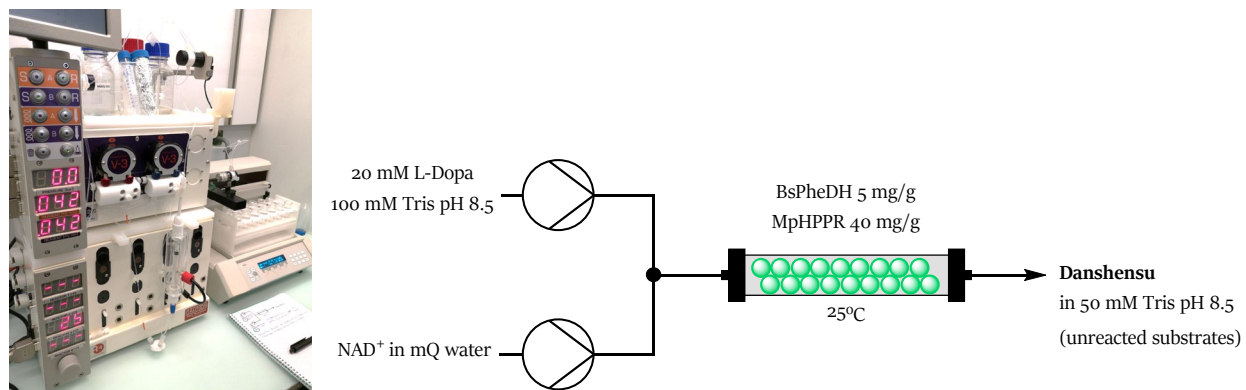


Figure 22. Set-up of the flow reactor for the continuous conversion of L-dopa to Danshensu.

Several conditions were tried, and all the results are presented in Table 7. No intermediate was detected along the reactions, meaning that MpHPPR was not limiting the overall conversion.

The lowest concentration of NAD<sup>+</sup> (0.1 mM) did not appear to be sufficient for the coupled reaction in flow, achieving only 5% of conversion at 30 minutes residence time. However, the conversion increased to 24% when 10 times higher cofactor was added (1 mM).

Rising the cofactor to 2 mM, however, did not enhance substantially the conversion, confirming that the cofactor regeneration was not limited at 1 mM scale.

60 minutes residence time improved the conversion, reaching the 36% with 3.6 mM of produced danshensu per hour at 25°C.

Setting the temperature to 30°C yielded the same conversion as at 25°C. Instead, using the preferred temperature for the MpHPPR, 37°C, led to a slight increase of conversion (39%). Since the increase was not significant, 25°C were chosen as best condition to maintain the stability of the biocatalysts over time.

Table 7. Conditions and related results of the continuous flow biotransformations.

NAD <sup>+</sup> concentration [mM]	Temperature [°C]	Residence Time [min]	Conversion [%]	Product concentration [mM]
0.1	25	30	5	0.5 ± 0.03
1.0	25	30	24	2.4 ± 0.04
1.0	30	30	23	2.3 ± 0.03
1.0	25	60	36	3.6 ± 0.1
1.0	37	60	39	3.9 ± 0.1
2.0	25	30	25	2.5 ± 0.05

### 8.2.10 Continuous production of Danshensu in the flow bioreactor

Danshensu has been successfully produced, while the immobilized enzymes demonstrated high stability over different cycles and reactions conditions (Table 7). Consequently, the system was evaluated over 24 hours of continuous flow biotransformation to assess the final biocatalysts productivity. Moreover, an in-line separation process was implemented for the continuous collection of pure danshensu (Figure 23). In this case, an acidification step followed by solvent extraction were employed through the addition of an inlet containing HCl 0.2 M (flow rate 0.03 mL/min) and a stream of ethyl acetate (flow rate 0.2 mL/min). Downstream of the process, a Zaiput system was placed to separate the two phases, so that the water could be potentially collected and, after pH adjustment, reused for other cycles of reactions, minimizing the waste. In parallel, the final product was extracted in the ethyl acetate phase and recovered by simple solvent evaporation, for an easier and faster work-up procedure.



For this reaction, 0.55 g of BsPheDH (5 mg/g) and 0.75 g of MpHPPR (40 mg/g) were adequately mixed in the reactor, which was set to 25°C. A flow rate of 0.036 mL/min was used for the two substrate inlets (total flow rate, 0.072 mL/min) giving a residence time of 30 minutes.

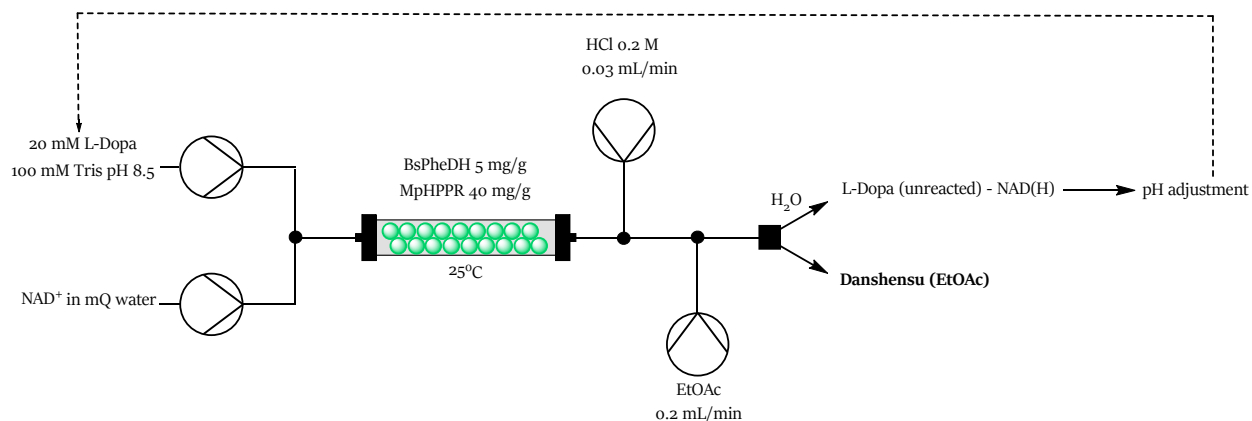


Figure 23. Set-up of the flow system for the 24 hours productivity test. Four peristaltic pumps were used for the purpose, two with the substrates (left) and two with the in-line separation process (HCl and EtOAc, on the right). The Zaiput separator is the red apparatus next to the packed bed reactor. Two bottles are placed at the downstream process for the collection of the two distinct phases.

Previous tests of danshensu extraction showed that the compound could be collected in ethyl acetate after acidification. With two sequential extractions, an 80% yield was obtained.<sup>30</sup> To simulate the double extraction in

flow, twice the volume of the aqueous phase was injected in the flow system (water: 0.102 mL/min, solvent: 0.2 mL/min).

After 1 hour of reaction, a sample was collected upstream for the HPLC analysis, which confirmed that 2.3 mM of danshensu were produced (23% conversion). After 24 hours, the concentration decreased to 1.93 mM (19% conversion), meaning that 85% of the activity was still retained despite the non-stop biocatalytic conversion over a long period of time. The downstream solutions were also collected for HPLC analysis, and the results showed that some danshensu was still present in the water phase, without being fully extracted in ethyl acetate. The solvent phase, instead, contained only danshensu without any unreacted L-dopa.

After the 24-hours reaction, between 40 and 47 mg of danshensu were expected.

The weight of the final product was 47 mg, however the  $^1\text{H-NMR}$  spectra (Figure 24) confirmed that some  $\beta$ -mercaptoethanol was also extracted. The final weight of danshensu was approximately calculated as 20 mg through the integration of the peaks area.

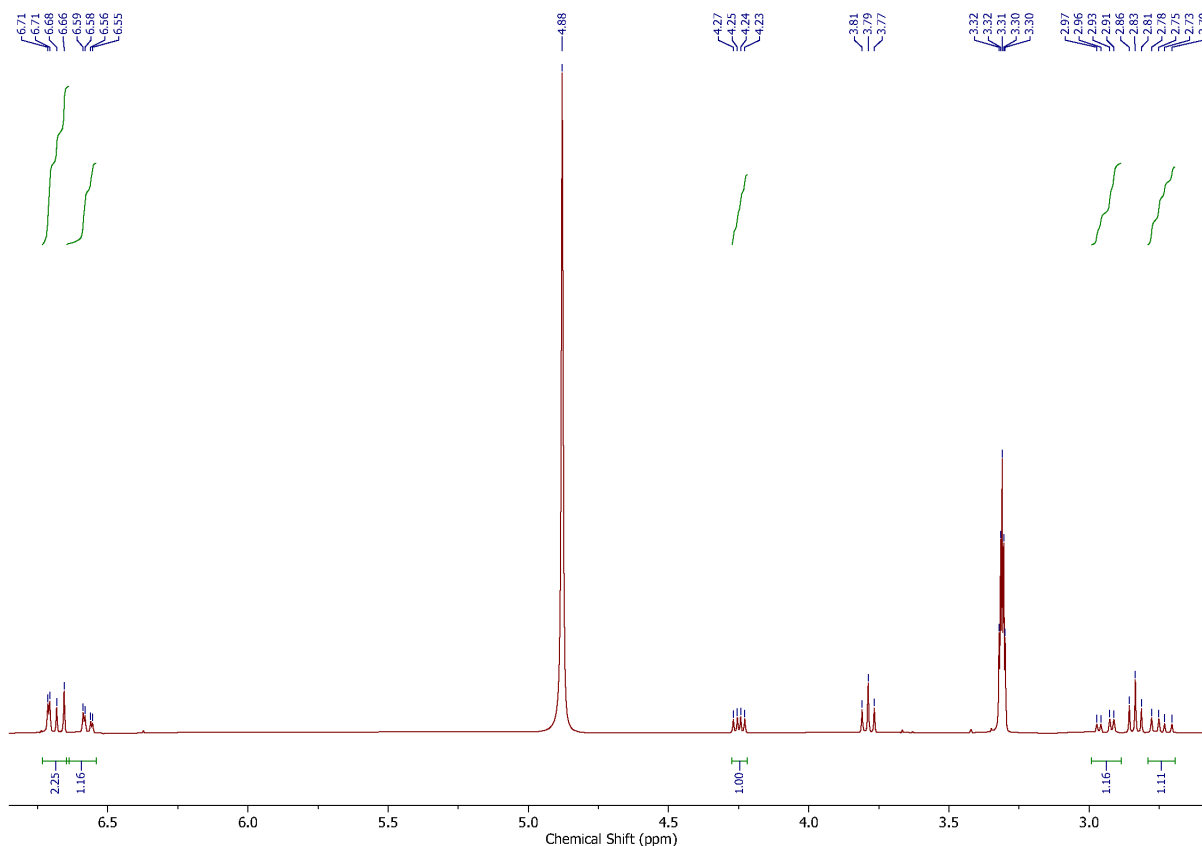


Figure 24. Characterization of the purified final product by  $^1\text{H-NMR}$ .

Consequently, the extraction yield of danshensu was 50% with 43% purity. Remarkably, the compound was not found in the oxidized form according to the NMR spectra.

As future work, optimizing this last experiment may result in higher yield and purity of danshensu. Probably, the presence of  $\beta$ -mercaptoethanol can be avoided by maintaining the substrate in anaerobic environment, so that 100% purity of danshensu may be achieved. The flow system itself excludes any contact between flowing solution and external oxygen, preventing substrate oxidation. With higher catalysts amounts, the reaction may happen faster without accumulation of L-dopa that can oxidize. Indeed, the intermediate DHPPA and the final product danshensu are not as reactive as L-dopa in the oxidation process.

The extraction process should also be improved to ensure high danshensu content in the solvent phase.

The final yield may be enhanced by decreasing the flow rate inside the bioreactor. In fact, with a corresponding residence time of 60 minutes, 3.6 mM of danshensu are obtained instead of 2.4 mM. This would give higher yield but lower productivity in terms of danshensu concentration generated per hour.

In this work, danshensu has been effectively produced in a continuous and sustainable manner. A catalyst productivity of 0.015 was obtained by dividing the 0.02 g of produced danshensu with the 1.3 g of immobilized biocatalysts. The space time yield resulted in 0.083 mM/min or 5 mM/h.

As a comparison, the production of danshensu reported in a previous publication, starting from L-dopa as substrate, achieved a productivity of 6.61 mM/h, which was slightly higher than the current work.<sup>14</sup> However, the publication reported a reaction system based on the addition of 125 mM L-dopa to form 118.9 mM (R)-danshensu in 18 hours. It is not clear how the solution was prepared, since the solubility of L-dopa in water is 5 mg/mL (at 20°C), corresponding to 25 mM.<sup>31</sup> As whole-cell biotransformation, the biocatalyst could not be recovered for further reactions after the 18 hours and probably, it lost stability over time as soluble form.

On the contrary, the BsPheDH – MpHPPR system was active and stable after one working day. Potentially, the immobilized biocatalysts could be continuously used for further hours to achieve higher yields, without the need for new enzyme expression.

This work could become suitable for industrial application, as highly sustainable process. After proper optimization, this method will attain higher efficiency for a competitive biocatalytic system.

### 8.3 CONCLUSION

Initially, the overall biotransformation was designed with the ubiquitous and low-priced caffeic acid as starting material. After optimizing the RgPAL amination reaction, a very low conversion rate was unfortunately achieved, thus making this first step impractical and wasteful. Nonetheless, L-dopa was found to be as inexpensive and valuable as the previous substrate, so that the first reaction became superfluous. Notably, when this work started in October 2021, approximately, the price of L-dopa was three times higher than caffeic acid.

Driving the attention to the following coupled reaction, the novel MpHPPR enzyme has been successfully expressed and characterized, showing activity in the reduction of DHPPA with NADH. Therefore, MpHPPR was efficiently coupled to BsPheDH for danshensu production. A fully optimized reusable system was obtained after immobilization of the two biocatalysts on a methacrylate resin. Their implementation in a flow bioreactor offered a 24% conversion with 30 minutes residence time and 36% conversion with 60 minutes. The two biocatalysts were then tested for a continuous flow biotransformation over 24 hours, in combination with an in-line separation method. Although the process could be further optimized, a productivity of 5 mM/h was successfully achieved. The final product was collected, and the dried form was yielded, even if the purity was not as expected. However, further studies might be carried out in order to improve the overall process.

Since the soluble biocatalysts demonstrated enhanced conversion rates in shorter reaction times, using smaller amounts of cofactor, it would be of high impact to perform the reaction in dialysis bags, as done in chapter 7. Indeed, both the two biocatalysts are extremely stable in their soluble form. Without the need for immobilization, this test may potentially open up new perspectives in the cost-efficient production of danshensu and consequently, the expanded pharmacological application.

### 8.4 BIBLIOGRAPHY

1. Li, L. N. Biologically active components from traditional Chinese medicines. *Pure Appl. Chem.* **70**, 547–554 (1998).
2. Findrik, Z., Poljanac, M. & Vasić-Rački, D. Modelling and optimization of the (R)-(+)-3,4-dihydroxyphenyllactic acid production catalyzed with D-lactate dehydrogenase from *Lactobacillus leishmannii* using genetic algorithm. *Chem. Biochem. Eng. Q.* **19**, 351–358 (2005).

3. Hu, P., Luo, G. A., Zhao, Z. & Jiang, Z. H. Quality assessment of Radix Salviae Miltiorrhizae. *Chem. Pharm. Bull.* **53**, 481–486 (2005).
4. Zhao, G. R. *et al.* Characterization of the radical scavenging and antioxidant activities of danshensu and salvianolic acid B. *Food Chem. Toxicol.* **46**, 73–81 (2008).
5. Bao, X. Y. *et al.* Danshensu for Myocardial Ischemic Injury: Preclinical Evidence and Novel Methodology of Quality Assessment Tool. *Front. Pharmacol.* **9**, (2018).
6. Zhang, J., Zhang, Q., Liu, G. & Zhang, N. Therapeutic potentials and mechanisms of the Chinese traditional medicine Danshensu. *Eur. J. Pharmacol.* **864**, 172710 (2019).
7. Chan, K. *et al.* Protective effects of Danshensu from the aqueous extract of Salvia miltiorrhiza (Danshen) against homocysteine-induced endothelial dysfunction. *Life Sci.* **75**, 3157–3171 (2004).
8. Yang, R. X. *et al.* Danshensu protects vascular endothelia in a rat model of hyperhomocysteinemia. *Acta Pharmacol. Sin.* **31**, 1395–1400 (2010).
9. Lam, F. F. Y., Yeung, J. H. K., Chan, K. M. & Mei Yu Or, P. Relaxant effects of danshen aqueous extract and its constituent danshensu on rat coronary artery are mediated by inhibition of calcium channels. *Vascul. Pharmacol.* **46**, 271–277 (2007).
10. Wang, T. *et al.* Neuroprotective effects of Danshensu on rotenone-induced Parkinson's disease models in vitro and in vivo. *BMC Complement. Med. Ther.* **20**, (2020).
11. Kwon, G. *et al.* Anxiolytic-like effect of danshensu [(3-(3,4-dihydroxyphenyl)-lactic acid)] in mice. *Life Sci.* **101**, 73–78 (2014).
12. Wang, W. *et al.* Danshensu alleviates pseudo-typed SARS-CoV-2 induced mouse acute lung inflammation. *Acta Pharmacol. Sin.* **43**, 771–780 (2022).
13. Gao, Y. *et al.* Acute and subchronic toxicity of danshensu in mice and rats. *Toxicol. Mech. Methods* **19**, 363–368 (2009).
14. Xiong, T. *et al.* Redox self-sufficient biocatalyst system for conversion of 3,4-Dihydroxyphenyl-l-alanine into (R)- or (S)-3,4-Dihydroxyphenyllactic acid. *J. Ind. Microbiol. Biotechnol.* **46**, 1081–1090 (2019).
15. Dong, C., Wang, Y. & Zhu, Y. Z. Asymmetric synthesis and biological evaluation of Danshensu derivatives as anti-myocardial ischemia drug candidates. *Bioorganic Med. Chem.* **17**, 3499–3507 (2009).

16. Lu, H. *et al.* Identification of a L-Lactate dehydrogenase with 3,4-dihydroxyphenylpyruvic reduction activity for L-Danshensu production. *Process Biochem.* **72**, 119–123 (2018).
17. Yao, Y. F., Wang, C. S., Qiao, J. & Zhao, G. R. Metabolic engineering of *Escherichia coli* for production of salvianic acid A via an artificial biosynthetic pathway. *Metab. Eng.* **19**, 79–87 (2013).
18. Ding, H. *et al.* Biosynthesis of 4-hydroxyphenylpyruvic acid from L-tyrosine using recombinant *Escherichia coli* cells expressing membrane bound L-amino acid deaminase. *Chinese J. Chem. Eng.* **26**, 380–385 (2018).
19. Wang, Y. H., Bai, Y. J., Fan, T. P., Zheng, X. H. & Cai, Y. J. Reducing 3,4-dihydroxyphenylpyruvic acid to d-3,4-dihydroxyphenyllactic acid via a coenzyme nonspecific d-lactate dehydrogenase from *Lactobacillus reuteri*. *J. Appl. Microbiol.* **125**, 1739–1748 (2018).
20. Nagy, E. Z. A. *et al.* Mapping the Hydrophobic Substrate Binding Site of Phenylalanine Ammonia-Lyase from *Petroselinum crispum*. *ACS Catal.* **9**, 8825–8834 (2019).
21. Louie, G. V. *et al.* Structural Determinants and Modulation of Substrate Specificity in Phenylalanine-Tyrosine Ammonia-Lyases. *Chem. Biol.* **13**, 1327–1338 (2006).
22. Asano, Y., Nakazawa, A. & Endo, K. Novel phenylalanine dehydrogenases from *Sporosarcina ureae* and *Bacillus sphaericus*. Purification and characterization. *J. Biol. Chem.* **262**, 10346–10354 (1987).
23. Seah, S. Y. K. *et al.* Alteration in relative activities of phenylalanine dehydrogenase towards different substrates by site-directed mutagenesis. *FEBS Lett.* **370**, 93–96 (1995).
24. Khorsand, F., Murphy, C. D., Whitehead, A. J. & Engel, P. C. Biocatalytic stereoinversion of d-: Para - bromophenylalanine in a one-pot three-enzyme reaction. *Green Chem.* **19**, 503–510 (2017).
25. Häusler, E., Petersen, M. & Alfermann, A. W. Hydroxyphenylpyruvate Reductase from Cell Suspension Cultures of *Coleus blumei* Benth. *Zeitschrift fur Naturforsch. - Sect. C J. Biosci.* **46**, 371–376 (1991).
26. Kim, K. H., Janiak, V. & Petersen, M. Purification, cloning and functional expression of hydroxyphenylpyruvate reductase involved in rosmarinic acid biosynthesis in cell cultures of *Coleus blumei*. *Plant Mol. Biol.* **54**, 311–323 (2004).

27. Velasco-Lozano, S., Benítez-Mateos, A. I. & López-Gallego, F. Co-immobilized Phosphorylated Cofactors and Enzymes as Self-Sufficient Heterogeneous Biocatalysts for Chemical Processes. *Angew. Chemie - Int. Ed.* **56**, 771–775 (2017).
28. Velasco-Lozano, S., da Silva, E. S., Llop, J. & López-Gallego, F. Sustainable and Continuous Synthesis of Enantiopure L-Amino Acids by Using a Versatile Immobilised Multienzyme System. *ChemBioChem* **19**, 395–403 (2018).
29. Janiak, V., Petersen, M., Zentgraf, M., Klebe, G. & Heine, A. Structure and substrate docking of a hydroxy(phenyl)pyruvate reductase from the higher plant *Coleus blumei* Benth. *Acta Crystallogr. Sect. D Biol. Crystallogr.* **66**, 593–603 (2010).
30. Zhang, Z. C. *et al.* Determination of danshensu in rat plasma and tissues by high-performance liquid chromatography. *J. Chromatogr. Sci.* **46**, 184–190 (2008).
31. Dannenfelser, R. M. & Yalkowsky, S. H. Data base of aqueous solubility for organic non-electrolytes. *Sci. Total Environ.* **109–110**, 625–628 (1991).

## 9. CONCLUSIONS

---

The main focus of the presented research work was the development and optimization of biocatalytic tools for the efficient application in cascade reactions, to provide then beneficial effects on industrial application.

In chapter 4, the phenylalanine ammonia lyase from *Anabaenas variabilis* (AvPAL) was successfully immobilized and employed in the continuous flow biotransformation of two aliphatic alanine derivatives. One of them, 3-trifluoromethyl-alanine, was not converted in the PAL deamination reaction since the substrate was not accepted. However, allylglycine was effectively transformed to the acrylate penta-2,4-dienoic acid even if only 3-5% conversion was achieved, corresponding to maximum 1.1 mM production in 1 hour of residence time.

For the quantification and remediation of ammonia, an efficient biocatalytic tool was developed by co-immobilizing the glutamate dehydrogenase from *Clostridium symbiosum* (CsGluDH) and the formate dehydrogenase from *Candida boidinii* (CbFDH) onto the methacrylate resin EP400/SS. Excellent immobilization yield and recovered activity were achieved as well as good stability over time. The bienzymatic system was tested in the removal of ammonia, showing full and rapid conversion of 50 mM substrate and 80% conversion in the 300 mM scale. In this regard, the immobilized form significantly surpassed the soluble enzymes, which were fast destabilized by the high substrates concentration.

To further optimize the described bienzymatic tool, a self-sufficient fusion protein was successfully created, yielding a completely active and stable bifunctional enzyme. The immobilized fusion protein showed outstanding results in the removal of low and high amounts of ammonia, indicating 100% conversion in both cases. Therefore, the closer proximity of the two enzymes has a beneficial impact on the reaction efficiency. Indeed, they fully exceeded the wild-type enzymes, proving the effective accomplished optimization.

In chapter 7, the versatility of the fusion protein system was investigated by fusing the alanine dehydrogenase from *Halomonas elongata* (HeAlaDH) with the CbFDH. The two orientations of the domains were obtained, and their comparison showed that different properties were retained depending on the protein structure. The AlaDH-FDH-His enzyme retained approximately 60% of FDH activity and 20-30% of the AlaDH one. This fusion protein was combined with the  $\omega$ -transaminase from *Halomonas elongata* (HeWT) to assist the conversion of vanillin to



## 9. CONCLUSIONS

vanillyl amine as test reaction. The soluble wild-type enzymes were previously described as poorly stable after 3 cycles of reuse in the dialysis bag assisted biotransformation. In comparison, the fusion protein proved to maintain the same conversion rate as the first cycle, meaning that an optimized biocatalytic tool for the transaminase reaction was successfully realized.

In the last chapter, a biocatalytic cascade reaction was developed for the sustainable production of danshensu. The amination of caffeic acid to L-dopa by the PAL from *Rhodotorula glutinis* did not offer considerable results, due to the low conversion rate in the flow system (maximum 8%). Moreover, the impact on the enzyme stability for the presence of 2 M ammonium sulphate and the oxidized by-product was impractical, as well as the high consequent price of the overall process. Thus, the cascade reaction was based on the still low-priced L-dopa as starting material. The phenylalanine dehydrogenase from *Bacillus subtilis* (BsPheDH) was envisaged for the oxidative deamination of the substrate. Since this enzyme requires NAD<sup>+</sup>, the addition of a second enzyme able to simultaneously reduce the reaction intermediate and regenerate the cofactor would significantly increase the cost- and reaction- efficiency of the system. The novel hydroxy phenyl pyruvate reductase from *Mentha x piperita* (MpHPPR) offered all these requirements, as confirmed by its characterization. The two biocatalysts were subjected to an immobilization screening, so an optimized combination was chosen, consisting of 5 mg/g BsPheDH and 40 mg/g MpHPPR covalently bound to EP400/SS with decent recovered activity (14% and 39% respectively) and excellent stability. The cascade biotransformation was performed in the flow bioreactor, yielding 24% conversion with 30 minutes residence time and 36% conversion with 60 minutes. Furthermore, the biocatalytic tool for danshensu production was assessed in a 24-hours flow reaction as potential industrial solution. Remarkably, the immobilized enzymes retained 85% activity after 24 hours of continuous reaction. Although the implemented in-line product separation still requires some improvements, the process achieved a reasonable productivity of 5 mM danshensu per hour. These promising results can be further optimized, offering a more sustainable, self-sufficient and less expensive tool for the biocatalytic manufacture of the valuable danshensu at industrial scale.

To summarize, the here described biocatalytic tools were efficiently developed after an accurate design. The following optimization strategies offered enhanced properties. Consequently, the enzymatic tools can be effectively applied in cascade reactions to improve the production even for industrial purpose.

## Declaration of consent

---

on the basis of Article 18 of the PromR Phil.-nat. 19

Name/First Name: Marchini Valentina

Registration Number: 19-122-506

Study program: PhD Chemistry and Molecular Sciences

Bachelor  Master  Dissertation

Title of the thesis: Biocatalytic Tools for Enzymatic Cascades

Supervisor: Francesca Paradisi

I declare herewith that this thesis is my own work and that I have not used any sources other than those stated. I have indicated the adoption of quotations as well as thoughts taken from other authors as such in the thesis. I am aware that the Senate pursuant to Article 36 paragraph 1 litera r of the University Act of September 5th, 1996 and Article 69 of the University Statute of June 7th, 2011 is authorized to revoke the doctoral degree awarded on the basis of this thesis.

For the purposes of evaluation and verification of compliance with the declaration of originality and the regulations governing plagiarism, I hereby grant the University of Bern the right to process my personal data and to perform the acts of use this requires, in particular, to reproduce the written thesis and to store it permanently in a database, and to use said database, or to make said database available, to enable comparison with theses submitted by others.

Bern 20/05/2022

Signature



# Curriculum Vitae

---

## EDUCATION:

### **Ph.D. in BIOCATALYSIS** (2018 - 2022)

School of Chemistry - University of Nottingham (UK) from 04.2018 to 08.2019

DCBP - Universität Bern (CH) from 09.2019 to 31.05.2022 (ph.D. defense in July 2022)

Supervisor: Prof. Francesca Paradisi

### **MSc in PHARMACY** (2011 - 2017)

Università degli Studi di Trieste (IT) - Final grade: 105/110

Master thesis: "Biocatalysed synthesis of azelaic acid's oligoesters for cosmetic and dermatologic applications"

Supervisors: Prof. Lucia Gardossi, Prof. Cynthia Ebert

### **HIGH SCHOOL DIPLOMA in BUSINESS CONSULTANT - PROFICIENT IN FOREIGN LANGUAGES**

(2006 - 2011) with focus on English, German and Spanish languages

Technical Commercial Institute (San Donà di Piave, Venezia, IT) - Final grade: 100/100

## PUBLICATIONS:

**As Author:** V. Marchini, A. I. Benítez-Mateos, D. Roura Padrosa, F. Paradisi. *Chimeric fusion of glutamate dehydrogenase and formate dehydrogenase yields a bifunctional efficient biocatalyst for the continuous removal of ammonia.* *Frontiers in Catalysis*, 2021. (10.3389/fctls.2021.790461)

**As Co-author:** D. R. Padrosa, V. Marchini, F. Paradisi. *CapiPy: python based GUI-application to assist in protein immobilization.* *Bioinformatics*, 2020. (10.1093/bioinformatics/btabo30)

## CONFERENCES:

17.10.2018 **Oral presentation** on "Development of an Alanine Ammonia-Lyase and 2,3-Alanine Aminomutase to improve the production of highly valuable compounds" Chemical Biology Forum at University of Nottingham, UK

07.12.2018 **Poster presentation** in the 17th Annual Symposium of CSCB in "Recent Advances in Synthesis and Chemical Biology XVII" at the Royal College of Surgeons in Dublin, IE

07/11.07.2019 **Poster presentation** in the 14th International Symposium on Biocatalysis and Biotransformations (BioTrans) in Groningen, NL

06.12.2019 **Poster presentation** in the 18th Annual Symposium of CSCB in “Recent Advances in Synthesis and Chemical Biology XVII” at the Royal College of Surgeons in Dublin, IE

04.02.2020 **Poster presentation** in the 2nd Anglo-Swiss Symposium 2020 in “Using Chemical Biology to Identify New Targets for Medicinal Chemistry” at University of Basel, CH

07/08.09.2020 **Oral presentation** on “*Development of one-pot sustainable production of acrylic acid derivatives using a Phenylalanine ammonia lyase, a Glutamate and a Formate dehydrogenase as biocatalysts*” Graduate Student Symposium 2020 at the University of Bern, CH

**with award for an excellent presentation of the Ph.D. research**

06/08.05.2021 **Poster presentation** in the 6th International Conference on Biocatalysis in Non-Conventional Media (BNCM) in Milano, IT

27/28.05.2021 **Oral presentation and Assistance during the Organization** on “*Design and development of a fusion protein employing a glutamate and a formate dehydrogenase as an efficient tool for the quantification of ammonia*” - International Symposium of The Next Generation of Biocatalysis in Bern, University of Bern, CH

19/22.07.2021 **Poster presentation** in the 15th International Symposium on Biocatalysis and Biotransformations (BioTrans) in Graz, A

25/26.04.2022 **Poster presentation** on “*Development of a fusion protein to yield a bifunctional efficient biocatalyst for the detection and the removal of ammonia*” in the Next Generation Biocatalysis (NextGenBiocat) Symposium in Delft, NL

**with the NextGenBiocat 2022 scientific committee award for the poster presentation**

31.05/03.06.2022 **Poster presentation** in the Girona Seminar in Girona, ES